Innovative Strategies for Enhancing Oncolytic Virus Therapy: From Delivery to Selective Translational Regulation

AIDA SAID

Thesis submitted to the University of Ottawa

in partial fulfillment of the requirements for the degree of

DOCTOR OF PHILOSOPHY

Department of Biochemistry, Microbiology and Immunology

Faculty of Medicine

University of Ottawa

Ottawa, Ontario, Canada

Abstract

Oncolytic viruses (OVs) are emerging as a promising therapeutic approach with the ability to achieve direct tumour cell death and the induction of antitumour immunity. Nevertheless, their clinical application is hampered by several obstacles, including inefficient delivery to solid tumours and the complex antiviral environment within infected cells that restricts protein production. This thesis focuses on these issues by investigating both the physical delivery of OVs and the translational mechanisms that govern gene expression during viral infection. First, we showed that needle-free injection (NFI) is a feasible and efficient technique for intratumoural injection of OVs, which enhances the distribution of viruses in tumours more efficiently than needle injection, without the loss of infectivity or therapeutic action. These results underscore the need to maximize delivery systems to promote viral propagation in solid tumours. Second, we examined how the antiviral state impacts transgene expression from OVs. Using an oncolytic herpes simplex virus-1 (HSV-1) platform, we showed that standard transgene mRNAs are inefficiently translated during infection. By incorporating a viral 5′ leader sequence into the transgene cassette, we significantly enhanced protein production and improved antitumour efficacy in vivo, demonstrating that adaptation to the host translational environment is critical for maximizing therapeutic output. Finally, using RNA sequencing and ribosome profiling, we characterized the translational landscape of glioblastoma cells during infection with the oncolytic Maraba virus MG1. Despite global suppression of protein synthesis, a subset of host mRNAs exhibited increased translational efficiency independent of transcript abundance, revealing a marked uncoupling between transcription and translation. We identified a purine-rich cis-regulatory element within the 5′ untranslated regions of some of the transcripts that promotes selective translation under antiviral stress conditions. Functional studies demonstrate that this R-motif enhances translation and regulates expression of genes such as GLDC, which acts as a host restriction factor limiting viral spread. Collectively, this work establishes translation as a critical regulatory layer shaping the outcome of oncolytic virotherapy. By integrating delivery optimization with mechanistic insights into translational control, this thesis provides a framework for improving OV design through both enhanced tumour targeting and sustained protein expression in the antiviral environment. These findings have broad implications for the development of more effective oncolytic viruses and other gene-based therapeutic platforms.

Acknowledgments

"Where there is a will, there is a way." This belief has carried me through the many challenges of my PhD. More than a scientific endeavor, this journey has been a process of building perseverance, discipline, and resilience. It has shaped not only how I think as a researcher, but also who I am as a person, teaching me to remain patient, to keep moving forward despite uncertainty, and to grow through every obstacle.

I would like to express my sincere gratitude to my supervisor, Dr. Tommy Alain, for his guidance and support throughout my PhD. I am also deeply thankful to Dr. Huy-Dung Hoang for his mentorship, generosity with his time, and constant willingness to help, all of which have greatly influenced my development as a scientist. I am especially grateful to my co-supervisor, Dr. Marceline Côté, for her support, understanding, and guidance at critical moments during my journey. Her encouragement and perspective were invaluable, and I truly appreciate the opportunity to have learned from her. I would also like to sincerely thank all the members of both labs for their support, collaboration, and the many enjoyable moments we shared along the way. The positive environment and teamwork made this journey both productive and memorable. I am equally grateful to my friends, especially Brad Mischuk, for his constant encouragement and for always pushing me to keep going, even during the most challenging and frustrating moments of my scientific journey.

I would also like to thank my thesis advisory committee members, Dr. Barbara Vanderhyden, Dr. Yannick Benoit, and Dr. Vanessa D'Costa, for their thoughtful feedback and continued support. I am equally grateful to my thesis examiners, Dr. Michael Brown, Dr. Barbara Vanderhyden, Dr. Carolina Solange Ilkow, and Dr. Mireille Khacho for accepting to evaluate my work and contribute to this important milestone.

On a personal level, I owe a very special thanks to my brother, Fares. Living far from home, his unwavering support, generosity, and presence made it possible for me to fully pursue this journey. He has been a constant source of strength and stability, and I am deeply grateful for everything he has done for me.

To my parents, thank you for your unconditional love, sacrifices, and belief in me. The values you instilled in me have guided me every step of the way, and this achievement is as much yours as it is mine.

Throughout this PhD, I learned far more than science. I learned resilience, professionalism, and emotional strength. I learned that growth comes with struggle, and that perseverance is built, not given. This journey has shaped me into a stronger and more mature person, and it has taught me that everything worth achieving comes through persistence, effort, and belief in oneself.

Table of Contents

List of Figures

List of Tables

List of Abbreviations

AAV — Adeno-Associated Virus

ACC — Animal Care Committee

AKT — Protein Kinase B

ALS — Amyotrophic Lateral Sclerosis

AMAP1 — Arf-GAP with SH3 Domain, Ankyrin Repeat and PH Domain 1

AMPK — AMP-Activated Protein Kinase

ANTXR1 — Anthrax Toxin Receptor 1

ARE — AU-rich Element

ARR2PB — Androgen-Responsive Probasin Promoter

ATCC — American Type Culture Collection

ATF4 — Activating Transcription Factor 4

BNT162b2 — Pfizer–BioNTech COVID-19 mRNA Vaccine

BSA — Bovine Serum Albumin

CAT — Chloramphenicol Acetyltransferase

CAVATAK — Coxsackievirus A21 Therapeutic Virus

CCL5 — C-C Motif Chemokine Ligand 5

CD123 — Cluster of Differentiation 123

CDK4 — Cyclin-Dependent Kinase 4

CDS — Coding Sequence

CIHR — Canadian Institutes of Health Research

CITE — Cap-Independent Translation Element

cGAS — Cyclic GMP-AMP Synthase

CLEC7A — C-Type Lectin Domain Containing 7A

CMV — Cytomegalovirus

CO_2 — Carbon Dioxide

COX-2 — Cyclooxygenase-2

CRC — Colorectal Cancer

CT — Cycle Threshold

CT26 — Murine Colorectal Carcinoma Cell Line

CV2CoV — CureVac Second-Generation COVID-19 mRNA Vaccine

CVB3 — Coxsackievirus B3

CVnCoV — CureVac First-Generation COVID-19 mRNA Vaccine

CXCL2 — C-X-C Motif Chemokine Ligand 2

CXCL3 — C-X-C Motif Chemokine Ligand 3

CXCL9 — C-X-C Motif Chemokine Ligand 9

CXCL10 — C-X-C Motif Chemokine Ligand 10

DAF — Decay-Accelerating Factor (CD55)

DAMPs — Damage-Associated Molecular Patterns

DC — Dendritic Cell

dl1520 — Adenovirus ONYX-015 Variant

DMEM — Dulbecco's Modified Eagle Medium

DNA — Deoxyribonucleic Acid

DPBS — Dulbecco's Phosphate-Buffered Saline

DPR — Dipeptide Repeat

DRD2 — Dopamine Receptor D2

dsDNA — Double-Stranded DNA

dsRNA — Double-Stranded RNA

DTT — Dithiothreitol

ECM — Extracellular Matrix

EDTA — Ethylenediaminetetraacetic Acid

EF1α — Elongation Factor 1 Alpha

EGFR — Epidermal Growth Factor Receptor

ELISA — Enzyme-Linked Immunosorbent Assay

ELISPOT — Enzyme-Linked Immunospot

EMCV — Encephalomyocarditis Virus

EMT — Epithelial–Mesenchymal Transition

ER — Estrogen Receptor

ERα — Estrogen Receptor Alpha

ERK — Extracellular Signal-Regulated Kinase

ESR1 — Estrogen Receptor 1

FBS — Fetal Bovine Serum

FCU1 — Fusion Cytosine Deaminase/Uracil Phosphoribosyltransferase

FLuc — Firefly Luciferase

FTD — Frontotemporal Dementia

G47Δ — Genetically Modified HSV-1 Oncolytic Virus

GARS — Glycyl-tRNA Synthetase

GC — Guanine–Cytosine Content

GEO — Gene Expression Omnibus

GFP — Green Fluorescent Protein

GLDC — Glycine Decarboxylase

GM-CSF — Granulocyte–Macrophage Colony-Stimulating Factor

gDNA — Genomic DNA

GSG — Glycine–Serine–Glycine

H101 — Oncorine Adenovirus

H3K27M — Histone H3 Lysine 27 to Methionine Mutation

HBB — Hemoglobin Subunit Beta

HCC — Hepatocellular Carcinoma

HEK293T — Human Embryonic Kidney 293T Cells

HERC5 — HECT and RCC1-Like Domain Containing Protein 5

HISAT2 — Hierarchical Indexing for Spliced Alignment of Transcripts

HNE — HEPES-NaCl-EDTA Buffer

HNSCC — Head and Neck Squamous Cell Carcinoma

HRV2 — Human Rhinovirus Type 2

HSV-1 — Herpes Simplex Virus Type 1

HSV-TK — Herpes Simplex Virus Thymidine Kinase

HVEM — Herpesvirus Entry Mediator

ICAM-1 — Intercellular Adhesion Molecule 1

ICD — Immunogenic Cell Death

ICP — Infected Cell Protein

ICP27 — Infected Cell Protein 27

IF — Immunofluorescence

IFITM1 — Interferon-Induced Transmembrane Protein 1

IFNγ — Interferon Gamma

IgG — Immunoglobulin G

IGF2BP1 — Insulin-Like Growth Factor 2 mRNA-Binding Protein 1

IL-10 — Interleukin 10

IL-12 — Interleukin 12

IL3RA — Interleukin 3 Receptor Subunit Alpha

IL8 — Interleukin 8

Incucyte — Live-Cell Imaging System

INPP5E — Inositol Polyphosphate-5-Phosphatase E

ISR — Integrated Stress Response

ISRIB — Integrated Stress Response Inhibitor

ISG — Interferon-Stimulated Gene

IVIS — In Vivo Imaging System

JAK — Janus Kinase

JX-594 — Pexa-Vec Vaccinia Virus

KOS — HSV-1 Strain KOS

KRAS — Kirsten Rat Sarcoma Viral Oncogene

LARP1 — La-Related Protein 1

LARP4 — La-Related Protein 4

LARS — Leucyl-tRNA Synthetase

Luc — Luciferase

LTN1 — Listerin E3 Ubiquitin Protein Ligase 1

MAPK — Mitogen-Activated Protein Kinase

MAPK13 — Mitogen-Activated Protein Kinase 13

MAVS — Mitochondrial Antiviral-Signaling Protein

MCS — Multiple Cloning Site

MDA5 — Melanoma Differentiation-Associated Protein 5

MDSCs — Myeloid-Derived Suppressor Cells

MEK — Mitogen-Activated Protein Kinase Kinase

MEME — Multiple Em for Motif Elicitation

METTL1 — Methyltransferase Like 1

MeV — Measles Virus

miR — MicroRNA

miRT — MicroRNA Response Target Site

MinION — Oxford Nanopore Sequencing Platform

MOI — Multiplicity of Infection

MPRA — Massively Parallel Reporter Assay

MRE — MicroRNA Response Element

mRNA — Messenger RNA

mTOR — Mechanistic Target of Rapamycin

mTORC1 — Mechanistic Target of Rapamycin Complex 1

MX1 — MX Dynamin-Like GTPase 1

NCBI — National Center for Biotechnology Information

NDV — Newcastle Disease Virus

NEMF — Nuclear Export Mediator Factor

NFI — Needle-Free Injection

NI — Needle Injection

NK — Natural Killer

NSCLC — Non-Small Cell Lung Cancer

NSERC — Natural Sciences and Engineering Research Council

NTC — Non-Targeting Control

OASL — 2′-5′-Oligoadenylate Synthetase Like

ONC201 — Imipridone Anticancer Compound

ORF — Open Reading Frame

OV — Oncolytic Virus

P2A — Porcine Teschovirus-1 2A Peptide

PABP — Poly(A)-Binding Protein

PAGE — Polyacrylamide Gel Electrophoresis

PBMC — Peripheral Blood Mononuclear Cell

PCR — Polymerase Chain Reaction

PDAC — Pancreatic Ductal Adenocarcinoma

PDK4 — Pyruvate Dehydrogenase Kinase 4

PECAM1 — Platelet and Endothelial Cell Adhesion Molecule 1

PERK — PKR-Like Endoplasmic Reticulum Kinase

PFU — Plaque-Forming Unit

PFA — Paraformaldehyde

PGK — Phosphoglycerate Kinase

PI3K — Phosphoinositide 3-Kinase

PIM1 — Proviral Integration Site for Moloney Murine Leukemia Virus 1

PKR — Protein Kinase R

PolIRES — Poliovirus Internal Ribosome Entry Site

PRR — Pattern Recognition Receptor

PTGS2 — Prostaglandin-Endoperoxide Synthase 2

PTI — Pattern-Triggered Immunity

PVSRIPO — Recombinant Poliovirus Therapy

qPCR / RT-qPCR — Quantitative Reverse Transcription PCR

RAN — Repeat-Associated Non-AUG Translation

RAS — Rat Sarcoma Viral Oncogene

Rb — Retinoblastoma Protein

ReoV — Reovirus

RIG-I — Retinoic Acid-Inducible Gene I

RIPA — Radioimmunoprecipitation Assay Buffer

RPF — Ribosome-Protected Fragment

RPKM — Reads Per Kilobase per Million

RLuc — Renilla Luciferase

RNA — Ribonucleic Acid

RNA-Seq — RNA Sequencing

Ribo-Seq — Ribosome Profiling

RNase I — Ribonuclease I

ROS — Reactive Oxygen Species

RPMI — Roswell Park Memorial Institute Medium

RSV — Respiratory Syncytial Virus

S6K — Ribosomal Protein S6 Kinase

saRNA — Self-Amplifying RNA

SD — Standard Deviation

SDS — Sodium Dodecyl Sulfate

SEM — Standard Error of the Mean

SINV — Sindbis Virus

SL1 — Stem-Loop 1

ssRNA — Single-Stranded RNA

STAT — Signal Transducer and Activator of Transcription

STING — Stimulator of Interferon Genes

SVV — Seneca Valley Virus

TAA — Tumour-Associated Antigen

TAC — Thesis Advisory Committee

TAMs — Tumour-Associated Macrophages

TBS — Tris-Buffered Saline

TE — Translational Efficiency

TGF-β — Transforming Growth Factor Beta

TK — Thymidine Kinase

TLR — Toll-Like Receptor

TME — Tumour Microenvironment

TNF-α — Tumour Necrosis Factor Alpha

TNFAIP3 — Tumour Necrosis Factor Alpha-Induced Protein 3

TOP — Terminal Oligopyrimidine Tract

TPL — Tripartite Leader Sequence

Tregs — Regulatory T Cells

TSC — Tuberous Sclerosis Complex

TSS — Transcription Start Site

TTP — Tristetraprolin

uORF — Upstream Open Reading Frame

UTR — Untranslated Region

UTRGAN — Untranslated Region Generative Adversarial Network

VACV — Vaccinia Virus

VEGF — Vascular Endothelial Growth Factor

Vero — African Green Monkey Kidney Cells

VSV — Vesicular Stomatitis Virus

VSVΔ51 — Vesicular Stomatitis Virus ΔM51 Mutant

VSVΔ51-Luc — Vesicular Stomatitis Virus ΔM51 Expressing Luciferase

WDR4 — WD Repeat Domain 4

ΔΔCt — Delta-Delta Cycle Threshold Method

ΔG — Gibbs Free Energy

ΔR — R-Motif Deletion Variant

1. CHAPTER ONE: GENERAL INTRODUCTION

One of the most successful pathogenic agents in human history is viruses, which have caused numerous world pandemics since the very beginning of the twentieth century. But now, in the age of molecular biology and genetic engineering, viruses have been rediscovered as potent tools to study the underlying biology and treat disease. Viral platforms have now found numerous applications in a wide variety of uses, including lentiviral vectors to deliver genes in a stable manner, adeno-associated viruses to deliver therapeutic genes, and viral vectors to develop vaccines. Of these, oncolytic viruses (OVs) are an especially promising therapeutic approach, where wild-type or engineered viruses selectively infect and kill cancerous cells, and also activate antitumour immune responses.

1.1 Introduction to Oncolytic Virus

1.1.1 A brief history of Oncolytic Viruses

Oncolytic virotherapy itself dates back to the late 1800s and early 1900s on the basis of clinical observations. Patients with myeloid leukemia showed transitory decreases in leukocyte counts, spleen size and lymphadenopathy in acute infections such as influenza-like illnesses, typhoid fever or sepsis[1–3]. Regression of a cervical tumour following administration of an attenuated rabies vaccine was also reported[3,4]. The antitumour effects were, however, temporary and the disease would reoccur after the infection was resolved. The idea of using viruses to treat cancer was more explicitly studied in the mid 20th century (1940s-1960s) where wild-type viruses were used to treat cancer patients. There were attempts to reproduce these effects with viruses like West Nile virus, adenovirus, hepatitis virus and mumps virus[2–4]. In spite of the fact that some tumour reduction was noted, such studies also had serious negative outcomes. One of the key weaknesses was the absence of tumour specificity resulting in encephalitis and hepatitis due to the inability to control viral dose and dissemination. Even with these issues, these initial investigations have confirmed that viruses can directly kill cancer cells via infection and inducing cell death[3,4]. The results also inspired continuous later studies that led to the creation of safer oncolytic viruses during the dawn of genetic engineering. The progress in recombinant DNA technology in the early 1990s made it possible to alter the genetic code of viruses to generate mutants with better tumour selectivity. Herpes simplex virus-1 (HSV-1) was one of the earliest engineered OVs where the thymidine kinase (TK) gene was removed to condition virus replication to rapidly growing cancer

cells and increase tumour selectivity[5]. ONYX-015, an adenovirus deleted of the E1B gene, can selectively replicate in cancer cells that are p53-deficient but not in normal cells and was the first OV to be tested in the clinic [6]. Later developments in OV engineering not only aimed to improve the safety profile, but also the therapeutic potency. In HSV-1 OVs, further tumour selectivity and viral proliferation in cancer cells was enhanced by the deletion of ICP34.5 and ICP47, while therapeutic transgenes such as human granulocyte-macrophage colony-stimulating factor (GM-CSF) was inserted to enhance the capacity of OVs to elicit an anti-tumour immune responses[7]. This led to the development of Talimogene laherparepvec (T-VEC) the first US FDA-approved oncolytic virus to treat cutaneous, subcutaneous, and nodal melanoma in 2015[7]. The oncolytic adenovirus H101 (Oncorine) was approved by the Chinese State Food and Drug Administration in 2005 for the treatment of head and neck cancers[8]. In Japan, the HSV-1–based G47Δ (Delytact), incorporating multiple deletions to enhance tumour selectivity and immune activation, has been approved for the treatment of glioma[9]. Alongside, other genetic manipulations have been involved, such as the insertion of tumour-targeting promoters like human telomerase reverse transcriptase hTERT that facilitate tumour-selective expression of viral genes or therapeutic transgenes[10–12]. All these developments have made oncolytic virotherapy a valid platform of cancer therapy.

1.1.2 Tumour Selectivity of Oncolytic Viruses

A defining feature of OVs is their ability to preferentially infect and replicate within cancer cells while sparing normal tissues. This selectivity arises from several factors:

1. <u>Dysfunction of antiviral pathways</u>

The antiviral state is one of the most sophisticated signaling networks in mammalian cells, involving hundreds to thousands of genes upregulated upon sensing of virus entry and replication within the cells.

Cancer cells commonly have defects in antiviral responses, including pattern recognition receptors (PRRs) and downstream effectors, which promote interferon induction. Pattern recognition receptors (PRRs) detect viral nucleic acids through both endosomal and cytosolic sensors. Endosomal Toll-like receptors (TLRs) recognize viral nucleic acids, including TLR3 (double-stranded RNA), TLR7/8 (single-stranded RNA), and TLR9 (DNA), whereas cytosolic PRRs include RIG-I, MDA5, cGAS, and PKR[13–16]. Cancer cells have defects in these pathways. For example, prostate cancer cells have decreased expression of TLR3 and TLR7, conferring

heightened sensitivity to virus, and cGAS in melanoma is epigenetically shut down, resulting in susceptibility for infection with HSV-1 and vaccinia[13–15]. Likewise, RIG-I signaling is defective in multiple myeloma, glioblastoma, and Ras-transformed cells; loss of downstream signaling pathways leads to increased viral replication[13–15]. Hepatocellular carcinoma exhibits loss of MDA5 expression, impairing IFN-β induction and leading to susceptibility to Sindbis virus[13–15]. STING, an adaptor protein that senses the presence of cytosolic DNA which triggers the production of IFN is commonly lost in colorectal cancer and melanoma[13–15]. In normal cells the cytosolic PRR PKR senses viral dsRNA which phosphorylates eIF2α, leading to shutdown of global translation hence blocking translation of viral proteins[17]. But PKR is often defective in cancers such as leukemias, lung and breast cancers which allow the continuous synthesis of viral proteins[18,19]. Overall failure to establish antiviral state and to detect virus and failure to shut down viral protein translation contribute to efficient oncolytic viruses replication in cancer cells.

Additionally, defects in type I IFN pathways in cancer cells are a major reason for the OV selectivity to cancer cells. Upon viral infection, IFN-α/β is produced and the IFN response is triggered via the IFNAR/JAK/STAT pathway, which in turn induces interferon-stimulated genes (ISGs) which limit viral replication[13,14]. But multiple alterations in this pathway occur in many cancers and prevent the induction of an antiviral state . For instance, loss or silencing of genes involved in IFN signaling is found in gliomas, leukemias and bladder cancer, and downregulated expression of IFN receptors (IFNAR1/2) occurs in hepatocellular, pancreatic, gastric and colorectal cancers enabling viral replication[13,14]. Significantly, cancer cells also frequently have defects in the JAK/STAT pathway, such as reduced expression of STAT1 in lymphomas and leukemias or lack of STAT phosphorylation in prostate cancer, which increase the vulnerability of cancer cells to virus infection[13–15].

2. <u>Oncogenic and tumour suppressor dysregulation</u>

Gain-of-function of oncogenes and loss-of-function of tumour suppressor genes in cancer cells represent another niche that oncolytic viruses exploit to selectively infect and replicate Oncogenic pathways that promote protein synthesis, cell cycle progression, and metabolic activity, including receptor tyrosine kinases (RTKs), epidermal growth factor receptor (EGFR), RAS, phosphoinositide 3-kinase (PI3K)/AKT/mTOR, and MEK/ERK, are frequently activated in cancer. When overactivated, these pathways suppress type I interferon signaling and inhibit PKR

activity, creating conditions that are commonly exploited by viruses to support viral gene expression and replication[20,21]. In parallel, loss of tumour suppressor genes such as p53 and Rb, which normally act as critical barriers to viral replication by inducing cell cycle arrest, apoptosis, and antiviral responses upon infection, allows the virus to replicate more efficiently[15,19,21].

Oncolytic viruses have been engineered to exploit these cancer-specific defects. For example, deletion of ICP34.5 in HSV-1 impairs the ability of the virus to counteract PKR-mediated eIF2α phosphorylation, thereby restricting replication in normal cells while permitting more efficient replication in cancer cells with defective PKR or interferon signaling[22,23]. Similarly, adenoviral vectors such as ONYX-015 (dl1520), which lack the E1B-55K protein, were originally developed to selectively replicate in p53-defective tumour cells, although later studies showed that this selectivity is not explained by p53 mutation alone[24–26]. Vaccinia viruses also preferentially replicate in tumours with activated EGFR/RAS signaling and elevated nucleotide metabolism[27,28]. Thus, engineering viruses to remove their ability to hijack normal cellular growth control mechanisms further restricts replication in healthy cells while enhancing tumour selectivity in cancer cells with pre-existing oncogenic alterations.

3. Overexpression of cell receptor in cancer cells

For a virus to enter cells, it needs to bind to surface receptors. In certain cancers, there is overexpression of specific types of receptors that are leveraged by oncolytic viruses to selectively enter cancer cells. For instance, CD46 (membrane cofactor protein), which is frequently upregulated in cancers such as ovarian, breast, colorectal, and hepatocellular tumours to evade complement-mediated lysis, serves as a primary receptor for the Edmonston strain of the measles virus. Similarly, Nectin-1 and HVEM (herpesvirus entry mediator) are highly expressed in various solid tumours, including melanoma, and act as entry receptors for HSV-1. Other receptors, such as ICAM-1 (CD54) and DAF (CD55), are commonly upregulated in cancers like multiple myeloma and breast cancer, facilitating infection by Coxsackievirus A21. In addition, CD155, also known as the poliovirus receptor, is overexpressed in tumours such as melanoma and glioma, enabling poliovirus targeting. The 67 kDa laminin receptor, which is associated with increased tumour invasion and motility, supports entry of the Sindbis virus. Furthermore, anthrax toxin receptor 1 (ANTXR1) serves as a receptor for Seneca Valley virus (SVV-001), and integrins

(αvβ3, αvβ5, α2β1), which are upregulated in tumour vasculature and certain cancers such as ovarian cancer, facilitate the entry of viruses including adenoviruses.[10,29–32]

4. Metabolic reprogramming and enhanced proliferation

Tumour cells have an increased anabolic environment, with elevated rates of glycolysis and glutamine metabolism and synthesis of nucleotides, lipids and amino acids, all needed for rapid growth. This physiological demand is similar to the needs of viruses for synthesis of genetic material. This creates a metabolically permissive environment for viruses to replicate. In contrast, less metabolically and mitotically active normal cells are less permissive to virus replication. As a result, the metabolic reprograming in cancer cells enables oncolytic viruses to replicate more efficiently than in normal cells[12,33,34]. High glycolysis (the Warburg effect) does not only supply rapid ATP but also supplies metabolic intermediates stimulating the pentose phosphate pathway, which is needed to produce ribose-5-phosphate essential for nucleotide production[35]. Enhanced production of de novo purine and pyrimidine by oncogenic pathways including MYC and RAS, which provide continuous supply of nucleotides required by cancer cells to proliferate and for viral genome replication[36,37]. Numerous tumours are glutamine-addicted, meaning that glutamine is a key carbon and nitrogen source that can be used to fuel the tricarboxylic acid cycle and provide the production and replication of nucleotides and amino acids, which are also essential to viral protein synthesis and proliferation[38,39]. The upregulation of lipid biosynthesis also occurs in cancer cells, which supply crucial membrane building blocks necessary to construct viral replication complexes and, in the case of enveloped viruses, viral assembly[40–42]. Moreover, cancer cells maintain elevated ROS alongside compensatory NADPH-dependent antioxidant responses, creating a balanced stress environment that supports metabolic activity and preserves cell viability, thereby allowing efficient viral replication[43–45]. All these metabolic changes collectively provide a permissive environment that oncolytic viruses can use to gain selective advantage in replicating in cancerous cells over normal tissues.

1.1.3 Mechanism of OV-induced cancer clearance

Another key advantage of OVs lies in their capacity for in situ amplification. Unlike conventional drugs with fixed dosing, OVs replicate within tumour tissue, increasing their local concentration and enabling sustained therapeutic activity. This self-amplifying property enhances efficacy while limiting systemic exposure and associated toxicity[46,47]. Furthermore, viral spread within the

tumour mass allows penetration into regions that are often inaccessible to chemotherapeutics, such as hypoxic or poorly vascularized areas. Beyond direct cytolysis, OVs exert profound immunological effects that distinguish them from traditional cytotoxic therapies. Viral replication within tumour cells leads to immunogenic cell death (ICD), characterized by the release of tumour-associated antigens (TAAs) and damage-associated molecular patterns (DAMPs), including ATP, HMGB1, and calreticulin. These signals promote dendritic cell maturation and antigen presentation, ultimately driving the activation of tumour-specific cytotoxic T lymphocytes. Importantly, this process effectively converts the tumour into an in situ vaccine, enabling systemic antitumour immunity and contributing to the elimination of distant, non-infected lesions[47]. This immune activation is particularly relevant in the context of immunologically "cold" tumours, which are characterized by low T-cell infiltration and poor responsiveness to immune checkpoint inhibitors. OV infection induces local inflammation, cytokine production, and immune cell recruitment, thereby transforming the tumour microenvironment into an immunologically "hot" state[47]. As a result, OVs not only function as direct cytotoxic agents but also as potent immune modulators capable of overcoming tumour-induced immunosuppression.

1.1.4 Arming oncolytic virus: Transgene expression to enhance efficacy and enable novel modalities

On top of promoting tumour clearance, OVs also provide a flexible platform for therapeutic gene delivery. Engineered viruses can be armed with transgenes encoding immune modulators or pro-apoptotic factors, thereby augmenting their antitumour effects. Among the most clinically advanced strategies is the expression of immunostimulatory transgenes, which aim to stimulate and regulate antitumour immune responses. A key example is granulocyte–macrophage colony-stimulating factor (GM-CSF), used in T-VEC and several adenoviral platforms. GM-CSF attracts dendritic cells (DCs) to the tumour site and stimulates their maturation and differentiation, which leads to increased phagocytosis of tumour debris generated by viral oncolysis, thereby improving tumour antigen presentation and enhancing the activation and expansion of tumour-specific CD8+ T cells. Similarly, interleukin-12 (IL-12) is a potent pro-inflammatory cytokine that enhances antigen presentation from lysed tumour cells and helps convert the tumour into a more immunologically "hot" environment. IL-12 induces multiple inflammatory cascades that promote the recruitment and activation of cytotoxic T lymphocytes and natural killer (NK) cells to produce interferon-γ, a key contributor to antitumour immune responses. IL-12 transgene expression has

demonstrated strong antitumour activity in multiple OV platforms in both clinical and preclinical studies[48–50].

Cytotoxic or pro-apoptotic transgenes were also armed in several OV to directly enhance tumour cell killing. For instance, TRAIL (TNF-related apoptosis-inducing ligand) selectively induces apoptosis in cancer cells through activation of death receptors (DR4/DR5), while sparing most normal cells. Another clinically relevant example is FCU1, a suicide gene that converts the non-toxic prodrug 5-fluorocytosine into the chemotherapeutic agent 5-fluorouracil within the tumour, enabling localized chemotherapy and increasing tumour-specific cytotoxicity and reducing systemic toxicity[48–51].

Several DNA and RNA viruses have been developed as oncolytic platforms and are currently being evaluated in clinical trials, including herpes simplex virus, adenovirus, reovirus, vaccinia virus, measles virus, Newcastle disease virus, and vesicular stomatitis virus[12,52–54], summarized in Table 1. Numerous additional viral platforms, including myxoma virus and Sindbis virus (SINV), are currently being investigated in preclinical studies but have not yet advanced to clinical trials.

Oncolytic Virus	Virus Family	Viral Genome Structure	Clinical Status	Cancer Types Tested / Treated	Key References
Talimogene laherparepvec (T-VEC)	Herpesviridae (HSV-1)	dsDNA, enveloped	FDA approved (2015)	Melanoma; trials in breast cancer, sarcoma	[55]
G47Δ HSV-1	Herpesviridae	dsDNA, enveloped	Approved in Japan (2021)	Glioblastoma	[56,57]
Reovirus (Pelareorep)	Reoviridae	dsRNA (segmented), non-enveloped	Phase II–III	Breast cancer, pancreatic cancer, glioma, myeloma	[58,59]
ONCOS-102 (Ad5/3-D24-GM-CSF)	Adenoviridae	dsDNA, non-enveloped	Phase I–II	Solid tumours including mesothelioma and breast cancer (in combination therapies)	[60,61]
Adenovirus (ONYX-015, DNX-2401)	Adenoviridae	dsDNA, non-enveloped	Phase I–III	Glioblastoma, pancreatic cancer,	[62–64]

				ovarian cancer, HNSCC	
Vaccinia virus (Pexa-Vec / JX-594)	Poxviridae	dsDNA, enveloped	Phase II–III	Hepatocellular carcinoma, colorectal cancer	65,66
Newcastle disease virus (NDV)	Paramyxoviridae	ssRNA (-), enveloped	Phase I–II	Glioblastoma, melanoma, colorectal cancer	67,68
Coxsackievirus A21 (CAVATAK)	Picornaviridae	ssRNA (+), non-enveloped	Phase I–II	Melanoma, bladder cancer, NSCLC	69,70
Measles virus (MV-NIS)	Paramyxoviridae	ssRNA (-), enveloped	Phase I–II	Multiple myeloma, ovarian cancer	71–73
Poliovirus (PVSRIPO)	Picornaviridae	ssRNA (+), non-enveloped	Phase I–II	Recurrent glioblastoma	74
Vesicular stomatitis virus (VSV)	Rhabdoviridae	ssRNA (-), enveloped	Phase I	Solid tumours, hepatocellular carcinoma	75,76
Parvovirus H-1 (H-1PV)	Parvoviridae	ssDNA, non-enveloped	Phase I–II	Glioblastoma, pancreatic cancer	77,78
Maraba virus (MG1)	Rhabdoviridae	ssRNA (-), enveloped	Phase I	Solid tumours, breast cancer (vaccine-boost strategy)	79,80
Seneca Valley virus (SVV-001)	Picornaviridae	ssRNA (+), non-enveloped	Phase I–II	Small- cell lung cancer, neuroendocrine tumours	81,82

Table1. 1. Oncolytic Viruses in Clinical Trials

1.2 Challenges of Oncolytic Virus Therapy

Despite significant advances in the design of OVs and clinical development, multiple biological and translational barriers continue to limit their therapeutic efficacy. These challenges span from delivery and biodistribution to antiviral immunity, tumour microenvironment constraints, and insufficient viral replication within tumours. Understanding these limitations is

essential for improving OV-based therapies and optimizing their integration with other treatment modalities.

1.2.1 Delivery and Biodistribution Barriers

Efficient delivery of OVs to tumour sites remains one of the most critical limitations in clinical application. Two primary administration routes are used: intratumoural (i.t.) and intravenous (i.v.) delivery, each associated with distinct challenges. Intratumoural injection enables direct delivery of high viral titers to accessible lesions and reduces systemic clearance; however, it is restricted to localized tumours and is not suitable for metastatic or anatomically inaccessible disease[83]. Additionally, repeated injections carry risks such as bleeding and potential tumour dissemination. In contrast, intravenous delivery allows systemic distribution and targeting of multiple lesions, including metastases, but suffers from significant inefficiencies. Following systemic administration, viral particles are rapidly diluted in circulation, making it difficult to achieve therapeutically effective concentrations at tumour sites[12,83]. Moreover, systemic delivery is associated with premature viral clearance before reaching the tumour, severely limiting efficacy. At the physiological level, multiple barriers impede viral trafficking. OVs must traverse the vascular endothelium and escape into tumour tissue, a process hindered by abnormal tumour vasculature, increased interstitial pressure, and dense extracellular matrix (ECM) components[12,84]. These structural constraints reduce viral penetration and limit uniform distribution within solid tumours. Furthermore, nonspecific sequestration of viral particles by organs such as the liver, spleen, and lungs further reduces the fraction of virus reaching tumour tissue[12,84,85]. Emerging delivery strategies, including cell-based carriers (e.g., mesenchymal stem cells or immune cells) and nanomaterial-based systems, aim to enhance tumour targeting and protect viruses from neutralization. However, these approaches face additional limitations, including reduced viability of carrier cells over time and challenges in clinical translation[12,84–86].

1.2.2 Limitation of Viral Spread Due to Host Antiviral Immunity and Viral Clearance

Although OVs are designed to selectively replicate within tumour cells, achieving sufficient viral amplification in vivo remains challenging. Viral replication is often limited by both intrinsic tumour factors and host responses. For example, incomplete defects in antiviral signaling pathways in some tumour cells can still restrict viral replication, reducing therapeutic efficacy[12,83,84]. Furthermore, the balance between viral attenuation and replication competence is critical. Genetic modifications introduced to improve safety, such as deletion of virulence genes, can inadvertently

reduce viral fitness and limit replication within tumours. Maintaining sufficient oncolytic potency while ensuring safety remains a key challenge in OV design[12,83,84]. In addition, insufficient viral spread within tumours can result in localized infection without complete tumour clearance. This limitation is particularly evident in large or poorly vascularized tumours, where viral dissemination is restricted.

A major obstacle to OV therapy is the rapid activation of host antiviral immune responses, which can significantly limit viral persistence and replication. Both innate and adaptive immune mechanisms contribute to viral clearance. Innate responses include activation of complement pathways, secretion of antiviral cytokines, and rapid recruitment of immune cells such as neutrophils and natural killer (NK) cells[4]. These responses can eliminate viral particles shortly after administration, particularly in systemic delivery settings. Adaptive immunity further complicates OV efficacy through the production of neutralizing antibodies. Many OVs are derived from common human pathogens (e.g., adenovirus or herpes simplex virus), and pre-existing immunity in patients can lead to rapid viral neutralization upon administration[4]. Even in seronegative individuals, rapid seroconversion following initial dosing limits repeated administration and reduces therapeutic benefit. Additionally, circulating blood components such as coagulation factors and complement proteins can bind viral particles, promoting their clearance and preventing tumour targeting[84,85]. Tissue-resident macrophages, particularly in the liver and spleen, also contribute to viral sequestration and degradation[84,85]. Importantly, OV therapy requires a delicate balance between antiviral and antitumour immunity. While antiviral responses limit viral replication, they are also necessary for generating robust antitumour immune responses. Achieving this balance remains a fundamental challenge in optimizing OV therapy[4].

1.2.3 Tumour Microenvironment (TME) Constraints

Even when OVs successfully reach tumour sites, the TME presents substantial barriers to effective viral replication and therapeutic activity. Solid tumours are characterized by an immunosuppressive environment, driven by factors such as transforming growth factor-β (TGF-β), interleukin-10 (IL-10), and arginase-1, which inhibit immune cell activation and function[85,86]. The TME also contains immunosuppressive cell populations, including regulatory T cells (Tregs), myeloid-derived suppressor cells (MDSCs), tumour-associated macrophages (TAMs), and cancer-associated fibroblasts. These cells suppress antiviral and antitumour immune responses, thereby limiting both viral replication and immune-mediated tumour clearance[85,86]. Additionally, physical

characteristics of the TME, including hypoxia, low pH, and abnormal vasculature, further impair OV efficacy. Hypoxic conditions can alter viral replication dynamics and promote resistance to therapy, while the dense ECM restricts viral spread within tumour tissue[85,86]. These factors collectively reduce the ability of OVs to uniformly infect tumour cells and achieve sustained oncolysis. Tumour heterogeneity represents another major limitation. Variability in receptor expression, antiviral signaling pathways, and metabolic states across tumour cell populations leads to inconsistent viral infection and replication, resulting in incomplete tumour eradication[85,86].

1.2.4 Clinical and Translational Challenges

Despite promising preclinical data, the clinical translation of OV therapy has been slower than anticipated. While several OVs have demonstrated safety and tolerability, their efficacy in late-stage clinical trials has been variable and often limited to subsets of patients[12,83,84]. This discrepancy highlights gaps in understanding OV pharmacokinetics, optimal dosing strategies, and patient selection. Regulatory and logistical challenges also contribute to the slow clinical adoption of OVs. As live, replicating agents, OVs require strict safety protocols, including monitoring of viral shedding and potential transmission. Although shedding has been observed in bodily fluids, the risk of transmission remains low under controlled conditions[12]. Additionally, manufacturing complexity, scalability, and standardization of viral products present further barriers to widespread clinical use. The diversity of viral platforms and engineering strategies complicates the establishment of uniform regulatory pathways.

1.2.5 Implications for Translational Control of the Antiviral State in OV Optimization

An important, yet often underappreciated, limitation of OV therapy lies in the dependence of viral replication on host cellular machinery, particularly the translational apparatus. Viral protein synthesis requires efficient engagement of host ribosomes and translation factors. Yet global translation repression is one of the most common host antiviral mechanisms to restrict viral replication via pathways such as PKR activation, eIF2α phosphorylation, and tRNA cleavage. While many tumours exhibit defects in these pathways that favor viral replication, this is not universally the case, and residual translational control mechanisms can limit viral gene expression. Moreover, competition between host and viral mRNAs for the translational machinery, particularly under stress conditions induced by infection, may further restrict viral protein production. These constraints highlight the importance of understanding host–virus interactions at the level of translation, particularly in the context of oncolytic virotherapy. Thus, optimizing OV efficacy may

require not only improving delivery and immune evasion but also enhancing viral access to the host translational machinery. This provides a strong rationale for investigating mechanisms of translational control during viral infection, which will be explored in the following section and constitute the main aims of this PhD thesis.

1.3 OV Delivery Methods

As mentioned earlier OV delivery to the intended site faces many challenges. The main delivery methods for OV currently are: direct (intratumoural) delivery, systemic delivery, and carrier-cell–mediated delivery.

1.3.1 Optimization of local (intratumoural) delivery

Intratumoural injection is a common method for delivery of accessible solid tumours due to the ability to inject high doses of virus directly into the tumour. But one of the key obstacles of this delivery method is limited and uneven viral distribution within the tumour. To address this, various approaches have been used to enhance intratumoural dispersion and penetration. In the clinic, intratumoural agents can be administered through multiple injection tracks or multiple insertion points in the same lesion to enhance distribution, as is the case for talimogene laherparepvec, where the virus is injected along multiple tracks and multiple insertion sites are used for lesions that are larger than the radial spread of the injection[87,88].

In addition to injection strategies, pressure-driven delivery approaches (such as convection-enhanced delivery) have been developed, especially for brain tumours, to improve penetration by generating bulk flow through tissue rather than relying only on passive diffusion[89,90]. At the same time, intratumoural matrix-modifying approaches have been used to eliminate barriers to viral distribution. These include co-delivery or expression of enzymes such as hyaluronidase, which breaks down hyaluronan, or can improve intratumoural diffusion and antitumour effects of oncolytic adenoviruses[91,92]. Other matrix-modifying agents include collagenase or matrix metalloproteinases (MMP-1 and MMP-8) that can modify and de-crosslink collagen-rich extracellular matrix and enhance viral spread[93,94]. These approaches demonstrate that local delivery of OVs is not only concerned with delivery of virus directly into the tumour, but with improving its physical distribution and penetration into the tumour microenvironment.

1.3.2 Optimizing systemic delivery

Intravascular administration of oncolytic viruses is crucial for metastatic cancer; however, this approach is limited by rapid elimination by the immune system, non-specific sequestration and poor tumour delivery. To overcome these limitations, various engineering approaches have been explored to improve viral stability, longevity, and tumour delivery. A key strategy is to mask viruses from the immune system via chemical and material engineering. This includes chemical modifications such as polymer coatings (e.g. polyethylene glycol) and lipid or nanoparticle encapsulation, which can protect viruses from being neutralized by antibodies and complement, allowing for extended circulation and a greater chance of reaching the tumour[95,96]. Another prominent area of development is the enhancement of tumour targeting through biomaterial delivery platforms, such as nanoparticles and virus-material hybrids, which can be used to enable controlled release and improve uptake by tumours. These not only shield the virus in circulation but can also be tailored to respond to tumour-specific environments to enhance delivery effectiveness[96].

Another approach involves genetic modifications to viral surface proteins to decrease immunogenicity and increase tumour cell specificity. Through changes in viral tropism or addition of ligands that bind to tumour-specific receptors, these strategies seek to enhance tumour-specific infection and reduce non-specific interactions. Other approaches include temporary immunomodulation, in which the antiviral immune response is temporarily dampened to prolong virus survival and circulation in the bloodstream[95].

1.4Canonical Cap-Dependent Translation Initiation in Eukaryotic Cells

Protein synthesis in eukaryotic cells occurs through four sequential stages: initiation, elongation, termination, and ribosome recycling. Among these steps, translation initiation represents the primary rate-limiting stage and is therefore the most tightly regulated. In eukaryotic cells, translation of most mRNAs occurs through a 5′ cap-dependent mechanism, in which recognition of the 7-methylguanosine (m^7G) cap structure by the translation initiation machinery directs ribosome recruitment and represents a major point of regulation of protein synthesis. Eukaryotic translation initiation is a highly ordered and regulated process that begins with assembly of the small ribosomal subunit and associated initiation factors. The 40S ribosomal subunit contains two key sites, the A site, which accommodates incoming aminoacyl-tRNAs, and

the P site, which holds the initiator tRNA during the first peptide bond formation. Translation initiation starts with binding of the initiation factors eIF1, eIF1A, eIF3, and eIF5 to the 40S subunit, creating a platform for recruitment of the initiator tRNA. The initiator methionyl-tRNA, which specifically recognizes the AUG start codon, is delivered to the P site by the GTP-bound factor eIF2 as part of the eIF2–GTP–Met-tRNAi ternary complex. Together, the 40S ribosomal subunit, eIF1, eIF1A, eIF3, eIF5, and the ternary complex assemble to form the 43S pre-initiation complex. In parallel, the mRNA is prepared for ribosome loading through recognition of its structural features, including the 5′ 7-methylguanosine cap and the 3′ poly(A) tail. The cap-binding protein eIF4E associates with the 5′ cap and recruits the scaffold protein eIF4G, which in turn interacts with the poly(A)-binding protein (PABP) bound to the 3′ end of the mRNA, promoting mRNA circularization. Secondary structures within the 5′ untranslated region are unwound by the RNA helicase eIF4A, facilitating ribosome access. The 43S pre-initiation complex is then recruited to the capped mRNA to form the 48S complex, which scans along the mRNA in a 5′-to-3′ direction until the AUG start codon is recognized. During this scanning process, accurate start codon selection is influenced not only by the presence of an AUG codon but also by the nucleotide context surrounding it, commonly referred to as the Kozak sequence. Favorable residues, particularly a purine at position −3 and a guanosine at position +4 relative to the AUG, enhance the stability of codon–anticodon interactions and promote efficient initiation. Structural studies have shown that start codon recognition is accompanied by conformational rearrangements within the pre-initiation complex, allowing the initiator tRNA to properly engage the AUG codon and enabling the ribosome to commit to translation initiation. Start codon recognition triggers GTP hydrolysis and release of initiation factors, followed by joining of the 60S ribosomal subunit, a step mediated by eIF5B, to form the translationally competent 80S ribosome. This completes the initiation phase and allows entry into elongation, during which aminoacyl-tRNAs are delivered to the A site by eEF1α and ribosomal translocation is driven by eEF2, until termination is achieved through recognition of a stop codon by the release factor eRF1 and release of the newly synthesized polypeptide.

1.5 Regulatory Pathways Governing Translation Initiation in Mammalian Cells

Translation initiation in mammalian cells is primarily controlled by three interconnected regulatory axes. The first and central axis is the mTORC1–TSC–4EBP1–eIF4F pathway, which is

regulated by growth factors and nutrient availability and determines whether ribosomes can be recruited to capped mRNAs. Under conditions of sufficient nutrients and growth signals, activation of PI3K leads to downstream activation of AKT, which inhibits the TSC1–TSC2 complex. Inhibition of TSC relieves repression on mTORC1, allowing mTORC1 activation and subsequent phosphorylation of the translational repressor 4EBP1. Phosphorylated 4EBP1 releases the cap-binding protein eIF4E, enabling its association with eIF4G and eIF4A to form the eIF4F complex and promote cap-dependent translation. In contrast, under conditions of metabolic stress or nutrient deprivation, activation of AMPK leads to activation of the TSC1–TSC2 complex, resulting in mTORC1 inhibition. In this context, 4EBP1 remains hypophosphorylated, binds eIF4E, prevents eIF4F assembly, and suppresses cap-dependent translation.

A second regulatory axis controlling translation initiation is the MNK–eIF4E pathway, which primarily modulates translational efficiency rather than acting as an on–off switch. Following eIF4F assembly, eIF4G recruits the MNK kinases, MNK1 or MNK2, which phosphorylate eIF4E at Ser209. Although this modification is not essential for translation initiation, it fine-tunes translational output and preferentially enhances translation of specific subsets of mRNAs.

The third axis represents an integrated stress response that shutdown global translation initiation in response to stress conditions, even in the presence of active mTORC1 signaling. Under normal conditions, the heterotrimeric factor eIF2 (composed of α, β, and γ subunits) binds GTP and initiator Met-tRNAi to form the ternary complex, which is required for loading Met-tRNAi onto the 40S ribosomal subunit and formation of the 43S pre-initiation complex. Upon cellular stress, such as double-stranded RNA accumulation, endoplasmic reticulum stress, or nutrient deprivation, stress-activated kinases including PKR, PERK, GCN2, and HRI phosphorylate the eIF2α subunit at Ser51. Phosphorylated eIF2α binds tightly to the guanine nucleotide exchange factor eIF2B, blocking GDP–GTP exchange and preventing formation of the ternary complex. As a result, global translation initiation is rapidly shut down, overriding mTORC1 and eIF4F activity.

1.6 Global Host Translation Shutoff During Viral Infection

Viruses are obligate intracellular parasites that rely entirely on host translational machinery to produce proteins required for replication. A hallmark of many viral infections is host translation shutoff, in which global cellular protein synthesis is suppressed to prioritize viral mRNA

translation. Consequently, a central feature of many viral infections is the reprogramming of host protein synthesis, often resulting in a phenomenon known as host translation shutoff, where global cellular protein synthesis is inhibited to prioritize viral mRNA translation. This process represents a critical aspect of the host–virus arms race: while host cells attempt to restrict viral replication by suppressing translation through innate antiviral pathways such as PKR-mediated phosphorylation of eIF2α, viruses have evolved diverse mechanisms to counteract these defenses and redirect ribosomes toward viral transcripts. As a result, many viruses selectively inhibit host mRNA translation while preserving or enhancing translation of viral mRNAs, thereby ensuring efficient viral protein production during infection[97–99]. For example: HSV-1 suppresses host mRNA translation through multiple mechanisms, including the virion host shutoff (vhs) endoribonuclease, which accelerates host mRNA degradation, and the viral protein ICP27, which disrupts host mRNA splicing and nuclear export while selectively promoting the export and translation of viral transcripts. In addition, HSV-1 infection alters poly(A)-binding protein (PABP) localization, leading to its accumulation in the nucleus and reduced association with eIF4F. This redistribution likely contributes to host translation shutoff, while viral mRNAs appear to retain translational competence despite reduced PABP engagement. Similar to HSV-1, vaccinia virus (VacV) relies on cap-dependent translation but enforces host shutoff through distinct mechanisms. In VacV infection, hyperphosphorylation of 4EBP1 is associated with a reduction in its steady-state protein levels, likely due to proteasome-mediated degradation, thereby maintaining eIF4F activity. VacV also promotes phosphorylation of eIF4E through activation of MNK kinases, and inhibition of MNKs strongly impairs viral replication. In parallel, VacV encodes the viral decapping enzymes D9 and D10, which remove the 5′ m^7G cap from host mRNAs and target them for rapid degradation. In contrast, RNA viruses such as VSV employ a distinct strategy to dominate the host translational landscape by actively suppressing cap-dependent translation through disruption of the eIF4F complex. VSV enhances the association of 4E-BP1 with eIF4E, which limits the availability of eIF4E for interaction with eIF4G, thereby preventing formation of the functional eIF4F complex and reducing host translation initiation[100]. During VSV infection, the viral matrix (M) protein inhibits AKT signaling, leading to reduced mTORC1 activity limiting eIF4F assembly and globally inhibiting cap-dependent translation, which represents the primary mode of translation in mammalian cells. In parallel, the VSV M protein inhibits the mRNA export factor RAE1, blocking nuclear export of host mRNAs and thereby restricting their access to cytoplasmic

ribosomes and favoring viral RNA translation in cytoplasm[97]. In SARS-CoV-2 infection, where the viral nonstructural protein 1 (Nsp1) acts as a potent inhibitor of host protein synthesis. Nsp1 binds directly to the 40S ribosomal subunit and occludes the mRNA entry channel, thereby preventing the loading of host mRNAs onto ribosomes and effectively blocking translation initiation. In addition to this direct inhibition, Nsp1 further reinforces host shutoff by promoting the degradation of cytosolic host mRNAs and impairing their nuclear export, reducing the pool of translatable transcripts available in the cytoplasm[101].

1.7 Host–Virus Interplay in Translational Stress Responses

Viral infection imposes significant stress on the host translational machinery and frequently activates cellular stress-response pathways that regulate protein synthesis. A central component of this response is the integrated stress response (ISR), which modulates translation initiation through phosphorylation of the translation initiation factor eIF2α, leading to global translational repression and the formation of cytoplasmic ribonucleoprotein assemblies known as stress granules (SGs). These structures function as hubs of translational regulation and innate antiviral defense, and many viruses have evolved mechanisms to manipulate or counteract these responses to support their replication[102]. SGs are dynamic, non-membranous cytoplasmic structures composed primarily of stalled pre-initiation complexes, untranslated mRNAs, and numerous RNA-binding proteins[103,104] form in response to a wide range of cellular stresses that impair translation initiation. Classical triggers include oxidative stress[105], heat shock[106], hypoxia[107], amino acid deprivation[108], UV irradiation[109], and endoplasmic reticulum stress[110], many of which activate the integrated stress response and lead to phosphorylation of eIF2α, resulting in translational arrest and SG assembly[111,112]. In addition to environmental stresses, pharmacological inhibition of translation initiation factors, such as eIF4A inhibitors or disruption of cap-dependent translation can also promote SG formation[113,114]. Viral infections are another major stimulus of SG assembly; depending on the virus and stage of infection, SGs may be induced transiently, persist, or be actively suppressed as part of the host–virus interplay. VSV infection activates PKR, leading to phosphorylation of eIF2α and inhibition of translation initiation[115,116]. This translational arrest promotes the accumulation of untranslated mRNAs and the formation of cytoplasmic stress granule (SG)-like structures containing host RNA-binding proteins such as TIA1, TIAR, and PCBP2, together with viral replication proteins and newly synthesized viral RNA. These structures

differ from canonical stress granules and likely represent sites where host stress-response factors interact with viral replication complexes. Consistent with an antiviral role for these components, depletion of TIA1 enhances viral gene expression and VSV replication, suggesting that SG-associated proteins act as restriction factors by sequestering viral components or modulating translation to limit infection[117]. Despite differences in viral replication strategies, several viruses interact with the host translational stress response in similar ways. For example, vaccinia virus (VacV) also engages the PKR–eIF2α pathway during infection. In the absence of the viral dsRNA-binding protein E3L, viral dsRNA activates PKR, resulting in eIF2α phosphorylation and inhibition of translation initiation, which restricts viral protein synthesis. Under these conditions, infected cells assemble SG containing proteins such as G3BP, TIA-1, and USP10, along with RNA molecules that contain a poly(A) tail. These structures form around viral replication factories and are thought to represent a host antiviral response associated with translational arrest and restriction of vaccinia virus replication[118]. HSV provides another example of how viruses manipulate host translational control pathways to support viral gene expression. Similar to many viral infections, HSV infection perturbs cellular stress responses that regulate translation, including pathways centered on phosphorylation of the translation initiation factor eIF2α, a key event that typically leads to translational arrest and can promote SG assembly. However, HSV encodes multiple mechanisms that limit the impact of this antiviral response. For instance, HSV can attenuate ER stress–associated signaling by modulating the PERK–eIF2α pathway, and evidence suggests that the viral glycoprotein B interacts with PERK and contributes to restraining its activation during infection, thereby helping sustain translation as viral protein synthesis increases[119,120]. In addition, HSV encodes the virion host shutoff endoribonuclease vhs (UL41), which remodels the cellular and viral RNA landscape during infection by destabilizing complementary viral transcripts and limiting the accumulation of viral dsRNA, vhs reduces activation of the dsRNA-sensing kinase PKR, thereby preventing excessive eIF2α phosphorylation and helping maintain translation in infected cells[119–122]. HSV further deploys additional factors, including γ134.5 and Us11, which antagonize PKR-mediated translational shutdown and help maintain translation in infected cells[123,124]. Together, these mechanisms illustrate how viruses employs multiple strategies to modulate host translation control pathways, allowing efficient viral protein synthesis while dampening antiviral signaling.

1.8 Viral Strategies to Sustain Translation in Infected Cells

Upon entering cancer cells, viral replication depends on the host translational machinery and therefore competes with host mRNAs for access to ribosomes. At the same time, infection rapidly activates the integrated stress response, resulting in global translation shutoff while promoting the selective translation of antiviral proteins that restrict viral replication[125]. As a result, many viruses have evolved alternative translational strategies that allow them to bypass host translational shutdown and maintain efficient viral protein production[126].

1.8.1 Hijacking Cap-Dependent Translation

The mRNAs of many DNA viruses, including herpes simplex virus type 1 (HSV-1) and vaccinia virus, are structurally similar to host mRNAs in that they contain a 5′ m^7G cap and a 3′ poly(A) tail, and therefore rely primarily on cap-dependent translation. Despite using the host translational machinery, HSV-1 efficiently suppresses host protein synthesis while maintaining robust viral translation. Upon infection, HSV-1 activates the host mTORC1 pathway through its virally encoded serine/threonine kinase US3, which acts as an AKT surrogate to phosphorylate and inhibit the mTOR repressor TSC2. This leads to mTORC1 activation, which drives the hyperphosphorylation of the translational repressor 4EBP1, and allows the release of eIF4E, thereby promoting assembly of the eIF4F complex and enhancing cap-dependent translation. Notably, HSV-1 further facilitates eIF4F assembly through the viral protein ICP6, which binds eIF4G and stabilizes its interaction with eIF4E, indicating that relief of 4EBP1-mediated repression alone is not sufficient for efficient initiation during infection. Similarly, VacV promotes viral translation by redistributing translation initiation factors. During VacV infection, eIF4E and eIF4G are relocalized to cytoplasmic viral replication factories, increasing the local concentration of initiation factors and favoring translation of viral transcripts over host mRNAs.

1.8.2 Cis-Elements Supporting Viral Translation

- Internal Ribosome Entry Sites

Internal ribosome entry sites (IRESs) are structured RNA elements that enable cap-independent initiation of translation by directly recruiting ribosomes to internal positions within an mRNA[127,128]. Unlike the canonical cap-dependent scanning mechanism, IRES-mediated translation allows ribosomes to initiate protein synthesis independently of the 5′ cap structure and, in some cases, with reduced dependence on canonical translation initiation factors[129]. IRES

elements were first discovered in picornaviruses and have since been identified in a wide range of viral RNAs as well as in a subset of cellular mRNAs[130,131]. These elements are typically located within the 5′ untranslated region (5′ UTR) and function through complex RNA secondary and tertiary structures that interact with ribosomal subunits, initiation factors, and additional host proteins known as IRES-transacting factors (ITAFs)[132]. Viral IRESs exhibit substantial diversity in size, sequence composition, and structural organization, and are commonly classified into distinct groups based on their structural features and their requirements for canonical initiation factors[129,132]. This structural and mechanistic diversity allows viruses to maintain efficient protein synthesis even under conditions where host cap-dependent translation is inhibited[97,98,133]. picornaviruses such as poliovirus, in which the viral protease 2Apro cleaves eIF4GI and eIF4GII[134]. This cleavage disrupts the interaction between eIF4E and the ribosome recruitment machinery, thereby shutting down host cap-dependent translation[134]. Importantly, the C-terminal fragment of eIF4G generated after cleavage interacts with poliovirus IRES and recruit ribosomal subunits, enabling continued translation of viral proteins[135].

IRES elements are highly heterogeneous and have been grouped into four major classes based on their conserved RNA architecture and their requirements for canonical initiation factors and ITAFs[132,136,137]. Type I and II IRESs, exemplified by poliovirus and encephalomyocarditis virus, respectively, are large multidomain elements that do not require eIF4E and instead recruit the translation machinery through non-canonical interactions with the central domain of eIF4G, together with eIF4A and IRES-specific ITAFs such as PTB and poly(rC)-binding protein (PCBP2)[138,139]. In contrast, type III IRESs, such as that of hepatitis A virus, display weaker initiation activity and depend on intact eIF4F and additional ITAF support[140,141]. Type IV IRESs, found in hepatitis C virus and pestiviruses, are more compact structured elements that bind directly to the 40S ribosomal subunit and eIF3, position the initiation codon without prior scanning, and can function through either eIF2-dependent or eIF2-independent mechanisms involving eIF5B[142,143]. Even more strikingly, dicistrovirus intergenic region IRESs can assemble translation complexes without canonical initiation factors, initiator tRNA, or even an AUG start codon, using highly compact pseudoknot-rich RNA structures that mimic tRNA-like interactions within the ribosome[144,145]. Importantly, some viral IRESs are partially or completely resistant to inhibition caused by eIF2α phosphorylation, allowing translation to continue under stress conditions in which host cap-dependent protein synthesis is suppressed[146–148].

A notable example of the functional diversity of viral IRES elements is observed in SVV, an oncolytic picornavirus with a structurally unique IRES. Unlike classical picornavirus IRES elements, the SVV IRES exhibits strong structural and functional similarity to HCV- and pestivirus-like (type IV) IRESs, despite belonging to a distinct viral family. The SVV IRES is capable of mediating cap-independent translation independently of key canonical initiation factors, including eIF4A and intact eIF4G, and directly recruits the 40S ribosomal subunit and eIF3. Interestingly, efficient SVV IRES activity requires the presence of downstream viral coding sequences, indicating that translation is regulated by an extended RNA structural context rather than the 5′ UTR alone. Furthermore, structural analyses have demonstrated that higher-order RNA elements, such as pseudoknots within the IRES, are essential for translation, emphasizing the critical role of RNA architecture in controlling viral protein synthesis[149].

Together, these observations highlight that viral IRESs are not a single mechanism, but rather a diverse set of structured RNA elements that enable viral mRNAs to maintain translation under conditions where canonical initiation is compromised.

- RNA structural motifs

RNA structure is a fundamental regulator of translation, controlling how viral mRNAs engage with the host translational machinery. RNA pseudoknots are highly structured RNA elements that play critical roles in regulating viral translation both within and outside IRES[150]. Structurally, pseudoknots are formed when a loop region base-pairs with a complementary sequence elsewhere in the RNA, generating a compact three-dimensional architecture that directly determines its ability to interact with ribosomes and regulate translation[150]. Within IRES elements, pseudoknots contribute to ribosome recruitment and positioning, as exemplified by the HCV IRES, where a pseudoknot located at the base of domain III participates in organizing the RNA structure and facilitating correct placement of the start codon in the ribosomal P site[151]. Beyond IRES-mediated initiation, pseudoknots also regulate translation during elongation and termination. In many viruses, including retroviruses and coronaviruses, pseudoknots located in coding regions stimulate programmed −1 ribosomal frame shifting. Programmed −1 ribosomal frameshifting is a translational recoding mechanism to expand virus coding capacity[152]. In this process, the ribosome shifts backward by one nucleotide during elongation, allowing translation to continue in an alternative reading frame and resulting in the production of a distinct protein from the same

mRNA. This event is directed by two key cis-acting elements: a slippery sequence, typically a heptanucleotide motif that permits realignment of tRNAs, and a downstream RNA pseudoknot structure that stimulates the shift[152]. The pseudoknot plays a critical mechanical role by forming a highly stable three-dimensional structure that resists unwinding by the ribosome's intrinsic helicase activity[153]. As the ribosome translocates along the mRNA and encounters the pseudoknot, it experiences a physical barrier that slows or stalls its movement. This pausing generates tension within the mRNA–tRNA complex, destabilizing codon–anticodon interactions at the slippery sequence and promoting a coordinated backward slippage of the ribosome by one nucleotide[153]. Additionally, pseudoknots positioned downstream of stop codons, such as in murine leukemia virus, promote stop codon readthrough, allowing synthesis of viral polyproteins encoded in the same reading frame but separated by a stop codon (UAG)[154]. Outside direct translation control, pseudoknots in untranslated regions contribute to viral RNA stability, replication, and translation–replication switching, as seen in plant viruses such as turnip yellow mosaic virus, where pseudoknot-containing tRNA-like structures enhance translation and coordinate replication processes[155]. Together, these examples illustrate that pseudoknots function as versatile cis-acting RNA structural motifs that regulate viral translation by influencing ribosome recruitment, pausing, and recoding events such as frameshifting and stop codon readthrough.

Another class of mRNA structural elements has recently been described by Sherlock et al.[156] These conserved viral cis-acting RNA structures, termed reinitiation-stimulating elements (RSEs) or termination upstream ribosome binding sites, promote translation of a downstream open reading frame (ORF) following termination of an upstream ORF through a termination–reinitiation mechanism, rather than de novo initiation. These elements are more widespread than previously appreciated and have been identified in viruses belonging to the *Caliciviridae, Orthomyxoviridae,* and *Rhabdoviridae* families. Mechanistically, RSEs contain a conserved ribosome complementary sequence that base-pairs with 18S rRNA expansion segment 7 in the 40S ribosomal subunit, thereby tethering the viral mRNA to the ribosome after termination. Structural analyses further revealed that the ribosome-bound RNA remains conformationally dynamic, which likely facilitates repositioning of nearby mRNA sequences to allow selection of a downstream start codon for reinitiation[156].

An additional example of cis-acting structural mRNA elements is the presence of Stem-loop structures that regulate translation efficiency and enable selective viral protein synthesis under conditions of host translational suppression. A well-characterized example is the stem-loop 1 (SL1) structure in the 5′ UTR of SARS-CoV-2 RNA. SL1 allows viral mRNAs to be translated despite Nsp1-mediated inhibition by enabling them to access the ribosome under conditions of global host shutoff. Consistently, removal of SL1 blocks viral translation, whereas its insertion is sufficient to restore translation in the presence of Nsp1[101]. HCV, the 5′UTR forms a highly structured RNA containing multiple stem-loops that mediate ribosome recruitment, with specific domains such as IIId and IIIe directly interacting with the 40S ribosomal subunit and domain III binding eIF3[157] . In addition to the IRES, a distinct 5′-proximal stem-loop structure located upstream of the IRES has been shown to modulate translation, as disruption of this structure results in a two- to fivefold reduction in translation efficiency without affecting RNA stability. These findings indicate that stem-loop structures can function beyond canonical IRES elements to fine-tune translation, likely by influencing ribosome accessibility or positioning. Similar regulatory roles for 5′ RNA structures have been described in other positive-strand RNA viruses, including poliovirus and bovine viral diarrhea virus[157]. Similarly, during MeV infection, global protein synthesis is suppressed through eIF2α phosphorylation; however, the viral nucleocapsid (N) mRNA remains efficiently translated. This is mediated by a short stem–loop structure located at the extreme 5′ end of the N mRNA, which recruits the host La/SSB RNA-binding protein and promotes selective ribosome engagement under stress conditions[158]. This mechanism ensures sustained production of the N protein, which is essential for efficient viral genome replication[159]. However, In WNV, a conserved stem-loop structure located within the 3′ UTR functions as a cis-acting element that represses translation. This SL reduces translation efficiency independently of the 5′UTR or cap structure, likely through binding and sequestration of host translation factors such as eEF1α, thereby limiting ribosome access to the viral RNA[160]. Although this appears counterintuitive, such translational repression is thought to play a critical regulatory role in the viral life cycle. Specifically, viral RNAs must balance their use as templates for translation and for replication. Translation is typically favored during early stages of infection to ensure production of viral proteins, whereas later stages require a shift toward genome replication[160]. SINV also contains translation-enhancing cis-acting elements outside the 5′UTR. Repeated stem-loop structures in the 3′UTR were shown to promote translation of both genomic and subgenomic viral

mRNAs specifically in insect cells, with minimal effect in mammalian cells. Mutational disruption of these loop sequences strongly reduced translation without major changes in RNA levels. These elements could also enhance translation of heterologous RNAs, supporting their function as bona fide intrinsic viral RNA motifs that contribute to host-specific translational adaptation[161].

- Upstream open reading frame

Upstream open reading frames (uORFs) are short coding sequences located within the 5′ untranslated region (5′UTR) of an mRNA that regulate translation of the downstream primary coding sequence[162]. During cap-dependent translation initiation, the scanning 43S pre-initiation complex encounters upstream start codons (uAUGs) and may initiate translation at these sites, resulting in production of short peptides and termination upstream of the main open reading frame[163]. The presence of uORFs can influence downstream translation through several mechanisms, including ribosome stalling, premature ribosome dissociation, or reinitiation of translation by the 40S ribosomal subunit following uORF termination[162,163]. In addition, the efficiency of uORF translation is strongly influenced by the sequence context surrounding the start codon, where weak initiation contexts allow ribosomes to bypass upstream start codons through leaky scanning and initiate translation at the downstream AUG[164]. Importantly, upstream initiation is not limited to canonical AUG codons, as non-canonical initiation codons such as CUG, GUG, and UUG can also serve as start sites for uORF translation[165]. Through these mechanisms, uORFs act as cis-regulatory RNA elements that fine-tune translation efficiency and allow dynamic control of protein synthesis in response to cellular conditions[166]. Many viruses exploit these regulatory features to control expression of viral proteins and to expand coding capacity from compact genomes.

Viruses frequently exploit uORFs, uAUGs, overlapping ORFs, and related start-site selection mechanisms such as leaky scanning and reinitiation to regulate translation from compact genomes. In these strategies, ribosomes may either initiate at an upstream start codon, thereby repressing or modulating downstream translation, or bypass a weak uAUG and initiate at a downstream ORF, allowing production of multiple proteins from a single transcript[167]. Across diverse virus families, including retroviruses such as HIV, hepadnaviruses such as HBV, herpesviruses such as HCMV and KSHV, filoviruses such as Ebola virus, coronaviruses and arteriviruses, caliciviruses, orthomyxoviruses, and enteroviruses, uORFs and overlapping ORFs

serve both regulatory and coding functions, fine-tuning viral protein stoichiometry, enabling stress-responsive translation, promoting ribosome shunting or termination-reinitiation, and expanding coding capacity through short peptides encoded in alternative reading frames[98,137]. In some cases, these elements are essential for efficient replication or viral propagation, underscoring that uORFs are not merely passive leader features but bona fide cis-acting regulatory modules in viral gene expression[98,137].

Although functional uORF–mediated translational control has been best characterized in non-oncolytic virus models, ribosome profiling studies have revealed extensive non-canonical translation in VacV, a prototypic poxvirus. In addition to the ~162 previously annotated viral open reading frames, ribosome profiling identified hundreds of previously unannotated translation events, including approximately 596 additional ORFs[168,169]. Many of these newly detected ORFs correspond to short open reading frames such as uORFs located in 5′ untranslated regions, truncated ORFs initiated from alternative start codons, frameshift-derived ORFs, and ORFs encoded within regions previously annotated as non-coding. These findings indicate that vaccinia virus possesses a highly complex translatome and suggest that small ORFs and upstream initiation events may contribute to the regulation of viral gene expression[137]. In addition, some short vaccinia-encoded proteins have well-defined functions during infection. For example, the O3L protein, a 35 amino acid transmembrane peptide incorporated into the viral membrane, is a component of the viral entry/fusion complex and is essential for viral entry, highlighting the functional importance of small viral ORFs in the vaccinia life cycle[170,171].

1.8.3 RNA stability / protection from degradation

In eukaryotic cells, mRNA stability is tightly regulated through coordinated pathways that control RNA turnover and maintain the fidelity of gene expression. Most cellular mRNAs are protected by two key structural features: the 5′ 7-methylguanosine cap and the 3′ poly(A) tail, which protect transcript ends from exonucleolytic degradation and also support efficient gene expression by facilitating mRNA processing, nuclear export, and translation initiation. Degradation of mRNAs generally begins with deadenylation, the shortening of the poly(A) tail by cellular deadenylase complexes, which is often the rate-limiting step in mRNA decay[172]. Once the poly(A) tail is removed, transcripts can be degraded either through 3′–5′ exonucleolytic decay mediated by the exosome or through decapping followed by 5′–3′ degradation by the exonuclease XRN1[172].

In addition to these constitutive decay pathways, eukaryotic cells possess specialized RNA surveillance and antiviral mechanisms that detect and eliminate aberrant or foreign RNAs. For example, nonsense-mediated decay (NMD) targets mRNAs containing premature termination codons or unusually long 3′ untranslated regions, while no-go decay (NGD) eliminates transcripts in which ribosomes stall during translation due to strong secondary structures or other obstacles[173]. Antiviral pathways also contribute to RNA degradation. The interferon-inducible endoribonuclease RNase L is activated by viral double-stranded RNA and cleaves both cellular and viral RNAs, thereby limiting viral replication. Similarly, The zinc-finger antiviral protein (ZAP) recognizes CpG-rich sequence motifs within viral RNAs, promoting their degradation by recruiting RNA decay machinery while also repressing their translation[174–176]. Because both RNA and DNA viruses rely on the host translation machinery in the cytoplasm to synthesize viral proteins, viral transcripts are inherently exposed to these cellular RNA decay and surveillance mechanisms. Consequently, viruses must evolve strategies to avoid detection, stabilize their RNAs, and ensure efficient translation within this hostile environment.

Viruses employ multiple strategies to evade cellular RNA decay pathways and maintain the stability of their transcripts in the cytoplasm. One common mechanism is the acquisition or synthesis of 5′ cap structures that mimic host mRNAs, thereby protecting viral RNAs from exonucleolytic degradation and facilitating translation[177]. Some viruses utilize host capping machinery, whereas others encode their own capping enzymes, as observed in vaccinia virus. In contrast, several negative-strand RNA viruses such as influenza viruses, arenaviruses, and bunyaviruses employ a cap-snatching mechanism in which capped fragments are cleaved from host mRNAs and used to prime viral transcription, simultaneously stabilizing viral RNAs while promoting degradation of host transcripts[178,179]. Other RNA viruses protect the 5′ end of their genomes through alternative mechanisms, such as the covalent attachment of the viral protein VPg in picornaviruses and caliciviruses, which can also promote translation through interactions with cap-binding factors[180,181]. Structural RNA elements further contribute to transcript stability. Highly structured regions within viral untranslated regions can both facilitate translation and limit nuclease accessibility. For example, poliovirus contains a 5′ cloverleaf RNA structure that binds the host poly(rC)-binding protein (PCBP), protecting the uncapped viral RNA from 5′ exonuclease activity and stabilizing viral transcripts within translating polysomes[182,183]. Similarly, IRESs present in several viral 5′UTRs support cap-independent translation while forming structural

barriers that restrict nuclease access. Viruses also evade specialized antiviral RNA decay pathways. Retroviruses such as Moloney murine leukemia virus and Rous sarcoma virus contain RNA elements that prevent recognition by the nonsense-mediated decay (NMD) pathway, while several viruses encode proteins that suppress the RNase L antiviral pathway, including vaccinia virus E3L, influenza virus NS1, and herpes simplex virus (HSV-1) Us11, which bind viral double-stranded RNA and inhibit activation of RNase L[184–186]. In addition, viruses frequently recruit host RNA-binding proteins that promote RNA stability; for instance, HuR and PCBP2 interact with viral untranslated regions in viruses such as hepatitis C virus, alphaviruses, poliovirus, and rabies virus, thereby enhancing viral RNA stability and translation[187,188]. Finally, some viruses directly disrupt host RNA decay machinery. Poliovirus infection induces degradation of several cellular RNA decay factors, including components of the deadenylation and decapping pathways as well as the exonuclease XRN1[189], while flaviviruses such as West Nile virus interfere with stress granule formation by relocalizing RNA-binding proteins to viral replication complexes[190].

Viruses can also modulate host epitranscriptomic pathways to influence RNA stability and gene expression. RNA methylation, particularly N6-methyladenosine (m6A), functions as a dynamic regulatory mark that determines RNA stability, translation, and processing[191]. For example, VSV infection dynamically regulates N6-methyladenosine (m6A) modification, initially increasing and subsequently decreasing m6A levels in host cells, where m6A demethylation by the enzyme ALKBH5 promotes viral replication. Mechanistically, ALKBH5-mediated removal of m6A marks from α-ketoglutarate dehydrogenase mRNA enhances its stability and expression, thereby supporting metabolic pathways, including itaconate metabolism, that are required for efficient viral replication[192]. Collectively, these mechanisms allow viruses to evade cellular RNA surveillance and degradation pathways while maintaining the stability and translational competence of viral transcripts.

1.8.4 Non-Canonical Mechanisms of Viral Translation

Viruses have evolved specialized non-canonical mechanisms to maintain protein synthesis under conditions where canonical translation is inhibited. A distinct but conceptually related strategy is observed in VacV, where late viral mRNAs contain non-templated (i.e., not genome-encoded) 5′ poly(A) leader sequences generated through transcriptional slippage at promoter regions[193]. These poly(A) leaders act as potent translational enhancers and support efficient protein synthesis in infected cells through a noncanonical mechanism that reduces dependence on key

initiation factors such as eIF4F and eIF3, while still allowing ribosome recruitment[194,195]. This process is further facilitated by the viral kinase B1, which phosphorylates the ribosomal protein RACK1 to enhance translation of poly(A) leader-containing mRNAs[196].

VSV utilizes a non-canonical mechanism of translation that relies on cis-acting RNA elements, located outside the coding sequence, and specialized ribosomal components rather than conventional initiation factor–dependent pathways. Despite possessing a 5′ cap and poly(A) tail, VSV mRNA translation remains efficient under conditions that inhibit cap-dependent translation, including eIF4E sequestration and disruption of the eIF4F complex. Instead, efficient translation of VSV transcripts requires the large ribosomal subunit protein rpL40, which is specifically necessary for 80S ribosome assembly on viral mRNAs but dispensable for the translation of most host mRNAs and IRES-mediated translation. Notably, this mechanism is conserved among other non-segmented negative-strand RNA viruses, including MeV and rabies virus[197].

1.8.5 Codon usage and tRNA availability

In addition to mechanisms regulating translation initiation, viruses can modulate translation efficiency at the level of elongation through codon usage and adaptation to host tRNA pools. During elongation, ribosomes decode mRNA codons by incorporating amino acids delivered by cognate aminoacyl-tRNAs, and the rate of elongation is strongly influenced by the availability of these tRNAs as well as by codon identity and local sequence context. Codons corresponding to abundant tRNAs are generally translated more efficiently, whereas rare codons or unfavorable amino acid motifs can slow elongation and induce ribosome pausing or stalling[198,199]. Consequently, codon usage bias often evolves to match the tRNA pool of the host organism[200]. However, viral codon usage does not always fully mirror host preferences. Increasing evidence suggests that viral infection and interferon signaling can dynamically remodel cellular tRNA pools, altering the relative abundance or aminoacylation of specific tRNAs. For example, analysis of influenza A virus evolution revealed that the PB1 gene progressively adapted its codon usage to an interferon-induced tRNA environment, enhancing viral replication in interferon-treated cells[201]. Conversely, several viruses, including human immunodeficiency virus (HIV) and herpes simplex virus (HSV-1), maintain suboptimal codon usage relative to human cells, suggesting that incomplete codon adaptation may help balance translation efficiency, prevent depletion of commonly used tRNAs, and regulate viral gene expression[202–204]. Moreover, viruses can influence

tRNA availability directly, either by encoding their own tRNA genes or by altering cellular tRNA usage within viral replication factories[205].

1.8.6 Virus modification of ribosome composition and function

Viruses can control translation not only through RNA elements or initiation factors but also by modulating the formation of specialized ribosomes. Ribosomes are not static machines; their composition and function can be altered during stress or viral infection to selectively translate specific mRNAs[206]. Unsurprisingly, viruses employ multiple strategies to modulate the formation of specialized ribosomes to inhibit host mRNA translation while redirecting ribosomes toward viral protein synthesis. For instance, in SARS-CoV-2, the viral protein NSP1 binds the 40S ribosomal subunit and inserts its C-terminal domain into the mRNA entry channel, thereby preventing host mRNA accommodation and inhibiting translation initiation[207]. Despite this global inhibition, viral translation is maintained through a cis-acting RNA hairpin (SL1) located in the 5′UTR, which enables viral mRNAs to bypass NSP1-mediated repression and remain competent for ribosome engagement[208]. In addition, SARS-CoV-2 exploits ribosomal proteins such as RPS3, a component of the 40S subunit involved in mRNA binding, scanning, and start codon selection; viral 5′UTR elements depend on RPS3 to promote efficient translation while contributing to host shutoff and mRNA decay[209]. Similarly, the oncolytic SVV utilizes its IRES to directly interact with the ribosomal protein RPL13, thereby facilitating ribosome recruitment and viral protein synthesis[210]. A comparable mechanism is observed in foot-and-mouth disease virus (FMDV), where RPL13 cooperates with the RNA helicase DDX3 to enhance 80S ribosome assembly on viral RNA[210].

Beyond selective recruitment, viral infection can induce ribosome specialization through alterations in ribosome biogenesis and function, leading to heterogeneous ribosomes with distinct translational properties[206]. For example, VacV does not alter ribosome composition but instead modifies ribosomal dynamics, including changes in 40S subunit movement and increased dependence on specific ribosomal proteins such as RACK1 and RPLP2, thereby enabling selective translation of viral mRNAs[209,211]. In contrast, HCV enhances rRNA production and promotes the formation of ribosomes that preferentially support viral translation[211,212]. Newcastle disease virus (NDV), an oncolytic virus, targets the nucleolus through its matrix protein to disrupt ribosome biogenesis and host protein synthesis[213]. Similarly, vesicular VSV inhibits the processing of precursor rRNA, reducing the production of functional ribosomes and contributing to host

translational shutoff while allowing efficient viral mRNA translation[197,214]. In addition to these changes, viruses can remodel ribosome conformation; for example, alphaviruses induce structural rearrangements in 18S rRNA that are required for efficient viral translation[215]. Viruses also reorganize the spatial distribution of the translational machinery, as seen in reoviruses, which form cytoplasmic viral factories that concentrate ribosomes and translation factors at sites of viral replication, thereby enhancing the efficiency of viral protein synthesis[206].

Furthermore, during infection with non-segmented negative-sense RNA viruses such as VSV and measles virus (MeV), viral entry induces ribosome remodeling through incorporation of an additional copy of the ribosomal protein rpL40 into 80S ribosomes at a non-canonical position near the mRNA entry channel. This modification generates specialized ribosomes that preferentially bind viral mRNAs and enhance viral protein synthesis, particularly under conditions where viral transcripts compete with host mRNAs early in infection. Notably, this mechanism does not globally increase translation efficiency but instead promotes selective translation of viral transcripts, thereby improving viral fitness under restrictive host conditions[216].

1.8.7 Viral exploitation of translation initiation factors

Viruses extensively exploit host translation initiation factors to suppress host protein synthesis while promoting selective translation of viral mRNAs. For example, VSV inhibits cap-dependent translation by modulating the mTOR pathway, leading to hypophosphorylation of 4E-BPs, which bind eIF4E and prevent assembly of the eIF4F complex, thereby reducing host translation initiation[100]. In contrast, human cytomegalovirus promotes translation by stabilizing the eIF4F complex through the viral protein pUL69, which directly interacts with eIF4A and prevents sequestration of eIF4E by 4E-BPs, thereby maintaining efficient cap-dependent translation of viral mRNAs[217]. Similarly, influenza virus utilizes eIF4A and eIF4G, but not eIF4E, to support translation of its mRNAs, indicating a non-canonical dependence on specific eIF4F components[218]. In contrast, FMDV encodes a protease (3C) that cleaves eIF4G and targets eIF4A, disrupting host cap-dependent translation while enabling viral RNA translation through IRES-mediated mechanisms[219]. Likewise, Cotesia plutellae bracovirus inhibits host translation by expressing a viral protein (CpBV15β) that sequesters eIF4A, thereby preventing eIF4F assembly and selectively favoring translation of viral mRNAs containing structured 5′UTRs[220]. In contrast, hantavirus bypasses the requirement for canonical initiation factors by encoding the N protein, which functionally replaces eIF4F components, including eIF4E, eIF4G, and eIF4A, thereby enabling

selective translation of viral transcripts[221]. In addition to targeting eIF4F, viruses also modulate the eIF2 pathway, a central regulator of translation initiation. For instance, Sindbis virus (alphavirus) activates GCN2 to induce eIF2α phosphorylation, leading to global inhibition of host translation while permitting selective translation of viral or stress-responsive transcripts[111,215]. Similarly, VSV activates PKR-mediated phosphorylation of eIF2α, contributing to host translational shutoff, although viral replication can still proceed under these restrictive conditions[100,115,197]. Furthermore, viruses such as HSV-1, VacV, and Kaposi's sarcoma-associated herpesvirus exploit MAPK/MNK signaling to regulate phosphorylation of eIF4E, thereby modulating translation initiation in a virus-specific manner and promoting efficient viral replication[222]. Collectively, these observations demonstrate that viruses target multiple nodes of the translation initiation machinery, including eIF4F complex assembly, eIF4A helicase activity, and eIF2-dependent ternary complex formation, to suppress host protein synthesis while ensuring efficient translation of viral mRNAs.

1.9 Study Rationale and Research Objectives

The high therapeutic potential of OVs is hindered by poor delivery and distribution in solid tumours. The most common method of injecting OVs into solid tumours is intratumourally, but this can lead to poor and uneven viral distribution because of physical barriers, such as high interstitial pressure and the abundance of extracellular matrix, which limit the spread of viral particles. This prompts an important question: is it possible to enhance the initial spread and penetration of OVs into tumour sites? To answer this question, the first chapter of this thesis examines the potential of needle-free injection (NFI) as an alternative delivery platform, as it is expected to improve the intratumoural distribution of virus particles by injecting with high pressure, without compromising the integrity and therapeutic efficacy of the virus.

Beyond oncolytic delivery, the therapeutic potential of OVs also relies on effective expression of transgenes encoding for factors that augment immune responses against the tumour. On the other hand, viral infection dramatically remodels host protein translational machinery, resulting in inadequate protein expression of these therapeutic transgenes, despite high levels of transcription. This raised a second question: is it possible to manipulate transgene translation to enhance therapeutic expression? The second chapter addresses this by exploring whether incorporation of viral 5′ leader sequences can enhance transgene mRNA translation within infected cells. The

rationale is that transgene design has largely focused on transcriptional control, while adaptation to the virus-specific translational environment remains underexplored, potentially limiting the effectiveness of current OV platforms.

Finally, little is known about how the host controls translation during OV infection to restrict viral replication and impact therapeutic success. Infection results in a global suppression of protein synthesis, but translation of a subset of mRNAs is spared through an undetermined mechanism, suggesting selective translation occurs. This raises the question in the third chapter: what translation mechanisms regulate selective translation during oncolytic virus infection and how do they affect viral growth? To this end, the third chapter maps the translational response during infection with the MG1 Maraba virus in glioblastoma cells, anticipating that the identification of cis-acting elements and host factors governing translation during an antiviral response will yield mechanistic insights, and unveil strategies to improve oncolytic virus-based therapies.

1.10 References

1. Dock, G. THE INFLUENCE OF COMPLICATING DISEASES UPON LEUKAEMIA.: Cases of Tuberculosis and Leukoemia. Miscellaneous Infections. Changes in the Red Blood Corpuscles. Qualitative Changes in the Blood, Especially in the Leukocytes. When Does the Change Occur? The Effects of Various Processes Other than Infection on Leukoemia. BIBLIOGRAPHY. *Am. J. Med. Sci. 1827-1924* 127, 563 (1904).
2. Pelner, L., Fowler, G. A. & Nauts, H. C. Effect of Concurrent Infections and Their Toxins on the Course of Leukemia. *Acta Med. Scand.* 162, 5–24 (1958).
3. PhD, Y. W. Milestone: The origins of oncolytic viral therapy. *Drug Discovery News* https://www.drugdiscoverynews.com/milestone-the-origins-of-oncolytic-viral-therapy-15984.
4. Javier, R. T. & Butel, J. S. The History of Tumour Virology. *Cancer Res.* 68, 7693–7706 (2008).
5. Zhou, M. & Shen, Z. Advanced progress in the genetic modification of the oncolytic HSV-1 virus. *Front. Oncol.* 14, 1525940 (2025).
6. Rothmann, T., Hengstermann, A., Whitaker, N. J., Scheffner, M. & zur Hausen, H. Replication of ONYX-015, a Potential Anticancer Adenovirus, Is Independent of p53 Status in Tumour Cells. *J. Virol.* 72, 9470–9478 (1998).
7. Talimogene Laherparepvec - an overview | ScienceDirect Topics. https://www.sciencedirect.com/topics/biochemistry-genetics-and-molecular-biology/talimogene-laherparepvec.
8. Larson, C. *et al.* Going viral: a review of replication-selective oncolytic adenoviruses. *Oncotarget* 6, 19976–19989 (2015).
9. Frontiers | Advances in immunotherapy for glioblastoma multiforme. https://www.frontiersin.org/journals/immunology/articles/10.3389/fimmu.2022.944452/full.
10. Yan, Z. *et al.* Enhancing cancer therapy: the integration of oncolytic virus therapy with diverse treatments. *Cancer Cell Int.* 24, 242 (2024).
11. Li, Y., Duan, H.-Y., Yang, K. & Ye, J.-F. Advancements and challenges in oncolytic virus therapy for gastrointestinal tumours. *Biomed. Pharmacother. Biomedecine Pharmacother.* 168, 115627 (2023).

12. Xiao, D. *et al.* Oncolytic viruses: advanced strategies in cancer therapy. *Signal Transduct. Target. Ther.* 11, 45 (2026).
13. Matveeva, O. V. & Chumakov, P. M. Defects in interferon pathways as potential biomarkers of sensitivity to oncolytic viruses. *Rev. Med. Virol.* 28, e2008 (2018).
14. Chen, C. *et al.* Oncolytic Virotherapy in Solid Tumours: A Current Review. *Biodrugs* 39, 857–876 (2025).
15. Chadwick, T. B., So, J., Hertzog, P. J., Haynes, N. M. & Parker, B. S. Striking the right balance with type I interferon signalling in cancer. *Nat. Rev. Cancer* 1–24 (2026) doi:10.1038/s41568-026-00915-1.
16. Chen, R. *et al.* Pattern recognition receptors: function, regulation and therapeutic potential. *Signal Transduct. Target. Ther.* 10, 216 (2025).
17. Lemaire, P. A., Anderson, E., Lary, J. & Cole, J. L. Mechanism of PKR Activation by dsRNA. *J. Mol. Biol.* 381, 351–360 (2008).
18. Watanabe, T., Imamura, T. & Hiasa, Y. Roles of protein kinase R in cancer: Potential as a therapeutic target. *Cancer Sci.* 109, 919–925 (2018).
19. Prestwich, R. J. *et al.* Oncolytic Viruses: Do They Have a Role in Anti-Cancer Therapy? *Clin. Med. Oncol.* 2, 83–96 (2008).
20. Fernandes, J. Oncogenes: The Passport for Viral Oncolysis Through PKR Inhibition. *Biomark. Cancer* 8, 101–110 (2016).
21. Lin, D., Shen, Y. & Liang, T. Oncolytic virotherapy: basic principles, recent advances and future directions. *Signal Transduct. Target. Ther.* 8, 156 (2023).
22. Li, Y. *et al.* ICP34.5 Protein of Herpes Simplex Virus Facilitates the Initiation of Protein Translation by Bridging Eukaryotic Initiation Factor 2α (eIF2α) and Protein Phosphatase 1. *J. Biol. Chem.* 286, 24785–24792 (2011).
23. Wylie, K. M., Schrimpf, J. E. & Morrison, L. A. Increased eIF2α Phosphorylation Attenuates Replication of Herpes Simplex Virus 2 vhs Mutants in Mouse Embryonic Fibroblasts and Correlates with Reduced Accumulation of the PKR Antagonist ICP34.5. *J. Virol.* 83, 9151–9162 (2009).
24. O'Shea, C. C. *et al.* Late viral RNA export, rather than p53 inactivation, determines ONYX-015 tumour selectivity. *Cancer Cell* 6, 611–623 (2004).

25. Heise, C. *et al.* ONYX-015, an E1B gene-attenuated adenovirus, causes tumour-specific cytolysis and antitumoural efficacy that can be augmented by standard chemotherapeutic agents. *Nat. Med.* 3, 639–645 (1997).
26. Bischoff, J. R. *et al.* An Adenovirus Mutant That Replicates Selectively in p53- Deficient Human Tumour Cells. *Science* 274, 373–376 (1996).
27. Guo, Z. S., Thorne, S. H. & Bartlett, D. L. Oncolytic Virotherapy: Molecular Targets in Tumour-Selective Replication and Carrier Cell-Mediated Delivery of Oncolytic Viruses. *Biochim. Biophys. Acta* 1785, 217–231 (2008).
28. Parato, K. A. *et al.* The Oncolytic Poxvirus JX-594 Selectively Replicates in and Destroys Cancer Cells Driven by Genetic Pathways Commonly Activated in Cancers. *Mol. Ther.* 20, 749–758 (2012).
29. Liszewski, M. K. & Atkinson, J. P. The multiverse of CD46 and oncologic interactions. *J. Clin. Invest.* 135, e188355.
30. Kaufman, H. L., Kohlhapp, F. J. & Zloza, A. Oncolytic viruses: a new class of immunotherapy drugs. *Nat. Rev. Drug Discov.* 14, 642–662 (2015).
31. Schwertner, B. *et al.* Nectin-1 Expression Correlates with the Susceptibility of Malignant Melanoma to Oncolytic Herpes Simplex Virus In Vitro and In Vivo. *Cancers* 13, 3058 (2021).
32. Bradley, S. *et al.* Applications of coxsackievirus A21 in oncology. *Oncolytic Virotherapy* 3, 47–55 (2014).
33. Mullen, P. J. & Christofk, H. R. The Metabolic Relationship Between Viral Infection and Cancer. *Annu. Rev. Cancer Biol.* 6, 1–15 (2022).
34. Ehrlich, M. & Bacharach, E. Oncolytic Virotherapy: The Cancer Cell Side. *Cancers* 13, 939 (2021).
35. Liberti, M. V. & Locasale, J. W. The Warburg Effect: How Does it Benefit Cancer Cells? *Trends Biochem. Sci.* 41, 211–218 (2016).
36. Liu, Y.-C. *et al.* Global Regulation of Nucleotide Biosynthetic Genes by c-Myc. *PLoS ONE* 3, e2722 (2008).
37. Dang, C. V. MYC on the Path to Cancer. *Cell* 149, 22–35 (2012).
38. Altman, B. J., Stine, Z. E. & Dang, C. V. From Krebs to clinic: glutamine metabolism to cancer therapy. *Nat. Rev. Cancer* 16, 619–634 (2016).

39. Li, X. *et al.* Glutamine addiction in tumour cell: oncogene regulation and clinical treatment. *Cell Commun. Signal. CCS* 22, 12 (2024).
40. Schoggins, J. W. & Randall, G. Lipids in Innate Antiviral Defense. *Cell Host Microbe* 14, 379–385 (2013).
41. Heaton, N. S. & Randall, G. Multifaceted roles for lipids in viral infection. *Trends Microbiol.* 19, 368–375 (2011).
42. Heaton, N. S. & Randall, G. Dengue virus-induced autophagy regulates lipid metabolism. *Cell Host Microbe* 8, 422–432 (2010).
43. Akter, S. *et al.* Reactive oxygen species (ROS) in cancer: from mechanism to therapeutic implications. *Signal Transduct. Target. Ther.* 11, 111 (2026).
44. Foo, J., Bellot, G., Pervaiz, S. & Alonso, S. Mitochondria-mediated oxidative stress during viral infection. *Trends Microbiol.* 30, 679–692 (2022).
45. Kayesh, M. E. H., Kohara, M. & Tsukiyama-Kohara, K. Effects of oxidative stress on viral infections: an overview. *Npj Viruses* 3, 27 (2025).
46. Zhang, S. & Rabkin, S. D. THE DISCOVERY AND DEVELOPMENT OF ONCOLYTIC VIRUSES: ARE THEY THE FUTURE OF CANCER IMMUNOTHERAPY? *Expert Opin. Drug Discov.* 16, 391–410 (2021).
47. Zhang, J., Chen, J. & Lin, K. Immunogenic cell death-based oncolytic virus therapy: A sharp sword of tumour immunotherapy. *Eur. J. Pharmacol.* 981, 176913 (2024).
48. Pérez-Domínguez, F., Quezada-Monrás, C., Cárcamo, L., Muñoz, J. P. & Carrillo-Beltrán, D. Oncolytic Viruses as a Novel Therapeutic Approach for Colorectal Cancer: Mechanisms, Current Advances, and Future Directions. *Cancers* 17, 1854 (2025).
49. de Graaf, J. F., de Vor, L., Fouchier, R. A. M. & van den Hoogen, B. G. Armed oncolytic viruses: A kick-start for anti-tumour immunity. *Cytokine Growth Factor Rev.* 41, 28–39 (2018).
50. Sampath, P. & Thorne, S. H. Arming viruses in multi-mechanistic oncolytic viral therapy: current research and future developments, with emphasis on poxviruses. *Oncolytic Virotherapy* 3, 1–9 (2013).
51. Thoidingjam, S. *et al.* Oncolytic virus-based suicide gene therapy for cancer treatment: a perspective of the clinical trials conducted at Henry Ford Health. *Transl. Med. Commun.* 8, 11 (2023).

52. Alemayehu, Y. A. & Getahun, Y. A. HARNESSING THE POWER OF ONCOLYTIC VIRUSES FOR ADVANCING CANCER THERAPY. *Cancer Treat. Res. Commun.* 101170 (2026) doi:10.1016/j.ctarc.2026.101170.
53. Li, Y., Qin, X., Liang, C. & Wang, L. Progress in the research and development of oncolytic virus therapies. *Front. Pharmacol.* 17, 1751206.
54. Fukuhara, H., Ino, Y. & Todo, T. Oncolytic virus therapy: A new era of cancer treatment at dawn. *Cancer Sci.* 107, 1373–1379 (2016).
55. Pol, J., Kroemer, G. & Galluzzi, L. First oncolytic virus approved for melanoma immunotherapy. *Oncoimmunology* 5, e1115641 (2015).
56. Todo, T. *et al.* Intratumoural oncolytic herpes virus G47Δ for residual or recurrent glioblastoma: a phase 2 trial. *Nat. Med.* 28, 1630–1639 (2022).
57. Todo, T., Ino, Y., Ohtsu, H., Shibahara, J. & Tanaka, M. A phase I/II study of triple-mutated oncolytic herpes virus G47Δ in patients with progressive glioblastoma. *Nat. Commun.* 13, 4119 (2022).
58. Noonan, A. M. *et al.* Randomized Phase 2 Trial of the Oncolytic Virus Pelareorep (Reolysin) in Upfront Treatment of Metastatic Pancreatic Adenocarcinoma. *Mol. Ther. J. Am. Soc. Gene Ther.* 24, 1150–1158 (2016).
59. Jonathan. Oncolytics Biotech's® Pelareorep Selected for Inclusion in Precision PromiseSM Pivotal Phase 3 Platform Trial | Oncolytics Biotech Inc. https://oncolyticsbiotech.com/press_releases/oncolytics-biotechs-pelareorep-selected-for-inclusion-in-precision-promisesm-pivotal-phase-3-platform-trial/ (2023).
60. Kuryk, L. *et al.* Antitumour-specific T-cell responses induced by oncolytic adenovirus ONCOS-102 (AdV5/3-D24-GM-CSF) in peritoneal mesothelioma mouse model. *J. Med. Virol.* 90, 1669–1673 (2018).
61. Ranki, T. *et al.* Phase I study with ONCOS-102 for the treatment of solid tumours – an evaluation of clinical response and exploratory analyses of immune markers. *J. Immunother. Cancer* 4, (2016).
62. Nemunaitis, J. *et al.* Phase II Trial of Intratumoural Administration of ONYX-015, a Replication-Selective Adenovirus, in Patients With Refractory Head and Neck Cancer. *J. Clin. Oncol.* 19, 289–298 (2001).

63. Lang, F. F. *et al.* Phase I Study of DNX-2401 (Delta-24-RGD) Oncolytic Adenovirus: Replication and Immunotherapeutic Effects in Recurrent Malignant Glioma. *J. Clin. Oncol.* 36, 1419–1427 (2018).
64. Fukuhara, H., Ino, Y. & Todo, T. Oncolytic virus therapy: A new era of cancer treatment at dawn. *Cancer Sci.* 107, 1373–1379 (2016).
65. Breitbach, C. J., Moon, A., Burke, J., Hwang, T.-H. & Kirn, D. H. A Phase 2, Open-Label, Randomized Study of Pexa-Vec (JX-594) Administered by Intratumoural Injection in Patients with Unresectable Primary Hepatocellular Carcinoma. *Methods Mol. Biol.* 1317, 343–357 (2015).
66. Xu, L., Sun, H., Lemoine, N. R., Xuan, Y. & Wang, P. Oncolytic vaccinia virus and cancer immunotherapy. *Front. Immunol.* 14, 1324744 (2024).
67. ReuvenOr. *Clinical Application of Intravenous New Castle Disease Virus - HUJ Oncolytic Virus in the Treatment of Advanced Glioblastoma Multiforme, Soft and Bone Sarcomas and Neuroblastoma Patients, Resistant to Conventional Anti- Cancer Modalities*. https://clinicaltrials.gov/study/NCT01174537 (2015).
68. Freeman, A. I. *et al.* Phase I/II trial of intravenous NDV-HUJ oncolytic virus in recurrent glioblastoma multiforme. *Mol. Ther. J. Am. Soc. Gene Ther.* 13, 221–228 (2006).
69. Annels, N. E. *et al.* Phase I Trial of an ICAM-1-Targeted Immunotherapeutic-Coxsackievirus A21 (CVA21) as an Oncolytic Agent Against Non Muscle-Invasive Bladder Cancer. *Clin. Cancer Res. Off. J. Am. Assoc. Cancer Res.* 25, 5818–5831 (2019).
70. Andtbacka, R. H. *et al.* Phase II calm extension study: Coxsackievirus A21 delivered intratumourally to patients with advanced melanoma induces immune-cell infiltration in the tumour microenvironment. *J. Immunother. Cancer* 3, P343 (2015).
71. Packiriswamy, N. *et al.* Oncolytic measles virus therapy enhances tumour antigen-specific T-cell responses in patients with multiple myeloma. *Leukemia* 34, 3310–3322 (2020).
72. Russell, S. J. *et al.* Remission of disseminated cancer after systemic oncolytic virotherapy. *Mayo Clin. Proc.* 89, 926–933 (2014).
73. Dispenzieri, A. *et al.* Phase I trial of systemic administration of Edmonston strain of measles virus genetically engineered to express the sodium iodide symporter in patients with recurrent or refractory multiple myeloma. *Leukemia* 31, 2791–2798 (2017).

74. Desjardins, A. *et al.* Recurrent Glioblastoma Treated with Recombinant Poliovirus. *N. Engl. J. Med.* 379, 150–161 (2018).
75. Smith, K. E. R. *et al.* A phase I oncolytic virus trial with vesicular stomatitis virus expressing human interferon beta and tyrosinase related protein 1 administered intratumourally and intravenously in uveal melanoma: safety, efficacy, and T cell responses. *Front. Immunol.* 14, 1279387 (2023).
76. Lichty, B. D., Breitbach, C. J., Stojdl, D. F. & Bell, J. C. Going viral with cancer immunotherapy. *Nat. Rev. Cancer* 14, 559–567 (2014).
77. Hajda, J. *et al.* Phase 2 Trial of Oncolytic H-1 Parvovirus Therapy Shows Safety and Signs of Immune System Activation in Patients With Metastatic Pancreatic Ductal Adenocarcinoma. *Clin. Cancer Res. Off. J. Am. Assoc. Cancer Res.* 27, 5546–5556 (2021).
78. Geletneky, K. & Rommelaere, J. Oncolytic parvovirus for cancer of the brain: are we approaching human trials? *Future Neurol.* 5, 783–785 (2010).
79. Breitbach, C. J. Considerations for Clinical Translation of MG1 Maraba Virus. *Methods Mol. Biol.* 2058, 285–293 (2020).
80. Jonker, D. J. *et al.* Phase I study of oncolytic virus (OV) MG1 maraba/MAGE-A3 (MG1MA3), with and without transgenic MAGE-A3 adenovirus vaccine (AdMA3) in incurable advanced/metastatic MAGE-A3-expressing solid tumours: CCTG IND.214. *J. Clin. Oncol.* 35, e14637–e14637 (2017).
81. Rudin, C. M. *et al.* Phase I Clinical Study of Seneca Valley Virus (SVV-001), a Replication-Competent Picornavirus, in Advanced Solid Tumours with Neuroendocrine Features. *Clin. Cancer Res. Off. J. Am. Assoc. Cancer Res.* 17, 888–895 (2011).
82. Schenk, E. L. *et al.* A randomized double-blind phase II study of the Seneca Valley Virus (NTX-010) vs placebo for patients with extensive stage SCLC (ES-SCLC) who were stable or responding after at least 4 cycles of platinum-based chemotherapy: NCCTG (Alliance) N0923 Study. *J. Thorac. Oncol. Off. Publ. Int. Assoc. Study Lung Cancer* 15, 110–119 (2020).
83. Ferguson, M. S., Lemoine, N. R. & Wang, Y. Systemic Delivery of Oncolytic Viruses: Hopes and Hurdles. *Adv. Virol.* 2012, 805629 (2012).
84. Shalhout, S. Z., Miller, D. M., Emerick, K. S. & Kaufman, H. L. Therapy with oncolytic viruses: progress and challenges. *Nat. Rev. Clin. Oncol.* 20, 160–177 (2023).

85. Zheng, M., Huang, J., Tong, A. & Yang, H. Oncolytic Viruses for Cancer Therapy: Barriers and Recent Advances. *Mol. Ther. - Oncolytics* 15, 234–247 (2019).
86. Appleton, E., Chiocca, E. A., Ungerechts, G., Melcher, A. & Vile, R. Oncolytic viruses as anticancer agents: clinical progress and remaining challenges. *The Lancet* 406, 1295–1312 (2025).
87. Imlygic, INN-talimogene laherparepvec.
88. Prot_SAP_000.pdf.
89. Palacios-Alonso, D. *et al.* Toxicity and Biodistribution of the Oncolytic Virus VCN-01 Following Intracranial Injection in Syrian Hamsters. *Hum. Gene Ther.* 36, 1237–1247 (2025).
90. Eissa, I. R. *et al.* The Current Status and Future Prospects of Oncolytic Viruses in Clinical Trials against Melanoma, Glioma, Pancreatic, and Breast Cancers. *Cancers* 10, (2018).
91. Guedan, S. *et al.* Hyaluronidase Expression by an Oncolytic Adenovirus Enhances Its Intratumoural Spread and Suppresses Tumour Growth. *Mol. Ther.* 18, 1275–1283 (2010).
92. Ganesh, S., Gonzalez-Edick, M., Gibbons, D., Van Roey, M. & Jooss, K. Intratumoural coadministration of hyaluronidase enzyme and oncolytic adenoviruses enhances virus potency in metastatic tumour models. *Clin. Cancer Res. Off. J. Am. Assoc. Cancer Res.* 14, 3933–3941 (2008).
93. Dolor, A. & Szoka, F. C. Digesting a path forward – the utility of collagenase tumour treatment for improved drug delivery. *Mol. Pharm.* 15, 2069–2083 (2018).
94. Mok, W., Boucher, Y. & Jain, R. K. Matrix Metalloproteinases-1 and -8 Improve the Distribution and Efficacy of an Oncolytic Virus. *Cancer Res.* 67, 10664–10668 (2007).
95. Xia, Y., Li, D., Yang, K. & Ou, X. Systemic Delivery Strategies for Oncolytic Viruses: Advancing Targeted and Efficient Tumour Therapy. *Int. J. Mol. Sci.* 26, 6900 (2025).
96. Zhu, J., Ma, J., Huang, M., Deng, H. & Shi, G. Emerging delivery strategy for oncolytic virotherapy. *Mol. Ther. Oncol.* 32, 200809 (2024).
97. Walsh, D. & Mohr, I. Viral subversion of the host protein synthesis machinery. *Nat. Rev. Microbiol.* 9, 860–875 (2011).
98. Stern-Ginossar, N., Thompson, S. R., Mathews, M. B. & Mohr, I. Translational Control in Virus-Infected Cells. *Cold Spring Harb. Perspect. Biol.* 11, a033001 (2019).
99. Liu, Y. *et al.* The role of host eIF2α in viral infection. *Virol. J.* 17, 112 (2020).

100. Connor, J. H. & Lyles, D. S. Vesicular stomatitis virus infection alters the eIF4F translation initiation complex and causes dephosphorylation of the eIF4E binding protein 4E-BP1. *J. Virol.* 76, 10177–10187 (2002).
101. Vora, S. M. *et al.* Targeting stem-loop 1 of the SARS-CoV-2 5' UTR to suppress viral translation and Nsp1 evasion. *Proc. Natl. Acad. Sci. U. S. A.* 119, e2117198119 (2022).
102. Wu, Y., Zhang, Z., Li, Y. & Li, Y. The Regulation of Integrated Stress Response Signaling Pathway on Viral Infection and Viral Antagonism. *Front. Microbiol.* 12, 814635 (2022).
103. Stress granules, RNA-binding proteins and polyglutamine diseases: too much aggregation? | Cell Death & Disease. https://www.nature.com/articles/s41419-021-03873-8.
104. Desai, M., Gulati, K., Agrawal, M., Ghumra, S. & Sahoo, P. K. Stress granules: Guardians of cellular health and triggers of disease. *Neural Regen. Res.* 21, 588–597 (2025).
105. Frontiers | Oxidative stress-induced stress granules: a central link to protein aggregation in neurodegenerative diseases. https://www.frontiersin.org/journals/neuroscience/articles/10.3389/fnins.2025.1686571/full.
106. Verma, A., Sumi, S. & Seervi, M. Heat shock proteins-driven stress granule dynamics: yet another avenue for cell survival. *Apoptosis Int. J. Program. Cell Death* 26, 371–384 (2021).
107. Li, S. *et al.* Aggregation of Stress Granules Induced by Hypoxia and Lipopolysaccharide via PKR-p-eIF2α Pathway and 4EBP1 Pathway Inhibits the Inflammatory Response in Peri-Implantitis. *J. Inflamm. Res.* 18, 10533–10544 (2025).
108. Reineke, L. C., Cheema, S. A., Dubrulle, J. & Neilson, J. R. Chronic starvation induces noncanonical pro-death stress granules. *J. Cell Sci.* 131, jcs220244 (2018).
109. Cabral, A. J., Costello, D. C. & Farny, N. G. The enigma of ultraviolet radiation stress granules: Research challenges and new perspectives. *Front. Mol. Biosci.* 9, 1066650 (2022).
110. Pincus, D. & Oakes, S. A. Unfolding emergency calls stress granules to the ER. *Nat. Cell Biol.* 26, 845–846 (2024).
111. Importance of eIF2α Phosphorylation and Stress Granule Assembly in Alphavirus Translation Regulation | Molecular Biology of the Cell. https://www.molbiolcell.org/doi/full/10.1091/mbc.e05-02-0124.
112. Mir, D. A., Ma, Z., Horrocks, J. & Rogers, A. Stress-Induced Eukaryotic Translational Regulatory Mechanisms. *J. Clin. Med. Sci.* 8, 1000277 (2024).

113. Low, W.-K. *et al.* Inhibition of Eukaryotic Translation Initiation by the Marine Natural Product Pateamine A. *Mol. Cell* 20, 709–722 (2005).
114. Slaine, P. D., Kleer, M., Smith, N. K., Khaperskyy, D. A. & McCormick, C. Stress Granule-Inducing Eukaryotic Translation Initiation Factor 4A Inhibitors Block Influenza A Virus Replication. *Viruses* 9, 388 (2017).
115. Baltzis, D. *et al.* Resistance to Vesicular Stomatitis Virus Infection Requires a Functional Cross Talk between the Eukaryotic Translation Initiation Factor 2α Kinases PERK and PKR. *J. Virol.* 78, 12747–12761 (2004).
116. Balachandran, S. *et al.* Essential Role for the dsRNA-Dependent Protein Kinase PKR in Innate Immunity to Viral Infection. *Immunity* 13, 129–141 (2000).
117. Dinh, P. X. *et al.* Induction of Stress Granule-Like Structures in Vesicular Stomatitis Virus-Infected Cells. *J. Virol.* 87, 372–383 (2013).
118. Simpson-Holley, M. *et al.* Formation of Antiviral Cytoplasmic Granules during Orthopoxvirus Infection. *J. Virol.* 85, 1581–1593 (2011).
119. Mulvey, M., Arias, C. & Mohr, I. Maintenance of Endoplasmic Reticulum (ER) Homeostasis in Herpes Simplex Virus Type 1-Infected Cells through the Association of a Viral Glycoprotein with PERK, a Cellular ER Stress Sensor. *J. Virol.* 81, 3377–3390 (2007).
120. Cheng, G., Feng, Z. & He, B. Herpes Simplex Virus 1 Infection Activates the Endoplasmic Reticulum Resident Kinase PERK and Mediates eIF-2α Dephosphorylation by the γ134.5 Protein. *J. Virol.* 79, 1379–1388 (2005).
121. Ma, H., Yin, R. & Ren, L. Recent advances on herpesvirus unique long protein 41. *Anim. Zoonoses* https://doi.org/10.1016/j.azn.2025.12.002 (2025) doi:10.1016/j.azn.2025.12.002.
122. Dauber, B., Saffran, H. A. & Smiley, J. R. The herpes simplex virus host shutoff (vhs) RNase limits accumulation of double stranded RNA in infected cells: Evidence for accelerated decay of duplex RNA. *PLoS Pathog.* 15, e1008111 (2019).
123. He, B., Gross, M. & Roizman, B. The γ134.5 protein of herpes simplex virus 1 complexes with protein phosphatase 1α to dephosphorylate the α subunit of the eukaryotic translation initiation factor 2 and preclude the shutoff of protein synthesis by double-stranded RNA-activated protein kinase. *Proc. Natl. Acad. Sci. U. S. A.* 94, 843–848 (1997).
124. Cassady, K. A., Gross, M. & Roizman, B. The herpes simplex virus US11 protein effectively compensates for the gamma1(34.5) gene if present before activation of protein kinase R by

precluding its phosphorylation and that of the alpha subunit of eukaryotic translation initiation factor 2. *J. Virol.* 72, 8620–8626 (1998).

125. Rozman, B., Fisher, T. & Stern-Ginossar, N. Translation—A tug of war during viral infection. *Mol. Cell* 83, 481–495 (2023).
126. Connor, J. H. & Lyles, D. S. Inhibition of host and viral translation during vesicular stomatitis virus infection. eIF2 is responsible for the inhibition of viral but not host translation. *J. Biol. Chem.* 280, 13512–13519 (2005).
127. Jackson, R. J., Hellen, C. U. T. & Pestova, T. V. The mechanism of eukaryotic translation initiation and principles of its regulation. *Nat. Rev. Mol. Cell Biol.* 11, 113–127 (2010).
128. Hellen, C. U. & Sarnow, P. Internal ribosome entry sites in eukaryotic mRNA molecules. *Genes Dev.* 15, 1593–1612 (2001).
129. Yamamoto, H., Unbehaun, A. & Spahn, C. M. T. Ribosomal Chamber Music: Toward an Understanding of IRES Mechanisms. *Trends Biochem. Sci.* 42, 655–668 (2017).
130. Jang, S. K. *et al.* A segment of the 5' nontranslated region of encephalomyocarditis virus RNA directs internal entry of ribosomes during in vitro translation. *J. Virol.* 62, 2636–2643 (1988).
131. Pelletier, J. & Sonenberg, N. Internal initiation of translation of eukaryotic mRNA directed by a sequence derived from poliovirus RNA. *Nature* 334, 320–325 (1988).
132. Lozano, G. & Martínez-Salas, E. Structural insights into viral IRES-dependent translation mechanisms. *Curr. Opin. Virol.* 12, 113–120 (2015).
133. Khan, D. & Fox, P. L. Host-like RNA Elements Regulate Virus Translation. *Viruses* 16, (2024).
134. Kempf, B. J. & Barton, D. J. Poliovirus 2APro Increases Viral mRNA and Polysome Stability Coordinately in Time with Cleavage of eIF4G. *J. Virol.* 82, 5847–5859 (2008).
135. Ohlmann, T., Rau, M., Pain, V. M. & Morley, S. J. The C-terminal domain of eukaryotic protein synthesis initiation factor (eIF) 4G is sufficient to support cap-independent translation in the absence of eIF4E. *EMBO J.* 15, 1371–1382 (1996).
136. Arhab, Y., Bulakhov, A. G., Pestova, T. V. & Hellen, C. U. T. Dissemination of Internal Ribosomal Entry Sites (IRES) Between Viruses by Horizontal Gene Transfer. *Viruses* 12, 612 (2020).

137. Khan, D. & Fox, P. L. Host-like RNA Elements Regulate Virus Translation. *Viruses* 16, (2024).
138. Abdullah, S. W., Wu, J., Wang, X., Guo, H. & Sun, S. Advances and Breakthroughs in IRES-Directed Translation and Replication of Picornaviruses. *mBio* 14, e00358-23.
139. de Breyne, S., Yu, Y., Unbehaun, A., Pestova, T. V. & Hellen, C. U. T. Direct functional interaction of initiation factor eIF4G with type 1 internal ribosomal entry sites. *Proc. Natl. Acad. Sci. U. S. A.* 106, 9197–9202 (2009).
140. Ali, I. K., McKendrick, L., Morley, S. J. & Jackson, R. J. Activity of the hepatitis A virus IRES requires association between the cap-binding translation initiation factor (eIF4E) and eIF4G. *J. Virol.* 75, 7854–7863 (2001).
141. Sadahiro, A. *et al.* Translation of Hepatitis A Virus IRES Is Upregulated by a Hepatic Cell-Specific Factor. *Front. Genet.* 9, 307 (2018).
142. Segar, K. E., Sherlock, M. E. & Kieft, J. S. Distribution and structural diversity of Type IV internal ribosome entry sites. 2025.05.12.653553 Preprint at https://doi.org/10.1101/2025.05.12.653553 (2025).
143. Li, Y. *et al.* Structure and function of type IV IRES in picornaviruses: a systematic review. *Front. Microbiol.* 15, (2024).
144. Thompson, S. R. Tricks an IRES uses to enslave ribosomes. *Trends Microbiol.* 20, 558–566 (2012).
145. Kieft, J. S. Comparing the three-dimensional structures of Dicistroviridae IGR IRES RNAs with other viral RNA structures. *Virus Res.* 139, 148–156 (2009).
146. González-Almela, E., Williams, H., Sanz, M. A. & Carrasco, L. The Initiation Factors eIF2, eIF2A, eIF2D, eIF4A, and eIF4G Are Not Involved in Translation Driven by Hepatitis C Virus IRES in Human Cells. *Front. Microbiol.* 9, (2018).
147. Hanson, P. *et al.* IRES-Dependent Translational Control during Virus-Induced Endoplasmic Reticulum Stress and Apoptosis. *Front. Microbiol.* 3, (2012).
148. Lancaster, A. M., Jan, E. & Sarnow, P. Initiation factor-independent translation mediated by the hepatitis C virus internal ribosome entry site. *RNA* 12, 894–902 (2006).
149. Willcocks, M. M. *et al.* Structural Features of the Seneca Valley Virus Internal Ribosome Entry Site (IRES) Element: a Picornavirus with a Pestivirus-Like IRES ▿ . *J. Virol.* 85, 4452–4461 (2011).

150. Brierley, I., Pennell, S. & Gilbert, R. J. C. Viral RNA pseudoknots: versatile motifs in gene expression and replication. *Nat. Rev. Microbiol.* 5, 598–610 (2007).
151. Berry, K. E., Waghray, S. & Doudna, J. A. The HCV IRES pseudoknot positions the initiation codon on the 40S ribosomal subunit. *RNA* 16, 1559–1569 (2010).
152. Brierley, I., Gilbert, R. J. C. & Pennell, S. Pseudoknot-Dependent Programmed —1 Ribosomal Frameshifting: Structures, Mechanisms and Models. *Recoding Expans. Decod. Rules Enriches Gene Expr.* 24, 149–174 (2009).
153. Namy, O., Moran, S. J., Stuart, D. I., Gilbert, R. J. C. & Brierley, I. A mechanical explanation of RNA pseudoknot function in programmed ribosomal frameshifting. *Nature* 441, 244–247 (2006).
154. Wills, N. M., Gesteland, R. F. & Atkins, J. F. Pseudoknot-dependent read-through of retroviral gag termination codons: importance of sequences in the spacer and loop 2. *EMBO J.* 13, 4137–4144 (1994).
155. Pettit Kneller, E. L., Rakotondrafara, A. M. & Miller, W. A. Cap-independent translation of plant viral RNAs. *Virus Res.* 119, 63–75 (2006).
156. Sherlock, M. E., Langeberg, C. J., Segar, K. E. & Kieft, J. S. A conserved class of viral RNA structures regulates translation reinitiation through dynamic ribosome interactions. *Cell Rep.* 44, (2025).
157. Luo, G., Xin, S. & Cai, Z. Role of the 5′-Proximal Stem-Loop Structure of the 5′ Untranslated Region in Replication and Translation of Hepatitis C Virus RNA. *J. Virol.* 77, 3312–3318 (2003).
158. Inoue, Y. *et al.* Selective Translation of the Measles Virus Nucleocapsid mRNA by La Protein. *Front. Microbiol.* 2, (2011).
159. Fields Virology 6th Edition. https://www.wolterskluwer.com/en/solutions/ovid/fields-virology-6th-edition-15514.
160. Li, W. & Brinton, M. A. The 3′ Stem Loop of the West Nile Virus Genomic RNA Can Suppress Translation of Chimeric mRNAs. *Virology* 287, 49–61 (2001).
161. Garcia-Moreno, M., Sanz, M. A. & Carrasco, L. A Viral mRNA Motif at the 3′-Untranslated Region that Confers Translatability in a Cell-Specific Manner. Implications for Virus Evolution. *Sci. Rep.* 6, 19217 (2016).

162. Morris, D. R. & Geballe, A. P. Upstream Open Reading Frames as Regulators of mRNA Translation. *Mol. Cell. Biol.* 20, 8635–8642 (2000).
163. Upstream Open Reading Frame - an overview | ScienceDirect Topics. https://www.sciencedirect.com/topics/agricultural-and-biological-sciences/upstream-open-reading-frame.
164. Dever, T. E., Ivanov, I. P. & Hinnebusch, A. G. Translational regulation by uORFs and start codon selection stringency. *Genes Dev.* 37, 474–489 (2023).
165. Kearse, M. G. & Wilusz, J. E. Non-AUG translation: a new start for protein synthesis in eukaryotes. *Genes Dev.* 31, 1717–1731 (2017).
166. Zhong, Z., Li, Y., Sun, Q. & Chen, D. Tiny but mighty: Diverse functions of uORFs that regulate gene expression. *Comput. Struct. Biotechnol. J.* 23, 3771–3779 (2024).
167. Jaafar, Z. A. & Kieft, J. S. Viral RNA structure-based strategies to manipulate translation. *Nat. Rev. Microbiol.* 17, 110 (2019).
168. Dai, A. *et al.* Ribosome Profiling Reveals Translational Upregulation of Cellular Oxidative Phosphorylation mRNAs during Vaccinia Virus-Induced Host Shutoff. *J. Virol.* 91, e01858-16 (2017).
169. Yang, Z. *et al.* Deciphering Poxvirus Gene Expression by RNA Sequencing and Ribosome Profiling. *J. Virol.* 89, 6874–6886 (2015).
170. Satheshkumar, P. S. & Moss, B. Characterization of a newly identified 35-amino-acid component of the vaccinia virus entry/fusion complex conserved in all chordopoxviruses. *J. Virol.* 83, 12822–12832 (2009).
171. Satheshkumar, P. S., Chavre, J. & Moss, B. Role of the vaccinia virus O3 protein in cell entry can be fulfilled by its Sequence flexible transmembrane domain. *Virology* 444, 148–157 (2013).
172. Dowdle, M. E. & Lykke-Andersen, J. Cytoplasmic mRNA Decay and Quality Control Machineries in Eukaryotes. *Nat. Rev. Genet.* 26, 463–478 (2025).
173. Shoemaker, C. J. & Green, R. Translation drives mRNA quality control. *Nat. Struct. Mol. Biol.* 19, 594–601 (2012).
174. Nchioua, R. *et al.* Host ZAP activity correlates with the levels of CpG suppression in primate lentiviruses. *Proc. Natl. Acad. Sci. U. S. A.* 122, e2419489122.

175. Shao, R., Visser, I., Fros, J. J. & Yin, X. Versatility of the Zinc-Finger Antiviral Protein (ZAP) As a Modulator of Viral Infections. *Int. J. Biol. Sci.* 20, 4585–4600 (2024).
176. Gokhale, N. S., Smith, J. R., Van Gelder, R. D. & Savan, R. RNA regulatory mechanisms that control antiviral innate immunity. *Immunol. Rev.* 304, 77–96 (2021).
177. Decroly, E., Ferron, F., Lescar, J. & Canard, B. Conventional and unconventional mechanisms for capping viral mRNA. *Nat. Rev. Microbiol.* 10, 51–65 (2012).
178. Ho, J. S. Y., Zhu, Z. & Marazzi, I. Unconventional viral gene expression mechanisms as therapeutic targets. *Nature* 593, 362–371 (2021).
179. Structural snapshots of phenuivirus cap-snatching and transcription | Nucleic Acids Research | Oxford Academic. https://academic.oup.com/nar/article/52/10/6049/7665631.
180. Goodfellow, I. The genome-linked protein VPg of vertebrate viruses - a multifaceted protein. *Curr. Opin. Virol.* 1, 355–362 (2011).
181. Genome Composition, Organization, and Expression. https://www.sciencedirect.com/science/chapter/monograph/pii/B9780123848710000066 doi:10.1016/B978-0-12-384871-0.00006-6.
182. Kempf, B. J. & Barton, D. J. Poly(rC) Binding Proteins and the 5′ Cloverleaf of Uncapped Poliovirus mRNA Function during De Novo Assembly of Polysomes. *J. Virol.* 82, 5835–5846 (2008).
183. Murray, K. E., Roberts, A. W. & Barton, D. J. Poly(rC) binding proteins mediate poliovirus mRNA stability. *RNA* 7, 1126–1141 (2001).
184. Drappier, M. & Michiels, T. Inhibition of the OAS/RNase L pathway by viruses. *Curr. Opin. Virol.* 15, 19–26 (2015).
185. Bryant, K. F. *et al.* Binding of herpes simplex virus-1 US11 to specific RNA sequences. *Nucleic Acids Res.* 33, 6090–6100 (2005).
186. Charron, A. J., Ward, S. L., North, B. J., Ceron, S. & Leib, D. A. The US11 Gene of Herpes Simplex Virus 1 Promotes Neuroinvasion and Periocular Replication following Corneal Infection. *J. Virol.* 93, e02246-18 (2019).
187. Narayanan, K. & Makino, S. Interplay between viruses and host mRNA degradation. *Biochim. Biophys. Acta Gene Regul. Mech.* 1829, 732–741 (2013).
188. Wang, L., Jeng, K.-S. & Lai, M. M. C. Poly(C)-Binding Protein 2 Interacts with Sequences Required for Viral Replication in the Hepatitis C Virus (HCV) 5′ Untranslated Region and

Directs HCV RNA Replication through Circularizing the Viral Genome ▿. *J. Virol.* 85, 7954–7964 (2011).

189. Ullmer, W. & Semler, B. L. Diverse Strategies Used by Picornaviruses to Escape Host RNA Decay Pathways. *Viruses* 8, 335 (2016).
190. Interaction of TIA-1/TIAR with West Nile and dengue virus products in infected cells interferes with stress granule formation and processing body assembly | PNAS. https://www.pnas.org/doi/10.1073/pnas.0703348104.
191. Hoang, H.-D., Neault, S., Pelin, A. & Alain, T. Emerging translation strategies during virus–host interaction. *WIREs RNA* 12, e1619 (2021).
192. Liu, Y. *et al.* N 6-methyladenosine RNA modification-mediated cellular metabolism rewiring inhibits viral replication. *Science* 365, 1171–1176 (2019).
193. Yang, Z., Bruno, D. P., Martens, C. A., Porcella, S. F. & Moss, B. Genome-Wide Analysis of the 5′ and 3′ Ends of Vaccinia Virus Early mRNAs Delineates Regulatory Sequences of Annotated and Anomalous Transcripts. *J. Virol.* 85, 5897–5909 (2011).
194. Shirokikh, N. E. & Spirin, A. S. Poly(A) leader of eukaryotic mRNA bypasses the dependence of translation on initiation factors. *Proc. Natl. Acad. Sci. U. S. A.* 105, 10738–10743 (2008).
195. Dhungel, P., Cao, S. & Yang, Z. The 5'-poly(A) leader of poxvirus mRNA confers a translational advantage that can be achieved in cells with impaired cap-dependent translation. *PLoS Pathog.* 13, e1006602 (2017).
196. Jha, S. *et al.* Trans-kingdom mimicry underlies ribosome customization by a poxvirus kinase. *Nature* 546, 651–655 (2017).
197. Lee, A. S.-Y., Burdeinick-Kerr, R. & Whelan, S. P. J. A ribosome-specialized translation initiation pathway is required for cap-dependent translation of vesicular stomatitis virus mRNAs. *Proc. Natl. Acad. Sci. U. S. A.* 110, 324–329 (2013).
198. Gardin, J. *et al.* Measurement of average decoding rates of the 61 sense codons in vivo. *eLife* 3, e03735 (2014).
199. Martin, S. *et al.* Oligodendrocyte differentiation alters tRNA modifications and codon optimality-mediated mRNA decay. *Nat. Commun.* 13, 5003 (2022).
200. Gingold, H. & Pilpel, Y. Determinants of translation efficiency and accuracy. *Mol. Syst. Biol.* 7, MSB201114 (2011).

201. Smith, B. L., Chen, G., Wilke, C. O. & Krug, R. M. Avian Influenza Virus PB1 Gene in H3N2 Viruses Evolved in Humans To Reduce Interferon Inhibition by Skewing Codon Usage toward Interferon-Altered tRNA Pools. *mBio* 9, e01222-18 (2018).
202. Bradel-Tretheway, B. G., Zhen, Z. & Dewhurst, S. Effects of codon-optimization on protein expression by the human herpesvirus 6 and 7 U51 open reading frame. *J. Virol. Methods* 111, 145–156 (2003).
203. Schachtel, G. A., Bucher, P., Mocarski, E. S., Blaisdell, B. E. & Karlin, S. Evidence for selective evolution in codon usage in conserved amino acid segments of human alphaherpesvirus proteins. *J. Mol. Evol.* 33, 483–494 (1991).
204. Ngumbela, K. C. *et al.* Quantitative Effect of Suboptimal Codon Usage on Translational Efficiency of mRNA Encoding HIV-1 gag in Intact T Cells. *PLoS ONE* 3, e2356 (2008).
205. Sirihongthong, T. & Auewarakul, P. Viral codon usage and the virus-host interactions. *Front. Microbiol.* 16, 1711603.
206. Wang, X., Zhu, J., Zhang, D. & Liu, G. Ribosomal control in RNA virus-infected cells. *Front. Microbiol.* 13, (2022).
207. Schubert, K. *et al.* SARS-CoV-2 Nsp1 binds the ribosomal mRNA channel to inhibit translation. *Nat. Struct. Mol. Biol.* 27, 959–966 (2020).
208. Tidu, A. *et al.* The viral protein NSP1 acts as a ribosome gatekeeper for shutting down host translation and fostering SARS-CoV-2 translation. *RNA* 27, 253–264 (2021).
209. Havkin-Solomon, T. *et al.* Selective translational control of cellular and viral mRNAs by RPS3 mRNA binding. *Nucleic Acids Res.* 51, 4208–4222 (2023).
210. Han, S. *et al.* Ribosomal Protein L13 Promotes IRES-Driven Translation of Foot-and-Mouth Disease Virus in a Helicase DDX3-Dependent Manner. *J. Virol.* 94, e01679-19 (2020).
211. Khalatyan, N. *et al.* Ribosome customization and functional diversification among P-stalk proteins regulate late poxvirus protein synthesis. *Cell Rep.* 44, 115119 (2025).
212. Raychaudhuri, S., Fontanes, V., Barat, B. & Dasgupta, A. Activation of Ribosomal RNA Transcription by Hepatitis C Virus Involves Upstream Binding Factor Phosphorylation Via Induction of Cyclin D1. *Cancer Res.* 69, 2057–2064 (2009).
213. Duan, Z. *et al.* The nucleolar phosphoprotein B23 targets Newcastle disease virus matrix protein to the nucleoli and facilitates viral replication. *Virology* 452–453, 212–222 (2014).

214. Zan, M., Evans, P. & Lucas-Lnard, J. The inhibition of mouse L-cell 45 S ribosomal RNA processing is a highly uv-Resistant property of vesicular stomatitis virus. *Virology* 177, 75–84 (1990).
215. Toribio, R., Díaz-López, I., Boskovic, J. & Ventoso, I. An RNA trapping mechanism in Alphavirus mRNA promotes ribosome stalling and translation initiation. *Nucleic Acids Res.* 44, 4368–4380 (2016).
216. Tsai, H.-Y. *et al.* Ribosome remodeling drives translation adaptation during viral infection and cellular stress. *bioRxiv* 2025.10.24.684008 (2025) doi:10.1101/2025.10.24.684008.
217. Aoyagi, M., Gaspar, M. & Shenk, T. E. Human cytomegalovirus UL69 protein facilitates translation by associating with the mRNA cap-binding complex and excluding 4EBP1. *Proc. Natl. Acad. Sci.* 107, 2640–2645 (2010).
218. Yángüez, E., Rodriguez, P., Goodfellow, I. & Nieto, A. Influenza virus polymerase confers independence of the cellular cap-binding factor eIF4E for viral mRNA translation. *Virology* 422, 297–307 (2012).
219. Belsham, G. J., McInerney, G. M. & Ross-Smith, N. Foot-and-mouth disease virus 3C protease induces cleavage of translation initiation factors eIF4A and eIF4G within infected cells. *J. Virol.* 74, 272–280 (2000).
220. Surakasi, V. P., Nalini, M. & Kim, Y. Host translational control of a polydnavirus, Cotesia plutellae bracovirus, by sequestering host eIF4A to prevent formation of a translation initiation complex. *Insect Mol. Biol.* 20, 609–618 (2011).
221. Mir, M. A. & Panganiban, A. T. A protein that replaces the entire cellular eIF4F complex. *EMBO J.* 27, 3129–3139 (2008).
222. Hoang, H.-D., Graber, T. E. & Alain, T. Battling for Ribosomes: Translational Control at the Forefront of the Antiviral Response. *J. Mol. Biol.* 430, 1965–1992 (2018).

2. CHAPTER TWO: HIGH-PRESSURE DELIVERY OF ONCOLYTIC VIRUSES VIA NEEDLE-FREE INJECTION PRESERVES THERAPEUTIC ACTIVITY

Authors: Aida Said, Huy-Dung Hoang, Nathalie Earl, Xiao Xiang, Nadeem Siddiqui, Marceline Côté, and Tommy Alain

Status: Published 2023

Cancers

DOI: 10.3390/cancers15235655

2.1 Author contribution

A.S. (Aida Said) led the study and was primarily responsible for the experimental design, data generation, formal analysis, and manuscript preparation. A.S., H.-D.H., and T.A. contributed to the investigation and interpretation of the results. Resources were provided by X.X., N.S., T.A., and M.C. Data curation was performed by A.S., with contributions from N.S. and N.E. The manuscript was written by A.S. and subsequently reviewed and edited with input from all co-authors. Project administration and supervision were provided by M.C. and T.A., and funding for the study was secured by T.A. All authors reviewed and approved the final version of the manuscript.

2.2 Simple Summary

We explored the use of needle-free injection (NFI) technology to deliver oncolytic viruses (OVs) for treating solid tumours. The study assesses the infectivity of OVs following NFI and compares the effectiveness of intratumoural administration of Vesicular Stomatitis Virus (VSV) to that of traditional needle injection (NI) in subcutaneous tumours in mice. NFI improves viral tissue distribution and preserves therapeutic activity of this virotherapy. The study establishes NFI as an efficient delivery method for OVs and underscores the need for further optimization to enhance therapeutic efficacy.

2.3 Abstract

Intratumoural delivery of oncolytic viruses (OVs) to solid tumours is currently performed multiple percutaneous methods of needle injections (NI). In this study, we investigated the use of a novel delivery approach, needle-free injection (NFI), to administer OVs to subcutaneous tumours. The stability and genetic integrity of several RNA and DNA viruses exposed to high-pressure jet injectors were first evaluated in vitro. We demonstrate that replication competence and infectivity of the viruses remained unchanged after NFI, as compared to traditional NI. Using the oncolytic Vesicular Stomatitis Virus expressing luciferase (VSVD51-Luc) in the syngeneic CT26 subcutaneous tumour model, we show that NFI administration not only successfully delivers infectious particles but also increases the dissemination of the virus within the tumour tissues when compared to NI. Furthermore, mice treated with VSVD51-Luc by NFI delivery showed similar reduction in tumour growth and survival compared to those with needle-administered virus. These results indicate that NFI represents a novel approach to administer and potentially increase the spread of OVs within accessible solid tumours, highlighting its usefulness in virotherapy.

Keywords: needle-free injection; oncolytic virus; tumour; immunotherapy

2.4 Introduction

Oncolytic viruses (OVs) represent a promising immunotherapeutic approach to cancer treatment. OVs selectively replicate in cancer cells while sparing normal cells [1]. This selective infection can mediate tumour regression by directly lysing cancer cells, as well as exposing tumour-associated antigens and triggering host antitumour immune response [2,3,4]. However, several challenges must be overcome to maximize OV infections of solid tumours, including physical barriers, immune restrictions against the virus, immunosuppressive tumour microenvironment and tumour heterogeneity [3].

The initial hurdles in achieving sufficient infection lie in the physical barriers and elevated interstitial pressure of solid tumours. These factors restrict the distribution of oncolytic viruses (OVs) and contribute to suboptimal deliveries, diminishing the spread of OVs within the tumour tissue. Consequently, this limitation hampers the overall therapeutic efficacy of the treatment [5]. Intratumoural injection by needle, which elicits fewer side effects than other administration methods, is the most commonly used route of administration for superficial, accessible, solid tumours [6,7]. However, the extracellular matrix of solid tumours can often prevent the diffusion of OV-containing fluid throughout the tumour [5,8,9,10]. To circumvent this limitation, current intratumoural OV delivery uses non-traditional needles such as multipronged needles to increase fluid penetration [11], and combines chemical [12,13] or viral bioengineering [14,15] approaches, for instance, OVs expressing ECM-degrading enzymes [15,16,17], to help promote viral spread within the tumour tissues. Developing novel OV delivery methods that maximize initial viral spread is another avenue to consider for improving the therapeutic efficacy of oncolytic viral immunotherapies.

Needle-free injection (NFI) technology is a method to deliver medications without the need of a needle or syringe. In NFI, the therapeutic agent is delivered via a high-pressure, narrow jet stream of liquid that penetrates the skin and reaches into subcutaneous or intramuscular layers. The original purpose of NFI technology was to provide a more user-friendly and pain-free alternative to needle injection systems. This technology is currently being used to deliver effectively a variety of therapeutic agents, including insulin, other hormones, antibiotics, and vaccines; it has been shown to induce potent immunogenicity in the case of the vaccines [18,19,20,21,22]. NFI was also reported to result in better diffusion of the injected liquids

compared to traditional needle injection in subcutaneous tumour [19,20], which could represent an added benefit for OV distribution.

In this study, we assessed the efficacy of first-generation NFI technology in delivering OVs to subcutaneous tumours. We first examined in vitro the replication competence of the oncolytic RNA viruses Vesicular Stomatitis Virus (VSVΔ51-GFP), Measles Virus (MeV-GFP) and Reovirus (ReoV), as well as the oncolytic DNA viruses Herpes Simplex Virus-1 (HSV1-GFP) and Vaccinia virus (VACV-GFP), when exposed to the high-pressure jet stream of needle-free injector system. All viruses subjected to NFI were found to infect and replicate to similar levels as compared to viruses delivered via traditional needle injection. We then investigated the intratumoural spread, as well as the effect on tumour growth and survival rate in vivo using a CT26 subcutaneous tumour- bearing mice administered VSVΔ51-Luc delivered either by NFI or NI. Improved luciferase expression, suggesting increased spread of virus, was detected in tumour tissues administered via NFI compared to that by NI. In addition, reduction in tumour growth and survival rate in mice treated with VSVΔ51-Luc delivered by NFI was found to be similar to those treated by NI. Overall, this study provides the first proof-of-principle for the use of NFI in delivering OVs, and our results demonstrate the potential of developing this delivery method for the treatment of solid tumours with OVs.

2.5 Materials and Methods

Cell Culture and Viruses

Murine colorectal carcinoma cell line CT26, human HEK293T, murine L929 and African green monkey Vero cells were obtained from the American Type Culture Collection (ATCC, Manassas, VA, USA). These cells were cultured in Dulbecco's Modified Eagle Medium (DMEM, Grand Island, NY, USA) (Fisher, New York, NY, USA) supplemented with 10% fetal bovine serum (Sigma, Tokyo, Japan) and 0.1% penicillin and streptomycin (Life Technologies, Waltham, MA, USA) at 37 °C in 5% CO_2.

HSV1 (HSV1-1716, strain 17–γ34.5 deleted, Sorrento Therapeutics, San Diego, CA, USA), VACV (JX-594 strain Wyeth, Tk-deleted expressing GM-CSF, Jennerex Biotherapeutics/Sillagen, Seoul, Republic of Korea) and ReoV (Type 3 Dearing, Oncolytics Biotech, Calgary, AB, Canada) were kindly provided by manufacturers. VSVΔ51-GFP and

VSVΔ51-Luc (ΔM51 with insertion of GFP or Luc genes, respectively) were kindly provided by Dr. John Bell (Ottawa Hospital Research Institute). Vero cells were used to propagate HSV1, VACV, VSVΔ51-GFP and VSVΔ51-Luc viruses, and L929 cells were used to propagate ReoV. Briefly, cells were inoculated with viruses at the appropriate MOIs. Cells were then subjected to three freeze–thaw cycles to release intracellular viruses. Freeze–thawed lysates were clarified by centrifugation at 500× g for 10 min, and the supernatants were collected. Viral supernatants were subjected to ultracentrifugation at 28,000× g for 90 min on a sucrose cushion layer (36% sucrose, 10 mM HEPES, 150 mM NaCl, 0.1 mM EDTA, pH 7.3), with the exception of VSVΔ51-Luc. VSVΔ51-Luc for use in animal studies was purified using a 10–40% opti-prep gradient as previously described [23]. Titers of HSV1, VACV, VSVΔ51-GFP and VSVΔ51-Luc were determined by plaque titration using Vero cells monolayer and using 1% carboxymethylcellulose.

Western Blotting

For Western blot (WB) analysis to assess viral protein expression, cells were cultured in 6-well plates. After 12 h of infection, the cells were lysed in RIPA buffer (150 mM NaCl, 1.0% IGEPAL® CA-630, 0.5% sodium deoxycholate, 0.1% SDS, 50 mM Tris, 50 mM NaF, 15 mM $NaVO_3$, pH 8.0) supplemented with cOmplete Protease Inhibitor Cocktail (Roche, Basel, Switzerland). Cell debris were removed by centrifugation at 12,000 rpm for 5 min at 4 °C. The protein concentration was quantified using the DC Protein assay (BioRad, Hercules, CA, USA). The protein samples were loaded onto a 10% SDS-polyacrylamide gel and separated by electrophoresis. The separated proteins were then transferred to a PVDF membrane and blocked with Intercept (TBS) Blocking Buffer (LI-COR). Primary antibodies specific to HSV1 (Dako, #B011402), VACV (a kind gift of Dr. John Bell, Ottawa Hospital Research Institute), β-actin (#A5441, Sigma), and ReoV anti-serum (a kind gift of Dr. Earl Brown, University of Ottawa) were used. For secondary antibodies, IRDye® 680RD Goat anti-Mouse IgG (LiCor, Lincoln, NE, USA, #926-68070) and IRDye® 800CW Goat anti-Rabbit IgG Secondary Antibody (LiCor, #926-32211) (1:10,000) were used.

First Generation Needle-Free Device

The Inolife needle-free device (Inolife R&D Inc., NuGen Medical Devices, Toronto, ON, Canada) comes with injector reset box and sterile ampules (Figure 2.1A). To recharge the injector, the safety ring is moved to the “safe on” position, then the injector is placed in the reset box and

the spring is fully loaded before closing the cover. When the injector is fully charged, the filled ampule is screwed into the injector, the safety ring is pulled to the "safe off" position. The injector is then placed on the subcutaneous tumour, and pressing the trigger releases the liquid contained inside the ampoule into the tissue via a high-pressure jet stream capable of tissue penetration. For in vitro virus stability assay, HSV1, VACV, VSV and ReoV were injected directly into a 6-well plate using either a one-end-hole needle or the Inolife needle-free device. The post-injection virus solutions then underwent three 10-fold dilutions before inoculated onto HEK293T cells (HSV1, VACV and VSV) or L929 cells (ReoV).

Immunofluorescence

To test for stability and virus replication of ReoV, the virus was inoculated onto L929 cells. After 48 h, the cells were fixed using 3.7% paraformaldehyde (PFA), then blocked for 30 min in blocking buffer (2% BSA + 0.1% Triton X-100). Cells were subsequently incubated with anti-ReoV anti-serum (Rabbit Ig, 1:1000) at room temperature for 30 min, then incubated with anti-rabbit Alexa Fluor 488 secondary antibody in blocking buffer (1:500, ThermoFisher, Waltham, MA, USA) at room temperature for 1 h. Immunofluorescent images was taking using EVOS cell imaging system (ThermoFisher).

Bromophenol Blue Injection and Detection Experiment

CT26 cells were subcutaneously injected, and when tumour volume reached approximately 1000 mm^3, 50 μL of bromophenol blue dye was injected intratumourally either using the needle-free or needle injection method. Immediately after injection, the tumours were dissected to observe the distribution of the dye. Subsequently, images were captured to document the extent of dye accumulation within the tumour tissue.

Live Cell Monitoring of Virus Infection

To assess virus replication efficiency, HSV1, VACV, VSV and MeV were injected into a 6-well plate using either the needle injection or NFI method. The viruses were then inoculated onto HEK293T cells that were seeded in a 48-well plate. The cells were subsequently monitored for 72 h using the IncuCyte ZOOM^{TM} Live-Cell Analysis System (Sartorius, Göttingen, Germany). Images were captured every 2 h at 10× magnification to monitor viral infection of live cells based on fluorescence. The acquired images were analyzed using the accompanying IncuCyte

ZOOM™ (Incucyte S3 Software v2018A) (Sartorius). Measurement of total green object area (μm^2/well) was utilized to determine the level of virus infection. Background subtraction was performed using the Top-Hat method with a disk-shaped structuring element containing a 10 mm radius in conjunction with a threshold of 1.0 green calibration unit. The analysis settings included edge split: Off, hole fill: No, adjust size: No.

CT26 Subcutaneous Tumour Model for In Vivo Imaging System (IVIS)

Female BALB/c mice, aged 5–6 weeks, were purchased from Charles River (Kingston, NY, USA). After one week of acclimatization, 5×10^5 CT26 cells were subcutaneously injected into one flank of each mouse. After 14 days, the mice received intratumoural injections of 50 µL VSV-Luc at 10^8 PFU/tumour using either the NI or NFI system. Twenty-four hours later, a solution of 15 mg/mL D-luciferin (GOLDBIO, CAT#: LUCK-1G) in DPBS was intraperitoneally injected at a dosage of 10 µL/g of body weight. Images were captured 5–8 min after luciferin injection. A series of 15 images, taken 1 min apart, with an acquisition time of 30 s per image, were obtained to determine the peak signal. The acquired images were analyzed using Living Image® software V4.7 (for IVIS® Spectrum images). The quantification of the region of interest was presented as the average radiance measurement, reported in units of photons per second per square centimeter per steradian (p/s/cm^2/sr). The average radiance represents the average intensity of light emitted from the sample over a given area and time, providing quantitative information about the level of bioluminescent signal detected. Following the imaging procedure, the animals were sacrificed.

CT26 Subcutaneous Tumour Model

When tumours reached palpable size, approximately 5 × 5 mm, they were injected intratumourally twice on day 1 and day 3 with VSV-Luc at 1×10^8 PFU/tumour. Tumour sizes were measured daily using a caliper, and their volumes were calculated using the formula [length × $(\text{width})^2$]/2. Animals were sacrificed either when an individual tumour reached 1500 mm^3 or at an alternative humane endpoint. All animal procedures were conducted with approval from the University of Ottawa Animal Care Committee.

2.6 Results

High-Pressure Needle-Free Injection Does Not Affect Stability and Replication Competence of RNA and DNA OVs

We first conducted in vitro experiments to assess whether several clinically relevant OVs would be affected when subjected to high-pressure liquid jet injections as compared to needle injections (Figure 2.1A, B). MeV [24] and VSVΔ51 [25] are single-stranded, negative-sense, enveloped, non-segmented RNA viruses with a small genome; HSV1 [26] and VACV [27] are large, enveloped, linear, double-stranded DNA viruses; and ReoV is a segmented, non-enveloped, double-stranded RNA virus. To determine whether these viruses can retain therapeutic potential under the high-pressure conditions of NFI, the viruses were ejected into 6-well plates either through a traditional syringe and needle, or via the needle-free jet injector. The virus-containing solutions were then used to infect HEK293T cells as NFI directly onto monolayer of cells would have resulted in irreversible damage to the cells. To examine the ability of viruses exposed to NFI to infect and spread within the culture, the infections were monitored for 3 days under live cell imaging (Incucyte) using the tagged green fluorescent protein (GFP) (for HSV1, MeV, VACV, VSV) or by immunofluorescence (IF) (ReoV). We observed equivalent viral spread, as measured by immunofluorescence or GFP signal from Incucyte images, for cells infected by viruses subjected to needle injection versus NFI (Figure 2.2A,B). Additionally, viral protein expression was examined by Western blotting using antibodies raised against HSV1, VACV, VSVΔ51 or ReoV. Similarly, no differences were observed in total viral protein synthesis from infections resulting from viruses passed through needles or the needle-free jet injector (Figure 2.2C). Together, these data demonstrate that the infectivity of viruses is preserved after high pressure NFI exposure.

Intratumoural Delivery and Spread of VSVΔ51-Luc via Needle-Free Jet Injector

Needle-free injection technology was previously shown to deliver medicine deep into the skin, and even intramuscularly, in a spray-like and highly dispersed form [18,19,20]. Therefore, we anticipated that this method of delivery could be applied to subcutaneous, accessible tumours and provide a dispersed distribution that could help the viruses reach and infect more tumour cells. As a proof of concept, we used bromophenol blue dye for tracking liquid distribution after intratumoural injection by either needle or NFI. We found that NFI delivered a wider distribution of the dye within the tumour as compared to needle administration (Figure 2.3A). To determine whether a more dispersed spread of injected liquid would result in a better distribution of OVs within the tumour tissues, we tested the use of NFI technology for OV administration in a CT26

subcutaneous mouse tumour model. We used the oncolytic virus VSVΔ51-Luc for the ease of tracking viral replication in vivo via its luciferase transgene using In Vivo Imaging System (IVIS). After 14 days of CT26 subcutaneous implantation, 10^8 PFU of VSVΔ51-Luc was administered intratumourally using a traditional needle or the needle-free jet injector system, and luciferase activity was measured 24 h post administration using IVIS (Figure 2.3B,C). The average radiance value obtained from IVIS imaging represents the average intensity of the emitted light across the region of interest, providing a quantitative measure of the bioluminescent signal emitted from the luciferase reporter gene. We found that NFI not only preserved OV replication, but also provided a significant increase in bioluminescence and intensity of VSVΔ51-Luc intratumourally ($p < 0.0001$) (Figure 2.3D,E). Notably, there was no significant difference in initial tumour volumes from the two mouse groups ($p = 0.9375$) (Figure 2.3F), suggesting the increase in luciferase activity appears to be a direct consequence of better virus distribution and infection rather than a variation in tumour sizes.

Therapeutic Efficacy of VSVΔ51-Luc Administered via Needle-Free Jet Injector

Given the promising effect of NFI on intratumoural spread of OV, we next tested whether this could translate into a better outcome in tumour volume reduction and survival. We repeated the subcutaneous CT26 tumour implantation model. When tumours reached 50–60 mm^3, two intratumoural injections of 1×10^8 PFU of VSVΔ51-Luc were administered on day one and three to maximize the antitumour effect of this OV (Figure 2.4A). As expected from previous experiences, NI of VSVΔ51-Luc resulted in a significant reduction in tumour volume, as well as a prolonged survival rate compared to the control (PBS) group ($p < 0.0001$ and $p = 0.0042$, respectively) (Figure 2.4B,C). However, NFI of VSVΔ51-Luc caused an equally significant reduction in tumour volume and improvement in survival rate when compared to the control group ($p < 0.0001$ and $p = 0.0018$, respectively). While in this model there was no significant difference in tumour volume and survival between the NI and NFI groups ($p = 0.6164$ and $p = 0.6758$, respectively), these results confirm that NFI of OVs can provide a similar performance in terms of therapeutic outcome for the treatment of subcutaneous solid tumours.

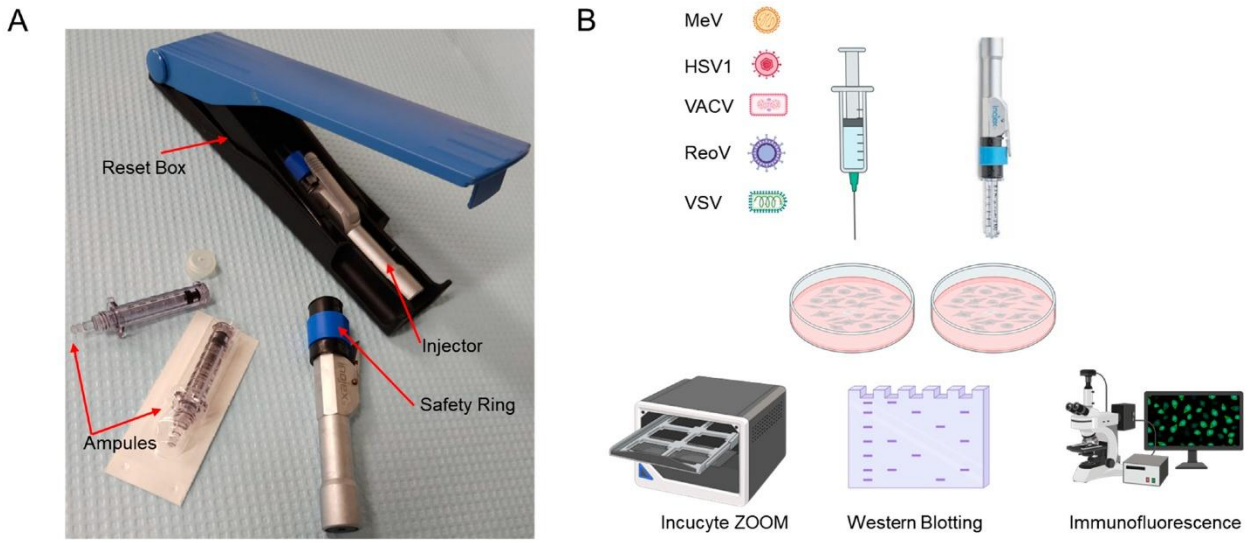

Figure 2. 1: Experimental schema of oncolytic viruses subjected to needle or needle-free injector.

(A): The first-generation Inojex Needle Free Injector System includes a reusable Inojex injector and reset box, as well as sterile, disposable ampules. (B): Two different delivery systems were utilized to infect HEK293T cells with five different oncolytic viruses, after which, viral infectivity was assessed. For MeV, HSV1, VACV and VSV, 72-h live-cell analysis was used to detect viral infection. For ReoV, immunofluorescence of viral protein after 24 h of infection was assayed. Additionally, for HSV1, VACV, VSV and ReoV, viral protein expression after 12 h of infection was analyzed via Western blotting.

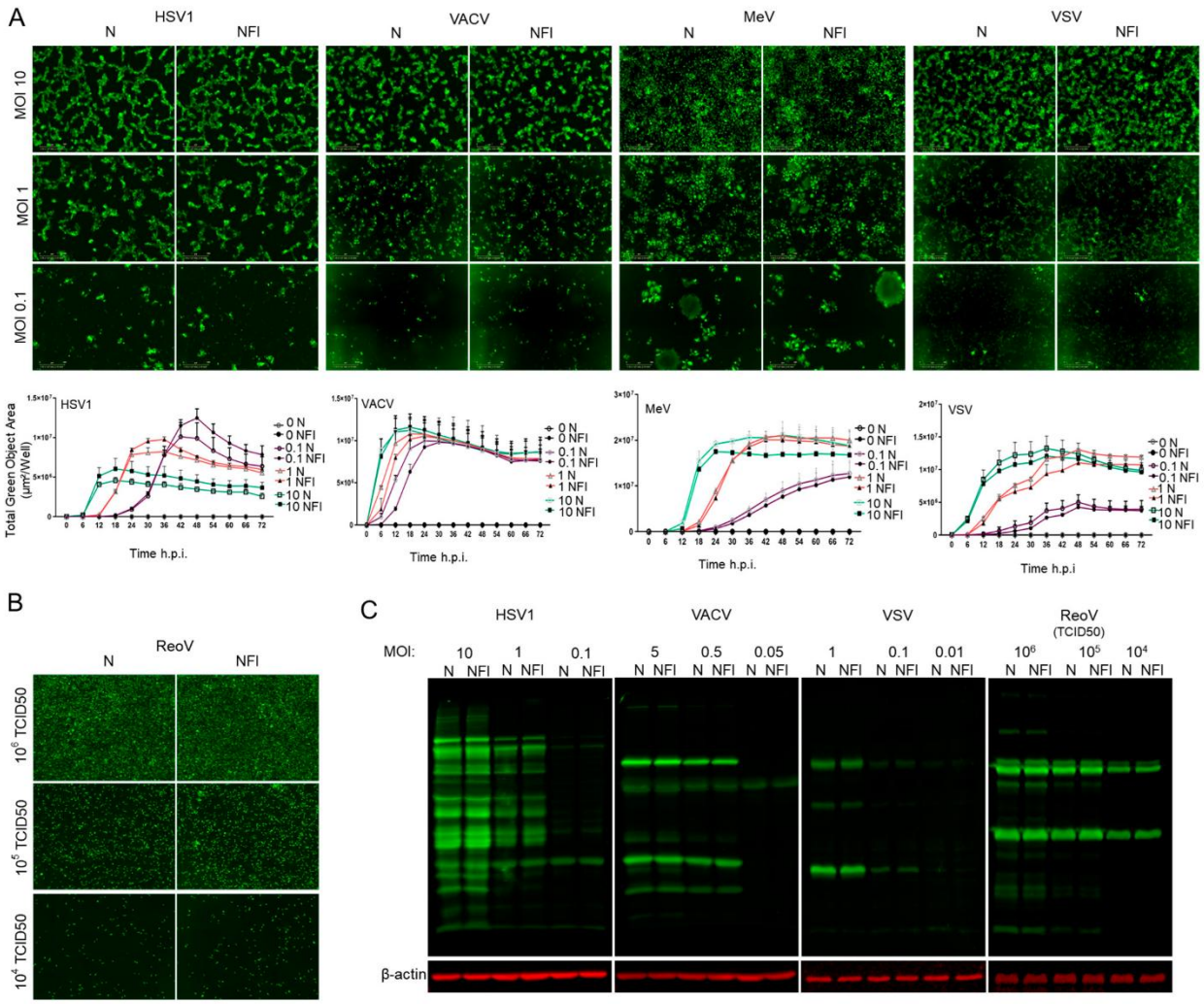

Figure 2. 2. Needle-free injection system does not compromise virus infectivity in vitro.

(A): Representative fluorescent images from Incucyte ZOOM^{TM} for MeV, HSV1, VACV, and VSV at 18 h post-infection from three different MOIs for each virus with respective quantifications below. Graphs depict the mean ± s.d. of four different images at 10X magnification taken every two hours for the total assay duration of 72 h. Data are representative of three independent experiments. (B): Representative immunofluorescent images of ReoV infectivity with 3 different titers ($TCID_{50}$). 48 h after infection with ReoV, HEK293T cells were fixed and labeled using immunofluorescence. (C): Representative Western blots of viral protein from HEK293T cells 12 h after infection with HSV1, VACV, VSV or ReoV.

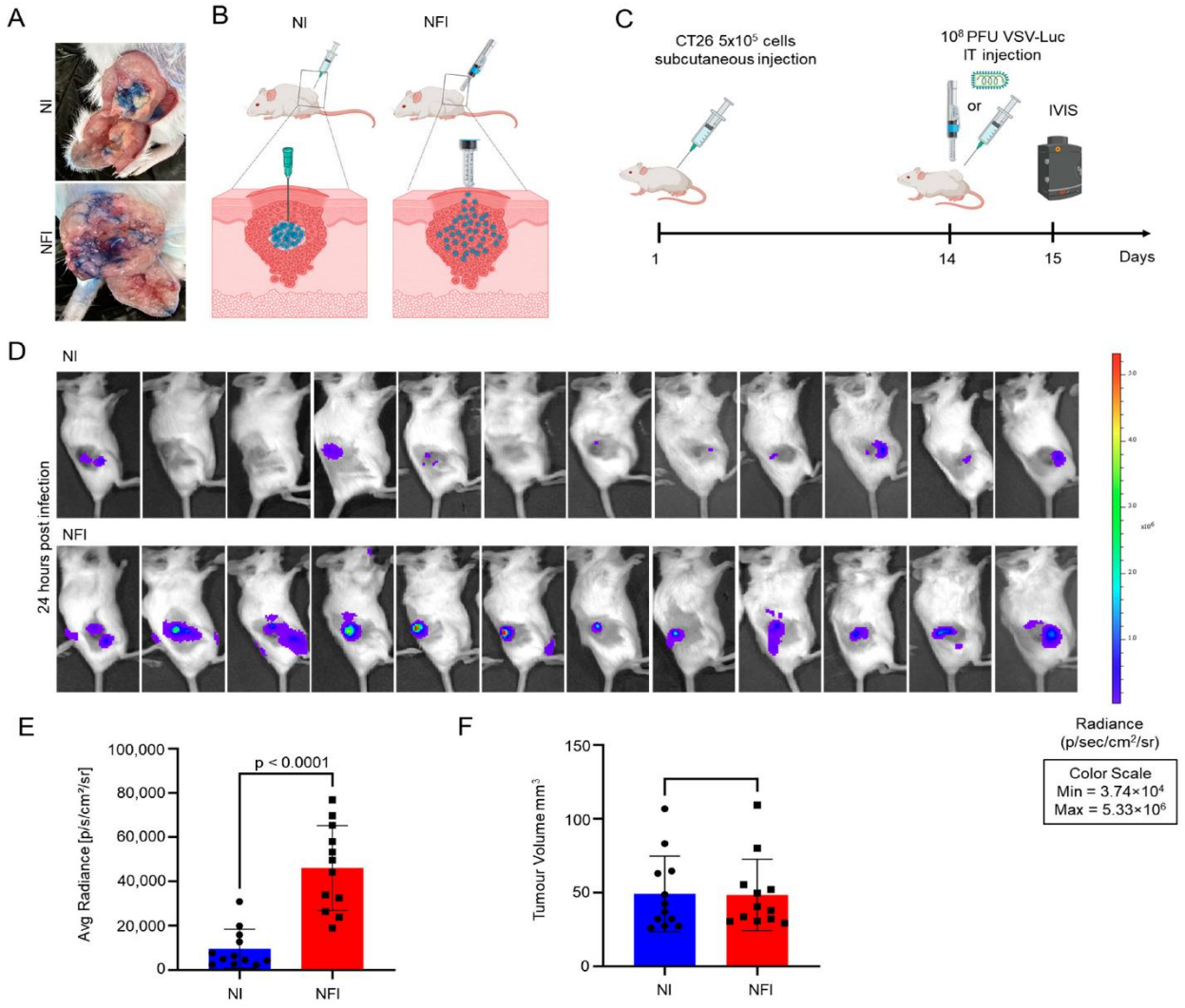

Figure 2. 3. A needle-free injection system can efficiently deliver viruses to tumours in vivo.

(A): Representative images for intratumoural delivery of bromophenol blue dye in large CT26 tumours using needle injection and needle-free injection. (B): Schematic representation of potential intratumoural viral distribution using a needle-free injection system. (C): Experiment timeline: 5×10^5 cells were injected subcutaneously into the flanks of mice, then 14 days later mice were injected intratumourally with 1×10^8 PFU of VSVΔ51-Luc. Twenty-four hours post-injection, mice were imaged to assess in vivo viral infection using IVIS imaging. (D): Representative bioluminescent images were taken using IVIS® Spectrum imaging 24 h after virus delivery. n = 12 for each group. (E): Quantification of luminescence images using Living Image® version 4.7 software. $p < 0.0001$ using a student's t-test. (F): Tumour volume of mice at the time of VSVΔ51-Luc injection. $p = 0.9375$ using a student's t-test.

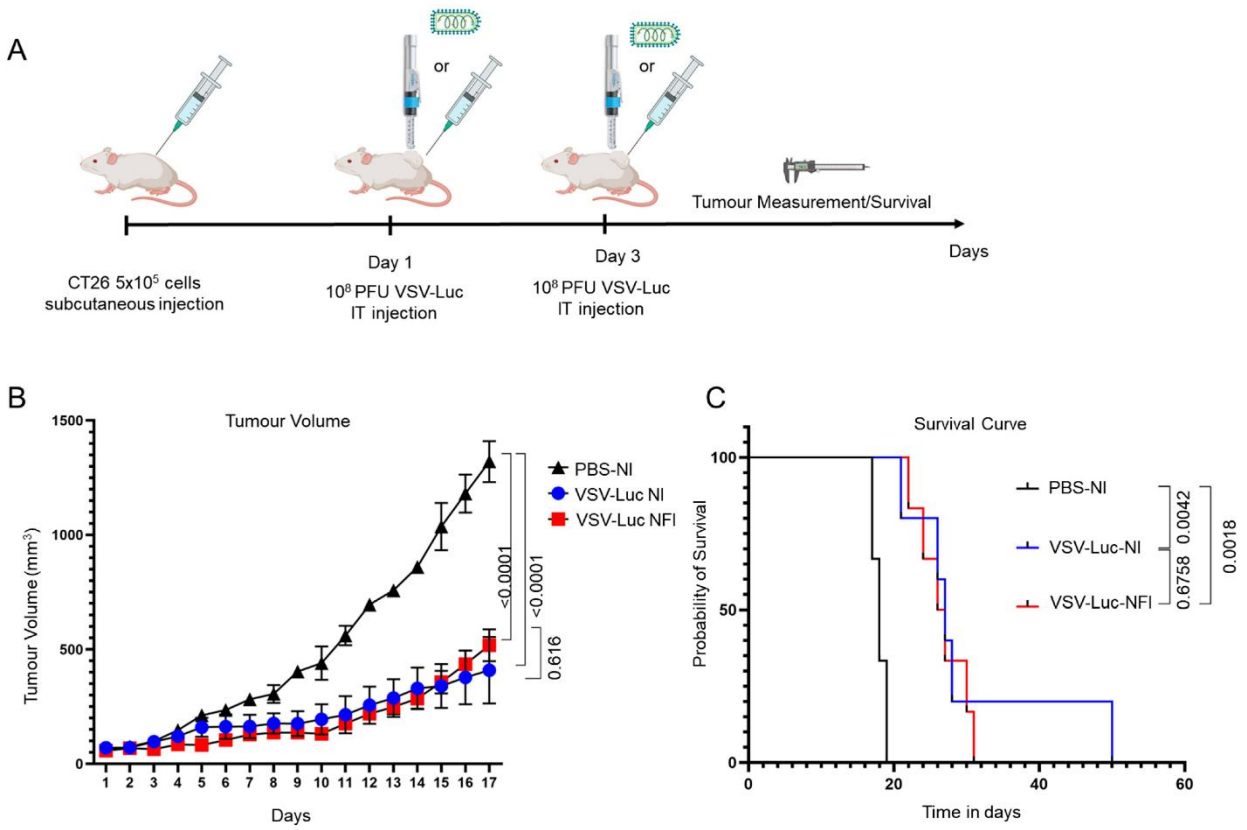

Figure 2. 4. Needle-free injection of VSVΔ51-Luc is as effective for tumour treatment as needle-based injection.

(A): Experiment outline: 5×10^5 cells were injected subcutaneously in the right flank of mice. When tumours reached 50–60 mm^3, a dose of 1×10^8 PFU of VSVΔ51-Luc was injected intratumourally, followed by a second identical dose on day 3. Tumour volumes were measured every day. (B): Tumour volume curves showing the effect of a needle-free injection system on tumour growth (PBS-N: n = 3; VSV-Luc-N: n = 5; VSV-Luc-NFI: n = 6). Data are represented as arithmetic mean ± SEM. $p < 0.05$ using a two-way ANOVA with Tukey's post-hoc test (C): Kaplan–Meier survival curve showing effects from the two different OV delivery systems (PBS-N: n = 3; VSV-Luc-N: n = 5; VSV-Luc-NFI: n = 6).

2.7 Discussion

The usage of needle-free injection technology is gaining attention as a promising technique for the delivery of small therapeutic molecules like insulin [28]. The use of NFI technology was also proven to be an effective method for transdermal delivery of exosomes [20], and was shown recently to be highly effective in delivery of more complex biologics such as vaccines or even mRNA-lipid complex. Until now, the largest macromolecules reported to be successfully delivered by NFI were mRNA-lipid nanoparticles [19]. Studies conducted thus far have demonstrated the dispersion and spray-like properties of NFI for vaccines and drugs. Furthermore, several lines of evidence indicate that this injection method can elicit robust immune responses upon vaccine administration. For example, when a needle-free injection system was used to administer the ZyCoV-D DNA or mRNA-based vaccine against SARS-CoV-2, significant antibody titers and immune responses were observed [19,29]. These responses included elevated levels of IgG and neutralizing antibodies, enhanced lymphocyte proliferation, and cytokine responses [19,29]. However, despite possessing favorable properties, NFI had yet to be tested for the delivery of OV. In this study, we are the first to evaluate the use of NFI for OV delivery and the effect of this administration method on OV efficacy in vivo. Using a collection of clinically important OVs, we showed that the high-pressure ejection by NFI does not compromise the replication competence of both RNA and DNA viruses. We also observed an improved distribution of VSVΔ51-Luc within tumour tissues using high-pressure needle-free administration in the subcutaneous CT26 tumour model. Finally, we confirmed that VSVΔ51-Luc injected by NFI into solid subcutaneous tumours provides equivalent tumour growth control and mouse survival to that provided by NI.

Intratumoural distribution and replication of different types of OVs plays a crucial role in stimulating effective antitumour immune responses [30]. OV infection induces immunogenic cell death, characterized by the release of damage-associated molecular patterns upon tumour cell death, which is essential for initiating immune reactions [31]. Compared to intravenous administration, intratumoural injection of OVs can concentrate the virus inside the tumour to facilitate induction of immunogenic cell death, better modulate the tumour microenvironment to overcome immunosuppression [32], and consequently enhance local and systemic antitumour immunity. Intratumoural delivery also overcomes potential unwanted side effects of systemic administration of OV [33,34]. Nonetheless, the biophysical properties of certain solid tumours

present significant obstacles to effective delivery of intratumourally administered OVs [34,35]. Current injection methods are presently being improved for intratumoural delivery of drugs in general [36,37,38]. The conventional end-hole needles are the widely used method to deliver drugs or OVs intratumourally, at least in experimental laboratory settings. However, closed diamond tip multisided hole needles have been shown to be significantly more efficient at promoting drug spread intratumourally and at inducing antitumour immunity compared to one end-hole needles [36]. Additionally, three-side-hole needles or three-pronged array needles can demonstrate better dispersion and distribution compared to single-side-hole needles, producing more spherical distributions within tissues, especially for percutaneous therapies [38,39]. All of these alternative injection methods are aimed at addressing the limitations associated with conventional needle injections, such as leakage out of the tumour, as well as achieving widespread distribution of drugs within cancerous tissues. Our results presented here propose the use and development of needle-free jet injector as a novel alternative to administer viral immunotherapeutics to accessible tumours such as melanoma or head and neck cancer.

This study was performed using a first-generation needle-free jet injector device designed for human administration of insulin into skin tissues. An important limitation of this study was that the injector's pressure and size were not ideal for administration to mouse models of cancer, requiring careful handling for successful injections. Even though the device was not optimized for mouse cancer models, we observed improved viral distribution into the tumour tissues by NFI as compared to NI. Improved initial viral infection could ultimately promote better tumour growth control; however, in this model, two doses of VSVΔ51-Luc already provided strong cancer regression, rendering the observed increased viral spread less impactful on tumour reduction compared to NI. Nonetheless, our results suggest that optimization of the technology could achieve useful outcomes for intratumoural delivery of OVs. Other oncolytic viruses with limited therapeutic efficacy due to poor viral spread, and additional hard-to-treat cancer models, could ultimately exhibit elevated benefits from administration by NFI. One potential improvement could be achieved via altering the nozzle geometry to optimize diffusion of OV-containing liquid inside solid tumour [40]. In addition, the injection volume and density of OV-containing vehicle could also be modified to adjust the penetration and diffusion of viruses inside tumour [41]. Finally, ejection pressure could be optimized for each tumour type, density, and size. In conclusion, our study establishes NFI as a novel and promising alternative for intratumoural delivery of viral

immunotherapeutics, and future advancements in needle-free injector system technology will optimize this approach to further enhance its therapeutic potential.

2.8 Conclusions

Needle-Free Injection technology represents an effective alternative delivery method for OVs to target accessible solid tumours. Overcoming the physical barriers of tumour microenvironments is a critical challenge for virotherapy, and this initial investigation demonstrates that NFI maintains the infectivity and therapeutic potential of OVs. In a subcutaneous mouse tumour model, NFI could even enhance the intratumoural distribution of virus, showcasing its promise as an efficient and convenient delivery method compared to traditional needle injections. While the study was performed using a first-generation device not originally designed for animal experiments, future optimization of this technology has the potential to improve the effectiveness and therapeutic distribution of OVs within tumour tissues, making it a promising route for the intratumoural administration of oncolytic virotherapies.

Funding

This work is supported partially by a Terry Fox Research Institute New Project Grant, a Natural Sciences and Engineering Research Council (NSERC) Discovery grant, a Cancer Research Society grant, a Canadian Cancer Society Research Institute Innovation to Impact Grant (#706852) and Canadian Institute of Health Research (CIHR) bridge funding to T.A. and H.H. This project was also supported by NuGen Medical Devices.

Institutional Review Board Statement

The animal study protocol was approved by the University of Ottawa Animal Care Committee (ACC). Protocol code: CHEOe-3084-R3 A1, approved on 8 August 2022.

Informed Consent Statement

Not applicable.

Data Availability Statement

The data presented in this study are available on request to the corresponding author.

Acknowledgments

Special thanks are extended to Brad Mischuk for his meticulous proofreading, which significantly enhanced the quality of this article. His dedication and expertise in reviewing the manuscript are deeply appreciated.

Conflicts of Interest

The authors declare no conflict of interest.

2.9 References

1. Singh, P.K.; Doley, J.; Kumar, G.R.; Sahoo, A.P.; Tiwari, A.K. Oncolytic Viruses & Their Specific Targeting to Tumour Cells. *Indian J. Med. Res.* 2012, *136*, 571–584. [Google Scholar] [PubMed]

2. Marelli, G.; Howells, A.; Lemoine, N.R.; Wang, Y. Oncolytic Viral Therapy and the Immune System: A Double-Edged Sword Against Cancer. *Front. Immunol.* 2018, *9*, 866. [Google Scholar] [CrossRef] [PubMed]

3. Lemos de Matos, A.; Franco, L.S.; McFadden, G. Oncolytic Viruses and the Immune System: The Dynamic Duo. *Mol. Ther. Methods Clin. Dev.* 2020, *17*, 349–358. [Google Scholar] [CrossRef] [PubMed]

4. Lichty, B.D.; Breitbach, C.J.; Stojdl, D.F.; Bell, J.C. Going Viral with Cancer Immunotherapy. *Nat. Rev. Cancer* 2014, *14*, 559–567. [Google Scholar] [CrossRef]

5. Zheng, M.; Huang, J.; Tong, A.; Yang, H. Oncolytic Viruses for Cancer Therapy: Barriers and Recent Advances. *Mol. Ther. Oncolytics* 2019, *15*, 234–247. [Google Scholar] [CrossRef]

6. Li, L.; Liu, S.; Han, D.; Tang, B.; Ma, J. Delivery and Biosafety of Oncolytic Virotherapy. *Front. Oncol.* 2020, *10*, 475. [Google Scholar] [CrossRef]

7. Tang, G.; Wang, D.; Zhao, X.; Feng, Z.; Chen, Q.; Shen, Y. The Dilemma of HSV-1 Oncolytic Virus Delivery: The Method Choice and Hurdles. *Int. J. Mol. Sci.* 2023, *24*, 3681. [Google Scholar] [CrossRef]

8. Beyer, I.; van Rensburg, R.; Lieber, A. Overcoming Physical Barriers in Cancer Therapy. *Tissue Barriers* 2013, *1*, e23647. [Google Scholar] [CrossRef]

9. Goradel, N.H.; Baker, A.T.; Arashkia, A.; Ebrahimi, N.; Ghorghanlu, S.; Negahdari, B. Oncolytic Virotherapy: Challenges and Solutions. *Curr. Probl. Cancer* 2021, *45*, 100639. [Google Scholar] [CrossRef]

10. Vähä-Koskela, M.; Hinkkanen, A. Tumour Restrictions to Oncolytic Virus. *Biomedicines* 2014, *2*, 163–194. [Google Scholar] [CrossRef]

11. Zeh, H.J.; Downs-Canner, S.; McCart, J.A.; Guo, Z.S.; Rao, U.N.M.; Ramalingam, L.; Thorne, S.H.; Jones, H.L.; Kalinski, P.; Wieckowski, E.; et al. First-in-Man Study of Western Reserve Strain Oncolytic Vaccinia Virus: Safety, Systemic Spread, and Antitumour Activity. *Mol. Ther.* 2015, *23*, 202–214. [Google Scholar] [CrossRef] [PubMed]

12. Montaguti, P.; Melloni, E.; Cavalletti, E. Acute Intravenous Toxicity of Dimethyl Sulfoxide, Polyethylene Glycol 400, Dimethylformamide, Absolute Ethanol, and Benzyl Alcohol in Inbred Mouse Strains. *Arzneimittelforschung* 1994, *44*, 566–570. [Google Scholar] [PubMed]

13. Eto, Y.; Yoshioka, Y.; Mukai, Y.; Okada, N.; Nakagawa, S. Development of PEGylated Adenovirus Vector with Targeting Ligand. *Int. J. Pharm.* 2008, *354*, 3–8. [Google Scholar] [CrossRef] [PubMed]

14. Cristi, F.; Gutiérrez, T.; Hitt, M.M.; Shmulevitz, M. Genetic Modifications That Expand Oncolytic Virus Potency. *Front. Mol. Biosci.* 2022, *9*, 831091. [Google Scholar] [CrossRef] [PubMed]

15. Guedan, S.; Rojas, J.J.; Gros, A.; Mercade, E.; Cascallo, M.; Alemany, R. Hyaluronidase Expression by an Oncolytic Adenovirus Enhances Its Intratumoural Spread and Suppresses Tumour Growth. *Mol. Ther.* 2010, *18*, 1275–1283. [Google Scholar] [CrossRef] [PubMed]

16. Dmitrieva, N.; Yu, L.; Viapiano, M.; Cripe, T.P.; Chiocca, E.A.; Glorioso, J.C.; Kaur, B. Chondroitinase ABC I-Mediated Enhancement of Oncolytic Virus Spread and Antitumour Efficacy. *Clin. Cancer Res. Off. J. Am. Assoc. Cancer Res.* 2011, *17*, 1362–1372. [Google Scholar] [CrossRef] [PubMed]

17. McKee, T.D.; Grandi, P.; Mok, W.; Alexandrakis, G.; Insin, N.; Zimmer, J.P.; Bawendi, M.G.; Boucher, Y.; Breakefield, X.O.; Jain, R.K. Degradation of Fibrillar Collagen in a Human Melanoma Xenograft Improves the Efficacy of an Oncolytic Herpes Simplex Virus Vector. *Cancer Res.* 2006, *66*, 2509–2513. [Google Scholar] [CrossRef] [PubMed]

18. Ravi, A.D.; Sadhna, D.; Nagpaal, D.; Chawla, L. Needle Free Injection Technology: A Complete Insight. *Int. J. Pharm. Investig.* 2015, *5*, 192–199. [Google Scholar] [CrossRef]

19. Mao, S.; Li, S.; Zhang, Y.; Long, L.; Peng, J.; Cao, Y.; Mao, J.Z.; Qi, X.; Xin, Q.; San, G.; et al. A Highly Efficient Needle-Free-Injection Delivery System for mRNA-LNP Vaccination against SARS-CoV-2. *Nano Today* 2023, *48*, 101730. [Google Scholar] [CrossRef]

20. Hu, S.; Li, Z.; Cores, J.; Huang, K.; Su, T.; Dinh, P.-U.; Cheng, K. Needle-Free Injection of Exosomes Derived from Human Dermal Fibroblast Spheroids Ameliorates Skin Photoaging. *ACS Nano* 2019, *13*, 11273–11282. [Google Scholar] [CrossRef]

21. Giudice, E.L.; Campbell, J.D. Needle-Free Vaccine Delivery. *Adv. Drug Deliv. Rev.* 2006, *58*, 68–89. [Google Scholar] [CrossRef] [PubMed]

22. Ledesma-Feliciano, C.; Chapman, R.; Hooper, J.W.; Elma, K.; Zehrung, D.; Brennan, M.B.; Spiegel, E.K. Improved DNA Vaccine Delivery with Needle-Free Injection Systems. *Vaccines* 2023, *11*, 280. [Google Scholar] [CrossRef] [PubMed]

23. Diallo, J.-S.; Vähä-Koskela, M.; Le Boeuf, F.; Bell, J. Propagation, Purification, and in Vivo Testing of Oncolytic Vesicular Stomatitis Virus Strains. *Methods Mol. Biol.* 2012, *797*, 127–140. [Google Scholar] [CrossRef] [PubMed]

24. Phan, M.V.T.; Schapendonk, C.M.E.; Oude Munnink, B.B.; Koopmans, M.P.G.; de Swart, R.L.; Cotten, M. Complete Genome Sequences of Six Measles Virus Strains. *Genome Announc.* 2018, *6*, e00184-18. [Google Scholar] [CrossRef] [PubMed]

25. Gaudier, M.; Gaudin, Y.; Knossow, M. Crystal Structure of Vesicular Stomatitis Virus Matrix Protein. *EMBO J.* 2002, *21*, 2886–2892. [Google Scholar] [CrossRef] [PubMed]

26. Smith, S.; Reuven, N.; Mohni, K.N.; Schumacher, A.J.; Weller, S.K. Structure of the Herpes Simplex Virus 1 Genome: Manipulation of Nicks and Gaps Can Abrogate Infectivity and Alter the Cellular DNA Damage Response. *J. Virol.* 2014, *88*, 10146–10156. [Google Scholar] [CrossRef] [PubMed]

27. Malkin, A.J.; McPherson, A.; Gershon, P.D. Structure of Intracellular Mature Vaccinia Virus Visualized by In Situ Atomic Force Microscopy. *J. Virol.* 2003, *77*, 6332–6340. [Google Scholar] [CrossRef]

28. Trimzi, M.A.; Ham, Y.-B. A Needle-Free Jet Injection System for Controlled Release and Repeated Biopharmaceutical Delivery. *Pharmaceutics* 2021, *13*, 1770. [Google Scholar] [CrossRef]

29. Yadav, P.D.; Kumar, S.; Agarwal, K.; Jain, M.; Patil, D.R.; Maithal, K.; Mathapati, B.; Giri, S.; Mohandas, S.; Shete, A.; et al. Needle-Free Injection System Delivery of ZyCoV-D DNA Vaccine Demonstrated Improved Immunogenicity and Protective Efficacy in Rhesus Macaques against SARS-CoV-2. *J. Med. Virol.* 2023, *95*, e28484. [Google Scholar] [CrossRef]

30. Crittenden, M.R.; Thanarajasingam, U.; Vile, R.G.; Gough, M.J. Intratumoural Immunotherapy: Using the Tumour against Itself. *Immunology* 2005, *114*, 11–22. [Google Scholar] [CrossRef]

31. Ma, J.; Ramachandran, M.; Jin, C.; Quijano-Rubio, C.; Martikainen, M.; Yu, D.; Essand, M. Characterization of Virus-Mediated Immunogenic Cancer Cell Death and the Consequences for Oncolytic Virus-Based Immunotherapy of Cancer. *Cell Death Dis.* 2020, *11*, 48. [Google Scholar] [CrossRef] [PubMed]

32. Labani-Motlagh, A.; Ashja-Mahdavi, M.; Loskog, A. The Tumour Microenvironment: A Milieu Hindering and Obstructing Antitumour Immune Responses. *Front. Immunol.* 2020, *11*, 940. [Google Scholar] [CrossRef] [PubMed]

33. Marabelle, A.; Tselikas, L.; de Baere, T.; Houot, R. Intratumoural Immunotherapy: Using the Tumour as the Remedy. *Ann. Oncol.* 2017, *28*, xii33–xii43. [Google Scholar] [CrossRef] [PubMed]

34. Brito-Orama, S.; Sheth, R.A. The Contemporary Landscape and Future Directions of Intratumoural Immunotherapy. *J. Immunother. Precis. Oncol.* 2023, *6*, 84–90. [Google Scholar] [CrossRef] [PubMed]

35. Baghban, R.; Roshangar, L.; Jahanban-Esfahlan, R.; Seidi, K.; Ebrahimi-Kalan, A.; Jaymand, M.; Kolahian, S.; Javaheri, T.; Zare, P. Tumour Microenvironment Complexity and Therapeutic Implications at a Glance. *Cell Commun. Signal.* 2020, *18*, 59. [Google Scholar] [CrossRef] [PubMed]

36. Muñoz, N.M.; Williams, M.; Dixon, K.; Dupuis, C.; McWatters, A.; Avritscher, R.; Manrique, S.Z.; McHugh, K.; Murthy, R.; Tam, A.; et al. Influence of Injection Technique, Drug Formulation and Tumour Microenvironment on Intratumoural Immunotherapy Delivery and Efficacy. *J. Immunother. Cancer* 2021, *9*, e001800. [Google Scholar] [CrossRef] [PubMed]

37. Sheth, R.A.; Murthy, R.; Hong, D.S.; Patel, S.; Overman, M.J.; Diab, A.; Hwu, P.; Tam, A. Assessment of Image-Guided Intratumoural Delivery of Immunotherapeutics in Patients with Cancer. *JAMA Netw. Open* 2020, *3*, e207911. [Google Scholar] [CrossRef]

38. Sudheendra, D.; Léger, R.; Groppo, E.R.; Sun, D.; Durrani, A.K.; Neeman, Z.; Wood, B.J. Comparison of Three Different Needles for Percutaneous Injections. *Cardiovasc. Intervent. Radiol.* 2007, *30*, 151–152. [Google Scholar] [CrossRef][Green Version]

39. Amalou, H.; Wood, B.J. Intratumoural Gene Therapy Injections with a Multi-Pronged, Multi-Side Hole Needle for Rectal Carcinoma. *Cardiovasc. Intervent. Radiol.* 2013, *36*, 561–562. [Google Scholar] [CrossRef][Green Version]

40. Wang, Y.; Yue, L.; Hu, L.; Wang, J. Needle-Free Jet Injectors' Geometry Design and Drug Diffusion Process Analysis. *Appl. Bionics Biomech.* 2021, *2021*, 5199278. [Google Scholar] [CrossRef]

41. Grant, T.M.; Stockwell, K.D.; Morrison, J.B.; Mann, D.D. Effect of Injection Pressure and Fluid Volume and Density on the Jet Dispersion Pattern of Needle-Free Injection Devices. *Biosyst. Eng.* 2015, *138*, 59–64. [Google Scholar] [CrossRef]

3. CHAPTER THREE: ADAPTATION OF TRANSGENE MRNA TRANSLATION BOOSTS THE ANTICANCER EFFICACY OF ONCOLYTIC HSV1

Authors: Huy-Dung Hoang, Aida Said, Nasana Vaidya, Victoria H. Gilchrist, Kyle Malone, Usha Kabilan, Serena Topshee, Xiao Xiang, An-Dao Yang, David Olagnier, Karen Mossman, Shawn T. Beug, Seyed Mehdi Jafarnejad, Samuel T. Workenhe, Tyson E. Graber, and Tommy Alain

Status: Published 2023

Journal for ImmunoTherapy of Cancer

DOI: 10.1136/jitc-2022-006408

3.1 Author Contributions

A.S. performed all in vivo experiments for this study, including optimization of treatment conditions and evaluation of therapeutic efficacy. T.A. and H.-D.H. conceived and designed the experiments. H.-D.H. performed the majority of the in vitro experiments. N.V. conducted translation reporter assays. V.H.G. carried out virus titration. H.-D.H. and A.S. performed polysome profiling. U.K. conducted RT-qPCR analyses. S.M.J. performed the wet-lab component of the RNA-seq experiments. H.-D.H. and T.A. wrote the manuscript. A.S., K.M., S.T.W., S.M.J., T.E.G., and T.A. reviewed and edited the final manuscript. All authors read and approved the final manuscript.

3.2 Abstract

Background: Transgenes deliver therapeutic payloads to improve oncolytic virus immunotherapy. Transgenes encoded within oncolytic viruses are designed to be highly transcribed, but protein synthesis is often negatively affected by viral infection, compromising the amount of therapeutic protein expressed. Studying the oncolytic herpes simplex virus-1 (HSV1), we found standard transgene mRNAs to be suboptimally translated in infected cells.

Methods: Using RNA-Seq reads, we determined the transcription start sites and 5'leaders of HSV1 genes and uncovered the US11 5'leader to confer superior activity in translation reporter assays. We then incorporated this 5'leader into GM-CSF expression cassette in oncolytic HSV1 and compared the translationally adapted oncolytic virus with the conventional, leaderless, virus in vitro and in mice.

Results: Inclusion of the US11 5'leader in the GM-CSF transgene incorporated into HSV1 boosted translation in vitro and in vivo. Importantly, treatment with US11 5'leader-GM-CSF oncolytic HSV1 showed superior antitumour immune activity and improved survival in a syngeneic mouse model of colorectal cancer as compared with leaderless-GM-CSF HSV1.

Conclusions: Our study demonstrates the therapeutic value of identifying and integrating platform-specific cis-acting sequences that confer increased protein synthesis on transgene expression.

3.3 Introduction

The use of viruses to deliver therapeutic payloads is becoming increasingly important in various biomedical applications such as viral vector-based vaccines, gene therapies, and oncolytic viruses (OVs).[1–3] In the case of OVs, high intratumoural transgene expression is crucial to elicit optimal antitumour immune responses[4] and therapeutic efficacy.[5 6] Consequently, OV platforms in clinical and preclinical development are engineered to encode one or more of the following: (1) immunomodulatory host proteins or tumour-associated antigens that can amplify antitumour immune responses, (2) suicide proteins intended to induce cancer cell death, and/or (3) reporter proteins that facilitate tracking and dosing (e.g., green fluorescent protein or luciferase).[7–10]

The components of a transgene expression cassette incorporated into a viral vector typically encode the transgene as an intron-less open reading frame (ORF—encoding the desired therapeutic payload) flanked by an upstream promoter and ended with a poly(A) signal.[11] Remaining sequences from the multiple cloning sites (MCS) between the transcription start site (TSS) following the promoter and the start codon, or the stop codon and poly(A) signal, act as short 5'UTR and 3'UTR, respectively. Much effort is spent on ensuring high transgene transcription in infected cells by incorporating a strong host promoter such as those from human phosphoglycerate kinase (PGK) or elongation factor 1α (EF1α), or from viruses such as the cytomegalovirus (CMV) immediate early promoter.[11] However, any bottlenecks in the subsequent translation of the transgene mRNA into protein have not been thoroughly investigated under the assumption that differences in the rate of translation would be nominal if the transcript is highly expressed. The innate antiviral response to the presence of replicating viruses challenges this assumption; dramatic changes in the subset of translated mRNAs are observed in infected cells, with replicating viruses actively reshaping the host protein synthesis machinery to favor the production of viral proteins while impeding those of their host.[12 13] Thus, the translation rate of non-viral transgene mRNAs is likely to be altered in infected cells. Ultimately, this could result in suboptimal transgene protein production and consequently compromise the therapeutic potential of the oncolytic viral therapy. An example is the expression cassette of GM-CSF in T-Vec: in a phase I clinical trial, detected GM-CSF levels from fine needle aspirates of several different tumour types plateaued or fell below detection at a mid-range dose, suggesting that expression is suboptimal in humans.[14] In another phase I trial, a clinical oncolytic vaccinia virus candidate also

engineered to express GM-CSF, Jennerex-594 (JX594), failed to elicit detectable GM-CSF with low doses of intravenously injected virus (10^5–10^6 viral plaque-forming units; pfu per kg); in stark contrast, an order of magnitude increase in viral dose yielded a positive detection of this therapeutic protein.[15] The requirement to increase dosing is, however, inopportune, as it is desirable to minimize viral dose to improve the safety profiles of these promising viral therapies. In other words, there is a want to increase the specific activity of an OV, enhancing the targeting and expression of its transgene(s) while reducing the accompanying toxic effects of its vector.

Recent studies revealed various translation enhancer motifs found in the 5'leader sequences of viral mRNAs, including non-templated poly(A) leaders in poxviruses[16 17] or ICP27-interacting motifs in herpes simplex virus-1 (HSV1) mRNA 5'leaders that facilitate nuclear export.[18 19] Viral internal ribosome entry sites such as those based on encephalomyocarditis virus (EMCV) are also used in recombinant gene expression to enhance translation of downstream ORFs.[20] However, the inclusion of translation enhancers has not been reported for clinically relevant OVs, including oncolytic poxviruses and HSV1. For example, T-VEC GM-CSF expression cassette does not contain a functionally authentic viral 5'leader, but residual cloning sequences of approximately 100 bp originating from the MCS of the plasmid pcDNA3 used in the cloning process.[21] We reasoned that the synthesis of therapeutic payloads from replicating oncolytic platforms may be enhanced by the incorporation of a viral 5'leader. Using RNA-Seq data of HSV1-infected cancer cells, we sought to identify HSV1 5'leaders that mediate high translation efficiency of downstream cistron mRNAs during viral replication. The 5'leader of the HSV1 late gene US11 increased translation of a downstream cistron in heterologous reporter constructs and, notably, this effect was only observed with concomitant HSV1 infection. HSV1 engineered to express a cassette containing the US11 5'leader upstream of the GM-CSF ORF conferred superior GM-CSF protein expression in several mammalian cell lines and dramatically improved antitumour efficacy and prolonged survival *in vivo* compared with its leaderless counterpart. Our study thus presents an opportunity to enhance therapeutic payload protein expression from oncolytic HSV1 platforms by incorporating a viral 5'leader into the expression transgene cassette.

3.4 Methods

Cell culture and viruses

The mouse breast cancer cell line 4T1, mouse colon cancer carcinoma CT26, human prostate cancer DU145, human renal carcinoma 786-O, HEK293T and Vero cells were acquired from American Tissue Culture Collection. 4T1 was maintained in Roswell Park Memorial Institute (RPMI) 1640 (Fisher) supplemented with 10% fetal bovine serum (FBS) (Sigma-Aldrich) and 1X penicillin/streptomycin (Fisher). HEK293T and Vero cells were maintained in Dulbecco's Modified Eagle Medium (DMEM) (Fisher) supplemented with 10% FBS and 1X penicillin/streptomycin (Fisher). Cells were incubated at 37°C, 5% CO_2 v/v. HSV1716 (HSV1 strain 17 with γ34.5 deleted, Sorrento Therapeutics) was kindly provided by the manufacturers. HSV1 strain KOS was kindly gifted by Dr Karen Mossman. All HSV1 strains were propagated in Vero cells. A monolayer of Vero cells was inoculated with HSV1 at 0.1 MOI, then cultured for approximately 24–48 hours until close to 100% cytopathic effect was observed. Supernatant was then collected separately, and infected cells were freeze-thawed three times to release intracellular virus. Both the cultured supernatant and the freeze-thawed lysate were clarified by centrifugation at 1000 g, 5 min to remove cell debris. The supernatants were combined and filtered through a 0.45 μm filter. Virus particle was further purified using a sucrose cushion by overlaying the supernatant on top of a 36% sucrose cushion in PBS and centrifuged at 18 000 g for 2 hours, 4°C. Virus in the pellet was resuspended in HNE buffer (HEPES 10 mM, NaCl 150 mM, EDTA 0.1 mM, pH 7.2) and stored at −80°C.

RNA-Seq mapping and TSS identification

RNA-Seq data of 4T1 cells infected by HSV1 was previously published.[22] For mapping of RNA-seq, RNA reads were mapped to the HSV1 reference genome JQ780693.1 using HISAT2.[23] Only one copy of the two flanking inverted repeat regions were used: the TRL region 1-8870 and TRS region 144602-151 023 were omitted. TSS was manually identified from RNA read coverage, defined by an abrupt increase of read coverage at a base position. The leader sequence was defined as the sequence from the TSS to the annotated start codon of the associated HSV1 gene, excluding any spliced intron if applicable. For converting leader sequence coverage between different HSV1 reference genomes (JQ780693.1 to JN555585.1), the sequence of the identified leader from JQ780693.1 was aligned to JN555585.1 using NCBI-BLAST to find the corresponding coordinates on JN555585.1. Raw data were deposited and analyzed on the Galaxy

server.[24] Gene expression level from mapped RNA-seq and Ribo-seq reads was calculated using Cuffdiff.[25]

Plasmid construction

For the leader translation activity screen using the CAT reporter assay, virus leader sequences were amplified by PCR from cDNA reverse-transcribed from mRNA of HSV1 infected 4T1 cells. Briefly, total RNA was extracted from cell using TRIzol reagent (Fisher), treated with Turbo DNA-free kit (Thermo Fisher) to remove potential contamination of virus genomic DNA, then reverse-transcribed by using the iScript Advanced cDNA Synthesis Kit (BioRad). The forward and reverse primers (NotI_*5'UTR*-F and XhoI_*5'UTR*-R) of each leader also contain the restriction sites of NotI and XhoI, respectively, for subsequent cloning. Amplification specificity was confirmed for each pair of primers by including a negative control cDNA from mRNA of uninfected 4T1. The PCR amplicons were cloned into the CAT reporter plasmid pMCpA (a kind gift from Dr. Martin Holcik, Carleton University) using the NotI-XhoI restriction sites.[26] A leaderless CAT reporter construct, in which only a short residual sequence from the plasmid MCS is transcribed with the CAT CDS, was used as control (this residual sequence also present in all viral 5'leader construct, directly 5' upstream of the leader sequence). For inserting transgene expression cassette into HSV1 genome, the cassette was cloned into the pTK-Green plasmid,[27] flanked by two regions of the HSV1 TK gene to allow for homologous recombination. The expression cassette consists of the leader, followed by the transgene (firefly luciferase or mouse GM-CSF), the self-cleaving peptide porcine teschovirus-1 2A (P2A) and GFP. The insert was generated by fusion PCR. The virus leader was amplified as described above using a forward primer containing an AgeI cutting site (AgeI_*5'UTR*-F) and a reverse primer with an overlap section of the transgene 5'end (*5'UTR*_LUC-R or *5'UTR*_CSF2-R). The second fragment containing the transgene CDS was amplified using a forward primer (*5'UTR*_LUC-F or *5'UTR*_CSF2-F), and a reverse primer consisting of the CDS 3' end, a GSG linker and a part of the P2A sequence (LUC-GSG-P2A-R). The third fragment containing the GFP was amplified using a forward primer (GSG-P2A-GFP-F) and a reverse primer that included a KpnI cutting side (GFP-KpnI-R). All three fragments were purified using the QIAquick PCR Purification Kit (Qiagen), then used as templates for fusion PCR using the 5'-most (AgeI_*5'UTR*-F) and 3'-most primer (GFP-KpnI-R). The resulting PCR product was cloned into the pTK-Green using AgeI and

XhoI sites. A leaderless LUC-GFP or CSF2-GFP construct, in which only a short residual sequence from the plasmid MCS is transcribed with the transgene CDS, was used as control (this residual sequence was also present in all viral 5'leader constructs, directly 5' upstream of the leader sequence). All plasmids were verified by Sanger sequencing.

CAT reporter assay

CAT reporter assay was performed as previously described.[22] Cells were seeded at approximately 75% confluency in a 6-well plate and incubated for 1 day before transfection. In the case of HSV1 infection, cells were infected with HSV1 at 5 MOI 1 hour before transfection. CAT reporter plasmid was co-transfected with β-Galactosidase plasmid (pBGal, a kind gift from Dr. Martin Holcik, Carleton University[26]) at 1 μg per each plasmid using Lipofectamine 2000 (Thermofisher) according to the manufacturer's protocol. Cells were lysed 24 hours post-transfection and assayed for CAT expression using the CAT ELISA kit (Roche). β-Galactosidase activity was also measured from lysate using ortho-Nitrophenyl-β-galactoside colourimetric assay. CAT expression was normalized to β-Galactosidase activity to control for transfection efficiency.

Quantitative RT-PCR

DNase-treated RNA and cDNA were prepared as described above. For RT-qPCR, SsoAdvanced Universal SYBR Green supermix (BioRad) was used with a CFX96 Touch Real-Time PCR Detection System (BioRad). The PCR condition was 95°C for 3 min, followed by 40 cycles of 95°C for 10 s and 60°C for 30 s, and ended with a standard melting curve cycle. Gene expression was calculated using the ΔΔCt method against the indicated reference genes. The list of primers for the genes or sequences of interest is in supplemental table S3.1.

Western blot

Cells were washed once with 1X PBS, then lysed on ice using RIPA buffer (150 mM NaCl, 1.0% IGEPAL CA-630, 0.5% sodium deoxycholate, 0.1% SDS, 50 mM Tris, 50 mM NaF, 15 mM $NaVO_3$, pH 8.0) supplemented with cOmplete Protease Inhibitor Cocktail (Roche). Lysate was centrifuged at 10,000 g, 10 min at 4°C to remove cell debris. Protein concentration was determined using the DC Protein assay kit (BioRad). An indicated amount of total protein was used for SDS-polyacrylamide gel electrophoresis (PAGE) using 10% SDS-polyacrylamide gel. Separated protein was transferred to PVDF membrane; the membrane was blocked with 5% w/v skim milk

in TBS-T buffer (10 mM Tris, 50 mM NaCl, 0.1% Tween-20, pH 7.5) and then blotted for the indicated antibody. The following antibodies and corresponding dilution were used: anti-GFP (Abclonal, CAT#AE011) at 1:2000, anti-β-actin (Sigma, #A5441) at 1:10,000, IRDye 800CW Goat anti-Mouse IgG Secondary Antibody (LICOR, CAT#926-32210) at 1:20,000 and IRDye 680RD Goat anti-Rabbit IgG Secondary Antibody (LICOR, CAT#926-68071) at 1:20,000.

Live-cell monitoring of GFP expression

Live-cell monitoring of GFP expression was performed using the IncuCyte Live-Cell Monitoring system (Sartorius). Transfection and/or infection were performed as indicated, then cell plates were placed inside the IncuCyte system and cultured and monitored at 37°C, 5% CO_2 with phase contrast and fluorescent images taken every 2 hours. Images were analyzed with the IncuCyte ZOOM software using the following parameters: background subtraction using Top-Hat method (disk shape structuring element with radius of 10 μm, threshold of 1.0 green calibrated unit), edge split: Off, Hole Fill: No, Adjust Size: No, Filters: No.

Generating recombinant HSV1 viruses

For inserting the expression cassette into HSV1 genome, we targeted the TK gene for insertion as previously described.[27] HSV1 genomic DNA was extracted from purified virus stock using the QIAamp DNA mini kit (Qiagen). HEK293T cells were seeded at 75% confluency 1 day before in six-well plates and then co-transfected with HSV1 gDNA:pTK-Green plasmid at a ratio of 1:40, for a total amount of 1 μg DNA/well, using Lipofectamine 2000 (Thermo Fisher) according to manufacturer protocol. Cells were then cultured for 3–5 days until cytopathic effect was observed. Cells were then freeze-thawed three times, centrifuged at 1000 g, 5 min to remove cell debris and supernatant was collected. Supernatants at various dilutions were then inoculated to a monolayer of Vero cells in order to separate individual plaques overlaid with DMEM supplemented with 10% FBS and 1% carboxymethylcellulose (CMC) to allow for the development of individual plaques. GFP-positive plaques were selected and subjected to multiple plaque purification rounds until a pure GFP-expressing HSV1 population was obtained. Insertion of the cassette into HSV1 genome was confirmed first by PCR genotyping using a forward primer on the TK gene (pTK-seq) and a reverse primer on the transgene (CSF2.e-R), followed by Sanger sequencing.

Plaque titration

Virus stock or solution was serially diluted, then inoculated a monolayer of Vero cells and incubated for 1 hour, 37°C, 5% CO_2 with frequent shaking. The virus-containing media was then removed and an overlay of DMEM + 10% FBS + 1% agar was added. Cells were then cultured at 37°C, 5% CO_2 until visible plaques could be observed using a brightfield microscope. Plaques were visualized using crystal violet staining and counted.

Polysome fractionation

Polysome fractionation was performed as previously described.[28] Briefly, cells were treated with cycloheximide (CHX) (Bioshop, CAT #66-81-9) at 100 µg/mL for 5 min to stop ribosomes, washed three times with ice-cold PBS supplemented with CHX (100 µg/mL) and lysed using polysome lysis buffer (5 mM Tris pH 7.5, 2.5 mM $MgCl_2$, 1.5 mM KCl, 100 µg/mL CHX, 2 mM DTT, 0.5% Triton X-100, 0.5% sodium deoxycholate) supplemented with 100 units RNAsin Ribonuclease inhibitor (Promega). Cell debris was cleared by centrifugation at 14,000 g for 10 min, 4°C. Supernatant was then loaded on a 10%–50% continuous sucrose gradient and centrifuged at 36,000 rpm, 90 min at 4°C in an SW41Ti rotor. Fractions were then collected, and the OD260 absorbance of fractions was monitored using a Brandel Fraction Collector System (Brandel). RNA was extracted from each fraction using TRIzol reagent (Thermo Fisher) according to the manufacturer's protocol.

GM-CSF quantification

To measure GM-CSF production from engineered HSV1 infection, cells were seeded at 80%–90% confluency and then infected with the indicated HSV1 at a MOI of 5. 24 hours postinfection, culture supernatant was collected and GM-CSF production was measured using the Mouse GM-CSF ELISA Kit (CSF2) (Abcam, CAT #ab100685) according to the manufacturer's protocol.

Single step-growth curve and monitoring HSV1 genes expression

For monitoring virus replication and viral gene transcription during a single-step growth curve, cells were seeded at 80%–90% confluency and infected the next day at a MOI of 5. Both cells and culture supernatant were collected at the indicated time points and used for virus titration

by plaque assay or RNA extraction for quantification of viral transcript expressions as described above.

CT26 subcutaneous tumour model

Female BALB/c were ordered from Charles River (Kingston, New York, USA). Animals were received at 5–6 weeks old, housed at 5 per cage, fed ad libitum, and acclimated to the facility for 2 weeks before experimental manipulation. For tumour implantation, 10^5 CT26 cells were injected subcutaneously into both flanks of the mouse. When tumours were palpable (~5×5 mm), the tumour on one flank was injected twice, 1 day apart, intratumourally with 50 µL DMEM or 5×10^5 PFU of the indicated virus, while the tumour on the other flank was left untreated (contralateral). Tumour sizes were measured every 2 days using a caliper. Animals were euthanized when an individual tumour reached 2000 mm^3, or at an alternate humane endpoint. The *in vivo* study was done single-blinded: the animal handler did not know the treatment given to each mice group. For assessing intratumoural GM-CSF level and HSV1 transcript abundance, tumours were excised and homogenized in PBS buffer using 2.0 mm zirconia beads (Thomas Scientific, CAT # 1197P96) with a TissueLyzer II (QIAGEN) at 20 Hz/s. Half of the homogenate was used for measuring GM-CSF using the Mouse GM-CSF ELISA Kit (CSF2) (Abcam, CAT #ab100685) according to the manufacturer's protocol. The other half of the homogenate was used for RNA extraction with Trizol Reagent (Thermo Fisher), and then the transcript mRNA was quantified by RT-qPCR as described above.

IFNγ ELISPOT assay

Splenocytes were isolated freshly from spleens of mice 8 days after the first injection and cultured in RPMI (Fisher) supplemented with 10% FBS (Sigma-Aldrich) and 1X penicillin/streptomycin (Fisher). IFNγ ELISPOT was done using the mouse interferon-gamma ELISPOT kit (Abcam, CAT# ab64029) according to the manufacturer's protocol. Briefly, 100,000 splenocytes were co-cultured with/without 50,000 UV-irradiated CT26 in the ELISPOT well for 24 hours. Cells were then thoroughly washed away from the well, and IFNγ spots from stimulated T-cells were developed. Individual wells were imaged using the stereomicroscope LEICA EZ4 W, and spots were counted manually.

Data and code availability

The RNA-seq data were published previously[22] and are available on the NCBI Gene Expression Omnibus (GEO: GSE137757), sample IDs GSM4086602 and GSM4086610 (HSV1 infected mRNA replicate).

Statistical analyses

All experiments were performed in at least three biological replicates. Statistical analyses were performed using GraphPad Prism V.8, using the method indicated in figure legends. Error bars indicate SD. $^{*}p<0.05$, $^{**}p<0.01$, $^{***}p<0.001$, $^{****}p<0.0001$, ns, non-significant.

3.5 Results

Determining HSV1 mRNA 5'leader sequences

HSV1 is an enveloped dsDNA virus with a 153 Kb genome arranged in covalently linked long (L) and short (S) segments that collectively encode approximately 80 genes.[29] Several single-gene studies identified and characterized the 5'leaders and 3'untranslated regions (3'UTRs) of a limited number of HSV1 genes[30–36] (see table 3.1). Most transcripts, however, have no such annotations in the public NCBI database (e.g., NCBI accession number JQ780693 for strain KOS and JN555585 for strain 17). We previously generated RNA-Seq data of HSV1 infected 4T1 murine breast cancer cells.[22] The HSV1 reads from this RNA-seq data can be used to identify and assess translationally active 5'leader (figure 3.1A). By mapping the HSV1 reads from this dataset to the KOS strain reference genome (JQ780693.1), we can distinguish RNA transcripts originating from each of the positive and negative gDNA strands (figure 3.1B). We can also discern the splice junctions of the four known spliced transcripts of HSV1 (i.e., UL15, US1, US12 and RL2) and the intron retention that was previously reported for RL2 (supplemental figure 3.1).[37]

Identification of transcription start sites (TSS) from long-read sequencing techniques (e.g., PacBio methods)[38] or full transcript sequencing (e.g., Oxford Nanopore MinION platform)[39] can be more straightforward than RNA-Seq that relies on aligning short reads, especially when there are overlapping ORFs present. However, we found that standard RNA-Seq read mapping can sufficiently identify the TSS for HSV1 genes. We scored TSS locations by monitoring for a 'wall' of stacked short reads that we interpreted as the start of a transcript (figure 3.1C,D). Whisnant *et al* have recently used a similar strategy to enumerate the HSV1 TSS, though their methods require more specialized RNA-Seq methods.[40] We detected reads that flanked the 5' and 3' ends of most

annotated ORFs (figure 3.1D,E, respectively), confirming that all annotated HSV1 transcripts harbor both a 5'leader and a 3'UTR. Although the 3'UTRs of a large portion of the viral genes overlapped with a downstream ORF, a spike in read density at a single nucleotide position upstream of the start codon consistent with a TSS could be clearly distinguished across 5'leaders (figure 3.1C, insets and table 3.1, the read density coverage at each identified TSS are shown in supplemental figure 3.2). Using these TSS coordinates, we identified 61 5'leader sequences of HSV1 genes (table 3.2). Importantly, when comparing the identified TSSs with the few annotated in NCBI, more recently identified by long-read sequencing done by Tombácz *et al*,[38] or RNA-Seq on enriched 5' end reads by Whisnant *et al*,[40] we found that the coordinates of the TSSs were exact or differed by only a few nucleotides (table 3.1). These studies confirmed our approach to robustly detect and confidently annotate each HSV1 transcript 5'leader.

The US11 5'leader enhances the translation of downstream ORFs in HSV1-infected cells

Having identified the 5'leader sequences of most HSV1 genes *in silico*, we next sought to determine their ability to modify the translation output of a downstream cistron. We hypothesized that the 5'leaders of HSV1 late genes expressed in an established infection stage should be best adapted to the altered translation control of HSV1 infection. We selected ten late genes for testing the translation modification effect of their 5'leader in HSV1 infected cells (supplemental figure 3.3).[41] HSV1 5'leaders of selected late genes were amplified from a cDNA library generated from HSV1-infected 4T1 cells and inserted upstream of the chloramphenicol acetyltransferase (CAT) reporter construct[42] (figure 3.2A and supplemental figure 3.4A). We performed the translation reporter assay under uninfected and HSV1-infected conditions by cotransfecting 4T1 cells with monocistronic plasmids expressing CAT and β-galactosidase postinfection, the latter construct included to standardize differences in transfection efficiency. In uninfected cells, the viral 5'leaders had both positive and negative effects on reporter expression, though no statistically significant differences were observed (figure 3.2B). The US11 5'leader was highest in augmenting the translation of CAT mRNA reporter. In contrast, the 5'leaders of UL1 and US8 were found to have none to inhibitory effects during HSV1 infection (supplemental figure 3.4B). However, following HSV1 infection, we found that US11 and UL27 5'leaders significantly enhanced CAT protein expression (figure 3.2B) compared with the reporter lacking a leader (leaderless). Importantly, these observations are not through 5'leader-mediated upregulation of CAT mRNA transcription

(figure 3.2C). We also predicted the folding free energy and potential secondary structure of the US11 and UL27 leaders (supplemental figure 3.4C) and the folding free energy of other screened HSV1 leaders (supplemental figure 3.4D). We found that despite having the strongest enhancement on CAT protein expression, the 5'leaders of US11 and UL27 have low predicted folding free energy compared with other HSV1 5'leaders. Together, these results suggest that the 5'leader sequences from US11 or UL27 mRNAs can mediate HSV1 infection-dependent increases in protein expression when inserted upstream of a transgene in cells.

Lytic infection by HSV1 induces a profound reprogramming of cellular transcription, splicing and nuclear export.[41 43] Thus, a plasmid-based overexpression reporter assay might be compromised by HSV1 infection and not faithfully reflect gene expression processes, including mRNA translation, of HSV1-encoded transgenes. Focusing on the US11 5'leader, we next investigated the effect of the US11 5'leader on regulating transgene expression directly from expression cassettes designed to be inserted within the *tk* locus of the HSV1 genome.[27] Briefly, transcription from the pTK plasmid expression cassette is driven by a CMV promoter and includes a SV40 polyadenylation signal (figure 3.2D). A bicistronic transgene cassette was created to allow concomitant expression of the therapeutic protein along with a reporter protein to facilitate recombinant virus selection and monitoring, all under the control of putative enhancer elements inserted at the 5'end of the expression cassette (figure 3.2D). The ORFs consist of luciferase (*luc*, which can be replaced with a desired therapeutic ORF) and *gfp* separated by the self-cleaving peptide porcine teschovirus-1 2A (P2A).[44 45] Western blot analysis of transfected cell lysates showed that inclusion of the US11 5'leader confers an increase in GFP protein levels in HSV1-infected cells (figure 3.2E,F). Consistent with our previous results, incorporation of the US11 5'leader did not affect levels of the *gfp* transcript in uninfected compared with HSV1-infected cells (figure 3.2G). GFP fluorescence was also quantified in 4T1 cells transfected with the leaderless plasmid or a plasmid harboring the US11 5'leader and subsequently infected with or without HSV1. Consistently, low fluorescence was observed in leaderless and uninfected cells, while HSV1 infection induced GFP fluorescence in the US11 5'leader construct (figure 3.2H).

The US11 5'leader enhances transgene protein expression from engineered HSV1 virions

To validate the potential of the US11 5'leader as a transgene enhancer, we constructed recombinant HSV1 strains based on the bicistronic pTK transgene expression plasmid described

above. The linearized pTK plasmid can be used to generate recombinant viruses following cotransfection with purified HSV1 genomic DNA. Homologous recombination of the expression cassette into the *tk* locus produces Δ*tk* virus progeny expressing the transgene in a constitutive manner under the CMV promoter (figure 3.3A). To better demonstrate the clinical potential, we replaced the *luc* ORF in the *luc-gfp* cassette with the *Csf2* (GM-CSF) ORF, a gene that is virally expressed in the FDA-approved oncolytic HSV1.[46] We generated a leaderless (HSV1 leaderless-Csf2) virus along with two virus clones incorporated with the US11 5'leader (HSV1 US11-Csf2) (figure 3.3B). In agreement with the enhanced expression of GFP conferred by the US11 5'leader in the plasmid-based systems, plaques on Vero cells of HSV1 US11-Csf2 showed elevated GFP fluorescence compared with plaques of HSV1 Csf2 (figure 3.3C). Cells infected with the HSV1 US11-Csf2 virus produced ~7–8 fold more GM-CSF compared with cells infected with HSV1 leaderless-Csf2 (figure 3.3D, supplemental figure 3.5). To assess if enhanced GM-CSF production is a result of higher viral replication, we measured replication kinetics by single-step growth curves and found that all virus clones exhibit comparable replication kinetics (figure 3.3E). RT-qPCR of mRNAs extracted from infected cells at various time points revealed that the presence of the 5'leader affected neither the expression kinetics of the HSV1 transcript US6 (figure 3.3F left panel) nor that of the transgene transcripts expressed in cis (*Csf2* and *gfp*, figure 3.3F middle and right panel) over the course of infection. To understand whether transgene-enhanced protein production might be a cell-type or species-dependent effect, we infected the human prostate cancer line DU145 and the human renal cell carcinoma line 786-O with wildtype, US11 5'leader, and leaderless viruses. Monitoring of GFP fluorescence intensity in these cells over the course of infection revealed a robust US11 5'leader-mediated enhancement of transgene protein expression in all cell lines tested (supplemental figure 3.6). These results demonstrate the ability of the US11 5'leader to augment the production of a clinically relevant therapeutic transgene in HSV1-infected mammalian cells.

The HSV1 US11 5'leader increases translational efficiency of associated transcript in a HSV1-dependent manner

We next sought to identify the mechanism underlying the increased expression of GM-CSF in cells infected with HSV1 US11-Csf2. We assessed whether the US11 5'leader has a bona fide effect on mRNA translation of the transgene by using the polysome profiling technique.

Briefly, ribosome-bound mRNAs were separated by ultracentrifugation on a sucrose gradient, which causes mRNAs to sediment based on the number of bound ribosomes. Accordingly, mRNAs that migrate toward heavier sucrose gradients have more bound ribosomes and higher translation efficiency. Vero cells were infected with HSV1 leaderless-Csf2 or HSV1 US11-Csf2 at a MOI of 5 (figure 3.4A), then the lysate containing ribosome-bound mRNAs was resolved on a 10%–50% sucrose gradient (figure 3.4B). We found that the presence of the US11 5'leader caused a shift of the *Csf2-gfp* transcript distribution toward heavier polysome fractions, demonstrating enhanced translation efficiency compared with the leaderless *Csf2-gfp* transcript (figure 3.4C,D). Interestingly, the *US6* and *US11* viral mRNAs are mostly distributed to the heavier polysome fractions (figure 3.4C,D), suggesting that HSV1 transcripts are generally highly translated despite the global shutoff of protein synthesis resulting from HSV1 infection.[22] Notably, without the US11 5'leader, the leaderless transgene *Csf2-gfp* mRNAs are suboptimally translated compared with the *US6* and *US11* viral mRNAs (supplemental figure 3.7A,B). To address whether the translation enhancement mediated by the US11 5'leader is specific for HSV1 infected cells or a result of a general antiviral state, we tested GFP expression from the plasmid pTK-*Csf2-gfp* in Vero cells transfected with the dsRNA mimic poly(I:C) or infected with another virus, VSV. We observed that neither poly(I:C) transfection nor VSV infection were capable of inducing GFP expression (figure 3.4E). Thus, the enhancement of US11 5'leader on gene expression appears to be specific to HSV1 infected cells. These data suggest that traditional transgene cassettes that lack *cis*-acting translation enhancing elements are suboptimally translated when compared with HSV1 endogenous transcripts. These data also demonstrate that incorporation of the HSV1 US11 5'leader can significantly and specifically improve translation of HSV1-encoded transgenes.

The US11 5'leader improves the antitumour effect of GM-CSF expressing HSV1 *in vivo*

A critical question is whether boosting the expression of a transgene beyond that achieved by current oncolytic HSV1 platforms ameliorates cancer outcomes. To answer this, we used the CT26 syngeneic tumour model of colon carcinoma that is routinely used to assess the efficacy of oncolytic HSV1.[47 48] Tumours were generated on both flanks of the mice, and tumour on one side was injected with resuspension buffer or 5×10^5 viral particles of HSV1 leaderless-Csf2 or HSV1 US11-Csf2 (figure 3.5A). Incorporating the US11 5'leader enhanced the intratumoural GM-CSF protein expression in treated animals by more than twofold (figure 3.5B), while both viruses shared

similar replication kinetics *in vivo* as shown by comparable transcription levels of the viral genes US6 and UL30 (figure 3.5C). This result suggests that while both viruses had similar infection rates, increased GM-CSF production was observed in HSV1 US11-Csf2 infected tumours. GM-CSF is known to be a proinflammatory cytokine but might exert anti-inflammatory properties in certain contexts.[49] Thus, we probed the tumour microenvironment of infected tumours by analyzing mRNA levels of representative inflammatory genes and found elevated levels of *Il1b*, *Il6,* and *Tnfa* mRNAs, and a statistically insignificant decrease of the immune suppressor gene *Arg1* in tumours treated with HSV1 US11-Csf2 (figure 5C). This observation suggests that HSV1 US11-Csf2 can induce a more inflammatory tumour microenvironment, even at the same treatment dose and growth rate as the leaderless virus. We also analyzed systemic antitumour response on the eighth day after the first injection by IFNγ ELISPOT on splenocytes co-cultured with UV-irradiated CT26 cells. We found no CT-26-specific immune cell response in the spleen of vehicle-treated mice, while the leaderless HSV1 was capable of inducing a certain level of CT26-specific immune cells. However, the HSV1 US11-*Csf2* induced a significantly higher CT26-specific T-cell response compared with the leaderless virus (figure 3.5D, supplemental figure 3.8). Finally, we directly compared the antitumour effect of both viruses (figure 3.5E, supplemental figure 3.9). As expected, regardless of viral clone, HSV1-injected tumours showed decreased growth relative to vehicle-injected tumours (figure 3.5F), a result consistent with the oncolytic and immunomodulatory properties of this viral platform.[14 47 50] Importantly, the growth of tumours injected with the US11 5'leader virus was significantly lower than that of tumours injected with the leaderless virus (figure 3.5F, left panel). More interestingly, treatment with the leaderless virus had no significant effect on the contralateral tumours, while treatment with the US11 5'leader virus significantly slowed tumour growth on the contralateral side, comparable to that observed in the treated one (figure 3.5F, right panel); suggesting an abscopal effect consistent with the elevated antitumour immune response observed by ELISPOT. Finally, we found that the US11 5'leader virus significantly improved mouse survival (figure 3.5G). Collectively, these data demonstrate that increasing the expression of GM-CSF via incorporation of the translation-enhancing US11 5'leader augments intratumoural cytokine production and boosts anticancer efficacy in a preclinical colon cancer model.

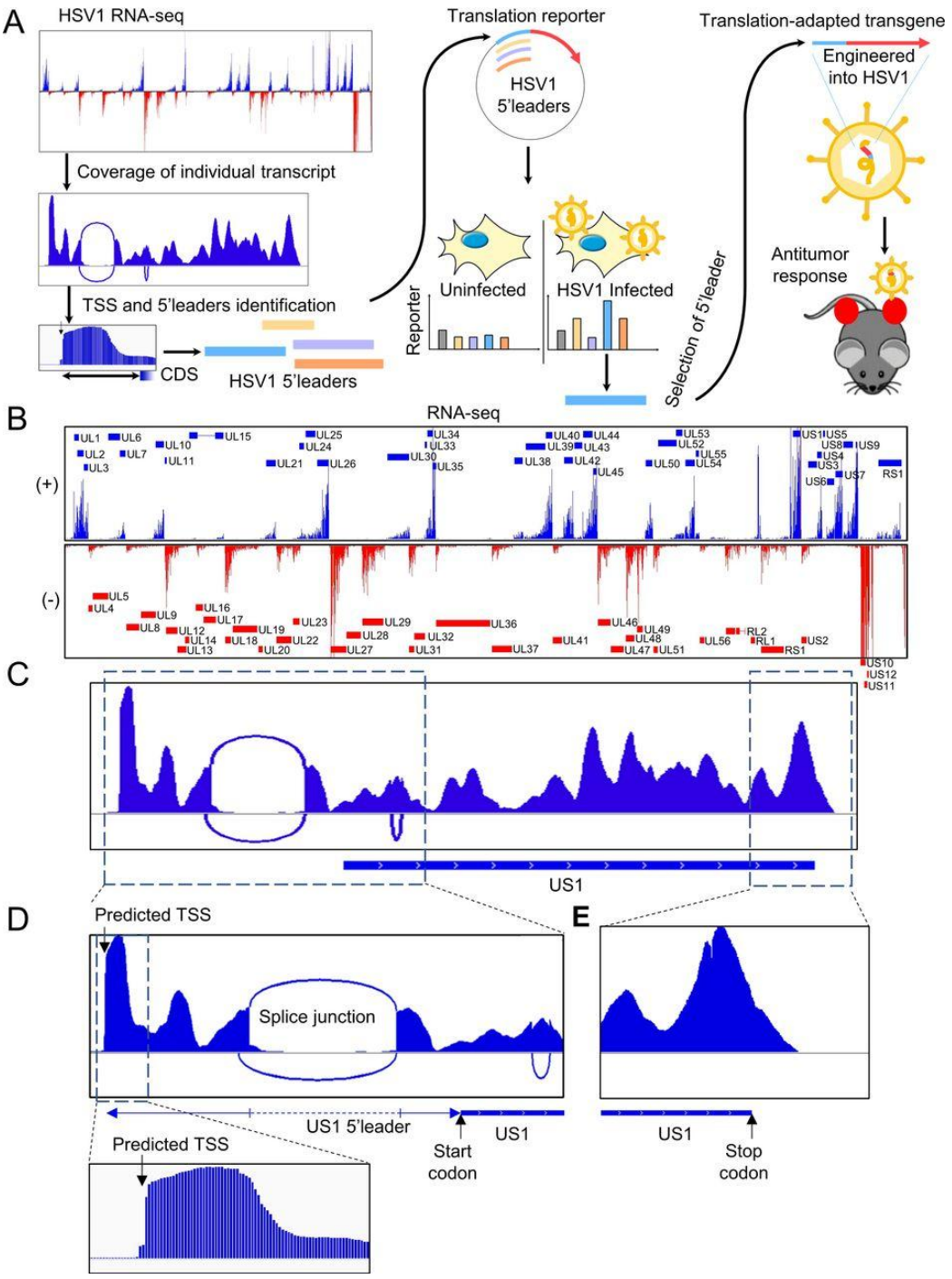

Figure 3. 1. Characterizing HSV1 individual transcript from RNA-seq coverage.

(A) Schematic overview of the workflow to identify HSV1 5'leaders from RNA-seq read, screen for translation enhancing 5'leaders specifically in HSV1-infected cells, and incorporate the 5'leader into transgene expression in an oncolytic HSV1 genome to test in a tumour model in vivo. (B) Total RNA-seq coverage of the HSV1 genome from 4T1 infected cells. Strand-specific RNA reads were mapped to HSV1 genome and separated by strand direction to avoid ambiguous mapping of overlapping genes. (C) RNA-seq coverage of the US1 gene. Intron-spanning reads were also detected and shown using Sashimi plot. (D) RNA-seq coverage in the 5' region of US1 gene. Lower plot shows the region of the predicted TSS at nucleotide resolution. (E) RNA-seq coverage at the 3' region of US1 gene. TSS, transcription start site.

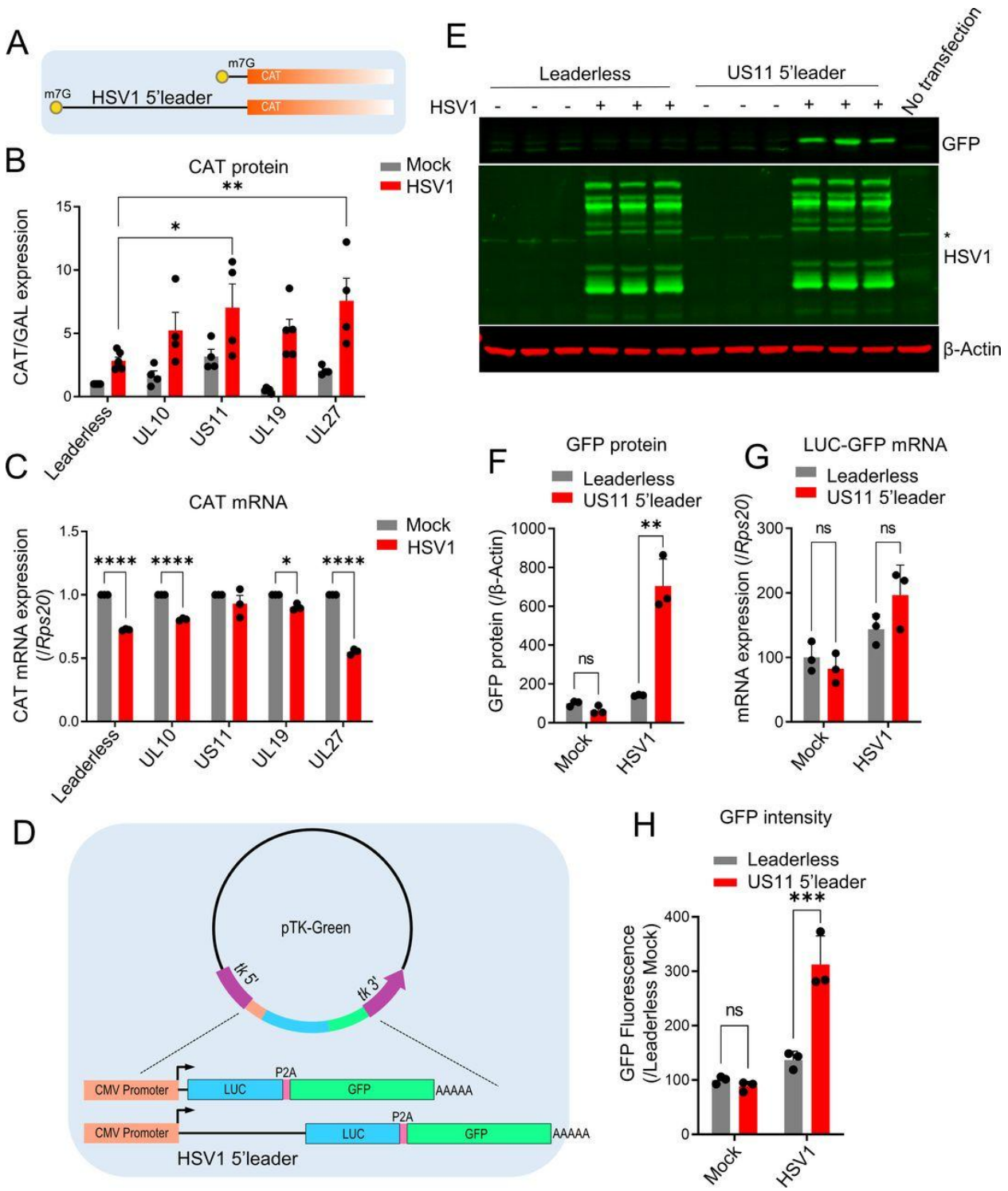

Figure 3. 4. HSV1 US11 5'leader sequence enhances expression of protein reporters in HSV1-infected mammalian cells.

(A) Schematic diagrams of the mRNAs expressed from CAT reporter construct without/with HSV1 5'leader. (B) Translation reporter assay to screen for HSV1 5'leader sequences that enhance translation during HSV1 infection. 4T1 cells were infected with HSV-1716-GFP at a MOI of 5,

then transfected with the CAT plasmid and a β-GAL expression plasmid that serves as a transfection control. Cells were lysed 24 hours post-infection and CAT expression was quantified by ELISA, while β-GAL activity was quantified by colorimetric assay using ortho-Nitrophenyl-β-galactoside substrate. Two-way ANOVA with Tukey's post-hoc test was performed. Only significant tests were shown. n=at least 3 biological replicates. Error bars: ±SD *p<0.05, **p<0.01. (C) Relative CAT mRNA expression from CAT translation reporter assay. 4T1 cells were treated as in (B), then lysed using Trizol. RT-qPCR was then used to quantifie mRNA expression of CAT mRNA normalized to the expression of *Rps20*. Two-way ANOVA with Sidak's post-hoc test was performed. n=3 biological replicates. Error bars: ±SD. *p<0.05, **p<0.01, ****p<0.0001. (D) Schematic diagram of the pTK-Green plasmids that harbor the HSV1 5'leader-reporter construct for insertion into the HSV1 TK gene and the resulting transcripts. The ribosome skipping sequence P2A is inserted between the luciferase CDS and GFP CDS, which allowed for synthesis of 2 proteins from one cistron. (E) Western Blot of lysates from 293T cells that were treated as in (B) with antibodies against GFP, HSV1 or β-Actin. (*): non-specific band. (F) Quantification of GFP expression from the Western Blots in (E). Two-way ANOVA with Sidak's post-hoc test was performed. n=3 biological replicates. Error bars: ±SD. *p<0.05, **p<0.01, ****p<0.0001. (G) RT-qPCR quantification of LUC-GFP mRNAs from the same experiment. Two-way ANOVA with Sidak's post-hoc test was performed. n=3 biological replicates. Error bars: ±SD. *p<0.05, **p<0.01, ****p<0.0001, ns, non-significant. (H) Quantification of GFP fluorescence. Cells were transfected with LUC-GFP reporter plasmid, then infected with the HSV1 (KOS strain) 4 hours post-transfection at a MOI of 2.5. Images were taken at 24 hours postinfection. ANOVA, analysis of variance; MOI, multiplicity of infection.

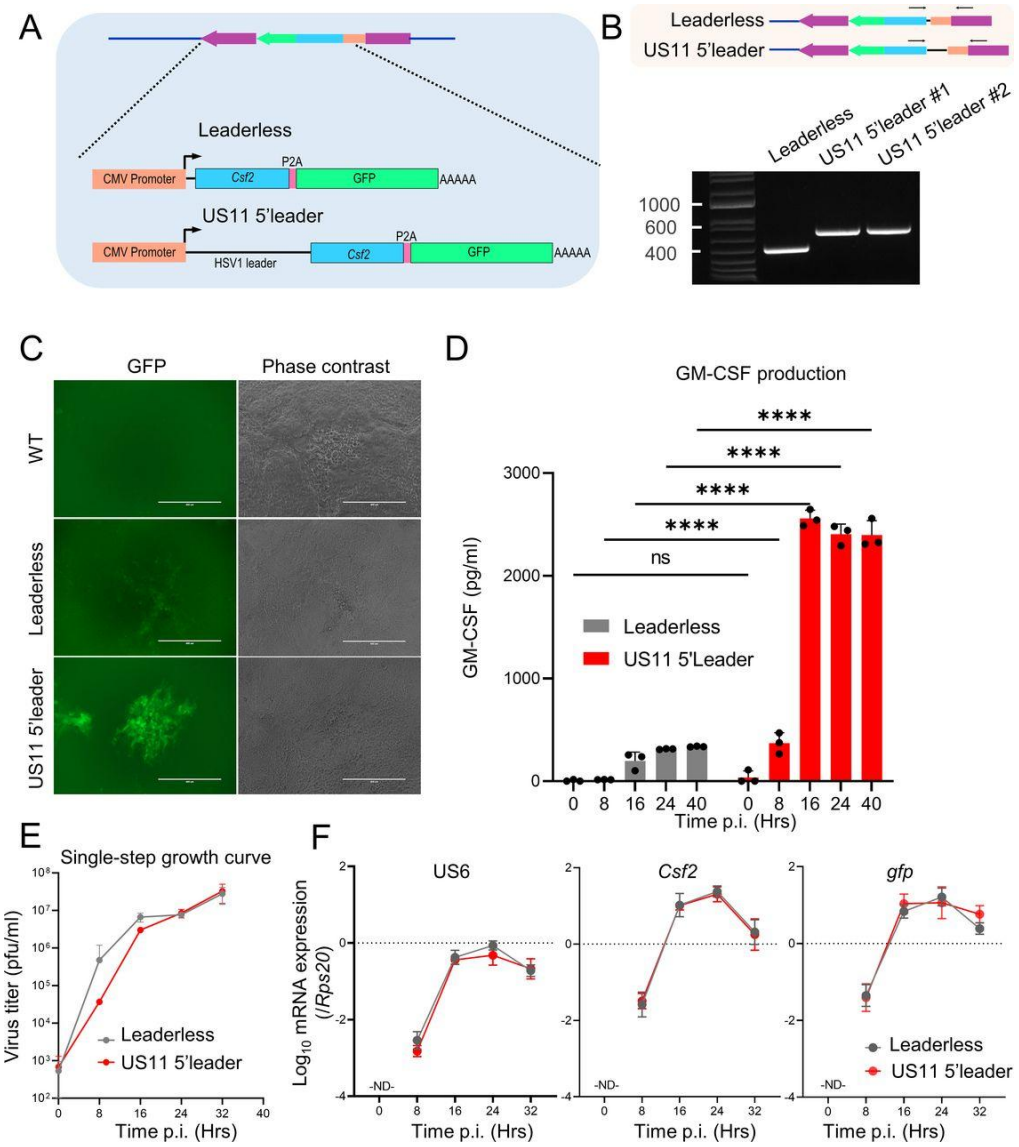

Figure 3. 5. A recombinant HSV1 virus exhibits a US11 5'leader-dependent boost in GM-CSF expression.

(A) Schematic illustration of the expression cassette insertion scheme from the pTK-CSF2-GFP plasmid into HSV1 genome (note that the TK gene is on the minus strand), and the resulting transcripts expressed from the inserted cassette. (B) Virus genotyping for confirmation of expression cassette insertion. PCR was done using HSV1 gDNA extracted from purified viruses to confirm the insertion of the leaderless CSF2-GFP cassette (~400 bp) and US11 5'leader-CSF2-GFP cassette (~600 bp) into the TK region of HSV1 genome. (C) Fluorescence imaging of individual plaques of wild-type HSV1, HSV1 Csf2 and HSV1 US11-Csf2. (D) Quantification of GM-CSF production in culture supernatant of Vero cells infected with HSV1 expressing leaderless CSF2-GFP or US11 5'leader-CSF2-GFP. Monolayers of Vero cells were infected with the indicated virus at a MOI of 5, and the culture supernatant was collected 24 hours post-infection. GM-CSF concentration was quantified by ELISA. One-way ANOVA with Dunnett's post-hoc test was performed. n=3 biological replicates. Error bars: ±SD. ****p<0.0001. (E) Single-step growth

curve of HSV1 Csf2 and HSV1 US11-Csf2. Monolayers of Vero cells were infected at a MOI of 5, then intracellular and extracellular virus was collected and titrated at the indicated time points. (F) Transcription level of HSV1 endogenous gene (US6) and transgenes. Monolayers of Vero cells were infected at a MOI of 5, then cells were lysed using Trizol at the indicated time points. mRNA abundance was quantified by RT-qPCR and normalized to *Rps20*. ANOVA, analysis of variance. MOI, multiplicity of infection.

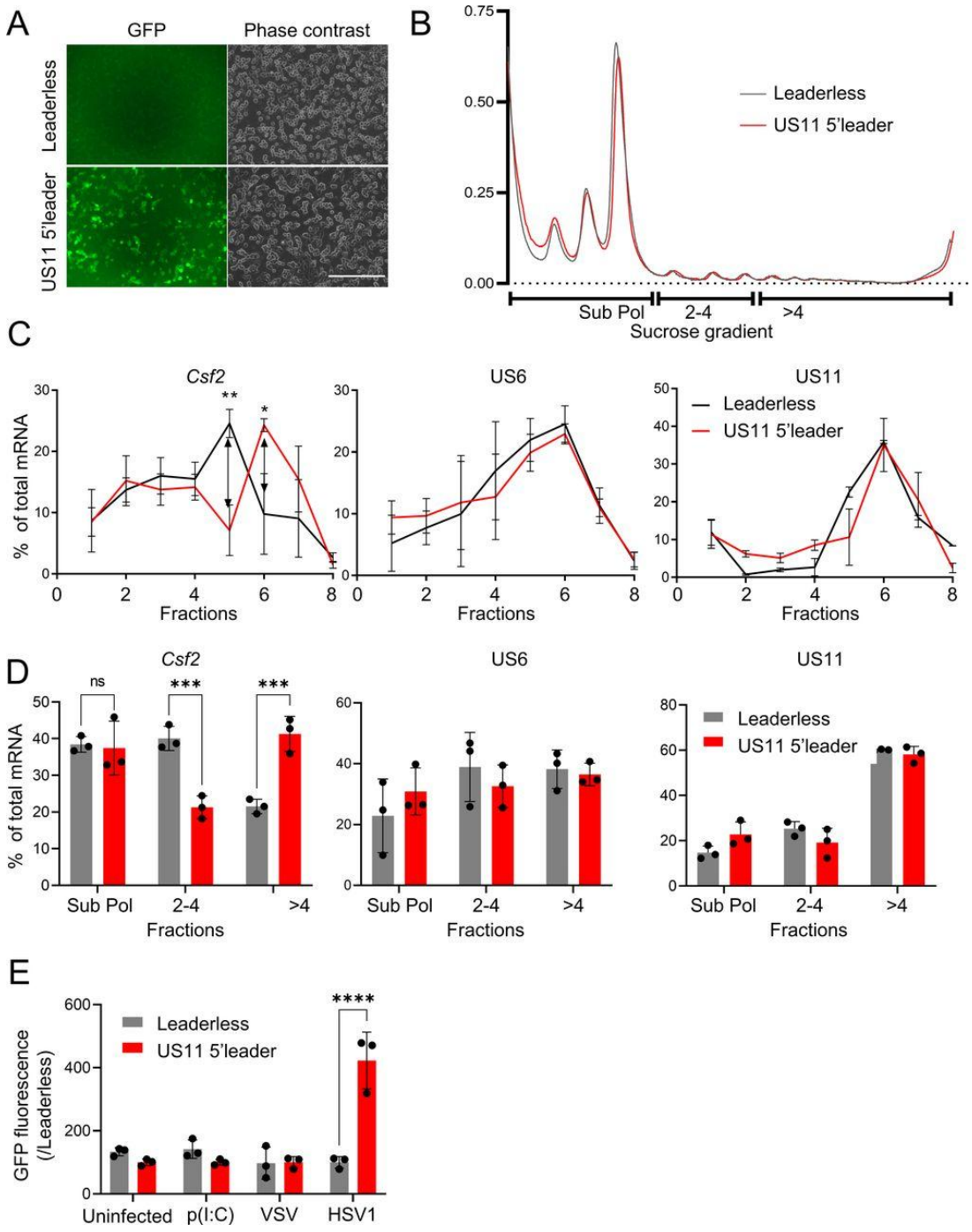

Figure 3. 6. The HSV1 US11 5'leader increases translation efficiency of a downstream transgene.

(A) Fluorescence and phase contrast images of HSV1-infected Vero cells used for the polysome fractionation experiment in (B) and (C). scale bar: 400 μm. (B) polysome traces of Vero cells infected with HSV1 Csf2 or HSV1 US11-Csf2 at a MOI of 5. Cells were lysed at 24 hours post-infection for polysome fractionation. (C) mRNA distribution in polysome fractions of *Csf2* (left panel) and the endogenous HSV1 transcripts US6 (middle panel) and US11 (right panel), quantified by RT-qPCR. Two-tailed unpaired t-test was performed. n=3 biological replicates. Error bars: ±SD. **p<0.01, *p<0.05. (D) mRNA distribution in non-translating fractions (subpolysome), poorly translating fractions (2–4 ribosomes) and highly translating fractions (>4 ribosomes) of *Csf2* (left panel), US6 (middle panel) and US11 (right panel) transcripts. Multiple unpaired *t*-test was performed. n=3 biological replicates. Error bars: ±SD. *** p<0.001 (E) Quantification of GFP fluorescence of Vero cells transfected with pTK-CSF2-GFP plasmid with or without US11 leader sequence, co-transfected with poly(I:C) or infected immediately after with VSV or wild-type HSV1 at a MOI of 5. Two-way ANOVA with Sidak's post-hoc test was performed. n=3 biological replicates. Error bars: ±SD. ****p<0.0001. ANOVA, analysis of variance. MOI, multiplicity of infection.

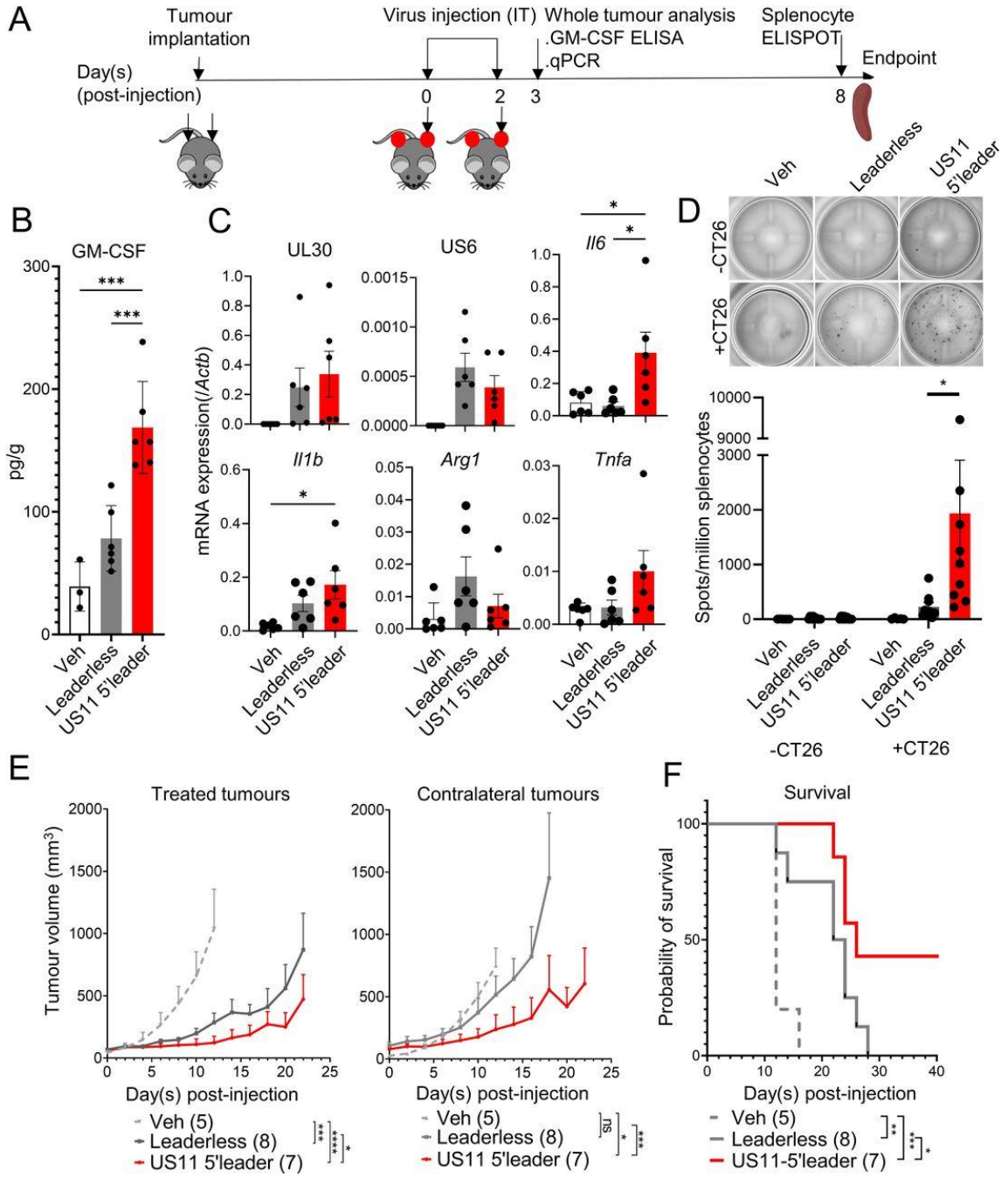

Figure 3. 9. US11 5'leader enhances the antitumour effect of GM-CSF expressing HSV.

(A) Schematic overview of the *in vivo* study to characterize the effect of HSV1 US11-Csf2 on tumour inflammation and systemic antitumour T-cells. 10^5 CT26 cells were injected in both flanks of BALB/c mice. When the tumour reached approximately 5×5 mm, two injections of 5×10^5 PFU of the indicated virus were performed intratumourally 2 days apart (day 0 and day 2). Tumour size was measured every 2 days. (B) Intratumoural GM-CSF level of tumour treated with leaderless or HSV1 US11-Csf2. Tumours as generated in (A) were excised 1 day after the second injection and homogenized in PBS. GM-CSF level was then quantified by ELISA. Two-tailed unpaired t-test

was performed. n=3 biological replicates. Error bars: ±SD. ***p<0.001. (C) Viral transcripts and inflammatory genes expression level in oHSV1-treated tumours. RNA from tumours in (B) were extracted with Trizol, then mRNA abundance of the indicated transcripts were quantified by RT-qPCR and normalized to *Actb*. Two-tailed unpaired t-test was performed. n=3 biological replicates. Error bars: ±SD. *p<0.05. (D) systemic tumour-specific T-cell responses after oHSV1 injection, evaluated by IFNγ ELISPOT. Eight days after the first injection, splenocytes were isolated from mice, and co-cultured with/without UV-irradiated CT26 at a 2:1 responder-to-stimulator ratio for 24 hours. Representative ELISPOT wells are shown, as well as quantification of CT26-specific spots in the bar graph. Two-tailed unpaired t-test was performed. Error bars: ±SD. *p<0.05. (E) the effect of Leaderless- or HSV1 US11-Csf2 treatment on tumour growth. Number of mice is shown in brackets. Two-way ANOVA with Tukey's post-hoc test was performed. Error bars: ±SD. *p<0.05, ***p<0.001, ****p<0.0001. (F) Kaplan-Meier survival curve of mice treated with the Leaderless or US11-Csf2 HSV1. Number of mice is shown in brackets. *p<0.05, **p<0.01, ***p<0.001. ANOVA, analysis of variance.

Table 3.1: HSV1 TSS identified in this study (Hoang et al.) compared to Tombacz et al., 2017 and Whisnant et al., 2020

_	Hoang et al., (This study)				Tombácz *et al.*, 2017		Whisnant *et al.*, 2020	
HSV1 Genes	TSS coordinates (JQ780693.1)	5'UTR coordinates (JQ780693.1)	5'UTR length	TSS coordinates (JN555585)	TSS coordinates (JN555585)	Differences to our study (nt)	TSS coordinates (JN555585)	Differences to our study (nt)
UL1+	8901	JQ780693.1+:8901-8994	92	9245	9242	3	9245	0
UL2+	9396	JQ780693.1+:9396-9541	145	9740	9739	1	9739	1
UL3+	X				10736			
UL4-	12151	JQ780693.1-:12079-12151	72	12495	12494	1	12494	1
UL5-	X				15581			
UL6+	X				15032			
UL7+	16613	JQ780693.1+:16613-16792	179	16957	16956	1	16956	1
UL8-	20337	JQ780693.1-:20134-20337	203	20680	20677	3	20679	1
UL9-	X				23358			
UL10+	22601	JQ780693.1+:22601-22862	261	22944	22943	1	22943	1
UL11-	25148	JQ780693.1-:24741-25148	407	25499	25498	1	25498	1
UL12-	26695	JQ780693.1-:26537-26695	158	27046	27045	1	27045	1

UL13-	X				28657			
UL14-	X				29249			
UL15 +	28451	JQ780693.1+:28451-28670	219	28802	28801	1	28801	1
UL16-	31261	JQ780693.1-:30949-31261	312	31608	31607	1	31607	-
UL17-	X				33719			
UL18-	35902	JQ780693.1-:35704-35902	198	36250	36249	1	36247	3
UL19-	40421	JQ780693.1-:40182-40421	239	40768	40768	0	40766	2
UL20-	X				41613			
UL21 +	41515	JQ780693.1+:41515-41726	211	41863	41862	1	41862	1
UL22-	46230	JQ780693.1-:46031-46230	199	46582	46581	1	46581	1
UL23-	47558	JQ780693.1-:47451-47558	107	47910	47906	4	47909	1
UL24 +	47008	JQ780693.1+:47008-47386	378	47360	47671	-311	47407	-47
UL25 +	47722	JQ780693.1+:47722-48461	739	48074	48630	-556	48630	-556
UL26 +	50311	JQ780693.1+:50311-50469	158	50664	50659	5	50663	1
UL26.5+	51249	JQ780693.1+:51294-51387	93	51635	51636	-1	51634	1
UL27-	55744	JQ780693.1-:55458-55744	286	56081	56080	1	56080	1
UL29-	61979	JQ780693.1-:61717-61979	262	62312	62312	0	62313	-1
UL30 +	X				62605			
UL31-	67123	JQ780693.1-:67044-67123	79	67458	67458	0	67457	1
UL32-	68885	JQ780693.1-:68827-68885	58	69220	69220	0	69219	1
UL33 +	68730	JQ780693.1+:68730-68826	96	69065	69065	0	69064	1
UL34 +	69107	JQ780693.1+:69107-69298	191	69442	69442	0	69441	1
UL35 +	70151	JQ780693.1+:70151-70231	80	70486	70489	-3	70488	-2
UL36-	X				?			
UL37-	83780	JQ780693.1-:83649-83780	131	84215	84215	0	84214	1

UL38+	83958	JQ780693.1+:83958-84088	130	84393	84394	-1	84393	0
UL39+	85774	JQ780693.1+:85774-86000	226	86217	86214	3	86216	1
UL40+	89331	JQ780693.1+:89331-89482	151	89774	89775	-1	89773	1
UL41-	92312	JQ780693.1-:92193-92312	119	92755	92755	0	92753	2
UL42+	924191	JQ780693.1+:92491-92669	178	92934	92936	-2	92934	0
UL43+	94323	JQ780693.1+:94323-94357	34	94765	94653	112	94764	1
UL44+	95723	JQ780693.1+:95723-95865	142	96171	96174	-3	96173	-2
UL45+	95706	JQ780693.1+:95706-97585	79	96154	97953	-1799	97953	-1799
UL46-	X				100995			0
UL47-	102866	JQ780693.1-:102672-102866	194	103312	103311	1	103309	3
UL48-	104814	JQ780693.1-:104635-104814	179	105258	105257	1	105257	1
UL49-	106099	JQ780693.1-:105949-106099	150	106542	106543	-1	106538	4
UL49A-	106686	JQ780693.1-:106551-106686	135	107129	107128	1	107126	3
UL50+	106387	JQ780693.1+:106387-106568	181	106830	106826	4	106829	1
UL51-	108863	JQ780693.1-:108569-108863	294	109306	109305	1	109302	4
UL52+	X				108985			
UL53+	111501	JQ780693.1+:111501-111737	236	111944	111943	1	111943	1
UL54+	113153	JQ780693.1+:113153-113292	139	113596	113598	-2	113598	-2
UL55+	115002	JQ780693.1+:115002-115054	52	115445	115447	-2	115444	1
UL56-	116643	JQ780693.1-:116485-116643	158	117084	117083	1	117083	1

RL2-	123628	JQ780693.1-:123482-123628	146	124258	124256	2	124255	3
RL1-	125310	JQ780693.1-:125206-125310	104	125965	125944	21	125964	1
RS1-	130404	JQ780693.1-:130103-130404	301	131431	131428	3	131429	2
US1+	131098		602					0
		JQ780693.1+:131098-131700	354 (spliced)	132128	132127	1	132129	-1
US2-	134359	JQ780693.1-:133983-134359	376	135307	135306	1	135305	2
US3+	134019	JQ780693.1+:134019-134277	258	134967	134958	9	134966	1
US4+	135787	JQ780693.1+:135787-135799	12	136735	136733	2	136734	1
US5+	X				137625			0
US6+	137395	JQ780693.1+:137395-137476	81	138342	138338	4	138345	-3
US7+	138754	JQ780693.1+:138754-138843	89	139699	139698	1	139699	0
US8+	140208	JQ780693.1+:140208-140282	74	141173	141170	3	141171	2
US8A+	141665	JQ780693.1+:141665-141783	118	142630	142626	4	142629	1
US9+	142287	JQ780693.1+:142287-142352	65	143252	143250	2	143251	1
US10-	144183	JQ780693.1-:144114-144183	69	145169	145171	-2	145168	1
US11-	144480	JQ780693.1-:144265-144480	215	145466	145461	5	145461	5
US12-	145247	JQ780693.1-:144596-145247	319 (spliced)	146069	146068	1	146066	3

Table 3. 1. HSV1 TSS identified in this study (Hoang et al.) compared to Tombacz et al., 2017 and Whisnant et al., 2020

Table 3.2: Sequence of HSV1 leaders identified in this study (Hoang et al.)

Gene name (strand)	5'leader length	5'Leader sequence
UL1+	92	gatacggggcttgtgtggcacgacgtcgtggttgtgttactgggcaaacacttggggactgtaggtttctgtgggtg ccgaccctaggcgct - atg
UL2+	145	agtcgcaagcaggccgccagccacacacctgtgaaggctgggtgtgtgaactttgactattcgcgcacccgccg ctgtgtagggcgacaggatttgggacctaccaacggaacgtctggacggaccccggttctgccgccggacg - atg
UL3+	221	gccatcaggccggaccctcgggtccattgcgtcctcaagttttcgcacccgtcgcccctctccaaggttccgttcg gaacctgccagcatttcctcgtggcgaaccgatacctcgagacccggtcgatttcacccatcgactggtcggtttg aaaggcatcgacgtccgggggtttttgtcggtgggggctttgggtatttccgatgaataaagacggtta - atg
UL4-	72	attgtctattaacccgccgtcccttacagttccaccgaacccggcccgggggactcactacccaccgcgag - atg
UL5-	450	gggccgcccggcgcaaagcaggcgaccaacccgtgggcaaagtccagcagcgtcgtcctaagcgtgttccgc cacgtgtcgaacacccgctcggccaccccggcgatatccgcctcccgggcgttcctgtaccggcgaaccagcc gttggggctgcagaccgcgggccgccacgtggccgagccagtccgcctcgaggtcccggtaagtggtggcgtt gaggagcgcgtgaaagatcgccgcctgcagctgccgggtggtcgcctcgctggaccggacgacgttgtacacc ccctggccctcggtataccccagctgcccgtggagaatctcgcggaacagcatcgtaccggggctggggtgaa cctttacccagccgtcctcgggggagcacagcgcttccgtgtccccccgcgcacgcgtagtgggggcccgcga gcgtggtgcggtc - atg
UL6+	98	cggccctccctggaacggctggtcggtccccgggttgctgaaggtgcggcgggccgggtttctgtccgtctagct ggcgctccccgccggccgccgcc - atg
UL7+	179	gacagacatcgcggccctgttcgtcgcggacgtccagcacgcagcgctgcccccgcccccctccccggtcggc gccgatttccggcccggcgcgtccccgcggggccggtccagatcgcggtcgcccggaagaactgcgcgagg cgcgccggaccagggcgggggcatcgggcaccggg - atg
UL8-	203	acgtggtcgtccgcggaccggcggcgctgttgccggaacgcaccgaggggccaagttggcccccggacccg ggccgtttcccacccccacccccaaccccaaaaaccgccccccccccgtcaccggtttccgcgacccaccgggc ccggccaggcacggcagcatgggacccacagaccgcccgtgatccttaggggccgtgcg - atg
UL9-	99	acagaggccaggacgaggagccccgtgacgcagaccgcagagaccacaaacgtcgccacctgcacacacca gacccaccacgccgtccgcgccccggtc - atg
UL10+	261	acactcgtgtccggagagtggatcgcttcccgcagccagcggatcagcgcggtagtttttcccgaccccattggc gcgcggaccacagtcacgcacctggccgtcggggcgctcgcgttggggaaggtgacgggtccgtgctgctgc cgctcgatcgttgttttcgggtgaacccggggcacccattcggccaaatcccccccgtacaacatccgcgctagc gatacgctcgacgtgtactgttcgcactcgtcgtcccca - atg
UL11-	407	ctgtttggcgcccccgacctcggacgccacaccatctcccccgtgtcctggagctccggggatctggtccgccgc gagcccgtcttcgcgaacccccgtcacccgaactttaagcagatcttggtgcagggctacgtgctcgacagccac ttccccgactgcccccccccacccgcatctggtgacgtttatcggcaggcaccgcaccagcgcggaggagggcg taacgttccgcctggaggacggcgccggggctctcggggccgcaggacccagcaaggcgtccattctcccgaa ccaggccgttccgatcgccctgatcattacccccgtccgcatcgatccggagatctataaggccatccagcgaag cagccgcctggcattcgacgacacgctcgccgagct - atg
UL12-	158	actgtcgtcggtggcgctgcctcccgagcttaagcctctcctggtgctggtgtcccgcctgtgtcacaccaacccg tgcgcgcggcacgcgctgtcgtgagaatcagcgttcacccggcggcgcgctcaaccaccgctccccccacgtc gtctcggaa - atg

UL13-	155	cgtcgtgactttctaaccgcacaccgacggtacctcgatccggcgcttggtgagcgcctggacgccgtggacgat cgtcttgcggaccaggaggagcaactcgaggaagcagcgaccaacgcttctctgtggggagacggcgacctg gccgaagg - atg
UL14-	334	gagaagagcggcgagtgctcgcagcagtcgtggagcgtcccgacgccagggaccacggtctggtggcgcttg ggggtcgcggtcgcgaaatctaaaaagggcactcgtagggcatcgccgcccatggtgaggcccgccgacgcc tcgtccgcgcccaccttaagttgcctctgtttctcgaggcgctccaggtactgctggacgtcggacgccagctgct gaccaaacatcgcgcacaccgggtggcgggtcgcggcggcgaagtaccccgatcacgggccttgggcacgc gagactatcagagcacccccccgggtcgcccgcagggtggcgga - atg
UL15+	219	gggtgctgacgccctcccggtgcagctgcagggtctggtccttgtaaatctcggctcggaggtgcgtctcggcca ggcgtcggcgcagggccgcgtgggcggcatctcggtccattccgccaccctgcgggcgacccgggggggtgct ctgatagtctcgcgtgcccaaggcccgtgatcggggtacttcgccgccgcgacccgccacccggtgtgcgcg - atg
UL16-	312	acagccccacgcagggtctgcgagcaatacctgcccggggaaagctacgcctacctctgcctggggtttaatcg ccgcctctgtggcatagttgtctttcccggcggctttgcgttcaccattaacatcgcggcctaccttagcctctcgga ccccgtcgcgcgggccgctgtccttaggttttgtcgcaaggtgtcgtccgggaacggccggtctcgctagcggg cgccttccccggccacctcgcccacccactcctccccgcgccgttggcccccgcctctggggtttgccctcccc ccgcccccggc - atg
UL17-	222	agcccataatcgtctggaccgcatccgggcgaataaagttggcctcgtcgacaaagagcaggttaaagtcctggc ctcggattccctagagacagaagaaacgcgccgcgcataagcacgcacgcctccgttggcgaatacgcatacg cgcgccaaacccacgcccttcccgcggactcgggggacccgcatcgcctacacacccacacccacccccgaa cc - atg
UL18-	198	ggattcgctctcggtgcgtctgggcccgacagacctccccgcgcatgctctggggtccctgtcgcctcccaaccc cctaagacccacccccgtcctatgcgaggttggtcgcccgtctctgctacgccgctgacccccaccgcgctcct cccgccacccgaaccaccactgcactccctgccgcgtggatcggcgcc - atg
UL19-	239	ggtctgttggggacactgggttctcctggaacgaggccgcagccttctcccggtgcctttcccccccgaccggca cccggcctctcacacagcatcccccgccttttttgggtccgggcccgtcgtgtctttcggtggaccttgggccgtc gggcacgtacacgggtggccgggcgttggggtggatcttagcctccccgggccaatatcgctagagacagccg atctccacgcgacccc - atg
UL20-	125	actcgcctccgcggatgcaacccgggtggtgtttgtgcaagaacccgggtgtctttgatctcgggatcctgctgac gtaagcgacccttgcggtttcggtctccccacctccaccgcacacccc - atg
UL21+	211	tcgttgtattcgagacctgcctgtgcaacgcacgtcggggttgcctgtgtccggttcggcccccaccgcgtgcggc acgcacgaggacgagtccgcgtgctttattggcgttccaagcgttgccctccagtttctgttgtcggtgttcccccat acccacgcccacatccaccgtagggggcctctgggccgtgttacgtcgccgcccgcg - atg
UL22-	199	ataaacgcggggttcggtcccagggctggcactctgtcgataccccaccgagaccccattgggaccaatacgcc cgcgtttcttccttttccccacccccaaccccccaagttcgggtgaaggcccagggctcgcagccaacgtcggggcg gcaagccctgccatagccacgggccccgtgggttagggacggggtccccc - atg
UL23-	107	accgagcgaccctgcagcgacccgcttaacagcgtcaacagcgtgccgcagatcttggtggcgtgaaactccc gcacctcttcggccagcgccttgtagaagcgcgt - atg
UL24+	378	cccagcctccccccgatatgaggagccagaacggcgtcggtcacggcataaggcatgcccattgttatctggg cgcttgtcattaccaccgccgcgtccccggccgatatctcaccctggtcgaggcggtgttgtgtggtgtagatgttc gcgattgtctcggaagcccccaacacccgccagtaagtcatcggctcgggtacgtagacgatatcgtcgcgcga acccagggccaccagcagttgcgtggtggtggttttccccatcccgtggggaccgtctatataaacccgcagtag cgtgggcattttctgctccaggcggacttccgtggctttttgttgccggcgagggcgcaacgccgtacgtcggttgt t - atg

UL25+	739	gcaaacgcgagcaacgggccacggggatgaagcagctgcgccactccctgaagctcctgcagtccctcgcgc ctccgggtgacaagatagtgtacctgtgccccgtcctggtgtttgtcgcccaacggacgctccgcgtcagccgcg tgacccggctcgtcccgcagaaggtctccggtaatatcaccgcagtcgtgcggatgctccagagcctgtccacgt atacggtccccattgagcctaggacccagcgagcccgtcgccgccgcggcggcgccgcccgggggtctgcga gcagaccgaaaaggtcacactctggggcgcgcgacccgcccgagtcagcggcccgccagttaccacccgcc gaccaaaccccccacctccacggagggcgggggggtgcttaagaggatcgcggcgctcttctgcgtgcccgtgg ccaccaagaccaaaccccgagccgcctccgaatgagagtgtttcgttccttcccccctcccccccgcgtcagacaaa ccctaaccaccgcttaagcggcccccgcgaggtccgaagactcatttggatccggcgggagccacccgacaac agcccccgggttttcccacgccagacgccggtccgctgtgccatcgcgcccccctcatcccacccccccatcttgtc ccaaataaaacaaggtctggtagttaggacaacgaccgcagttctcgtgtgttatttttcgctctccgcctctcgcag - atg
UL26+	158	gctccagtcccggcccggcggttggcgtgaacgcaacggcgggagctgggttagcgtttagtttagcattcgctc tcgcctttccgcccgcccccccgaccgttgcgcctttttttttttcgtccaccaaagtctctgtgggtgcgcgcatggca gccg - atg
UL26.5+	93	ataccgcccggctcgatcgctgccgcgccgcagggtgaccggtgcccaatcgtccgtcagcgcggggtcgcct tgtccccggtactgcccccc - atg
UL27-	286	acactctttgcctcggtctaccggtgcggggagctcgagttgcgccgcccggactgcagccgcccgacctccga aggtcgttaccgttacccgcccggcgtatatctcacgtacgactccgactgtccgctggtggccatcgtcgagagc gcccccgacggctgtatcggcccccggtcggtcgtggtctacgaccgagacgttttctcgatcctctactcggtcc tccagcacctcgcccccaggctacctgacgggggggcacgacgggcccccgtagtcccgcc - atg
UL28-	270	ggggaatgtgtgtaaaataaattattgctacgacatccgtgcttgtttgtgttccgtgtctatatctctgggcgggccgt gattcctctccgcggtgtctgggaatagagcagaaacgcacgcgccgccgactcccggcttgccggtcggcgg gcccgcgggaggccgccccgaagaggggggaccccggggctcagccagacgccgggtagcgtacggaccg cctcggtccaccgcatactccggccgcggtacagatcggcgccgcgag - atg
UL29-	262	cgacccggagcacctgaccgtaagcatctgtgcctctcgcagggaccccgcgttgccggccgccggggttcatc ggcgaccccgtggttacccgggggggttgtcggtgaaggggagggattcattccccaaccccggtctccaaccct ccccttgaccgtcgccgccccccccccggattttgacgctcgggagacataccttgtcgggcgtccgtcgtcgtgc cgggattacctccgttcgcggaccgattgacaaaaggac - atg
UL30+	202	gaataaaccgggccgccggccggggcgccgcgcagcagctcgccgcccggatccgccagacaaacaaggc ccttgcacatgccggcccgggcgagcctgggggtccggtaattttgccatcccacccaagcggctttttgggttttt ctcttcccccctccccacattcccctctttaggggttcgggtgggaacaaccgcg - atg
UL31-	79	acatttgtccgtgaggcgggcgcgctgcttagacgccactcgatctcgctcctgtccctggagcacaccctgtgta cct – atg
UL32-	58	gcagtcggggattgtgtcccgtaaagttcgctggcgcgtgcgcccctcccgcccagcc - atg
UL33+	96	acatacgcgcgctcgaacgcccccgccttccagctgctgccgggggactcttcgcacaccgcgacgctcgcca ggaccccgggggggcgaagttgcc - atg
UL34+	191	gcagaccccggacaccgcgtgtgtgcacggcgagctgctcgccgccaagcgggaaagattcgcggcggtcat taaccggttcctggacctgcaccagattctgcggggctgacgcgcgtgctgttgggcgggacggttcgcgaacc ctttggtgggtttacgcgggcacgcacgctcccatcgcgggcgcc - atg
UL35+	80	gccagtgcgttccggacgccttcgccccacacagccctcccgaccgacacccccatatcgcttcccgacctccg gtcccg - atg
UL36-	75	gtgggtggcggaaacaacactaaccccgggggtccggtccataaacaggccgggtctctggcccgcagggca cat - atg

UL37-	131	gcaacgcctgcgggggtcctggagggccgcgggggatcgataattcgccgctccctacagcgcacgacagtc attcccgcccggtctcgtcgttggtctacgctgtcccccacccacgcgagccgggcgtc - atg
UL38+	130	caacacaacccaccggaggcggtagccgcgtttggctgtggggtgggtggttccgccttgcgtgagtgtcctttc gacccccccccccctccctcccccgggtcttgctaggtcgcgatctggggtcgca - atg
UL39+	226	ccacaggtgggtgctttggaaacttgccggtcgccgtgctcctgtgagcttgcgtccctccccggtttcctttgcgct cccgccttccggacctgctctcgcctactcttctttggctctcggtgcgattcgtcaggcagcggccttgtcgaatct cgaccccaccactcgccggacccgccgacgtcccctctcgagcccgccgaaacccgccgcgtctgttgaa - atg
UL40+	151	actactgcaaggttcgcaaggcgaccaacagcggggtctttggcggcgacgacaacattgtctgcatgagctgc gcgctgtgaccgacaaacccctccgcgccaggcccgccgccactgtcgtcgccgtcccacgctctcccctgct gcc - atg
UL41-	119	cctcttgtgtcggtgttgttgtctgggtcaccatacacagagagacaggctcgggtgtcccggaccgtcgcaccaa ccacgccttagttaggccgatccgcagttacaattgacctgac - atg
UL42+	178	cgtagtttctggctcggtgagcgacggtccggttgcttgggtcccctggctgccatcaaaaccccacccctcgcagc ggcatacgcccccctccgcgtcccgcacccgagaccccggcccggctgccctcaccaccgaagcccacctcgtc actgtggggtgttcccagcccgcgttggg - atg
UL43+	34	gtgtatttcctttccctgtccttataaaagccgt - atg
UL44+	142	ccctcactatcgagggcgcttggtcgggaggccgcatcgaacgcacacccccatccggtggtccgtgtggaggt cgttttcatgcccggtctcgctttgccgggaacgctagccgatccctcgcgaggggggaggcgtcgggc - atg
UL45+	79	atccttggtcgatcccgaacgacacacggcgtggagcaaaacgcctccccctgagccgctttcctaccaacacaa cggc - atg
UL46-	43	ggcataactccgaccggcgggtcccgaccgaacgggcgtcacc - atg
UL47-	194	catttggccgggggctggggcggcgggtagccttcgcgggagatactgcgttttttgcgccggccccgtcgctc ccgtccattcccatcgcgaggggtccggcggcacctaccccggcctccatccgcgctgtggggtctttttctttttt ggggggtagcggacatccgataacccgcgtctatcgccacc - atg
UL48-	179	cattcctcgggaacggacggggttcccgctgcccacttccccccataaggtccgtccggtcctctaacgcgtttgg gggttttctcttcccgcgccgtcgggcgtcccacactctctgggcgggcggggacgatcgcatcaaaagcccgat atcgtctttcccgtatcaaccccaccca - atg
UL49-	150	gccactcacgcatccccagtgggttttgcggaccctctcttctctcccgggccgcccctatcgctcgacctctccac acctgcaccacccccgccgtccgaacccaggcctaattgtccgcgcatccgaccctagcgtgttcgtggaacc - atg
UL49A-	135	aggttcagttgcacgactccgcccccgcgagtagcgacggccgtgtgccagtcgccatcgtacccccgacccaa gctgtccggctggacaaggatcgccccggatccccactgactcatcttcctgttagggacg - atg
UL50+	181	agacatttggccagtgttttgggtctcgcaccgcgcgcccccgatcccatcgcgcccgccctcctcgccgggcg gctccccgcgcgggcccgcgtctcccgccgctaaggcgacgagcaagacaaacaacaggcccgcccgacag acccttctgggggggcccatcgtccctaacaggaag - atg
UL51-	294	gccatttagcccgcccgacgcttggtagagcgcccgactctcttcgaacctgtcttgctccgtgggcccgtcggca cggccatcgtgcgtgtatgcgtcgtagctgaatatataaaccggctcggcccccagtagagagtttgtgaggagg gcgatcgaagaggtaataacgcacccgtcggtcgcataaagcgcggtcacctccacgggagtcccggccgccc gcctctccccgcggttcccgtcttcctgccccattgcgtccgcgcgcccaagggccagtacccgcccgcg - atg
UL52+	63	acatatagccccgagaagagaagccatcgcgggcgggtactggcccttgggcgcgcggacgca - atg

UL53+	236	agtaaggacgactgggtcctcctacagctagtccccgttcgcggtaccctgcagcaaagcctgtcgtgtctgcgctttaagcacggccgggcgagtcgcgccacggcgcggacattcgtcgcgctgagcgtcggggccaacaaccgcctgtgcgtgtccttgtgtcagcagtgctttgccgccaaatgcgacagcaaccgcctgcacacgctgtttaccattgaccggcacgcc - atg
UL54+	139	ggtggtgtgcagccgtgttccaaccacggtcacgcttcggtgcctctccccgattcgggcccggtcgctcgctaccggtgcgccaccaccagaggccatatccgacaccccagccccgacggcagccgacagcccggtc - atg
UL55+	52	gtcatagtgcccttaggagcttcccgcccgggcgcatccccccttttgcact - atg
UL56-	158	ggttgggcgacgcatgccagcccaacaaaatccgccggggtgccagtcccattcccgaaggcgtagcccgttaacttggctggcttggatggggagtagggccttttccattaccccaaggacctagcgcgcgggagtcgtggctttggggcgcatcc - atg
RL2-	146	tcgcatttgcacctcggcactcggagcgagacgcagcagccaggcagactcgggccgccccctctccgcatcaccacagaagccccgcctacgttgcgacccccagggaccctccgtccgcgaccctccagccgcatacgacccccc - atg
RL1-	104	cccccgcggccgagactagcgagttagacaggcaagcactactcgcctctgcacgcacatgcttgcctgtcaaactctaccaccccggcacgctctctgtctcc - atg
RS1-	301	ccacacggagcgcggctgccgacacggatccacgacccgacgcgggaccgccagagacagaccgtcagacgctcgccgcgccgggacgccgatacgcggacgaagcgcgggaggggatcggccgtccctgtccttttttcccacccaagcatcgaccggtccgcgctagttccgcgtcgacggcgggggtcgtcggggtccgtgggtctcgccccctccccccatcgagagtccgtaggtgacctaccgtgctacgtccgccgtcgcagccgtatccccggaggatcgccccgcatcggcg - atg
US1+	517	gcagacggcgccggccacgaacgacgggagcggctgcggagcacgcggaccgggagcgggagtcgcagagggccgtcggagcggacggcgtcggcatcgcgacgccccggctcgggatcgggatcgcatcggaaagggacacgcggacgcgggggggaaagacccgcccacccccacccacgaaacacaggggacgcaccccgggggcctccgacgacagaaacccaccggtccgcctttttgcacgggtaagcaccttgggtgggcggaggaggggggggacgcgggggcggaggaggggggacgcgggggcggaggaggggggacgcgggggcggaggaggggggacgcgggggcggaggaggggggacgcgggggcggaggaggggggctcacccgcgttcgtgccttcccgcaggaggaacgtcctcgtcgaggcgaccggcggcgaccgttgcgtggaccgcttcctgctcgtcgggcgggggggaagccactgtggtcctccgggacgttttctgg – atg
US2-	376	gacggctttgtctccggcgggacggcctcctccttcctcctgccctgtccccgtaaacgcgacaaaacttacgacaggccattcgccgcaccgtgagtgccaaccaacgagcaccccgaacgacgggccccggggttttaaggagcggcagtttgacgacccacccccctgacctaccccccccgtaaatcaccctcccctccccccggacgcctccgctgccggtcgctccaagggcccccccgggaaggcgggtctgtggaccgtagggcccttaaatttttagagcagcccccgcgtcggcctgtctccccgccgtgcgtggccttacaaatctgcaagtgccccaaatcggacacgggcctgtaatatacccaac - atg
US3+	258	acttgcagatttgtaaggccacgcacggcggggagacaggccgacgcgggggctgctctaaaaatttaagggccctacggtccacagacccgccttcccgggggggccttggagcgaccggcagcggaggcgtccgggggaggggagggtgatttacgggggggtaggtcaggggtgggtcgtcaaactgccgctccttaaaaccccggggcccgtcgttcggggtgctcgttggttggcactcacggtgcggcga - atg
US4+	12	gtttttggcatc - atg
US5+	106	gcgcgacttccgggcctcagaacccacccgaaacggccaacggacgtctgagccaggcctggctatccggagaaacagcacacgacttggcgttctgtgtgtcgcg - atg
US6+	81	ggtcataagcttcagcgcgaacgaccaactaccccgatcatcagttatccttaaggtctcttttgtgtggtgcgttccggt - atg
US7+	89	gtggacagtcgataagtcggtagcgggggacgcgcacctgttccgcctgtcgcacccacagctttttttgcgaaccgtcccgttccggg - atg

US8+	74	tcttctggcgggttggtgcggtgctgtttgttgggctcccattttacccgaagatcggctgctatccccgggac - atg
US8A+	118	acgtacattcgcgtggccgacagcgagctgtacgcggactggagctcggacagcgagggagaacgcgaccag gtcccgtggctggcccccccggagagacccgactctccctccacca - atg
US9+	65	agcaaattaaaaatcgtgagtcacagcgaccgcaacttcccacccggagctttcttccggcctcg - atg
US10-	69	accccagaggtgttcacgcacctcgaggacacccgcgcatgatctccggacccccgcaacggggtgata - atg
US11-	215	ggccagaaccgccgtgcacgacccggagcgtcccctgctgcgctctcccgggctgctgcccgaaatcgccccc aacgcatccttgggtgtggcacatcgaagaaccggcgggaccgtgaccgacagtccccgtaatccggtaaccc gttgagtcccgggtacgaccatcacccgagtctctgggcggagggtggttcccccccgtggctctcgag - atg
US12-	486	gcagacggcgccggccacgaacgacgggagcggctgcggagcacgcggaccgggagcgggagtcgcaga gggccgtcggagcggacggcgtcggcatcgcgacgccccggctcgggatcgggatcgcatcggaaagggac acgcggacgcgggggggaaagacccgcccacccccacccacgaaacacaggggacgcaccccgggggcct ccgacgacagaaacccaccggtccgccttttttgcacgggtaagcaccttgggtgggcggaggaggggggac gcgggggcggaggaggggggacgcgggggcggaggaggggggacgcgggggcggaggaggggggac gcgggggcggaggaggggggacgcgggggcggaggagggggctcacccgcgttcgtgccttcccgcagg aggaacgtcctcgtcgaggcgaccggcggcgaccgttgcgtggaccgcttcctgctcgtcgggggggagc - atg

Table 3. 2. Sequence of HSV1 5'leaders identified in this study (Hoang et al)

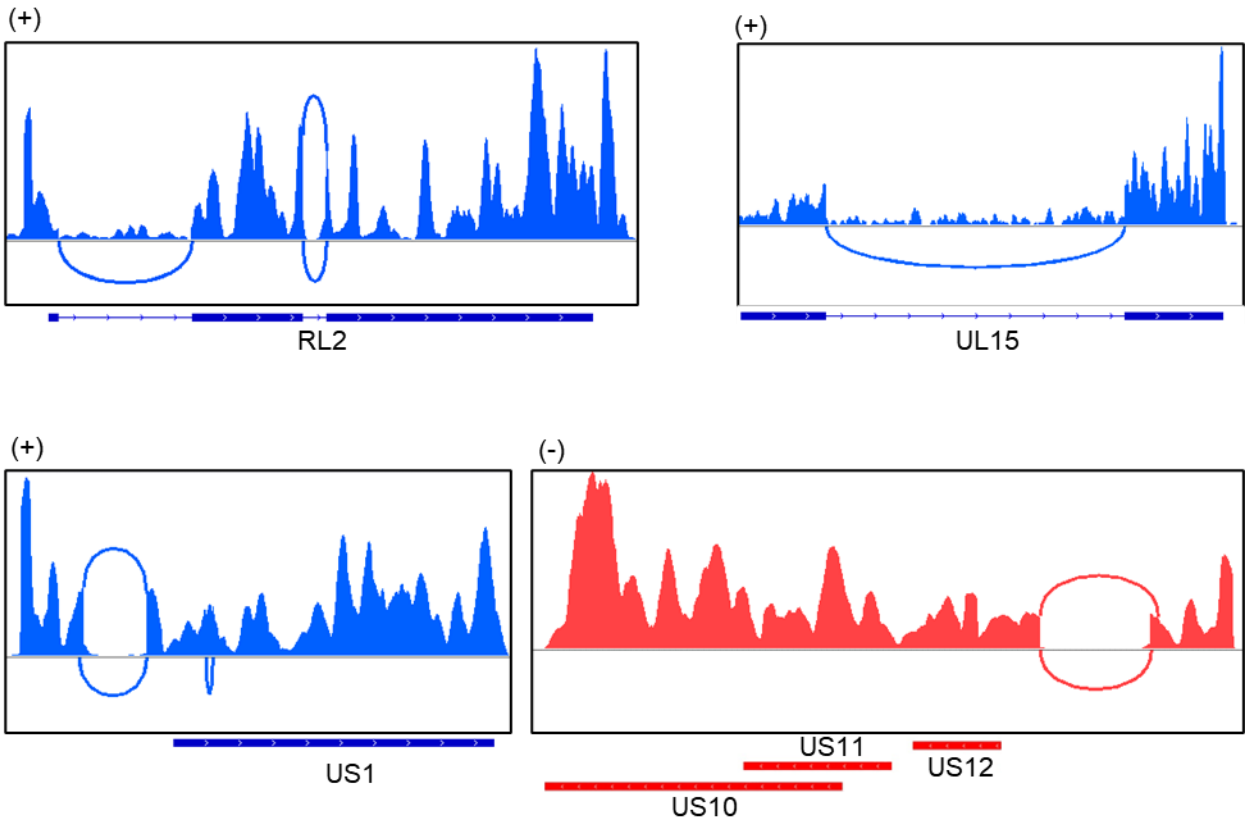

Supplementary 3. 1 Examples of spliced junction detected on known HSV1 spliced transcripts.

Individual transcripts (RL2, UL15, US1, US12) identified by RNA-seq coverage on the positive strand (blue) and negative strand (red).

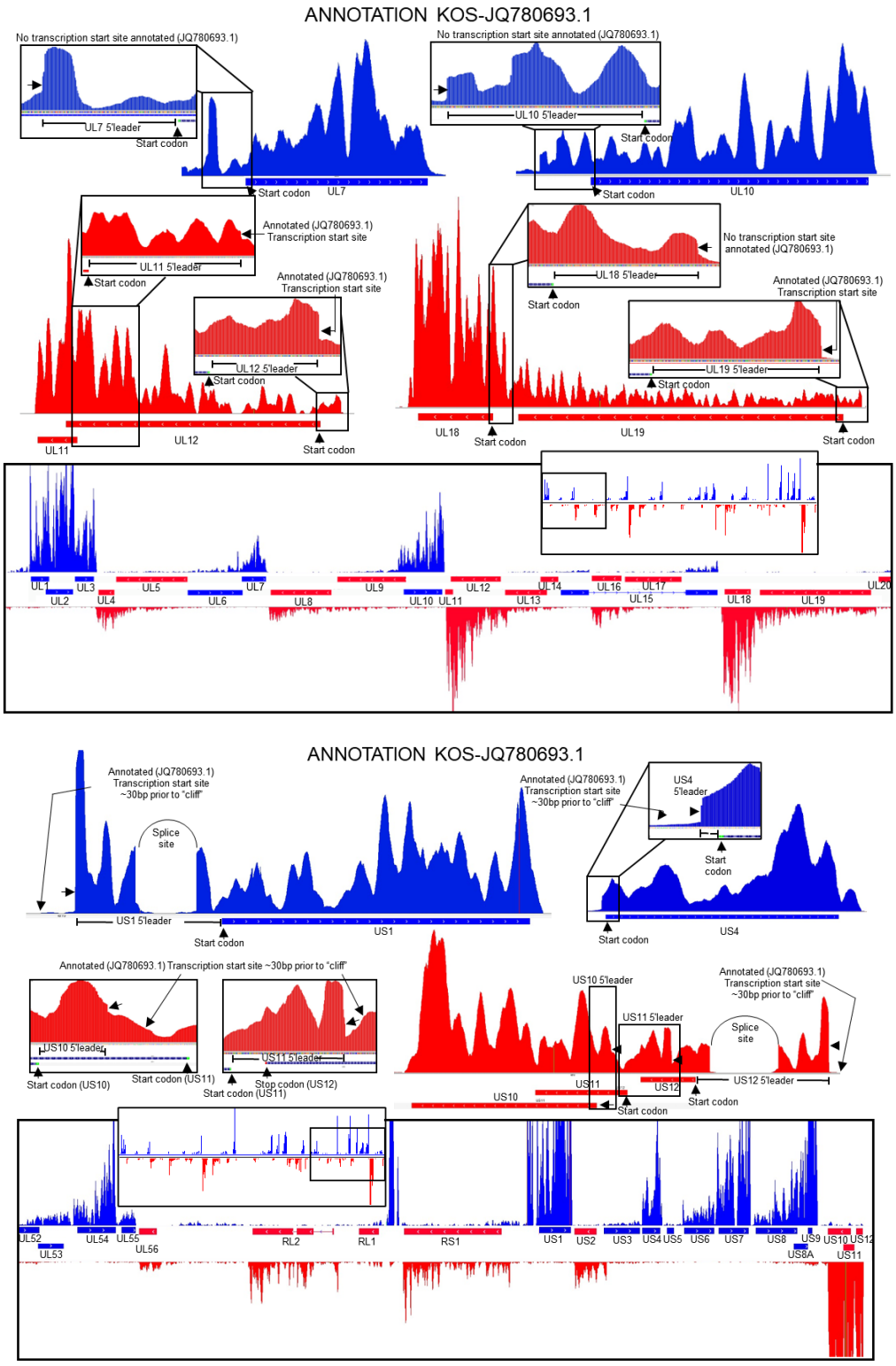

Supplementary 3. 2. Full RNA-seq coverage of HSV1 genome.

RNA-seq data from 4T1 infected with HSV1 previously published (Hoang et al., 2019). Strand-specific RNA reads were mapped to HSV1 (JQ780693.1) and separated by direction to avoid ambiguous mapping of overlapping genes. This graph shows the inset for every identified TSS of all HSV1 genes.

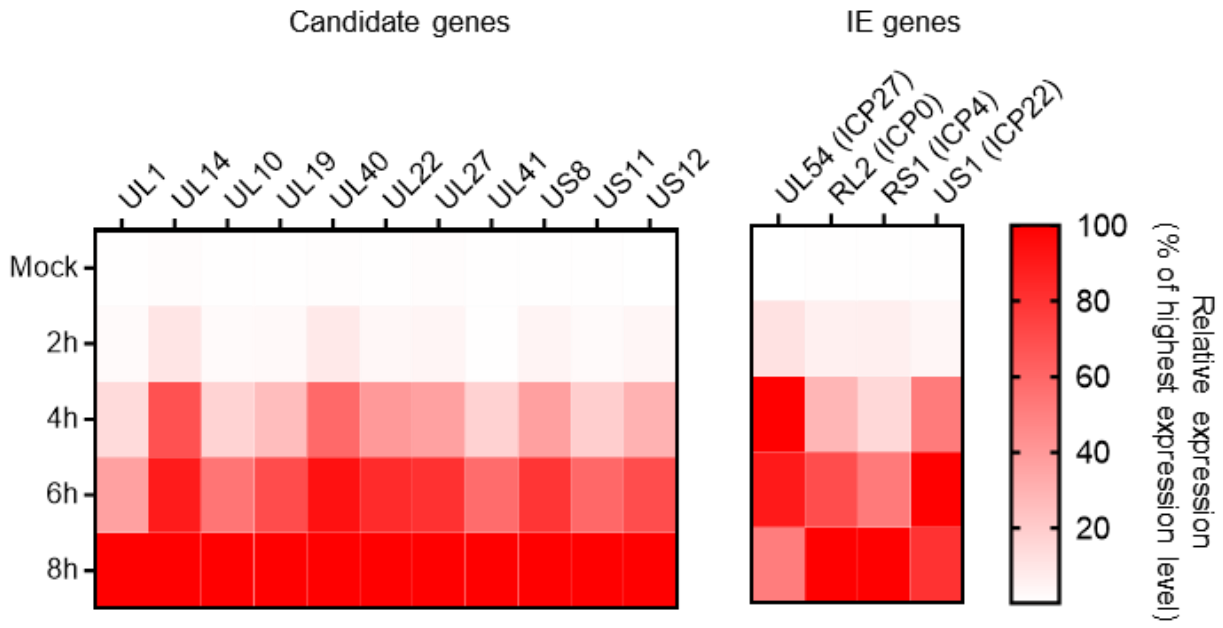

Supplementary 3. 3. Relative mRNA expression level of the 10 late genes selected as candidates (left heatmap), as well as 4 immediate early genes (right heatmap). mRNA expression were obtained from a previous study by Rutkowski et al., 2015. Expression level was normalized as a percentage of the highest expression level across all time points

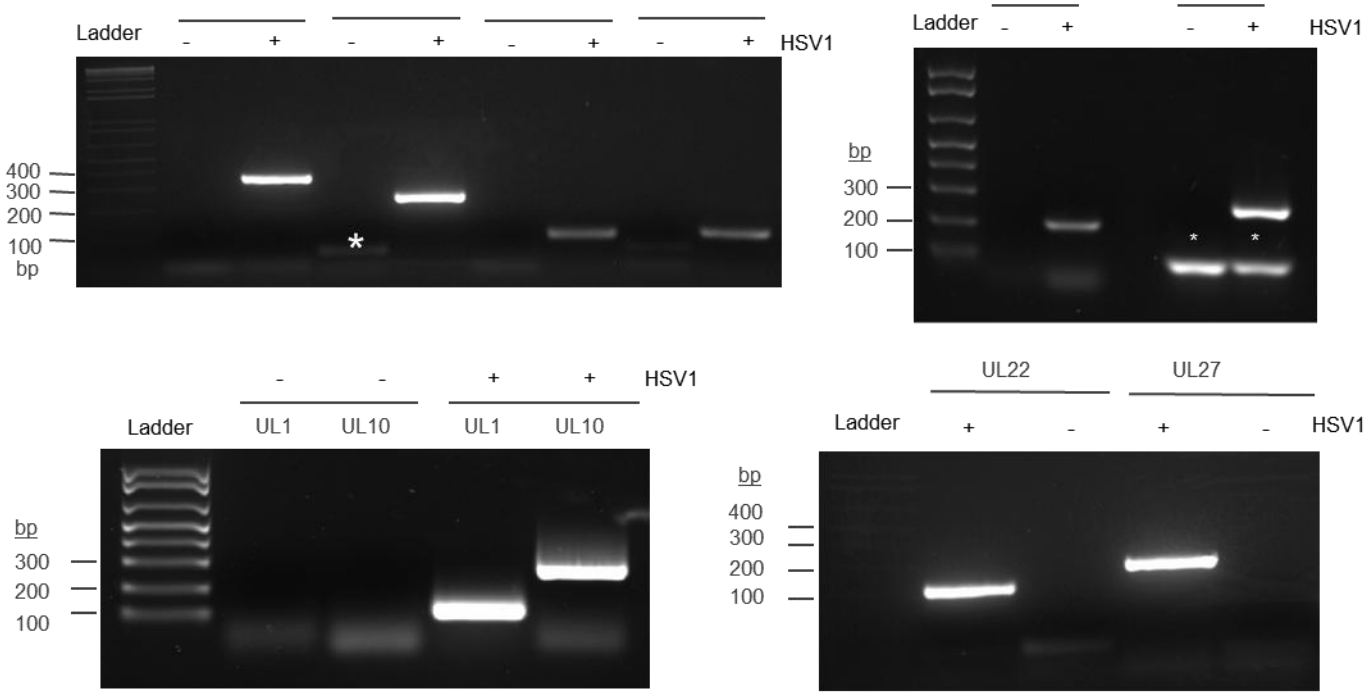
Ladder
HSV1
bp
400
300
200
100
UL1
UL10
UL22
UL27

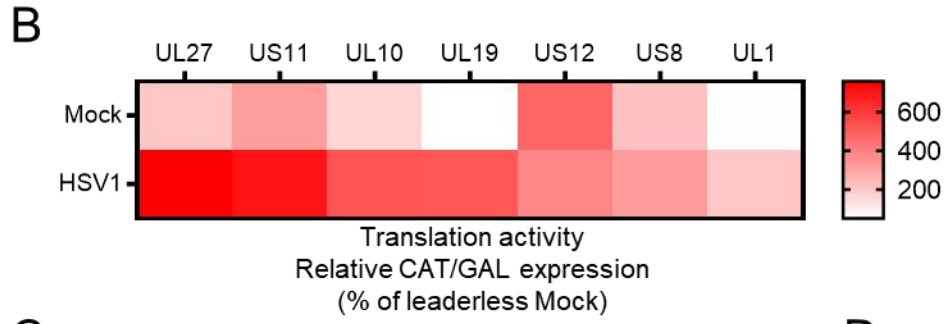
B
UL27
US11
UL10
UL19
US12
US8
UL1
Mock
HSV1
600
400
200
Translation activity
Relative CAT/GAL expression
(% of leaderless Mock)

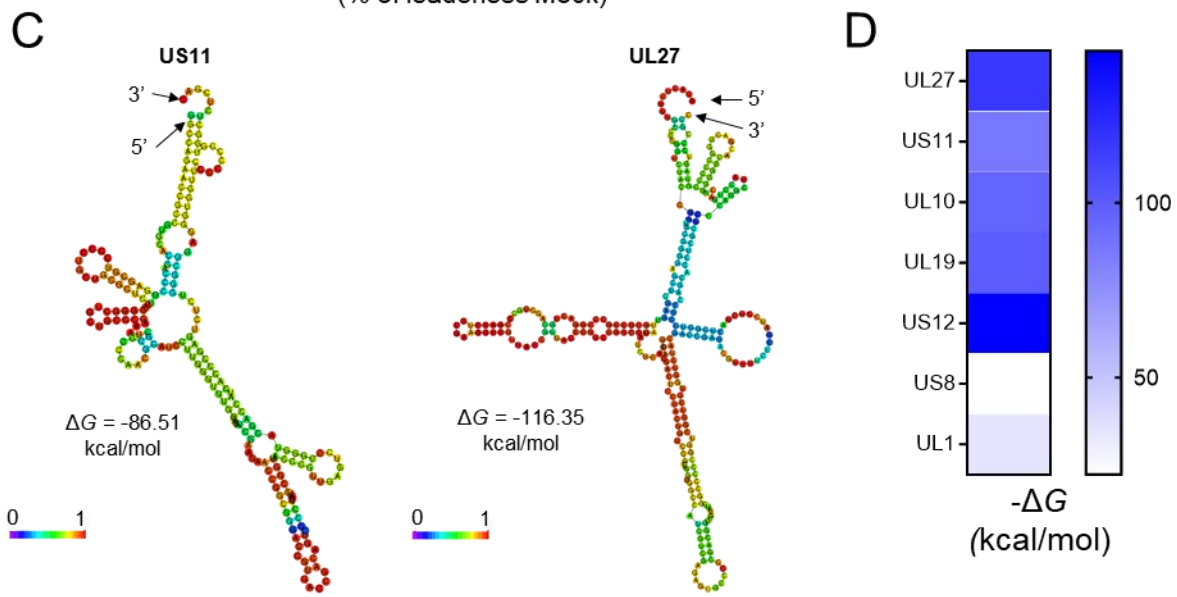
C
US11
UL27
3'
5'
ΔG = -86.51
kcal/mol
ΔG = -116.35
kcal/mol
0
1
D
UL27
US11
UL10
UL19
US12
US8
UL1
100
50
-ΔG
(kcal/mol)

Supplementary 3. 4. Translation reporter screen for 5'leaders that enhance translation during HSV1 infection.

(A) Agarose gel visualization of other HSV1 5'leaders (including the rest of the 5' leader in Figure 2) amplified from total RNA of HSV1 infected cells. Negative controls (RNA from uninfected cells) confirmed the specificity of the PCR products for HSV1 transcripts only. (*): unspecific band. (B) Translation reporter assay to screen for HSV1 leader sequences that enhance translation during HSV-1 infection. 4T1 cells were transfected with the CAT plasmid and a β-GAL expression plasmid that serve as a transfection control. 8 hours post transfection, cells were infected with HSV-1716-GFP at an MOI of 5. Cells were lysed 18 hours post infection and CAT expression was quantified by ELISA, while β-GAL activity was quantified by colorimetric assay using ONPG substrate. (C) Predicted secondary structure and folding free energy of US11 (left panel) and UL27 (right panel) leaders using Vienna RNAfold[33]. Color scale bars represent base pairing probabilities. (D) Heatmap representing folding free energy of candidate HSV1 leaders, calculated using Vienna RNAfold.

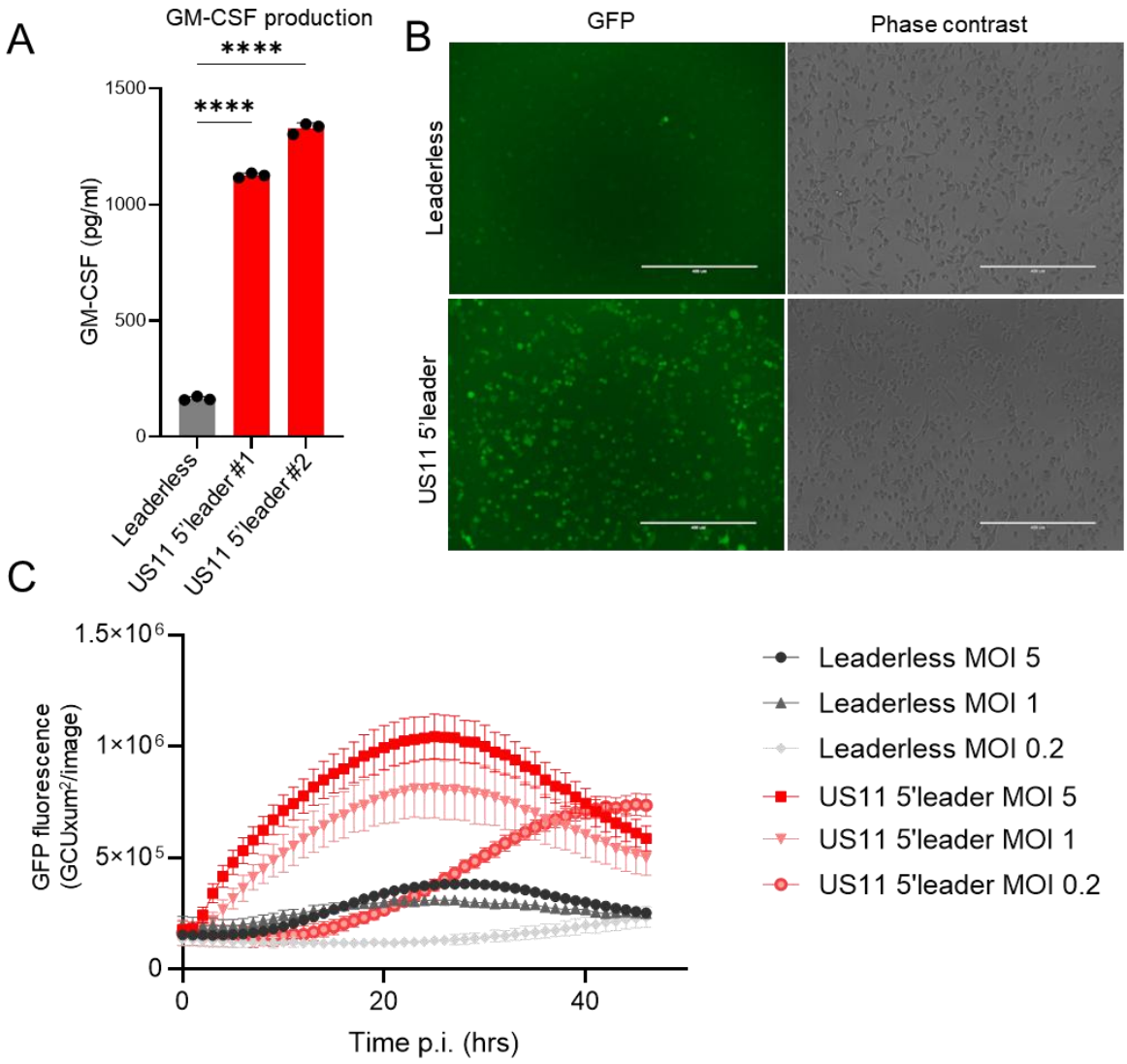
A
GM-CSF production
****
****
1500
1000
500
0
GM-CSF (pg/ml)
Leaderless
US11 5'leader#1
US11 5'leader#2
B
GFP
Phase contrast
Leaderless
US11 5'leader
C
1.5×10^6
1×10^6
5×10^5
0
GFP fluorescence (GCUxum²/image)
0
20
40
Time p.i. (hrs)
Leaderless MOI 5
Leaderless MOI 1
Leaderless MOI 0.2
US11 5'leader MOI 5
US11 5'leader MOI 1
US11 5'leader MOI 0.2
D
GM-CSF production
3000
2000
1000
0
GM-CSF (pg/ml)
****
****
****
ns
Mock
0.2
1
5
Mock
0.2
1
5
Leaderless
US11 5'Leader

Supplementary 3. 5. Characterizing expression enhancement by US11 5' Leader in oncolytic HSV1.

(A) Monolayer of Vero cells was infected with the indicated virus at a MOI of 5, and the culture supernatant was collected 24 hours post infection. GM-CSF concentration was quantified by ELISA. One-way ANOVA with Dunnett's post-hoc test was performed. n = 3 biological replicates. Error bars: ±sd. ****p < 0.0001. (B) Representative GFP fluorescence of HSV1 expressing Leaderless CSF2-GFP or US11 5'leader-CSF2-GFP. Monolayer of CT26 was infected with the indicated virus at an MOI of 5, then fluorescence microscopy images were taken at 24 hours post-infection. (C) Time course of GFP fluorescence of HSV1 expressing Leaderless CSF2-GFP or US11 5'leader-CSF2-GFP. Monolayer of CT26 was infected with the indicated virus at an MOI of 0.2, 1 or 5, then GFP fluorescence was monitored over 2 days post-infection using the Incucyte live cell imaging system. (D) Dose dependency analysis of secreted GM-CSF. CT26 cells were infected with the indicated virus at an MOI of 0.2, 1 or 5, then culture supernatant was collected 24 hours post-infection. GM-CSF concentration was quantified using ELISA. Two-way ANOVA with Sidak post-hoc test was performed. n = 3 biological replicates. Error bars: ±sd. ****p < 0.0001.

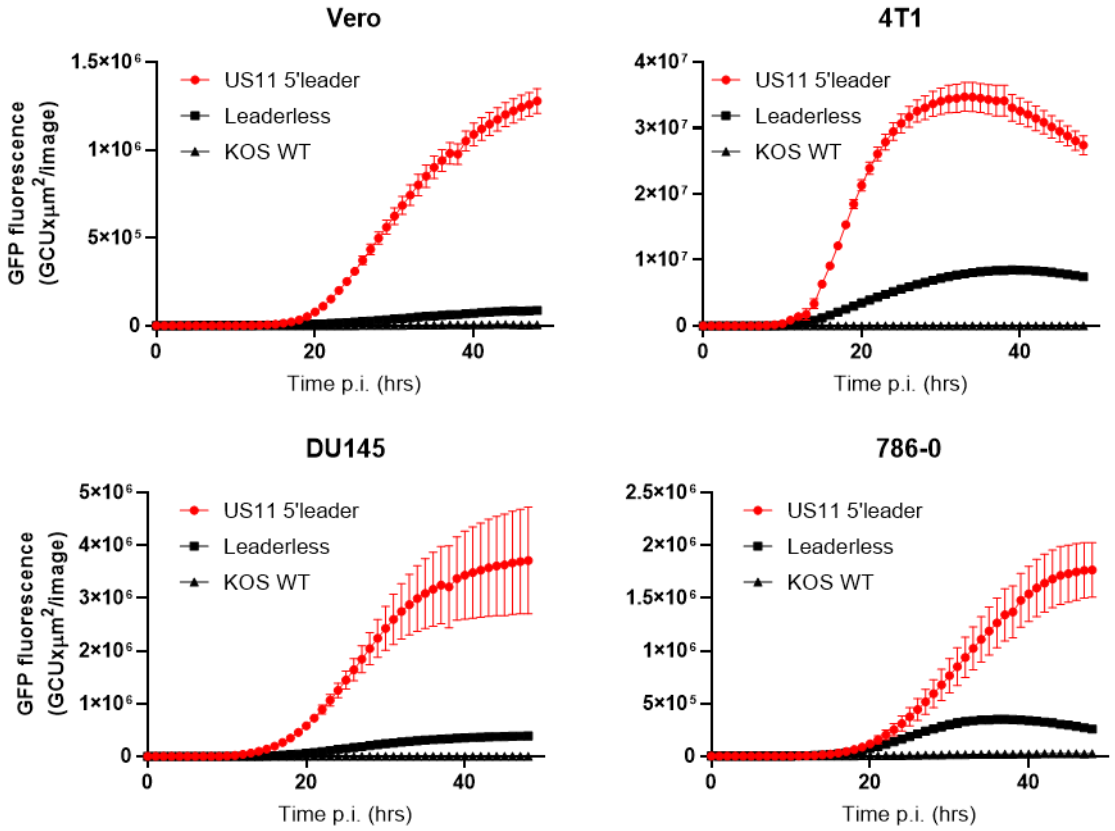

Supplementary 3. 6. US11 5'leader enhancement is robust in different cell types and species.

Monolayer of the African green monkey kidney cell line Vero, mouse breast cancer cell line 4T1, human prostate cancer cell line DU145 and human renal carcinoma cell line 786-O were infected with HSV1 KOS, HSV1 Csf2 or HSV1 US11-Csf2 at an MOI of 0.1, then GFP fluorescence intensity was followed for 48 hours using the Incucyte live cell imaging system.

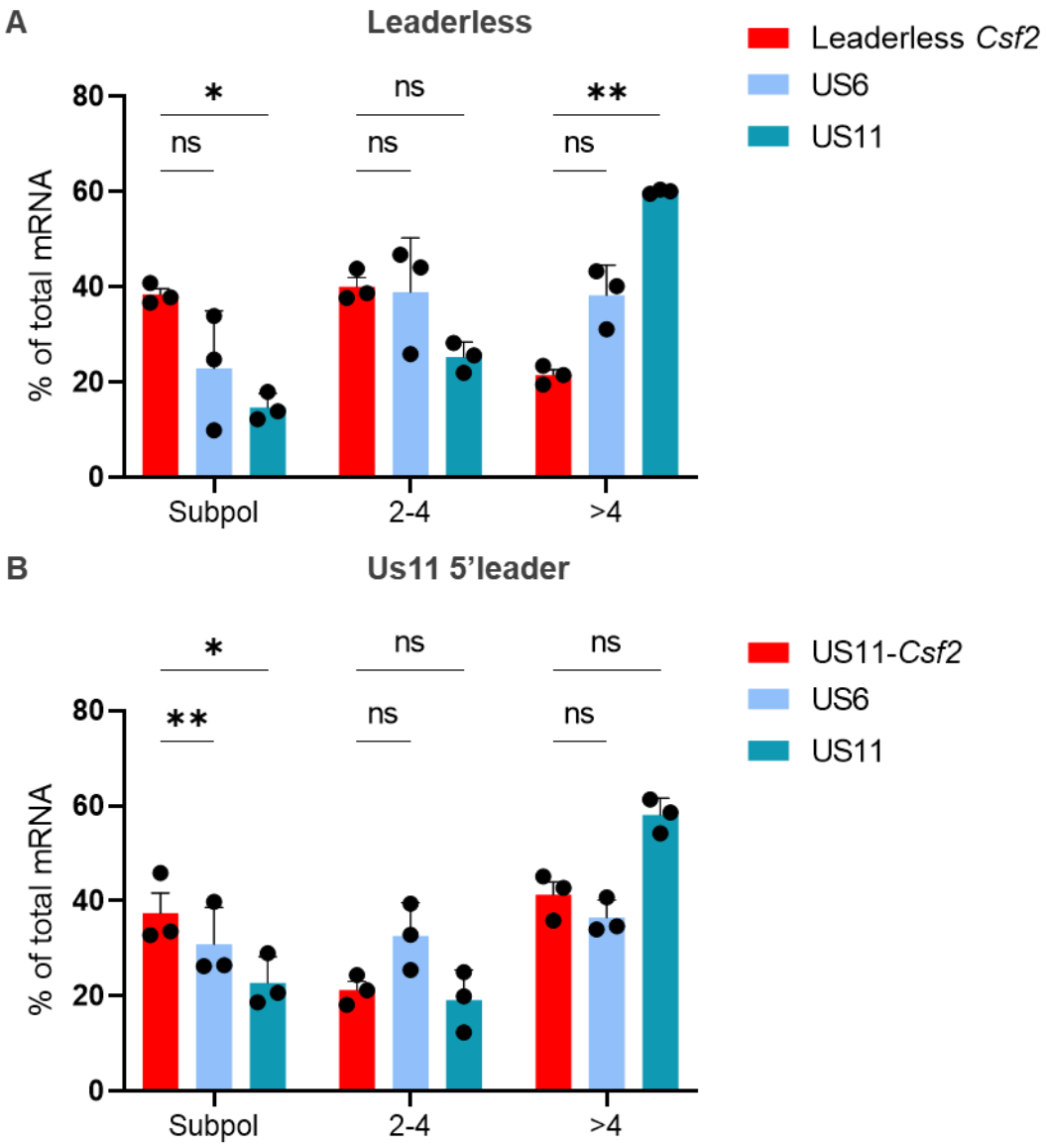

Supplementary 3. 7. Leaderless transgene mRNAs are suboptimally translated compared to viral mRNA.

In the same polysome profiling experiment described in Figure 4, the mRNA distribution of US6 and US11 were compared to that of leaderless Csf2 (A) or US11-Csf2 (B) mRNA.

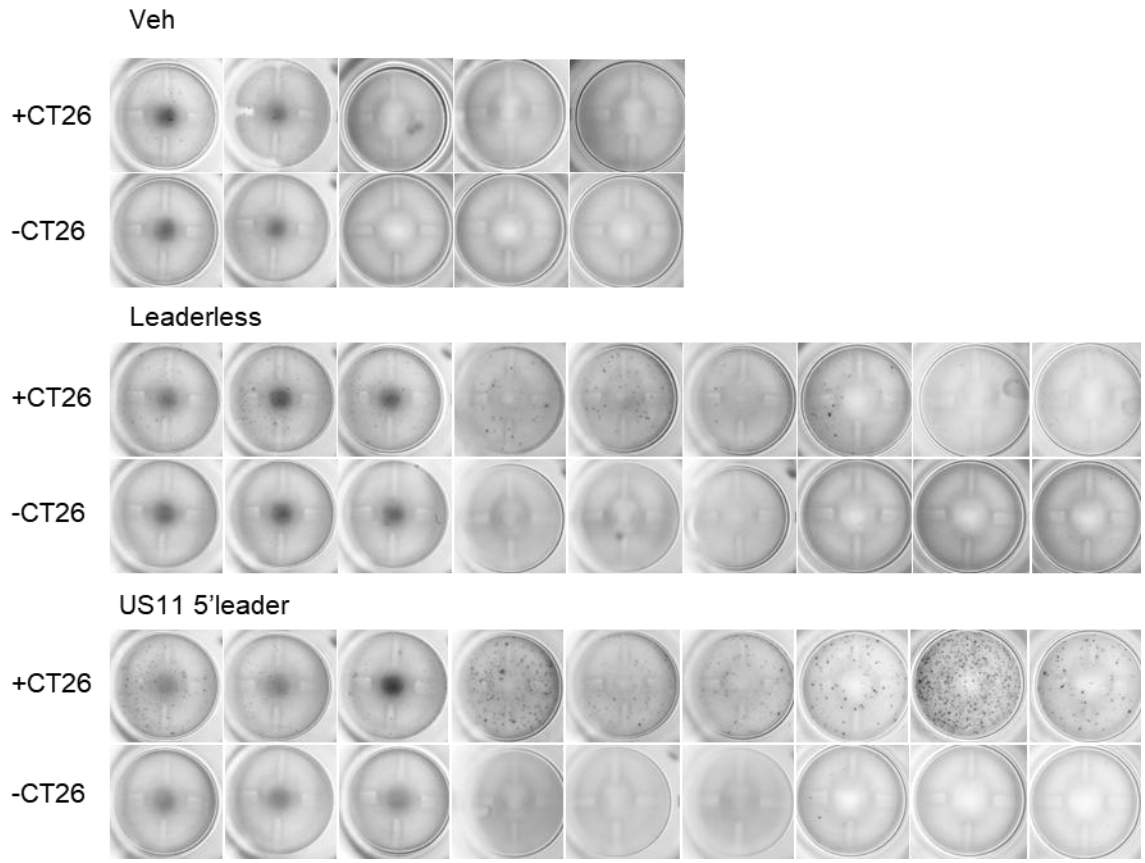

Supplementary 3. 8. Raw data of individual wells from the IFNγ ELISPOT experiment in Figure 3.5D.

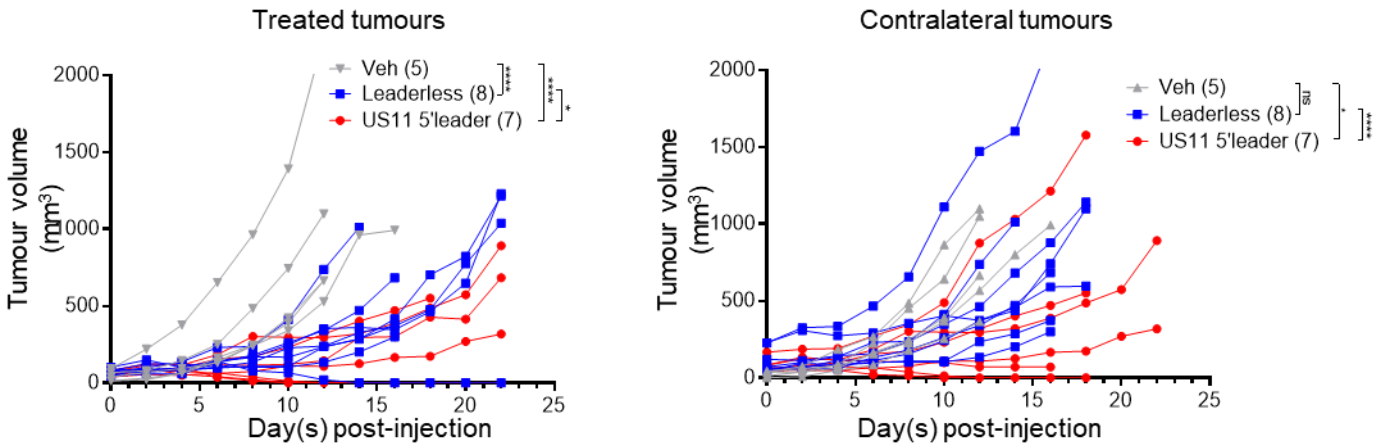

Supplementary 3. 9. Size of individual tumours in Figure 3.5E.

3.6 Discussion

In this work, we show that incorporating a HSV1 5'leader sequence enhances downstream transgene protein expression from a recombinant HSV1 virus. Our system tested for transgenes that are intracellular (CAT, LUC, GFP) or secreted (GM-CSF), and expression levels were consistently induced by the incorporation of the US11 5'leader during HSV1 infection. The elevated expression is mediated through increased mRNA translation of the modified transgene transcript within infected cancer cells. Importantly, we found that an oncolytic HSV1 harboring a 5'leader upstream of a therapeutic transgene has superior antitumour activity compared with a leaderless HSV1. This approach represents a simple yet highly effective way to improve the current generation of oncolytic HSV1 platforms that are presently in clinical trials. This strategy can be complementary to those that employ either a strong heterologous promoter to drive transgene expression, or an approach that inserts the transgene into a highly transcriptionally active region of the HSV1 genome. As an example of the former strategy, Toda *et al* found that a GM-CSF expression cassette driven by a CMV promoter and inserted into the TK region yielded approximately 55 pg of GM-CSF per 10^5 Vero cells.[51] In the present study, which also employed a CMV-driven GM-CSF expression cassette inserted in the TK region of the HSV1 genome, we saw 41.75±2.35 pg GM-CSF per 10^5 Vero cells, a value very close to that previously reported (supplemental figure 3.5A; calculated based on 167±9.4 pg/mL of GM-CSF observed in a 12-well plate format at confluency, which typically contains 4×10^5 cells in 1 mL of culture media). Yet, with the introduction of the US11 5'leader, close to an eightfold increase in GM-CSF production was obtained, representing a significant improvement in transgene protein expression. It is possible that transgene production could be improved even further by combining a strong HSV1 promoter (e.g., the one driving HSV1 RL2 expression)[47 52] with a translation enhancer found in viral 5'leaders and potentially also viral 3'UTRs. Additionally, minimal translation enhancing motif(s) specific for HSV1 infection could provide less recombination risk than full length 5'leaders, especially if to be applied to a novel generation of oncolytic HSV1 encoding for multiple therapeutic transgenes.

We have found that the enhanced translation of *Csf2* transcript expressed from a HSV1 backbone improved antitumour efficacy in a dual transplanted flank mouse cancer model. As expected, tumours treated with the leaderless-Csf2 HSV1 had slower progression, and the

corresponding mice had a better survival rate compared with mock-treated counterparts (figure 3.5F,G). However, the HSV1 US11-Csf2 virus not only inhibited tumour growth to a greater extent in the injected side, but also induced significant growth inhibition in the contralateral tumours and resulted in a further improved survival rate. Consistently, we observed a higher intratumoural GM-CSF concentration in tumours from mice administered the US11 5'leader HSV1, which also correlated with upregulation of proinflammatory genes (figure 3.5B,D) and elevated levels of tumour-specific immune cells in the spleens of treated mice (figure 3.5D), suggesting a modification of the tumour microenvironment toward a desired inflammatory milieu that resulted from an augmented anticancer immune response. As GM-CSF was previously shown to enhance systemic antitumour immune responses,[53] our data indicate that an increase in GM-CSF production can induce a more inflammatory tumour microenvironment and lead to an improved systemic anticancer immune response against distant tumours. Overall, our data show that the use of a strong promoter (CMV promoter) alone does not maximize transgene protein expression, but that incorporation of a translation enhancer can boost the payload levels further, leading to increased oncolytic virus efficacy.

The findings presented herein identified *cis*-acting sequences within virus-based therapies that can be exploited to enhance transgene protein expression. The method was first conceptualized by the comprehensive annotation of viral 5'leader sequences through TSS identification by RNA-Seq and mapping translational efficiency across a viral genome by ribosome profiling. During the lytic cycle, HSV1 expresses its genes in an orderly manner, classified into immediate-early (ie), early (E), and late (L) genes.[54] We screened for selected 5'leaders that are highly expressed in the late stage of HSV1 infection and thus might also be better tuned to enhance translation at this stage of infection (figure 3.2). Our mini-screen did not cover all HSV1 5'leaders; thus, there might be other specific viral sequences with potentially superior translation enhancing activity at a different time of infection that could be revealed with a more comprehensive study of all HSV1 5'leaders. This study provides an impetus to investigate whether HSV1 5'leaders mediate an additional layer of temporal regulation on HSV1 gene expression by translational regulation.

We have shown here that the HSV1 US11 5'leader sequence fused upstream of transgenes encoded within HSV1 can be used to enhance therapeutic payload expression and improve the antitumour efficacy of the virus. Our study exemplifies a novel method for optimizing the

expression level of a desired transgene that can be applied to other virus-based therapeutic contexts. These findings also invite further studies to better understand post-transcriptional gene expression in perturbed cellular conditions, such as in virally infected cells.

3.7 References

1. Rauch S, Jasny E, Schmidt KE, et al. New vaccine technologies to combat outbreak situations. Front Immunol 2018; 9.
2. Macedo N, Miller DM, Haq R, et al. Clinical landscape of oncolytic virus research in 2020. J Immunother Cancer 2020; 8.
3. Bulcha JT, Wang Y, Ma H, et al. Viral vector platforms within the gene therapy landscape. Signal Transduct Target Ther 2021; 6.
4. Serafini P, Carbley R, Noonan KA, et al. High-Dose granulocyte-macrophage colony-stimulating factor-producing vaccines impair the immune response through the recruitment of myeloid suppressor cells. Cancer Res 2004; 64:6337–43.
5. Conner J, Braidwood L. Expression of inhibitor of growth 4 by HSV1716 improves oncolytic potency and enhances efficacy. Cancer Gene Ther 2012; 19:499–507.
6. Pearl TM, Markert JM, Cassady KA, et al. Oncolytic virus-based cytokine expression to improve immune activity in brain and solid tumours. Mol Ther Oncolytics 2019; 13:14–21.
7. Zhang Q, Liu F. Correction: advances and potential pitfalls of oncolytic viruses expressing immunomodulatory transgene therapy for malignant gliomas. Cell Death Dis 2020; 11.
8. Zheng M, Huang J, Tong A, et al. Oncolytic viruses for cancer therapy: barriers and recent advances. Mol Ther Oncolytics 2019; 15:234–47.
9. Todo T, Ito H, Ino Y, et al. Intratumoural oncolytic herpes virus G47Δ for residual or recurrent glioblastoma: a phase 2 trial. Nat Med 2022; 28:1630–9.
10. Todo T, Ino Y, Ohtsu H, et al. A phase I/II study of triple-mutated oncolytic herpes virus G47Δ in patients with progressive glioblastoma. Nat Commun 2022; 13.
11. Cripe TP, Chen C-Y, Denton NL, et al. Pediatric cancer gone viral. part I: strategies for utilizing oncolytic herpes simplex virus-1 in children. Mol Ther Oncolytics 2015; 2.
12. Walsh D, Mohr I. Viral subversion of the host protein synthesis machinery. Nat Rev Microbiol 2011; 9:860–75.

13. Hoang H-D, Graber TE, Alain T, et al. Battling for ribosomes: translational control at the forefront of the antiviral response. J Mol Biol 2018; 430:1965–92.

14. Hu JCC, Coffin RS, Davis CJ, et al. A phase I study of oncovexgm-CSF, a second-generation oncolytic herpes simplex virus expressing granulocyte macrophage colony-stimulating factor. Clin Cancer Res 2006; 12:6737–47.

15. Breitbach CJ, Burke J, Jonker D, et al. Intravenous delivery of a multi-mechanistic cancer-targeted oncolytic poxvirus in humans. Nature 2011; 477:99–102.

16. Dhungel P, Cao S, Yang Z, et al. The 5'-poly (a) leader of poxvirus mrna confers a translational advantage that can be achieved in cells with impaired cap-dependent translation. PLoS Pathog 2017; 13.

17. Jha S, Rollins MG, Fuchs G, et al. Trans-kingdom mimicry underlies ribosome customization by a poxvirus kinase. Nature 2017; 546:651–5.

18. Mears WE, Rice SA. The RGG box motif of the herpes simplex virus ICP27 protein mediates an RNA-binding activity and determines in vivo methylation. J Virol 1996; 70:7445–53.

19. Sandri-Goldin RM. Icp27 mediates HSV RNA export by shuttling through a leucine-rich nuclear export signal and binding viral intronless RNAs through an RGG motif. Genes Dev 1998; 12:868–79.

20. Rivera AA, Wang M, Suzuki K, et al. Mode of transgene expression after fusion to early or late viral genes of a conditionally replicating adenovirus via an optimized internal ribosome entry site in vitro and in vivo. Virology 2004; 320:121–34.

21. Liu BL, Robinson M, Han Z-Q, et al. Icp34.5 deleted herpes simplex virus with enhanced oncolytic, immune stimulating, and anti-tumour properties. Gene Ther 2003; 10:292–303.

22. Hoang H-D, Graber TE, Jia J-J, et al. Induction of an alternative mrna 5' leader enhances translation of the ciliopathy gene INPP5E and resistance to oncolytic virus infection. Cell Rep 2019; 29:4010–23.

23. Kim D, Langmead B, Salzberg SL, et al. HISAT: a fast spliced aligner with low memory requirements. Nat Methods 2015; 12:357–60.

24. Afgan E, Baker D, Batut B, et al. The galaxy platform for accessible, reproducible and collaborative biomedical analyses: 2018 update. Nucleic Acids Res 2018; 46:W537–44.

25. Trapnell C, Williams BA, Pertea G, et al. Transcript assembly and quantification by RNA-seq reveals unannotated transcripts and isoform switching during cell differentiation. Nat Biotechnol 2010; 28:511–5.

26. Graber TE, Baird SD, Kao PN, et al. Nf45 functions as an IRES trans-acting factor that is required for translation of cIAP1 during the unfolded protein response. Cell Death Differ 2010; 17:719–29.

27. Minaker RL, Mossman KL, Smiley JR, et al. Functional inaccessibility of quiescent herpes simplex virus genomes. Virol J 2005; 2.

28. Gandin V, Sikström K, Alain T, et al. Polysome fractionation and analysis of mammalian translatomes on a genome-wide scale. J Vis Exp 2014;

29. Bommareddy PK, Peters C, Saha D, et al. Oncolytic herpes simplex viruses as a paradigm for the treatment of cancer. Annu Rev Cancer Biol 2018; 2:155–73.

30. Huang CJ, Wagner EK. The herpes simplex virus type 1 major capsid protein (VP5-UL19) promoter contains two cis-acting elements influencing late expression. J Virol 1994; 68:5738–47.

31. Steffy KR, Weir JP. Upstream promoter elements of the herpes simplex virus type 1 glycoprotein H gene. J Virol 1991; 65:972–5.

32. Pederson NE, Person S, Homa FL, et al. Analysis of the GB promoter of herpes simplex virus type 1: high-level expression requires both an 89-base-pair promoter fragment and a nontranslated leader sequence. J Virol 1992; 66:6226–32.

33. Goodart SA, Guzowski JF, Rice MK, et al. Effect of genomic location on expression of beta-galactosidase mRNA controlled by the herpes simplex virus type 1 UL38 promoter. J Virol 1992; 66:2973–81.

34. Mavromara-Nazos P, Roizman B. Delineation of regulatory domains of early (beta) and late (gamma 2) genes by construction of chimeric genes expressed in herpes simplex virus 1 genomes. Proc Natl Acad Sci U S A 1989; 86:4071–5.

35. Rixon FJ, Clements JB. Detailed structural analysis of two spliced HSV-1 immediate-early mRNAs. Nucleic Acids Res 1982; 10:2241–56.

36. Greco A, Simonin D, Diaz JJ, et al. The DNA sequence coding for the 5' untranslated region of herpes simplex virus type 1 ICP22 mRNA mediates a high level of gene expression. J Gen Virol 1994; 75 (Pt 7):1693–702.

37. Tang S, Patel A, Krause PR, et al. Hidden regulation of herpes simplex virus 1 pre-mrna splicing and polyadenylation by virally encoded immediate early gene ICP27. PLOS Pathog 2019; 15.

38. Tombácz D, Csabai Z, Szűcs A, et al. Long-read isoform sequencing reveals a hidden complexity of the transcriptional landscape of herpes simplex virus type 1. Front Microbiol 2017; 8.

39. Tombácz D, Moldován N, Balázs Z, et al. Multiple long-read sequencing survey of herpes simplex virus dynamic transcriptome. Front Genet 2019; 10.

40. Whisnant AW, Jürges CS, Hennig T, et al. Integrative functional genomics decodes herpes simplex virus 1. Nat Commun 2020; 11:2038.

41. Rutkowski AJ, Erhard F, L'Hernault A, et al. Widespread disruption of host transcription termination in HSV-1 infection. Nat Commun 2015; 6:7126.

42. Zhao TT, Graber TE, Jordan LE, et al. Hnrnp A1 regulates UV-induced NF-kappaB signalling through destabilization of cIAP1 mRNA. Cell Death Differ 2009; 16:244–52.

43. Tang S, Patel A, Krause PR, et al. Herpes simplex virus ICP27 regulates alternative pre-mRNA polyadenylation and splicing in a sequence-dependent manner. Proc Natl Acad Sci U S A 2016; 113:12256–61.

44. Donnelly MLL, Luke G, Mehrotra A, et al. Analysis of the aphthovirus 2A/2B polyprotein " cleavage" mechanism indicates not a proteolytic reaction, but a novel translational effect: a putative ribosomal " SKIP.". J Gen Virol 2001; 82:1013–25.

45. Kim JH, Lee S-R, Li L-H, et al. High cleavage efficiency of a 2A peptide derived from porcine teschovirus-1 in human cell lines, zebrafish and mice. PLoS One 2011; 6.

46. Pol J, Kroemer G, Galluzzi L, et al. First oncolytic virus Approved for melanoma immunotherapy. Oncoimmunology 2016; 5.

47. Malhotra S, Kim T, Zager J, et al. Use of an oncolytic virus secreting GM-CSF as combined oncolytic and immunotherapy for treatment of colorectal and hepatic adenocarcinomas. Surgery 2007; 141:520–9.

48. Moesta AK, Cooke K, Piasecki J, et al. Local delivery of oncovexmgm-CSF generates systemic antitumour immune responses enhanced by cytotoxic T-lymphocyte-associated protein blockade. Clin Cancer Res 2017; 23:6190–202.

49. Bhattacharya P, Budnick I, Singh M, et al. Dual role of GM-CSF as a pro-inflammatory and a regulatory cytokine: implications for immune therapy. J Interferon Cytokine Res 2015; 35:585–99.

50. Kim K-J, Moon D, Kong SJ, et al. Antitumour effects of IL-12 and GM-CSF co-expressed in an engineered oncolytic HSV-1. Gene Ther 2021; 28:186–98.

51. Toda M, Martuza RL, Rabkin SD, et al. Tumour growth inhibition by intratumoural inoculation of defective herpes simplex virus vectors expressing granulocyte-macrophage colony-stimulating factor. Mol Ther 2000; 2:324–9.

52. Thomas S, Kuncheria L, Roulstone V, et al. Development of a new fusion-enhanced oncolytic immunotherapy platform based on herpes simplex virus type 1. J Immunother Cancer 2019; 7.

53. Yan WL, Shen KY, Tien CY, et al. Recent progress in GM-CSF-based cancer immunotherapy. Immunotherapy 2017; 9:347–60.

54. Honess RW, Roizman B. Regulation of herpesvirus macromolecular synthesis. I. cascade regulation of the synthesis of three groups of viral proteins. J Virol 1974; 14:8–19.

CHAPTER FOUR: A PURINE-RICH 5′UTR ELEMENT DRIVES SELECTIVE TRANSLATION DURING RHABDOVIRUS INFECTION

Authors: Aida Said, Huy-Dung Hoang, Christa Osei, David Stojdl, Tyson Graber, Seyed Mehdi Jafarnejad, Marceline Côté, and Tommy Alain

Status: Manuscript submitted

4.1 Author Contributions

A.S. performed the majority of the experimental work and data analysis presented in this study. C.O. contributed to the generation of CRISPR–Cas9 plasmids and prepared supplementary figures related to motif enrichment from transcriptional datasets. T.A., H.-D.H., and M.C. conceived the study and guided the overall experimental design and interpretation of results. H.-D.H. provided continuous support in shaping experimental strategies and data interpretation. D.S. provided the MG1 virus and contributed key experimental resources. T.G., S.M.J., and T.A. performed ribosome profiling preparation and processing. All authors contributed to manuscript preparation and approved the final version.

4.2 Abstract

Viral infection triggers global repression of host protein synthesis, yet selective translation of specific transcripts persists under these restrictive conditions. The mechanisms enabling such escape remain poorly defined. Here, combining transcriptome and ribosome profiling during oncolytic Maraba virus (MG1) infection of glioblastoma cells, we reveal extensive transcription–translation decoupling and identify a subset of host mRNAs whose translational efficiency increases despite global shutdown. Motif analysis of translationally upregulated transcripts uncovers a conserved purine-rich element within their 5′ untranslated regions (5′UTRs). Functional reporter assays demonstrate that this R-motif is necessary to confer infection-induced translational activation. Among motif-containing genes, glycine decarboxylase (GLDC) is selectively upregulated at the translational level and functions as a host restriction factor limiting MG1 spread. Loss of GLDC enhances viral dissemination, linking motif-driven translation to antiviral defense. Together, these findings define a previously unrecognized cis-acting translational program in mammalian cells during viral infection and provide a modular strategy to sustain gene expression in translationally constrained environments, with implications for oncolytic virotherapy and gene-based therapeutics.

4.3 Introduction

Viral infection create a unique disturbance on the host translation machinery, generating a molecular "tug-of-war": the virus attempt to hijack this machinery to synthesize its own viral protein, while the cell shut down protein synthesis to restrict viral replication while maintaining translation of a subset of antiviral mRNAs[1]. A central antiviral mechanism of host cells is the global protein synthesis shutdown by phosphorylation of the translation initiation factor eIF2α via PKR[1,2]. Several interferon-stimulated genes (ISGs) also inhibit viral protein synthesis by targeting distinct steps of translation. For example, Interferon-Induced Protein with Tetratricopeptide Repeats 1 (IFIT1) blocks cap-dependent initiation by binding non-canonical RNA caps[3,4], and ISG15 or OAS/RNase L pathways degrade viral RNA and reduce ribosome loading[5–7]. Some viruses, on the other hand, evolved mechanisms to bypass the host's antiviral translation inhibition through cap-independent cis-element termed the internal ribosome entry site (IRES), viral cap-independent translation elements (CITEs), structured RNA elements within untranslated regions, as well as eIF4F-independent initiation pathways and m^{6}A-mediated regulation. These diverse strategies enable viral and cellular mRNAs to sustain protein synthesis[8–13]. Multiple prominent gene therapy platforms, including oncolytic virus, mRNA and saRNA therapies, require the expression of transgenes in this unique translation control environment. However, little is known about this translation environment severely limit expression output of therapeutic transgene and therapeutic efficacy.

Despite being one of the two major gene expression layers during infection, the translation program of the antiviral state remains poorly characterized compared to the transcription program. However, advancement in the last decade in high-throughput techniques to measure translation output at the global scale, such as ribosome-profiling and polysome profiling, has shed light to a dynamically regulated program as complex as the transcription level[14,15]. Various studies show extensive decoupling between mRNA levels and ribosome occupancy, with many antiviral transcripts induced at the mRNA level but not efficiently translated, while others become selectively translated despite having stable or declining transcript abundance[16–18]. While this uncoupling suggests mechanisms at the translation level that play a key role in determining whether a transcript is repressed or induced during infection, the molecular mechanisms for this regulatory network remain largely unknown.

Several studies have shown that cis-acting elements in mRNA can regulate translation output during host-pathogen interaction. The most well-studied translation enhancing motif is the 5'terminal oligopyrimidine (5'TOP) motif[19,20]. Found mostly at the 5'end of genes of the translation machinery, the motif mediates translation enhancement by mTORC1, which frequently occur during innate immune and inflammation activation[21]. In plants, a purine-rich "R-motif" in 5′UTRs enables defence mRNAs to escape global translational repression during innate immunity triggered by microbe-associated molecular pattern[22]. It was later revealed that this motif can mediate cap-independent translation initiation through Poly(A)-Binding Protein (PABP)[23,24]. Alternatively, cis-element can also suppress translation and stability of the associated mRNAs, such as the case of AU-rich element (ARE) and interferon gamma-activated inhibitor of translation (GAIT) element[25,26], both of which are found in the 3'UTR of inflammatory cytokine mRNAs and suppress their expression to prevent runaway inflammation that can lead to tissue damage.

Oncolytic viruses (OVs) are wildtype or engineered viruses that have high oncotropism. Treatment of tumour tissue with OVs leads to direct tumour lysis by virus infection, but also induce local inflammation, recruitment of immune cell and induction of tumour-specific immune response[27]. OVs are generally armed with a "payload", therapeutic transgenes that further promote tumour cytotoxicity or antitumour immune response[28]. MG1 is a genetically engineered oncolytic Maraba virus, a rhabdovirus closely related to vesicular stomatitis virus (VSV), that exhibits potent oncolytic activity due to a double mutation in the matrix (M; L123W) and glycoprotein (G; Q242R) proteins, which enhances tumour selectivity while limiting pathogenicity in normal tissues[29,30]. To determine the translational regulation during rahbdovirus oncolysis, we profiled both mRNA abundance and ribosome footprints to measure transcription and translation rates in glioblastoma cells during early infection. MG1 induced substantial transcription–translation decoupling and revealed a subset of host transcripts whose translational efficiency increased despite a global shutdown of protein synthesis. Motif analysis of these translational efficiency (TE)-upregulated genes uncovered a purine-rich 5′UTR element resembling plant R-motifs but operating in human cells. We find that this motif acts as a cis-acting enhancer of translation during infection, requires PABP activity, and contributes to the selective translation of Glycine decarboxylase (GLDC), a metabolic antiviral effector whose loss increases MG1 spread.

Altogether, these findings uncover a novel translation mechanism that enhance translation output during the antiviral state via purine-rich cis-acting motif. This element can be exploit for engineering translationally-enhanced expression of therapeutic payloads encoded in oncolytic virus genome to maintain optimal expression level by adapting to the translation regulation of the infected cells .

4.4 Methods

Cell Culture and Viruses

Glioblastoma human cell lines U434 and U373, human HEK293T, and African green monkey Vero cells were obtained from the American Type Culture Collection (ATCC, Manassas, VA, USA). These cells were cultured in Dulbecco's Modified Eagle Medium (DMEM, Grand Island, NY, USA) (Fisher, New York, NY, USA) supplemented with 10% fetal bovine serum (Sigma, Tokyo, Japan) and 0.1% penicillin and streptomycin (Life Technologies, Waltham, MA, USA) at 37 °C in 5% CO2.

VSVΔ51-Red were kindly provided by Dr. John Bell (Ottawa Hospital Research Institute). Vero cells were used to propagate MG1, VSVΔ51-RFP. Briefly, cells were inoculated with viruses. Cells were then subjected to three freeze–thaw cycles to release intracellular viruses. Freeze–thawed lysates were clarified by centrifugation at 500× g for 5 min, and the supernatants were collected. Viral supernatants were subjected to ultracentrifugation at 10,000× g for 90 min. VSV was ultracentrifuged again with at 28,000 × g on a sucrose cushion layer (36% sucrose, 10 mM HEPES, 150 mM NaCl, 0.1 mM EDTA, pH 7.3). For palleted MG1 was ultra purified using a 10–40% opti-prep gradient as previously described [23]. Titers were determined by plaque titration using Vero cells monolayer and using 1% carboxymethylcellulose.

Ribosome profiling

Ribosome profiling was carried out on two independent biological replicates following the approach described by Jafarnejad et al. (2018)[31]. To preserve actively translating ribosomes, U343 cells were treated with cycloheximide prior to lysis. Cell lysates were subsequently divided into two parallel processing streams. One portion was used for total RNA extraction and RNA-seq analysis (described below), while the other portion underwent RNase I digestion to generate ribosome-protected fragments.

For RNA-seq library preparation, 150 µg of total RNA was isolated, and polyadenylated [poly(A)+] mRNA was enriched using magnetic oligo(dT) Dynabeads (Thermo Fisher Scientific) according to the manufacturer's protocol. The purified mRNA was eluted and combined with an equal volume of 2× alkaline fragmentation buffer (2 mM EDTA, 10 mM Na_2CO_3, 90 mM $NaHCO_3$), followed by incubation at 95°C for 20 minutes to induce fragmentation. Reactions were terminated using a stop/precipitation solution containing 300 mM sodium acetate (pH 5.5) and GlycoBlue, and RNA was recovered by isopropanol precipitation using standard procedures.

Fragmented mRNA was size-fractionated on a denaturing 10% urea–polyacrylamide gel, and RNA fragments corresponding to 35–50 nucleotides were excised, eluted, and precipitated. In parallel, ribosome-protected fragments of approximately 28–32 nucleotides were purified from the RNase I–treated samples. Both total RNA fragments and RPFs were used for cDNA library construction as previously described (Jafarnejad et al., 2018)[31].

To minimize ribosomal RNA contamination, subtractive hybridization was performed using biotinylated oligonucleotides complementary to highly abundant rRNA species. Libraries derived from mRNA fragments and RPFs were PCR-amplified (10 cycles) with indexed primers and sequenced on an Illumina HiSeq 2000 platform using 50-nucleotide single-end reads at the McGill University and Génome Québec Innovation Centre.

Ribosome Profiling and RNA-Seq Data Processing and Analysis

Ribosome profiling (Ribo-seq) and total RNA-sequencing (RNA-seq) data were analyzed using the Galaxy online platform following a standardized workflow (https://usegalaxy.org). Raw sequencing reads were obtained as FASTQ files from the sequencer. Adapter sequences and low-quality bases were removed using Trimmomatic, with reads containing low-quality nucleotides filtered according to default quality parameters. Following preprocessing, cleaned reads were aligned to a combined reference consisting of the human genome (hg38) and the Maraba virus genome using Bowtie2 with the very-sensitive-local alignment setting. This mode was selected to maximize alignment sensitivity while allowing for soft-clipping of residual adapter or low-quality sequence. Only successfully mapped reads were retained for downstream analyses. Gene expression levels were quantified using Cufflinks, which calculates transcript abundance as Reads Per Kilobase of transcript per Million mapped reads (RPKM). Gene-level RPKM values were derived from mapped reads for both RNA-seq and ribosome-protected fragment (RPF) libraries.

To reduce background noise from lowly expressed genes, only genes with an expression level of ≥ 5 RPKM were retained for downstream analyses. This filtering step was applied at the gene expression quantification stage, following read alignment and RPKM calculation, and was used to exclude genes with minimal or unreliable signal. Translation efficiency was defined as the ratio of RPF RPKM to RNA-seq RPKM for each gene.

Pathway and Interferon Signature Analysis of Transcriptional and Translational Datasets

Differentially expressed gene (DEG) lists derived from RNA-seq, ribosome profiling (RPF), and translation efficiency (TE) analyses were subjected to functional pathway and interferon signature analyses. For pathway enrichment, genes were analyzed separately at the mRNA, RPF, and TE levels using QIAGEN Ingenuity® Pathway Analysis (IPA®, QIAGEN, Redwood City, CA). Canonical pathway enrichment was assessed using IPA's right-tailed Fisher's exact test, and pathway significance was reported as $-\log_{10}$(p-value), with enriched pathways ranked based on statistical significance and visualized together with their associated molecules. In parallel, gene lists generated for the MG1 versus MOCK comparison at the mRNA, RPF, and TE levels were submitted to the Interferome database (v2.0) to identify genes annotated as interferon-regulated based on curated experimental evidence (https://www.interferome.org)[32].

Motif analysis

Translationally upregulated genes were ranked based on translational efficiency (TE) , and the top candidates were selected for downstream analysis. After restricting to protein-coding transcripts with annotated 5′UTRs, a final set of 83 genes was used for motif discovery. To assess the robustness of motif enrichment, we extended the analysis to larger gene sets (e.g., top 150–200 ranked genes). For each gene, the canonical transcript was identified using the Ensembl database. The corresponding 5′ untranslated region (5′UTR) sequences of the selected transcripts were then extracted using R. These 5′UTR sequences were uploaded to the MEME Suite motif discovery tool for analysis[33] (https://meme-suite.org). Motif discovery was performed using parameters allowing multiple occurrences of a motif within a single sequence and restricting motif identification to the given strand only.

Luciferase plasmid cloning and luciferase assay

Six 5′UTR sequences corresponding to the genes MEF2C, SCNN1D, CLEC7A, NPIPB4, GLDC, and IL3RA, beta actin with and without R motif, (see Table 4.1 for all cloned sequences in LUC plasmid) were cloned into the pcDNA3 RLUC–PolIRES–FLUC plasmid (Addgene plasmid #45642) downstream of the T7 promoter. The resulting constructs were transfected into cells using Lipofectamine 3000 (Thermo Fisher Scientific; cat. #L3000008). Two hours post-transfection, cells were infected with MG1 at a multiplicity of infection (MOI) of 1 or 5 or VSV at MOI of 0.5 or 1. Twenty-four hours post-infection, luciferase activity was measured using the Dual-Luciferase Reporter Assay System according to the manufacturer's instructions (Promega; cat. #E2920).

Polysome profiling

U343 cells were seeded in 15-cm dishes and, after 24 h, were infected with MG1 at MOI of 1. At 8 or 12 hours post infection (hpi), cycloheximide (CHX) was added directly to the culture medium to a final concentration of 100 μg/mL and cells were incubated at 37°C for 5 min to arrest ribosomes on mRNAs. Cells were then washed with ice-cold PBS containing CHX, scraped, and collected by centrifugation at 500 × g for 5 min at 4°C.

Cell pellets were lysed in hypotonic lysis buffer (5 mM Tris, pH 7.5; 2.5 mM $MgCl_2$; 1.5 mM KCl) supplemented with cycloheximide (100 μg/mL), DTT (2 mM), RNase inhibitor (200 U/mL), 0.5% Triton X-100, and 0.5% sodium deoxycholate. Lysates were clarified by centrifugation, and the supernatant containing ribosome-bound mRNAs was loaded onto a 10–50% sucrose gradient prepared in buffer containing 200 mM HEPES-KOH (pH 7.6), 1 M KCl, 50 mM $MgCl_2$, and cycloheximide (1000 μg/mL).

Gradients were ultracentrifuged at 36,000 rpm for 2 h at 4°C with maximum acceleration and deceleration set to 5. Following centrifugation, gradients were fractionated at a flow rate of 0.75 mL/min, and 15 fractions were collected for RNA extraction using TRIZOL following the manufacturer protocol.

Western Blot

U343 cells were infected with MG1, and at 24 h post-infection cells were collected and lysed using RIPA buffer supplemented with supplemented with 10 mM NaF, 10 mM Na2VO3 and cOmplete Protease Inhibitor Cocktail (Roche). Protein concentration was determined using a BCA

assay, and 25 μg of total protein was resolved on a 10% Bis-Tris polyacrylamide gel (Cat#: 1610183, Bio-Rad). Proteins were then transferred onto a PVDF membrane using a semi-dry transfer system (Cat#: 10026938, Bio-Rad) . Membranes were blocked with blocking buffer (Cat#: 2010020, Bio-Rad) for 30 min, followed by incubation with the primary antibody against β-actin (1:10,000), PABP (Cat#: 4992S, cell signaling, 1:1000), GLDC (Cat#: PA522102, Invitrogen, 1:500) overnight at 4°C. Membranes were subsequently incubated with fluorescently labeled or HRP-conjugated secondary antibodies for 1 h. HRP-conjugated signals were detected using ECL substrate (Cat#:1705061, Bio-Rad).

Quantitative RT-PCR (RT-qPCR)

At 24 h post-infection (hpi) with MG1 at a MOI of 1 or 5, total RNA was extracted from cells using TRIzol reagent according to the manufacturer's instructions. 1 μg of total RNA was reverse-transcribed into cDNA ca the iScript™ Advanced cDNA Synthesis Kit (Bio-Rad). RT-qPCR was performed using iQ™ SYBR Green Supermix (Bio-Rad) on a Realplex 2 thermocycler (Eppendorf). The PCR cycling conditions consisted of 95°C for 5 min, followed by 40 cycles of 95°C for 10 s, 60°C for 30 s, and 72°C for 30 s. GLDC mRNA abundance was quantified using the ΔΔCt method and normalized to β-actin expression.

Generation of Cas9-stable U343 cells and dual-gRNA CRISPR constructs

To generate a Cas9-stable U343 cell line, lentivirus encoding Cas9 were produced by co-transfecting HEK293T cells with pCW-Cas9, psPAX2, and pMD2.G plasmids (Addgene) at a ratio of 4:3:1, respectively, using lipofectamine 3000. Lentiviral supernatants were collected at 48 and 72 h post-transfection, filtered through a 0.45-μm filter, and used to transduce U343 cells in the presence of polybrene (10 μg/mL). Transduced cells were selected with puromycin (1 μg/mL) for 4 days, followed by single-cell cloning. Monoclonal populations were screened for Cas9 expression following induction with doxycycline (1 μg/mL) for 48 h, and the clone with the highest Cas9 expression and without leaky expression was selected for downstream experiments.

For dual-gRNA plasmid construction, two guide RNAs (gRNAs) per gene (non-targeting control, GLDC, and PABP) were designed using CHOPCHOP, targeting two distinct exons per gene. Dual-gRNA inserts (~110 bp) were generated by PCR amplification of four fragments: Fragment 1 (43 bp), Fragment 2 containing gRNA1 (60 bp), Fragment 3 containing gRNA2 (60

bp), and Fragment 4 (40 bp). The amplified fragment were assembled using Gibson assembly together with the U6 promoter and gRNA scaffold excised from the pDonor-sU6 plasmid (Addgene), and subsequently cloned into the lenti-sgRNA(MS2)_zeo backbone plasmid (Addgene), as described previously[34].

For CRISPR lentivirus production and transduction, HEK293T cells were co-transfected using Lipofectamine 3000 with pMD2.G (VSV-G), psPAX2 (packaging), and CRISPR transfer plasmid at a ratio of 1:3:4, respectively. Lentiviral supernatants were collected at 48 and 72 h, filtered through a 0.45-µm filter, and used to transduce the selected Cas9-U343 monoclonal cell line in the presence of polybrene (10 µg/mL). Transduced cells were selected with zeocin (500 µg/mL) for 7 days. All constructs were verified by Sanger sequencing prior to use.

Live Cell Monitoring of Virus Infection

MG1 infectivity and spread were monitoried using the IncuCyte ZOOM™ Live-Cell Analysis System (Sartorius, Göttingen, Germany). CRISPR GLDC and non-targeted CRISPR U343 cell lines were infected with MG1 of MOI 0.1. Images were captured every 2 h at 10× magnification to monitor viral infection of live cells based on fluorescence. The acquired images were analyzed using the accompanying IncuCyte ZOOM™ (Incucyte S3 Software v2018A) (Sartorius). Measurement of total green object area (µm^2/well) was utilized to determine the level of virus infection.

Table 4. 1. Oligos Used in this study

Oligonucleotides	SOURCE
5'UTR cloning in pcDNA3 RLUC–PolIRES–FLUC plasmid	
MEF2C	
GTTGTTGCTAGCGCAGTCACAGACACTTGAGCACACGCGTACACCC AGACATCTTCGGGCTGCTATTGGATTGACTTTGAAGGTTCTGTGTG GGTCGCCGTGGCTGCATGTTTGAATCAGGTGGAGAAGCACTTCAAC GCTGGACGAAGTAAAGATTATTGTTGTTATTTTTTTTTCTCTCTCT CTCTCTCTTAAGAAAGGAAAATATCCCAAGGACTAATCTGATCGGG TCTTCCTTCATCAGGAACGAATGCAGGAATTTGGGAACTGAGCTGT GCAAGTGCTGAAGAAGGAGATTTGTTTGGAGGAAACAGGAAAGAG AAAGAAAAGGAAGGAAAAAATACATAATTTCAGGGACGAGAGAG AGAAGAAAAACGGGGACTGCTAGCGTTGTT	Thermofisher
SCNN1D	

GTTGTTGCTAGCCCTGGGCGACAGCGAGACTCCATCTCAATAAATA AAAAAAAAAAAGAGTTGTTATCAGTAGAAGGGAATGTCTGGTTAC AGTATGGCGTTGTGCAGATGAAGGTCTTATCGCAGATGAAGCCACC AGGTCACAAGCCTCAGAGAGAATCAACTATAAATGCTTCTCATCAG ACTCAAGGCCTGAGGTGATGCTGATGCTGTGCCTGAATTCCAGCAG GGAGGAGGCGCTAGCGTTGTT	Thermofisher
CLEC7A	
GTTGTTGCTAGC AGTACCTAGCCCACATGATTTGACTCAGAGATTCTCTTTTGTCCAC AGACAGTCATCTCAGGAGCAGAAAGAAAAGAGCTCCCAAATGCTA TATCTATTCAGGGGCTCTCAAGAACAGCTAGCGTTGTT	Thermofisher
NPIPB4	
GTTGTTGCTAGCGTTTCAGGCACAGAACTGTATATCCAATAATAGT GAAATGGATCCCACTAATTATGACAGAAATGATGATACATTTAAAT GACTTGGATGTTTTATAGGTATGATCTCGTGAAATCTTGAGAGAAA CTGAATGACGAATGAAACTATTGTTCCTGTTTCACACAGAAGAAAA CTGAGGTTGGCACTCATCATGAGCCCCTGTTCTCATTCTGCAAGCT AGCGTTGTT	Thermofisher
IL3RA	
GTTGTTGCTAGCCTTCGGTTTCTCTTCGGGGAAAGCTGCTTTCAGCG CACACGGGAAGATATCAGAAACATCCTAGGATCAGGACACCCCAG ATCTTCTCAACTGGAACCACGAAGGCTGTTTCTTCCACACAGTACT TTGATCTCCATTTAAGCAGGCACCTCTGTCCTGCGTTCCGGAGCTG CGTTCCCGGCTAGCGTTGTT	Thermofisher
GLDC	
GTTGTTGCTAGC AAAGTGTGCGGAGCAGGTGCCTTGGGTGGAGCCACAACTTTGCGC GAGTGTCTTGGTTGAGCGCAGCGCCCATTCATTGCCCGCGAGCGTC CATCCATCTGTCCGGCCGACTGTCCAGCGAAAGGGGCTCCAGGCCG GGCGCAGCCGCCACCCGGGGGACCGAGGCCAGGAGAGGGGCCAA GAGCGCGGCTGACCCTTGCGGGCCGGGGCAGGGGACGGTGGCCGC GGCCGCTAGCGTTGTT	Thermofisher
GLDC-ΔR	

GTTGTTGCTAGCGGTGCCTTGGGTGGAGCCACAACTTTGCGCGAGT GTCTTGGTTGAGCGCAGCGCCCATTCATTGCCCGCGAGCGTCCATC CATCTGTCCGGCCGACTGTCCAGCGAAAGGGGCTCCAGGCCGGGC GCAGCCGCCACCCGGGGGACCGAGGCCAGGAGAGGGGCCAAGAG CGCGGCTGACCCTTGCGGGCCGGGGCAGGGGACGGTGGCCGCGGC CGCTAGCGTTGTT	Thermofisher
Reverse Fluc:	
5’ ttctggatcataaactttcg 3’	Thermofisher
F-MEF2C:	
5’ GCAGTCACAGACACTTGAGC 3’	Thermofisher
F-SCNN1D	
5’ CCTGGGCGACAGCGAGACTC 3’	Thermofisher
F-CLEC7A	
5’ AGTACCTAGCCCACATGATT 3’	Thermofisher
F-NPIPB4	
5’ GTTTCAGGCACAGAACTGTA 3’	Thermofisher
F-IL3RA	
5’ TCTTCGGGGAAAGCTGCTTT 3’	Thermofisher
F-GLDC	
5’ AGTGTGCGGAGCAGGTGCCT 3’	Thermofisher
ACTB-F	
GTTGTTGCTAGCACCGCCGAGACCGCGTCCGCCCCGCGAGCACAG AGCCTCGCCTTTGCC	Thermofisher
ACTB-R	
AACAACGCTAGCGGTGAGCTGGCGGCGGGTGTGGACGGGCGGCGG ATCGGCAAAGGCGAG	Thermofisher
ACTB-F-Motif	
GTTGTTGCTAGCAAAGTGTGCGGAGCAACCGCCGAGACCGCGTCC GCCCCGCGAGGAGCACAGAGCCT	Thermofisher
GLDC-F qPCR	
GTACAGCTCAGGCCCTCTTG	Thermofisher
GLDC-R qPCR	
TGCTCGCTTGAGACCTTCTG	Thermofisher
gRNAs	
GLDC	
TCATCAATCCGGGCAATCGTTGG	IDT
AGGACAGGTCTACCTAGACGGGG	IDT
PABPC1	

AAGCACGCTCCGCTGCAGGAAGG	IDT
ATGGCAGCTATCCCACAGGTAGG	IDT
NTC	
GGGACGCGAAAGAAACCAGT	IDT
GTATTACTGATATTGGTGGG	IDT

4.5 Results

MG1 Infection Suppresses Global Gene Expression and Decouples Transcription from Translation

MG1 activity *in vitro* is characterized by rapid innate antiviral sensing and clearance, and multiple studies indicate that antiviral barriers can act post-transcriptionally through stress- and translation-control pathways (e.g., eIF2α/4E-BP1 signalling), raising the possibility that transcriptional changes alone cannot comprehensively reflect proteins output during MG1 infection[35–38]. To define conditions that preserve measurable translation during infection, we first evaluated the impact of MG1 on global protein synthesis. Polysome profiling and S^{35} metabolic labeling revealed substantial translation suppression at MOI = 1 and 12 h post-infection (Figure 4.1A–B). Therefore, RNA-seq and ribosome profiling were performed at 6 h post-infection to capture early gene expression changes prior to extensive translational shutdown and to define how MG1 infection reprograms gene expression in glioblastoma cells. U343 cells were infected with MG1 (MOI = 1) for 6 h and processed for paired transcriptome (RNA-seq) and translatome (Ribo-seq) profiling (Figure 4.1C). After adapter trimming and quality filtering (Supplementary Fig. 4.1A), reads were aligned to the human and MG1 genomes. Gene expression at the RNA and RPF level were computed, and TE of individual gene were calculated using the formula TE = RPF/RNA. RNA and RPF reads from mock samples mapped almost exclusively to human transcripts, whereas infected samples displayed abundant viral RNA and RPF reads (Supplementary Fig. 4.1B), confirming active viral transcription and translation.

MG1 infection has been reported to trigger global translational repression while permitting selective translation of specific host mRNAs[38]. Consistent with this, MG1 infection in U343 cells caused a global decrease in mRNA abundance, ribosome occupancy, and translational efficiency (Supplementary Fig. 4.1C). Under mock or MG1 conditions, steady-state mRNA and RPF values remained strongly correlated at the genome-wide level ($r = 0.8574$, $r = 0.8020$) (Fig. 4.1D–E). In contrast, decoupling between transcription and translation regulation occur during infection, as we

observe an inverse correlation between fold-change at the RNA and RPF level (Figure 4.1F, r = −0.2826) and RNA and TE (Figure 4.1G, r = −0.5088) of differentially expressed genes modulated by infection. Table 4.2 and 4.3 show the upregulated genes at mRNA and TE level respectively revealed minimal overlap, confirming that MG1 infection rapidly uncouples transcription from translation regulation of differentially expressed genes. Together, these data demonstrate that without accounting for translation regulation, pathway activation inferred from mRNA levels alone may incompletely reflect global response to infection.

Distinct Transcriptional and Translational Responses During MG1 Infection

Next, we sought to characterize the host response to MG1 infection at the transcription and translation levels. We applied a cut-off of 2 fold-change in expression, and identified genes that are up- and down-regulated at the transcription level (Table 4.2), and genes that are up- and down-regulated at the translation level (Table 4.3). To detect activated biological pathways, Ingenuity Pathway Analysis (IPA) was performed separately on transcriptionally- and translationally-upregulated gene sets (RNA-up and TE-up, respectively). As expected, transcriptionally-upregulated genes were strongly enriched for canonical antiviral programs, such as interferon signalling, chemokine signaling, or pathogen induced cytokine storm signaling (Figure 4.2A). These pathways belong to three main functional categories of antiviral interferon response, chemokine-mediated recruitment and MAPK-IL17 inflammatory pathway, representing a mixture of direct antiviral response and cell-mediated inflammatory response. Representative transcripts within these pathways showed robust mRNA induction, but with minimal changes or even a reduction in TE (Figure 4.2B). On the other hand, translationally-upregulated genes are enriched in a distinct set of processes, such as crosstalk between dendritic cells and NK cells, Th2 pathway or glycine biosynthesis (Figure 4.2C). These pathways belong to the three main function categories of Immune crosstalk & Checkpoint pathway, CA2+/MAPK Stress-responsive pathway and Metabolic Adaptation pathways, which show a focus on cell-mediated immune response and metabolic adaptation. Although these genes displayed marked increases in translation efficiency, their mRNA abundance remains stable or even reduced during infection (Figure 4.2D), corroborating the transcription-translation decoupling observed in RNAseq and ribose data (Table S4.1 and 4.2).

As interferon signalling defines the dominant antiviral and inflammatory response during viral infection, we asked whether there is a translation component to the expression program of interferon stimulated genes. We intersected differentially expressed genes with the Interferome database, which aggregated publicly available data for gene regulated by Type I, II or III interferon to assess how interferon-responsive programs are regulated at the transcription and translation level during MG1 infection. 87 of the 251 top transcriptionally up-regulated genes are interferon regulated genes (Supplementary Fig. 4.2A-D). Intriguingly, 95 out of 255 top translationally up-regulated genes are also regulated by interferon, suggesting that a significant fraction of translation regulated genes contribute to the interferon response of the antiviral state (Supplementary Fig. 4.2E-H).

A Conserved Purine-Rich Motif Is Enriched in Translationally-Induced Genes During MG1 Infection

After confirming that there are distinct subset of translationally regulated genes that define the host reaction to virus infection, we sought to determine the translation regulation mechanism(s) that may govern the expression of theses genes. Cis-acting motifs has been shown to be a major mechanism for modulating translation output of associated mRNA in response to specific cellular state, with known motifs associated with suppressing translation of inflammatory and antiviral genes such as the GAIT element and AU-rich elements[26,39–41]. However, there is no known motif that mediate translation upregulation in response to the antiviral or inflammatory state to date. To determine if such a motif exists in our list of TE-up genes, the sequence of the 5′UTRs of the top TE-induced genes were analyzed using the MEME suite to search for enrichment of any RNA motif (Figure 4.3A). Translationally upregulated genes were ranked based on translational efficiency, and the top candidates were selected for downstream analysis. After restricting to protein-coding transcripts with annotated 5′UTRs, a final set of 83 genes was used for motif discovery. Motif discovery uncovered a significantly enriched purine-rich sequence ($E = 7.3 \times 10^{-19}$) that we subsequently referred to as the R-motif (Figure 4.3B). To assess the robustness of motif enrichment, we extended the analysis to larger gene sets (e.g., top 150–200 ranked genes). While the statistical significance (E-value) varied with input size, purine-rich motifs with similar sequence features were consistently identified, supporting enrichment of this motif class among translationally active transcripts (supplementary Fig. 4.3A). To assess whether this motif

represents a general feature for upregulated genes or is specific to translationally regulated transcripts, we performed the same motif discovery analysis on the 5′UTRs of transcriptionally upregulated genes. In contrast to TE-high genes, no purine-rich motif with comparable sequence features or statistical significance was identified in this gene set, supporting the specificity of this motif for translationally active transcripts (Supplementary Fig. 4.3B). The motif appeared in ~22% of TE-high transcripts and was often present at multiple positions within individual 5′UTRs (Figure 4.3C). According to interferome database, twelve of the motif-enriched genes were interferon-regulated gene (Figure 4.3D), corroborating the notion that R-motif containing genes are involved in host response to virus infection.

To test whether motif-containing 5'UTRs confer translational advantages during virus infection, six representative 5′UTRs corresponding to genes that displayed consistent RNA-seq and Ribo-seq RPKM values were evaluated using a translation reporter assay in mock and MG1 infected cells. They were cloned upstream of the Renilla luciferase CDS, which is transcribed together with firefly luciferase CDS under translation control of poliovirus IRES into a poly-cistronic mRNA (Figure 4.3E). Normalization of the activity of Renilla luciferase to firefly luciferase allows for bypassing transcription variation and measuring the translation output of the 5'UTR of interest. Although baseline translation in uninfected cells varied, MG1 infection significantly increased RLuc expression in 4 out of 6 genes tested in a dose-dependent manner (Figure 4.3F-G).

To assess whether this translational enhancement is restricted to a specific cellular or viral context, we extended the analysis to an independent glioblastoma cell line (U373) and to infection with an alternative rhabdovirus (VSV). Consistent with our findings in U343 cells infected with MG1, motif-containing 5′UTRs exhibited increased translational output in U373 cells (Supplementary Fig. 4.3C). Although the magnitude of translational enhancement was reduced during VSV infection, several motif-containing transcripts still showed significant increases in translation, supporting a conserved regulatory effect across distinct viral contexts (Supplementary Fig. 4.3D).

The R-Motif Drives Infection-Induced Translation Through the GLDC 5′UTR

To determine whether the R-motif directly contributes to infection-induced translational activation, we focused on the 5′UTR of the gene glycine decarboxylase (*GLDC*), which exhibited

one of the strongest translational responses to MG1 infection and contains a prominent R-motif at the 5’ end of the transcripts. Dual-luciferase reporters harboring the full GLDC 5′UTR, an R-motif deletion variant (ΔR-GLDC), or a control construct lacking a 5′UTR were generated (Figure 4.4A). MG1 infection significantly enhanced translation from the full GLDC 5′UTR, whereas deletion of the R-motif markedly impaired this induction (Figure 4.4B), demonstrating that the motif is required for infection-stimulated translation.

To assess whether the R-motif is sufficient to confer infection-responsive translation, the motif was inserted into the ACTB 5′UTR (Figure 4.4C). While MG1 infection alone did not alter translation from the native ACTB 5′UTR, insertion of the R-motif significantly increased reporter expression during infection (Figure 4.4D), indicating that the motif contributes to translational activation but is not sufficient to fully recapitulate the activity of the native GLDC 5′UTR.

Multiple cis-acting features within 5′UTRs, including upstream open reading frames (uORFs) and RNA secondary structure, are well-established regulators of translational efficiency, with uORFs influencing ribosome scanning and initiation and structured elements modulating ribosome access and initiation factor recruitment[42–46]. Thus, we next sought to exclude the contribution of these elements to the infection-induced translational activation mediated by the GLDC 5′UTR by performing systematic dissection of the UTR. Analysis of aggregated ribosome footprint data from publicly available datasets (GWIPS-viz) revealed a section of the 5’UTR possess high ribosome occupancy within the central region of the GLDC 5′UTR, with two ribosome footprint peaks corresponding to two CTG nucleotide sequences that can function as alternative translation start site (Figure 4.4E), suggesting the presence of upstream open reading frames (uORFs). However, sequential truncation of GLDC 5’UTR demonstrated that deletion of the first 60 nucleotides, encompassing the R-motif, substantially reduced infection-induced translation (Figure 4.4F–G), whereas removal of predicted uORF-containing regions did not enhance translation, indicating minimal uORF-mediated repression in this context.

Given that purine-rich RNA transcripts have been shown to require poly(A)-binding protein (PABP) for selective translation during immune challenge in plant[23,47,48], we examined whether the mammalian PABPC1 contributes to R-motif–dependent translation in human cells. A doxycycline-inducible Cas9-expressing U343 clone was generated for genome editing (Supplementary Fig. 4.4A). CRISPR-mediated deletion of PABPC1 was confirmed by

immunoblotting (Figure 4.4H) significantly reduced infection-induced activation of the GLDC 5′UTR reporter (Figure 4.4I). MG1 infection was also associated with increased eIF4G, but not eIF4A, levels (Supplementary Fig. 4.4B-D), consistent with remodeling of translation initiation capacity that may preferentially support motif-containing transcripts

Despite having a highly stable and complex predicted secondary structure (ΔG = −100.6 kcal/mol; Supplementary Fig. 4.4E), which would be expected to impede ribosomal scanning and suppress translation initiation, the GLDC 5′UTR supported robust basal and infection-induced translation. Additionally, shorter fragments of the GLDC 5'UTR promote poorer translation, suggesting that there are maybe other cis-acting elements that contribute to high basal translation activity of this 5'UTR. Collectively these results emphasizes the role of R motif in enhancing translation upon MG1 infection.

GLDC Is Translationally Upregulated and Restricts MG1 Spread in Glioblastoma Cells

To validate the translational activation of GLDC identified by our profiling analyses and assess its functional relevance during MG1 infection, we examined endogenous GLDC translation and its impact on viral replication. U343 cells infected with MG1 (MOI = 1, 8 h) were subjected to polysome profiling to assess ribosome loading. Lysates prepared under ribosome-preserving conditions were separated on 10–50% sucrose gradients, yielding monosomal and polysomal fractions for RNA quantification. MG1 infection showed a global repression in translation as seen in the polysomal trace (Figure 4.5A). As a control, ACTB mRNA shifted toward lighter fraction in MG1 compared to mock (Figure 4.5B) in agreement with the global translation repression, In contrast, GLDC mRNA redistributed to heavy polysomes in MG1 compared to mock condition (Figure 4.5C), confirming selective enhancement of GLDC translation. Despite reduced transcript levels, GLDC protein increased during infection (Figure 4.5D–E), confirming that its protein level are driven by translational upregulation and decouple with transcription.

To investigate the functional relevance of GLDC induction to MG1 infection, GLDC was deleted using CRISPR–Cas9 in U343 cells. GLDC knockout was confirmed by immunoblotting (Figure 4.5F). Upon MG1-GFP infection, GLDC-deficient cells exhibited a marked increase in GFP-positive regions, indicating increased viral spread compared to control cells, as quantified by Incucyte live-cell imaging over 24 h (Figure 4.5G–H), indicating that GLDC acts as a host restriction factor limiting MG1 dissemination in glioblastoma.

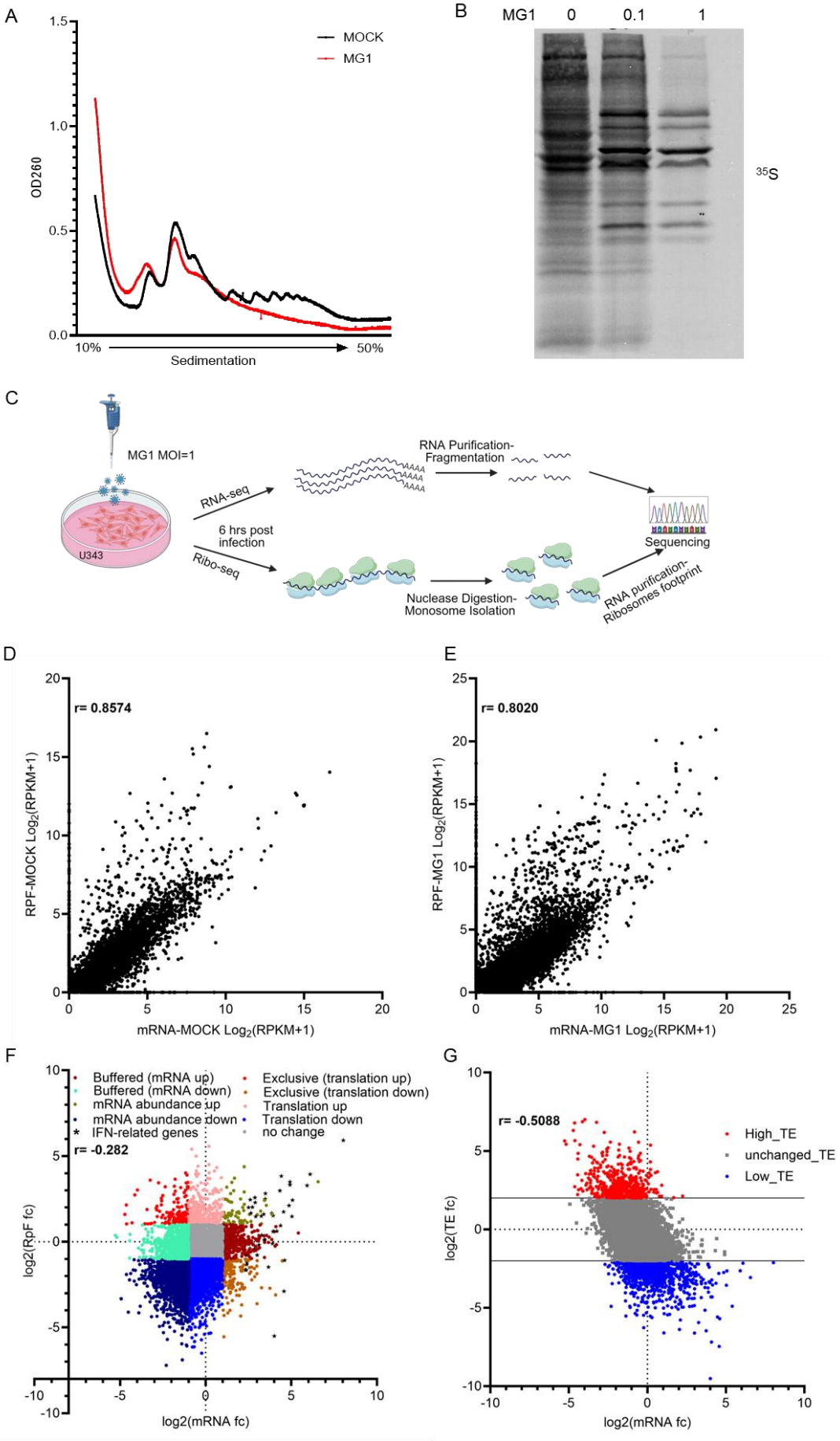
A
MOCK
MG1
OD260
1.5
1.0
0.5
0.0
10%
50%
Sedimentation
B
MG1 0 0.1 1
35S
C
MG1 MOI=1
U343
6 hrs post infection
RNA-seq
Ribo-seq
RNA Purification-Fragmentation
Sequencing
Nuclease Digestion-Monosome Isolation
RNA purification-Ribosomes footprint
D
r= 0.8574
RPF-MOCK Log2(RPKM+1)
mRNA-MOCK Log2(RPKM+1)
E
r= 0.8020
RPF-MG1 Log2(RPKM+1)
mRNA-MG1 Log2(RPKM+1)
F
Buffered (mRNA up)
Buffered (mRNA down)
mRNA abundance up
mRNA abundance down
IFN-related genes
Exclusive (translation up)
Exclusive (translation down)
Translation up
Translation down
no change
r= -0.282
log2(RpF fc)
log2(mRNA fc)
G
r= -0.5088
High_TE
unchanged_TE
Low_TE
log2(TE fc)
log2(mRNA fc)

Figure 4. 1. Transcriptional and Translational Remodeling of Glioblastoma Cells During Maraba-MG1 Infection.

(A) Polysome Profiling of MG1. Representative sucrose gradient traces (10–50%) showing ribosome distribution in mock-treated (black) and MG1-infected (red) U343 cells, measured by absorbance at OD260 12 hpi (B) Global protein synthesis by S^{35} metabolic labeling. U343 cells were infected with MG1 at MOI 0, 0.1, and 1. Newly synthesized proteins were labeled with S^{35}-methionine/cysteine, resolved by SDS–PAGE, and visualized by autoradiography. (C) Experimental workflow. U343 cells were infected with MG1 (MOI = 1) and harvested 6 h post-infection for RNA-seq and ribosome profiling (Ribo-seq). Total RNA was purified and fragmented for RNA-seq libraries, while ribosome-protected fragments (RPFs) were generated by nuclease digestion and monosome isolation. All libraries were sequenced to quantify transcript abundance, ribosome occupancy, and to calculate translational efficiency (TE). (D) Correlation between mRNA and RPF levels in mock-treated cells. Scatterplot of $\log_2$(RPKM+1) between mRNA abundance and ribosome footprint density under mock conditions (r = 0.8574). (E) Correlation between mRNA and RPF levels in MG1-infected cells. Scatterplot of $\log_2$(RPKM+1) values for infected between transcript abundance and ribosome footprint density (r = 0.8020). (F) Relationship between mRNA and RPF fold changes. Scatterplot showing $\log_2$ fold-change in RPFs plotted against $\log_2$ fold-change in mRNA levels (MG1 vs. mock). (G) Correlation between mRNA abundance and translational efficiency (TE). Scatterplot showing $\log_2$ fold-change in TE plotted against $\log_2$ fold-change in mRNA levels. Transcripts with increased TE were defined using a TE fold-change cutoff of ≥ 2 (blue), while unchanged-TE transcripts are shown in grey and TE-decreased transcripts in red.

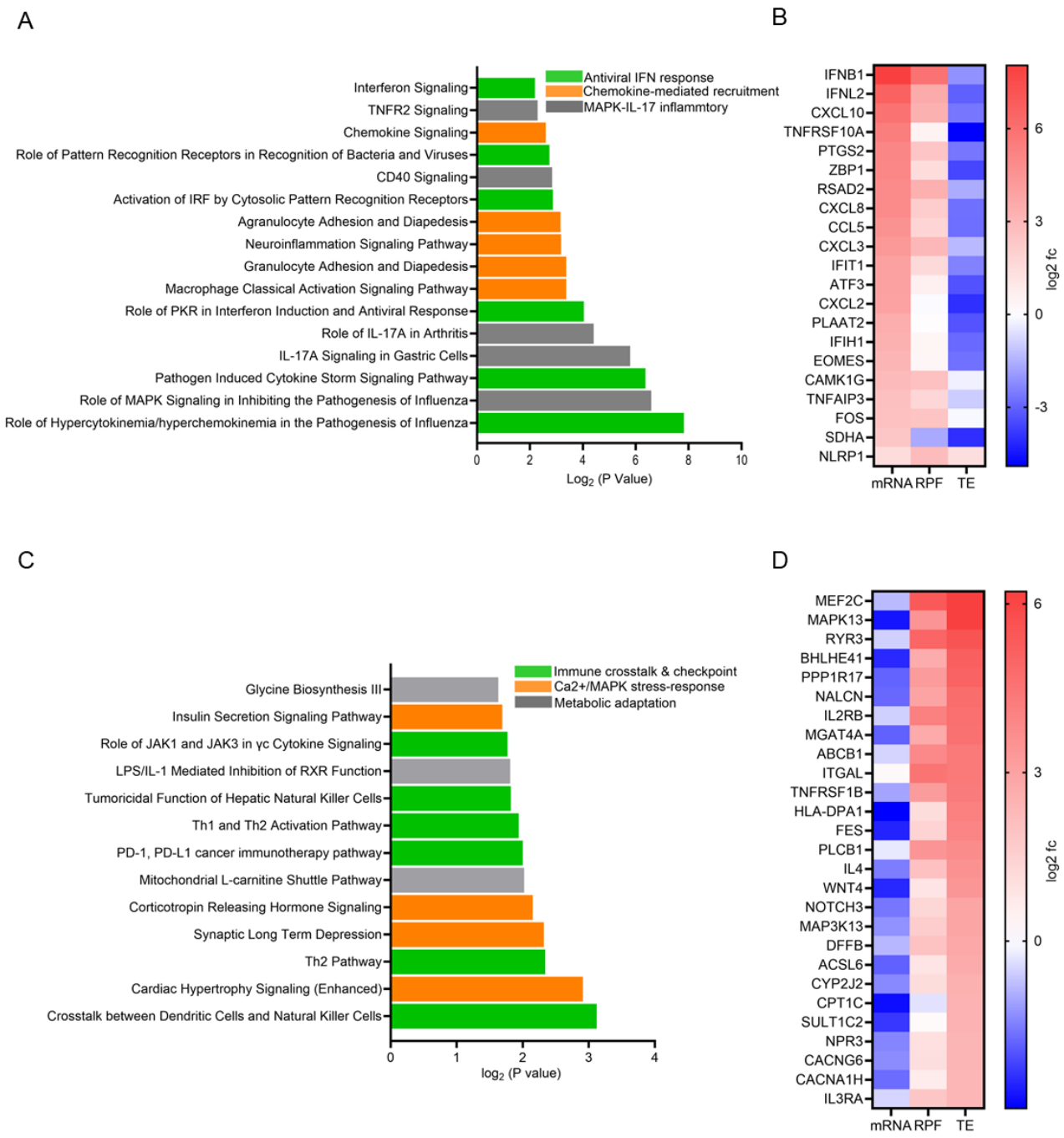

Figure 4. 2. IPA Reveals Pathway Enrichment of Transcriptionally Versus Translationally Regulated Genes During MG1 Infection.

(A) mRNA-enriched pathways identified by IPA. Bar plot (left) shows the top IPA pathways significantly enriched among genes upregulated at the mRNA level during MG1 infection. Pathways are grouped into three functional categories: Antiviral Interferon Response, Chemokine-Mediated Recruitment, and MAPK/IL-17-Driven Inflammatory Signaling. (B) Heatmap summarizes log2FC in mRNA, RPF, and TE for representative genes within each pathway in (A). (C) TE-enriched pathways identified by IPA. Bar plot (left) shows pathways significantly enriched among genes with increased translational efficiency (TE). These pathways cluster into Immune Crosstalk & Checkpoint Signaling, Ca^{2+}/MAPK Stress-Responsive Signaling, and Metabolic Adaptation Pathways. (D) Heatmap summarizes log2FC in mRNA, RPF, and TE for representative genes within each pathway in (C).

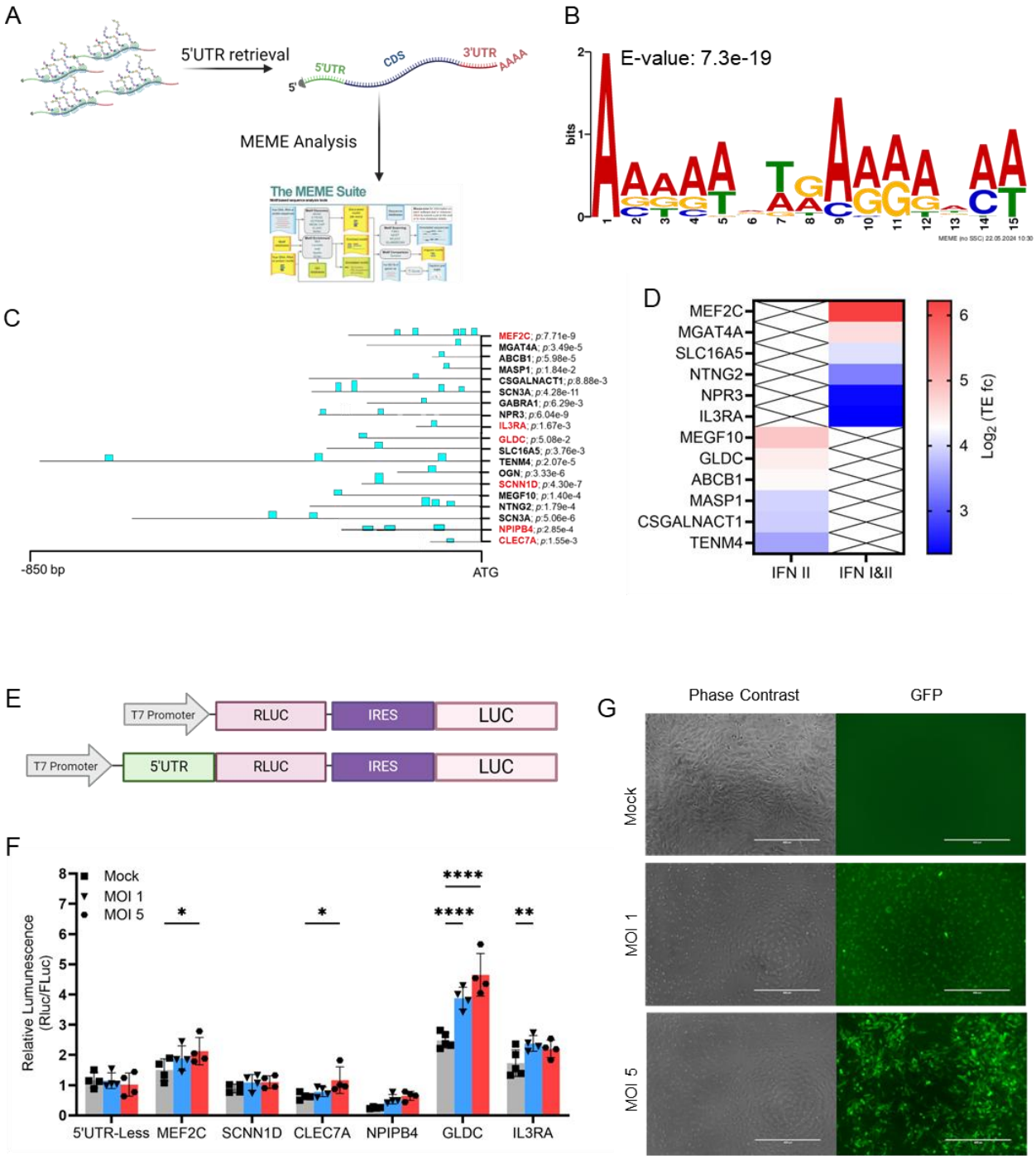
A
5'UTR retrieval
5'UTR
CDS
3'UTR
AAAA
5'
MEME Analysis
The MEME Suite
B
E-value: 7.3e-19
bits
C
MEF2C; p:7.71e-9
MGAT4A; p:3.49e-5
ABCB1; p:5.98e-5
MASP1; p:1.84e-2
CSGALNACT1; p:8.88e-3
SCN3A; p:4.28e-11
GABRA1; p:6.29e-3
NPR3; p:6.04e-9
IL3RA; p:1.67e-3
GLDC; p:5.08e-2
SLC16A5; p:3.76e-3
TENM4; p:2.07e-5
OGN; p:3.33e-6
SCNN1D; p:4.30e-7
MEGF10; p:1.40e-4
NTNG2; p:1.79e-4
SCN3A; p:5.06e-6
NPIPB4; p:2.85e-4
CLEC7A; p:1.55e-3
-850 bp
ATG
D
MEF2C
MGAT4A
SLC16A5
NTNG2
NPR3
IL3RA
MEGF10
GLDC
ABCB1
MASP1
CSGALNACT1
TENM4
IFN II
IFN I&II
Log2 (TE fc)
E
T7 Promoter
RLUC
IRES
LUC
T7 Promoter
5'UTR
RLUC
IRES
LUC
F
Mock
MOI 1
MOI 5
Relative Lumunescence (Rluc/FLuc)
5'UTR-Less
MEF2C
SCNN1D
CLEC7A
NPIPB4
GLDC
IL3RA
G
Phase Contrast
GFP
Mock
MOI 1
MOI 5

Figure 4. 3. Identification, distribution, and functional validation of a purine-rich translational enhancer motif enriched in top TE-high genes.

(A) Workflow for motif discovery. The 5′UTR sequences of the top TE-high genes were retrieved and analyzed using the MEME Suite to identify enriched sequence motifs associated with enhanced translational efficiency. (B) Purine-rich motif identified by MEME. Sequence logo representation of the significantly enriched motif (E-value = 7.3×10^{-19}). (C) Motif distribution across 5′UTRs. Genomic positions of the motif within the 5′UTRs of representative TE-high genes. (D) Fold-change distribution of interferon-stimulated genes containing the motif. Motif-enriched interferon-related genes display elevated TE fold-changes across IFN-I, IFN-II, and combined IFN-I/II categories. (E) Dual luciferase translation reporter constructs for testing 5'UTR-mediated translation control. Schematic of the dual-luciferase reporters containing either a 5′UTR-less control or the indicated 5′UTRs upstream of Renilla luciferase (RLuc), followed by an IRES-driven firefly luciferase (FLuc) internal control. (F) Luciferase assays validate translational enhancement by motif-containing 5′UTRs. U343 cells were transfected with the indicated dual luciferase reporter plasmid, then infected with MG1 at the indicated MOI. 24h post infection, Rluc and Fluc activity were measured. Bars represent mean ± SEM. Stat: n=4, 2-way anova followed by Dunnett's multiple comparisons test. *p<0.05, ** p<0.01, ****p<0.001 (G) Phase contrast and GFP imaging of infected cells. Representative phase contrast and GFP fluorescence images of U343 cells under mock conditions and following MG1 infection at MOI 1 and MOI 5. Scale bars are shown.

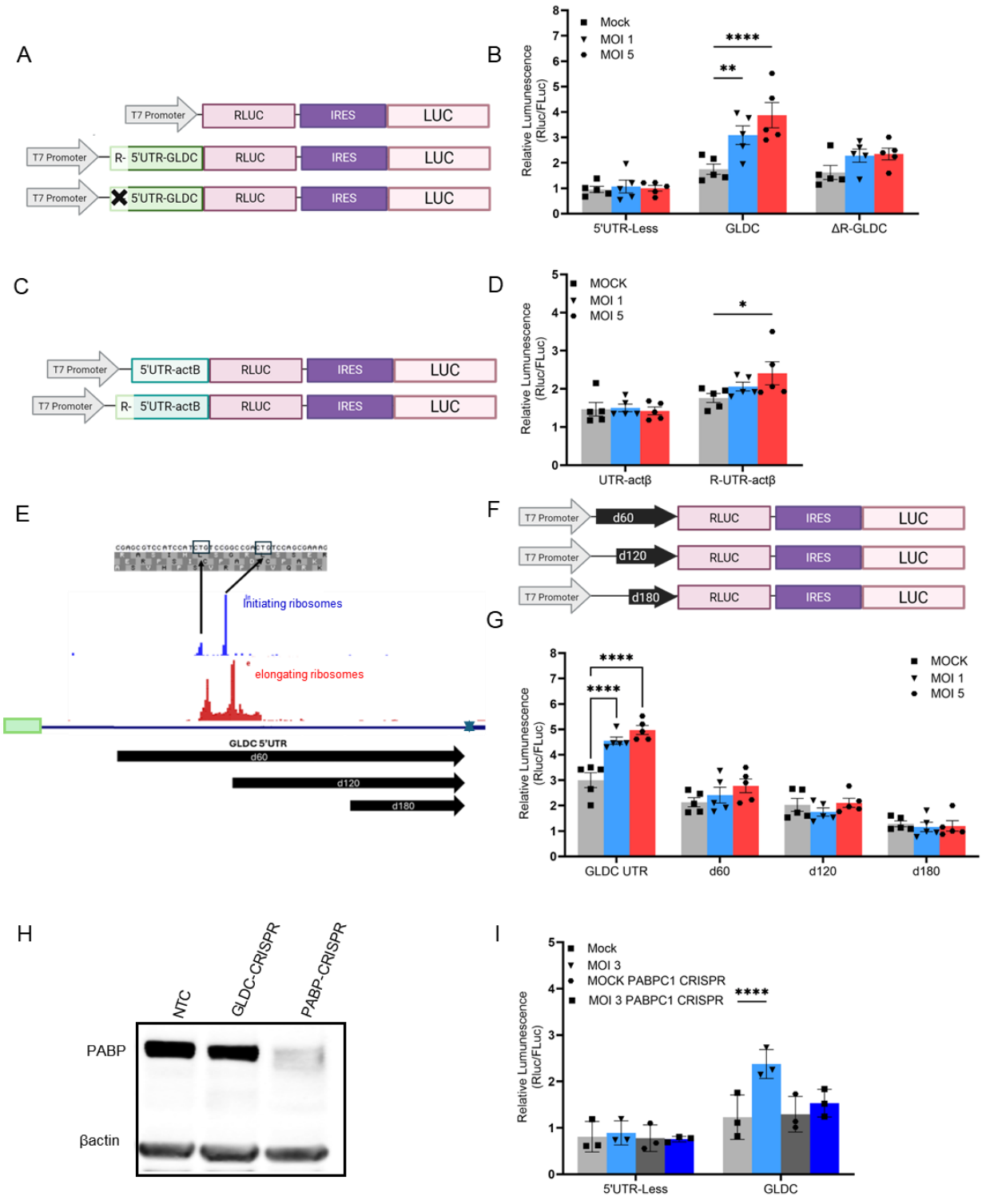
A
T7 Promoter
RLUC
IRES
LUC
R-
5'UTR-GLDC
B
Mock
MOI 1
MOI 5
Relative Lumunescence (Rluc/FLuc)
****
**
5'UTR-Less
GLDC
ΔR-GLDC
C
5'UTR-actB
D
MOCK
*
UTR-actβ
R-UTR-actβ
E
Initiating ribosomes
elongating ribosomes
GLDC 5'UTR
d60
d120
d180
F
G
GLDC UTR
H
NTC
GLDC-CRISPR
PABP-CRISPR
PABP
βactin
I
MOI 3
MOCK PABPC1 CRISPR
MOI 3 PABPC1 CRISPR

Figure 4. 4. The GLDC 5′UTR confirms the R-motif as a driver of infection-induced translation.

(A) Reporter constructs for testing GLDC 5′UTR and R-motif function. Dual-luciferase reporters containing either a 5′UTR-less control, the full GLDC 5′UTR or an R-motif–deleted variant (ΔR-GLDC) upstream of Renilla luciferase (RLuc) were generated to evaluate the contribution of the R-motif to translational induction during MG1 infection. (B) GLDC 5′UTR validation of R-motif–dependent translational enhancement. Rluc and Fluc activity were measured after 24 hrs of MG1 infection. Data represent mean ± SEM. Statistical analysis: n=5, two-way ANOVA followed by Dunnett's multiple comparisons test. . *p<0.05, ** p<0.01, ****p<0.001. (C) Testing sufficiency of the R-motif to enhance translation. Reporter constructs containing the ACTB 5′UTR (with or without insertion of the GLDC R-motif) were generated to determine whether transferring the motif into a different 5′UTR background is sufficient to drive translational activation. (D) Moderate enhancement by R-motif insertion into ACTB. Rluc and Fluc activity were measured after 24 hrs of MG1 infection. Data are mean ± SEM. Statistical analysis: n=5, two-way ANOVA followed by Dunnett's multiple comparisons test. . *p<0.05, ** p<0.01, ****p<0.001. (E) Identification of putative upstream ORFs (uORFs) in the GLDC 5′UTR and design of truncation constructs. Ribosome profiling data from GWIPS-viz mapped onto the GLDC 5′UTR revealed two footprint peaks upstream of the annotated start codon, corresponding to non-AUG start codons. Three truncation constructs (d60, d120, d180) of the whole 5’UTR were generated. (F) Schematic representation of GLDC 5′UTR truncation constructs used in the luciferase reporter assay. Diagram showing the three truncation variants (d60, d120, d180) cloned upstream of Renilla luciferase (RLuc). (G) Luciferase reporter assay for GLDC 5′UTR truncation constructs. Relative RLuc/FLuc activity measured 24 h after MG1 infection (MOI 1 or 5) for the full-length GLDC 5′UTR and the three truncation variants (d60, d120, d180). Bars represent mean ± SEM from biological replicates. Statistical analysis: n=5, two-way ANOVA followed by Dunnett's multiple comparisons test. *p<0.05, ** p<0.01, ****p<0.001. (H) PABPC1 knockout validation. Immunoblot of PABP in NTC, GLDC-CRISPR, and PABP-CRISPR cells. β-actin, loading control. (I) Luciferase assay in control and PABPC1-CRISPR cells. U343 cells (control and PABPC1-CRISPR) were transfected with the indicated dual luciferase reporter constructs and infected at MOI 3. Relative luminescence (RLuc/FLuc) was measured 24 h post-infection for 5′UTR-less control and GLDC 5′UTR constructs. Bars represent mean ± SEM. Statistical analysis was performed using two-way ANOVA followed by Tukey's multiple comparisons test (*p < 0.05, **p < 0.01, ****p < 0.001).

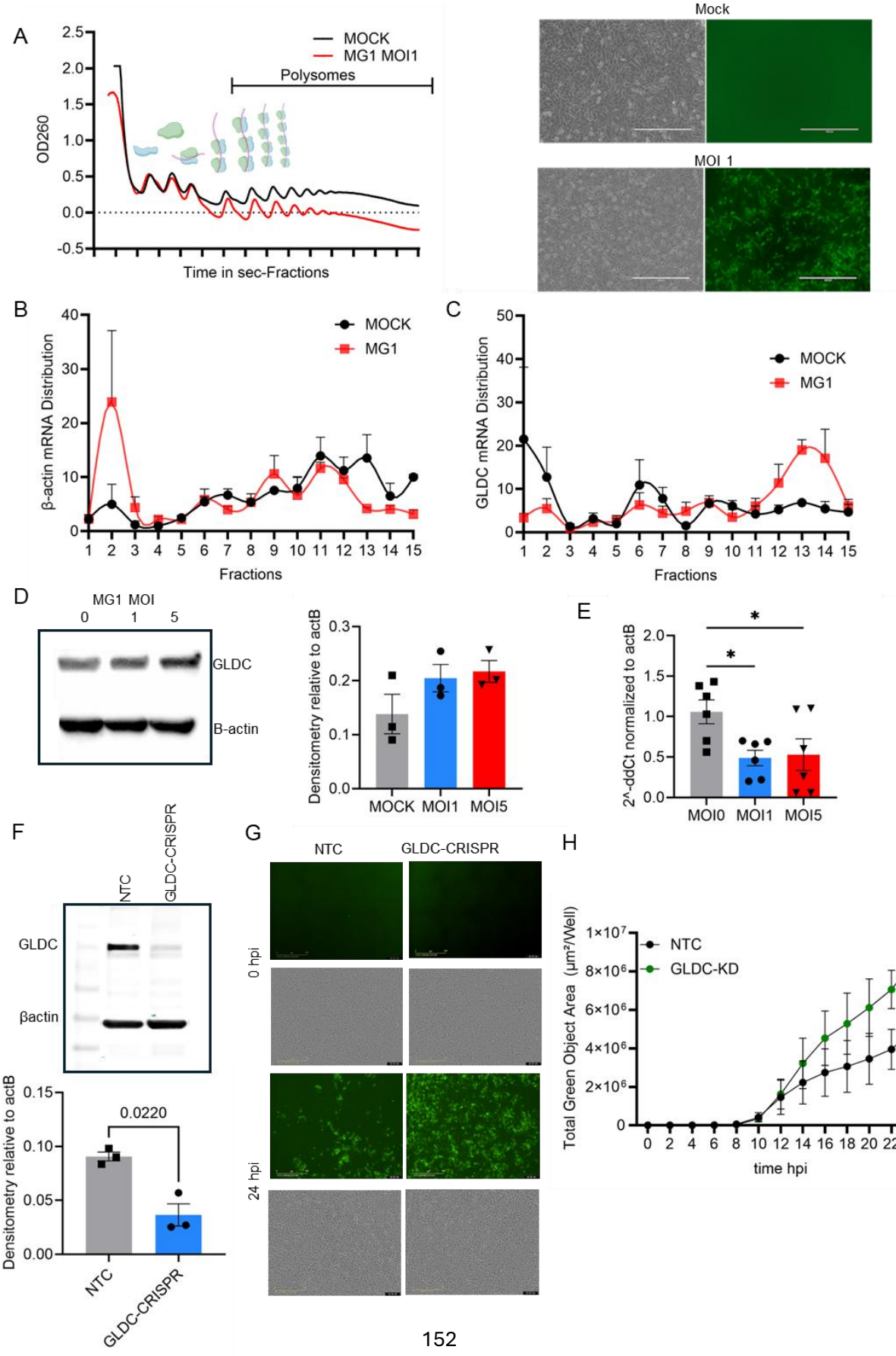
A
MOCK
MG1 MOI1
Polysomes
OD260
Time in sec-Fractions
Mock
MOI 1
B
MOCK
MG1
β-actin mRNA Distribution
Fractions
C
MOCK
MG1
GLDC mRNA Distribution
Fractions
D
MG1 MOI
0 1 5
GLDC
B-actin
Densitometry relative to actB
MOCK MOI1 MOI5
E
2^-ddCt normalized to actB
MOI0 MOI1 MOI5
F
NTC
GLDC-CRISPR
GLDC
βactin
Densitometry relative to actB
0.0220
NTC
GLDC-CRISPR
G
NTC
GLDC-CRISPR
0 hpi
24 hpi
H
NTC
GLDC-KD
Total Green Object Area (µm²/Well)
time hpi

Figure 4. 5. GLDC Is Translationally Upregulated Antiviral Gene.

(A) Polysome profiling of MG1-infected cells. Sucrose gradient polysome profiles of mock- and MG1-infected U343 cells (MOI 1) showing infection-associated changes in ribosome distribution. Representative phase-contrast and GFP images (right) illustrate MG1 infection. (B, C) Distribution of β-actin and GLDC mRNAs across polysome fractions. RT-qPCR quantification of β-actin (B) and GLDC (C) mRNA across gradient fractions. (D) GLDC protein levels increase following MG1 infection. Western blot (left) and densitometry (right) of GLDC in mock-, MOI 1–, and MOI 5–infected cells. (E) GLDC is transcriptionally downregulated. Relative GLDC transcript levels were quantified by RT-qPCR and normalized to housekeeping genes. Data represent mean ± SEM. Statistical analysis: n=6, two-way ANOVA followed by Dunnett's multiple comparisons test. *$p<0.05$. (F) GLDC depletion using CRISPR. CRISPR-mediated knockdown of GLDC confirmed by WB. Densitometry. non-targeting controls (NTC). (G) Increased MG1 Spread in GLDC-CRISPR Cells Representative Incucyte GFP fluorescence and phase-contrast images of NTC and GLDC-CRISPR cells at 0 h and 24 h post-MG1 infection. (G) Quantification of viral spread over time. Automated Incucyte analysis of total green object area, representing the cumulative GFP-positive region generated by MG1-GFP infection, was measured over a 24-hour time course. Bars represent mean ± SEM.

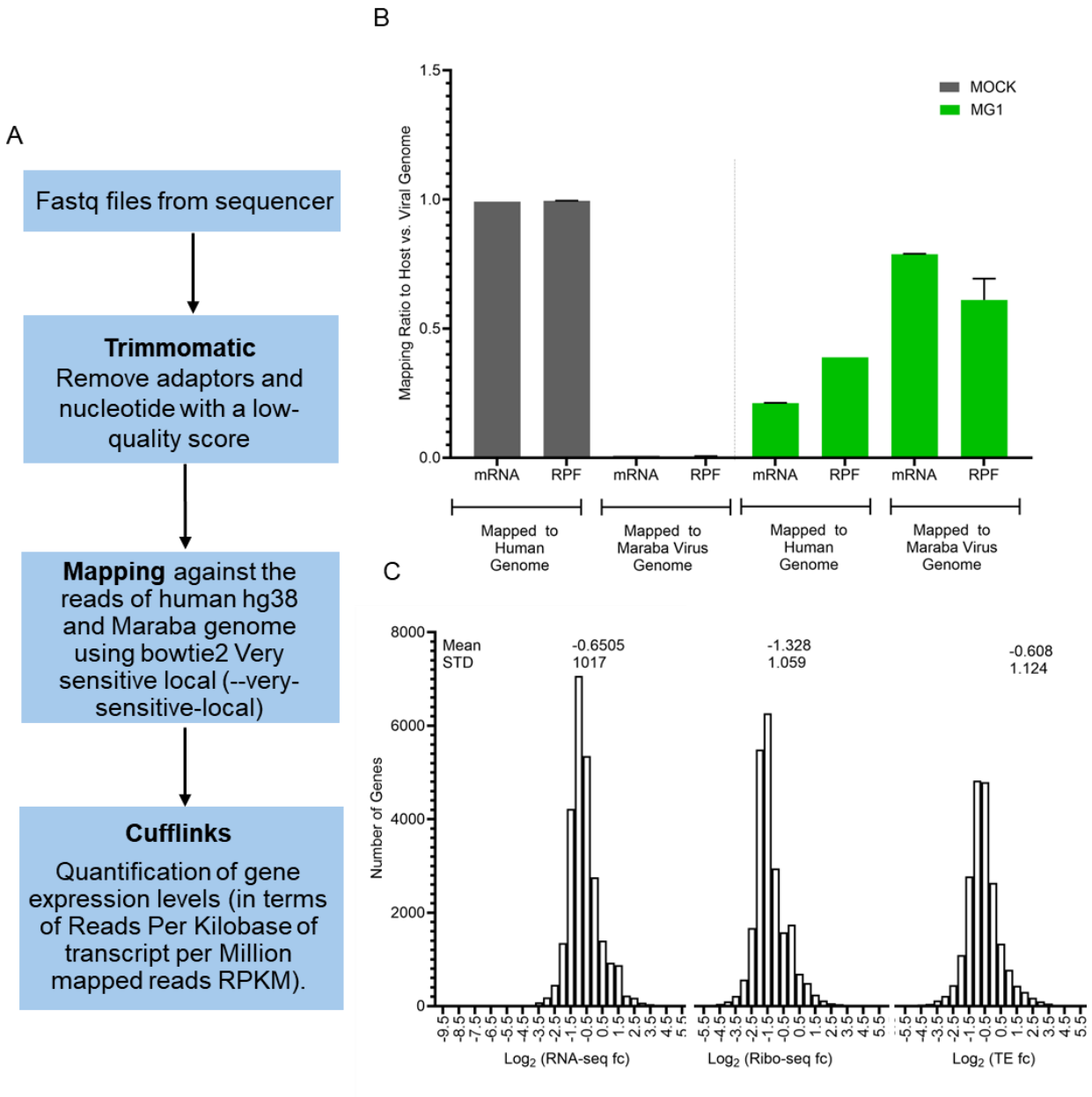

Supplementary Figure 4. 1. Quality Control and Data Processing Pipeline for RNA-seq and Ribo-seq Analyses

(A) Bioinformatic workflow for RNA-seq and Ribo-seq processing. Raw FASTQ files were trimmed using Trimmomatic to remove adaptors and low-quality bases. Reads were mapped to both the human hg38 genome and the Maraba MG1 viral genome using Bowtie2 with the "very sensitive local" setting. Gene expression levels were quantified using Cufflinks and reported as RPKM values. (B) Mapping ratio of host versus viral reads across libraries. Bar plot showing the proportion of sequencing reads aligned to the human transcriptome relative to the MG1 viral genome for each RNA-seq and Ribo-seq sample. Differences in host–virus representation reflect infection dynamics and library type. (C) Distribution of $\log_2$ fold-changes for RNA-seq, Ribo-seq, and translational efficiency (TE). Histograms display the global distribution of $\log_2$ fold-changes (MG1 / Mock) for transcript abundance, ribosome occupancy, and TE. Mean and standard deviation values are indicated above each panel.

A

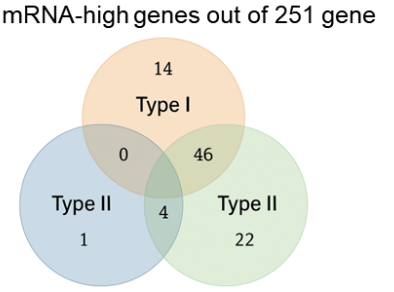
87 mRNA-high genes out of 251 gene
14
Type I
0
46
Type II
1
4
Type II
22

B

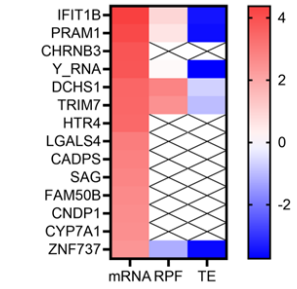
Type I Interferon-Related genes
IFIT1B
PRAM1
CHRNB3
Y_RNA
DCHS1
TRIM7
HTR4
LGALS4
CADPS
SAG
FAM50B
CNDP1
CYP7A1
ZNF737
mRNA RPF TE
4
2
0
-2

C

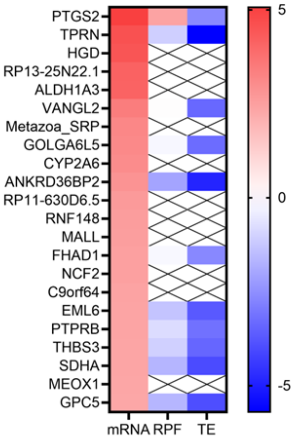
Type II Interferon-Related genes
PTGS2
TPRN
HGD
RP13-25N22.1
ALDH1A3
VANGL2
Metazoa_SRP
GOLGA6L5
CYP2A6
ANKRD36BP2
RP11-630D6.5
RNF148
MALL
FHAD1
NCF2
C9orf64
EML6
PTPRB
THBS3
SDHA
MEOX1
GPC5
mRNA RPF TE
5
0
-5

D

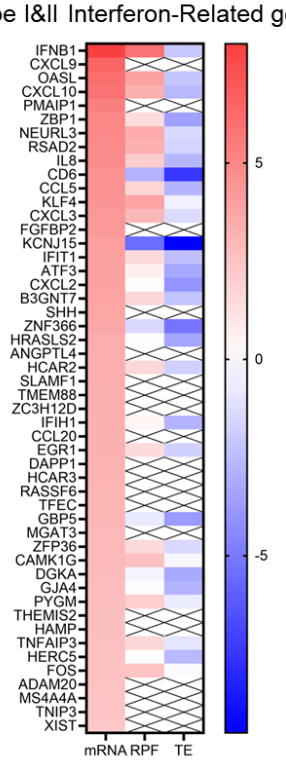
Type I&II Interferon-Related genes
IFNB1
CXCL9
OASL
CXCL10
PMAIP1
ZBP1
NEURL3
RSAD2
IL8
CD6
CCL5
KLF4
CXCL3
FGFBP2
KCNJ15
IFIT1
ATF3
CXCL2
B3GNT7
SHH
ZNF366
HRASLS2
ANGPTL4
HCAR2
SLAMF1
TMEM88
ZC3H12D
IFIH1
CCL20
EGR1
DAPP1
HCAR3
RASSF6
TFEC
GBP5
MGAT3
ZFP36
CAMK1G
DGKA
GJA4
PYGM
THEMIS2
HAMP
TNFAIP3
HERC5
FOS
ADAM20
MS4A4A
TNIP3
XIST
mRNA RPF TE
5
0
-5

E

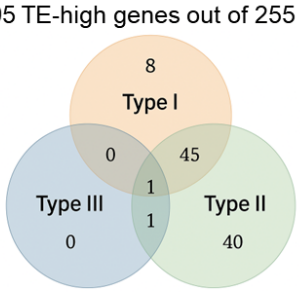
95 TE-high genes out of 255 gene
8
Type I
0
45
1
Type III
0
1
Type II
40

F

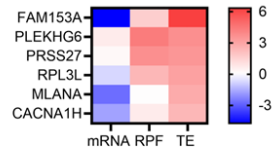
Type I Interferon-Related genes
FAM153A
PLEKHG6
PRSS27
RPL3L
MLANA
CACNA1H
mRNA RPF TE
6
3
0
-3

G

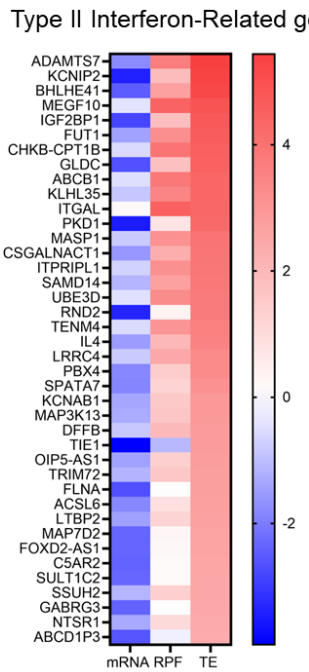
Type II Interferon-Related genes
ADAMTS7
KCNIP2
BHLHE41
MEGF10
IGF2BP1
FUT1
CHKB-CPT1B
GLDC
ABCB1
KLHL35
ITGAL
PKD1
MASP1
CSGALNACT1
ITPRIPL1
SAMD14
UBE3D
RND2
TENM4
IL4
LRRC4
PBX4
SPATA7
KCNAB1
MAP3K13
DFFB
TIE1
OIP5-AS1
TRIM72
FLNA
ACSL6
LTBP2
MAP7D2
FOXD2-AS1
C5AR2
SULT1C2
SSUH2
GABRG3
NTSR1
ABCD1P3
mRNA RPF TE
4
2
0
-2

H

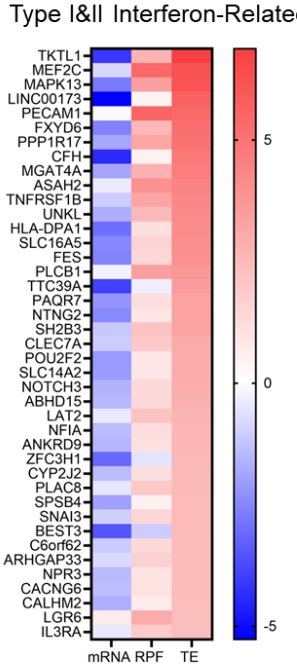
Type I&II Interferon-Related genes
TKTL1
MEF2C
MAPK13
LINC00173
PECAM1
FXYD6
PPP1R17
CFH
MGAT4A
ASAH2
TNFRSF1B
UNKL
HLA-DPA1
SLC16A5
FES
PLCB1
TTC39A
PAQR7
NTNG2
SH2B3
CLEC7A
POU2F2
SLC14A2
NOTCH3
ABHD15
LAT2
NFIA
ANKRD9
ZFC3H1
CYP2J2
PLAC8
SPSB4
SNAI3
BEST3
C6orf62
ARHGAP33
NPR3
CACNG6
CALHM2
LGR6
IL3RA
mRNA RPF TE
5
0
-5

Supplementary Figure 4. 2. Distribution and expression profiles of interferon-related genes among mRNA-high and TE-high gene sets.

(A) Distribution of interferon-related genes within mRNA-high and TE-high categories. Venn diagrams show the overlap of Type I, Type II, and Type III interferon-related genes among the mRNA-high (87 of 251 genes) and TE-high (95 of 255 genes) groups. (B) Type I interferon–related genes. Heatmap showing FC in mRNA, RPF, and TE for Type I interferon genes that meet the TE-high threshold. (C) Type II interferon–related genes. Heatmap of Type II interferon genes enriched in the TE-high category. (D) Genes responding to both Type I and Type II interferon pathways. Heatmap of genes annotated to both interferon responses that are selectively enriched in the TE-high set. (E) Type I interferon–related genes. Heatmap showing FC in mRNA, RPF, and TE for Type I interferon genes that meet the mRNA-high Category. (F) Type II interferon–related genes. Heatmap of Type II interferon genes enriched in the mRNA-high category. (G) Genes responding to both Type I and Type II interferon pathways. Heatmap of genes annotated to both interferon responses that are selectively enriched in the mRNA-high set.

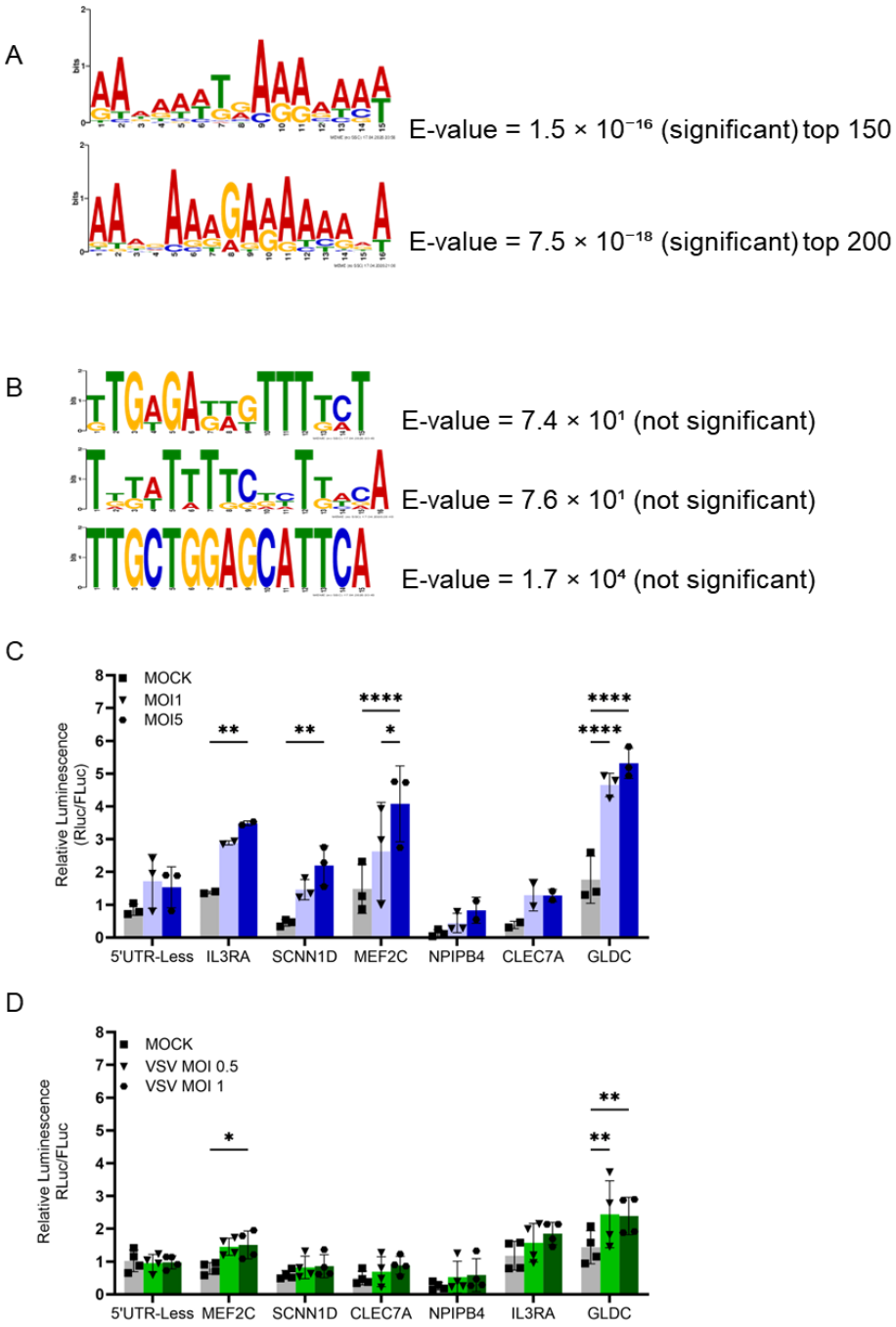

Supplementary Figure 4. 3. Motif analysis and context-dependent validation of motif-containing 5′UTRs. (A) Motif analysis of translationally upregulated genes using different bins. Sequence logos derived from 5′UTRs of top translationally upregulated genes using different gene set sizes (top 150 and top 200). Motifs resembling the R motif are shown with corresponding E-values. (B) Motif analysis of transcriptionally upregulated genes. Sequence logos identified from 5′UTRs of transcriptionally upregulated genes. Motifs are shown with corresponding E-values. (C) Luciferase reporter assay in U373 cells. U373 cells were transfected with the indicated dual luciferase reporter plasmids and infected at the indicated MOIs. Relative luminescence (RLuc/FLuc) was measured 24 h post-treatment. Bars represent mean ± SEM (n = 3). Statistical analysis was performed using two-way ANOVA followed by Dunnett's multiple comparisons test (*p < 0.05, **p < 0.01, ****p < 0.001). (D) Luciferase reporter assay. U343 cells were transfected with the indicated dual luciferase reporter plasmids then infected with VSV. Relative luminescence (RLuc/FLuc) was measured. Bars represent mean ± SEM (n = 4). Statistical analysis was performed using two-way ANOVA followed by Dunnett's multiple comparisons test (*p < 0.05, **p < 0.01, ****p < 0.001).

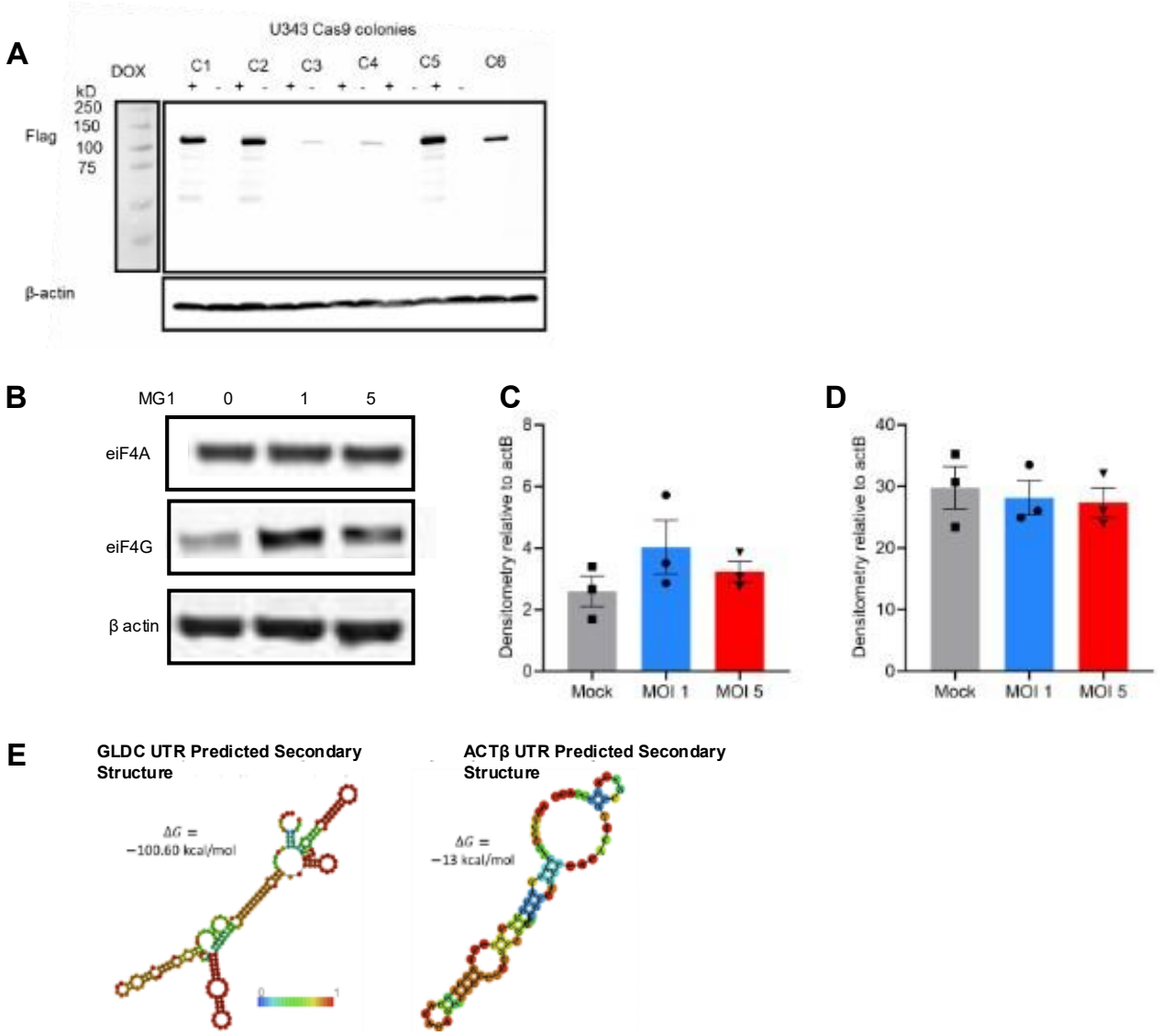

Supplementary Figure 4. 4. Structural features of 5′UTRs and validation of Cas9 induction and translation-related factors during MG1 infection.

(A) Immunoblot screening of U343 Cas9 monoclonal lines. U343 Cas9 clonal lines (C1–C6) were treated with or without doxycycline (DOX) and analyzed by immunoblot for inducible Cas9 (Flag). β-actin is shown as a loading control. (B) Immunoblot of translation initiation factors. Immunoblot analysis of eIF4G and eIF4A in U343 cells under mock and MG1 infection conditions (MOI 1 and MOI 5). β-actin is shown as a loading control. (C) Densitometry of eIF4G. Quantification of eIF4G protein levels normalized to β-actin under mock and MG1 infection conditions. Bars represent mean ± SEM. (D) Densitometry of eIF4A. Quantification of eIF4A protein levels normalized to β-actin under mock and MG1 infection conditions. Bars represent mean ± SEM. (E) Predicted secondary structure and folding free energy of the GLDC and ACTB 5′UTRs. Predicted secondary structures and minimum free-energy values for the GLDC (left) and ACTB (right) 5′UTRs generated using the ViennaRNA RNAfold web server. The GLDC 5′UTR displays a highly structured and thermodynamically stable secondary structure (ΔG = –100.6 kcal/mol) compared to the less structured ACTB 5′UTR (ΔG = –13 kcal/mol).

4.6 Discussion

Our findings shed light on the previously poorly understood translation control environment during host-virus interaction. First, MG1 infection causes extensive post-transcriptional regulation of a subset of gene, demonstrating that mRNA abundance alone is insufficient to predict protein output and host response during infection. Second, we identify a conserved purine-rich cis-acting element within the 5′ untranslated regions of a subset of infection-induced transcripts that promotes selective translation under conditions of global translational repression. Third, this motif is necessary, and partially sufficient, to confer infection-stimulated translation upregulation. Finally, we show that selective translation mediated by this cis-element contributes to antiviral gene expression program, as exemplified by its translational upregulation of GLDC, which limits MG1 spread in glioblastoma cells. Together, these results establish cis-acting translational control as a novel mechanism in mammalian cells that shapes host responses to Rhabdovirus infection.

Comparative RNA-seq and ribosome-profiling studies have repeatedly shown that transcriptional output does not reliably predict steady-state protein level. In yeast, genome-wide analyses revealed that while severe stress elicits correlation changes in transcript levels and translation, mild stress uncouples these layers, with many transcripts undergoing translational regulation without corresponding mRNA changes[49]. In plant pattern-triggered immunity (PTI), global translational reprogramming constitutes a fundamental regulatory layer, where defence responses are driven largely by changes in translational efficiency rather than transcript abundance[23,24]. Viral infection also promotes this uncoupling by reshaping host translation responses independently of mRNA levels[16,50]. In cancer-relevant contexts, ribosome profiling has shown that pathways such as mTOR selectively modulate translation efficiency of defined mRNA subsets without proportional changes in RNA levels, emphasize the importance of translation-based regulatory programs [51]. Consistent with these models, our MG1 infection data reveal a marked decoupling and in many cases an inverse relationship between mRNA abundance and translation efficiency, supporting translational control as a major regulator of host response to viral infection.

In mammalian cells, purine-rich sequences modulate translation in context-specific ways: eIF4A1 promotes translation of structured, purine-rich 5′UTRs by facilitating local RNA unwinding[52], whereas eIF4A2 binds binds similar motifs to repress translation initiation through

recruitment of the Ccr4-Not complex[53]. PABP autoregulates its translation through adenosine-rich 5′UTR elements[47]. Intriguingly, a 5′ poly(A) leader generated independently of the template sequence was also reported to confer translation advantage for poxvirus viral mRNA[54]. Together, these studies show that purine-rich motifs are versatile cis-acting modules that shape mRNA access to ribosomes. Yet, their involvement in translation control in glioblastoma cells infected by rhabdoviruses mainly MG1 has not been investigated.

Purine-rich elements in 5′ untranslated regions have emerged as regulators of translation that are engaged under non-homeostatic cellular states such as stress, immune activation, or altered growth signaling. In plant PTI, a conserved purine-rich element termed R-motif in the 5′ leaders of defense mRNAs was identified and demonstrated to supports cap-independent translation through a PABP-dependent initiation module when canonical cap-dependent translation is attenuated[23,24]. Similarly, in yeast, A-rich or poly(A)-like sequences within 5′UTRs enable cap-independent translation during nutrient stress, facilitating selective protein synthesis required for adaptive responses[48]. In mammalian systems, studies in proliferating human cancer cell lines (including HeLa and HCT116) have linked AG-rich 5′UTR motifs to selective translational activation; under conditions of active or perturbed mTOR signaling, these motifs recruit eIF4A1 to locally unwind structured leaders and enhance translation of growth- and stress-associated transcripts[52]. Together, these studies support a model in which purine-rich 5′UTR elements ensure translation when global initiation capacity is constrained or selectively remodeled. Importantly, purine-rich motifs can also mediate translational repression under steady-state growth conditions. In human HeLa cells, purine-rich sequences positioned proximal to the start codon were found to preferentially engage eIF4A2, resulting in inhibition of translation initiation[55]. Although this study did not examine stress or infection, it underscores that the translational output of purine-rich elements is shaped by motif position within the 5′UTR and the identity of the associated helicase. In contrast, immune-, stress-, or infection-associated states preferentially engage alternative initiation factors such as PABP or eIF4A1, thereby supporting selective translational activation. Consistent with this framework, our data support a role for the R-motif in promoting selective translation during MG1 infection, a condition characterized by global translational remodeling rather than steady-state growth.

Accumulating evidence across systems supports a role for poly(A)-binding protein (PABP) as a trans-acting factor that promotes selective translation through purine- or A-rich elements in 5′ untranslated regions under stress or immune conditions. In plant PTI PABP engages a purine-rich R-motif to drive cap-independent translation of defense mRNAs when canonical translation is attenuated[23]. Similarly, in yeast, A-rich sequences within 5′UTRs recruit PABP1 to mediate internal initiation, bypassing the requirement for the 5′ cap[48]. Extending this concept to mammalian viral infection, de Rozières et al. (2022)[57] reported that PABP1 binding to viral 5′UTRs enables eIF4E-independent recruitment of eIF4G and sustains translation under inhibitory conditions. Consistently Akabane virus infection suppress host translation by redistributing PABP1 from the cytoplasm to the nucleus[58]. Together, these studies support a conserved model in which PABP can enable selective translation of specific mRNAs via purine-rich 5′UTR elements during stress or immune activation, consistent with our observation that PABPC1 is required for R-motif–dependent translational activation during MG1 infection.

GLDC encodes the P-protein of the mitochondrial glycine cleavage system and catalyzes glycine catabolism coupled to NADH production, directly linking one-carbon metabolism to mitochondrial redox homeostasis[59,60]. By contributing NADH to the mitochondrial electron transport chain, GLDC supports energy production and limits excessive redox stress, a state known to influence innate immune signaling pathways[61]. Mitochondrial redox balance is a critical determinant of antiviral signaling, as MAVS-dependent interferon induction occurs on the mitochondrial membrane and is sensitive to changes in mitochondrial function and oxidative stress[62]. In parallel, redox imbalance and mitochondrial stress can potentiate PKR activation and eIF2α phosphorylation, reshaping translational control during infection[63]. Together, these mechanisms provide a biological framework through which GLDC activity can modulate innate immune and translational responses during viral infection. GLDC has also been implicated in suppressing MHC-I–mediated antigen presentation to promote immune evasion in cancer, supporting a broader role in host immune response pathways[64].

Previous studies have identified GLDC as a host susceptibility factor in influenza A virus infection, where genetic or pharmacological inhibition of GLDC enhances type I interferon signaling and suppresses viral replication[65,66].These studies, conducted primarily in epithelial cell systems and focused on nuclear-replicating influenza viruses, support a model in which GLDC-

driven one-carbon metabolism sustains nucleotide availability and constrains innate immune activation, thereby favoring viral propagation. In contrast, our data demonstrate that GLDC restricts MG1 spread in glioblastoma cells, as loss of GLDC markedly accelerates viral spread. This divergence likely reflects fundamental differences in virus class, cellular state, and regulatory layer. Rhabdoviruses such as MG1 and VSV replicate exclusively in the cytoplasm and are highly sensitive to perturbations in host translational capacity and mitochondrial homeostasis, features that are distinct from influenza virus biology. Notably, whereas prior studies focused on GLDC regulation at the metabolic or transcriptional level, our data reveal selective translational upregulation of GLDC during MG1 infection, uncovering a previously unrecognized post-transcriptional mode of host restriction.

4.7 References

1. Rozman, B., Fisher, T. & Stern-Ginossar, N. Translation—A tug of war during viral infection. *Mol. Cell* 83, 481–495 (2023).

2. Walsh, D., Mathews, M. B. & Mohr, I. Tinkering with Translation: Protein Synthesis in Virus-Infected Cells. *Cold Spring Harb. Perspect. Biol.* 5, a012351 (2013).

3. Diamond, M. S. IFIT1: A dual sensor and effector molecule that detects non-2′-O methylated viral RNA and inhibits its translation. *Cytokine Growth Factor Rev.* 25, 543–550 (2014).

4. Habjan, M. *et al.* Sequestration by IFIT1 Impairs Translation of 2′O-unmethylated Capped RNA. *PLoS Pathog.* 9, e1003663 (2013).

5. Schneider, W. M., Chevillotte, M. D. & Rice, C. M. Interferon-stimulated genes: a complex web of host defenses. *Annu. Rev. Immunol.* 32, 513–545 (2014).

6. Brennan-Laun, S. E., Ezelle, H. J., Li, X.-L. & Hassel, B. A. RNase-L Control of Cellular mRNAs: Roles in Biologic Functions and Mechanisms of Substrate Targeting. *J. Interferon Cytokine Res.* 34, 275–288 (2014).

7. Li, Y. *et al.* Activation of RNase L is dependent on OAS3 expression during infection with diverse human viruses. *Proc. Natl. Acad. Sci.* 113, 2241–2246 (2016).

8. Hoang, H.-D., Neault, S., Pelin, A. & Alain, T. Emerging translation strategies during virus–host interaction. *WIREs RNA* 12, e1619 (2021).

9. Walsh, D. & Mohr, I. Viral subversion of the host protein synthesis machinery. *Nat. Rev. Microbiol.* 9, 860–875 (2011).

10. Newburn, L. R. & White, K. A. *Cis*-acting RNA elements in positive-strand RNA plant virus genomes. *Virology* 479–480, 434–443 (2015).

11. Meyer, K. D. *et al.* 5′ UTR m6A Promotes Cap-Independent Translation. *Cell* 163, 999–1010 (2015).

12. Coots, R. A. *et al.* m6A Facilitates eIF4F-Independent mRNA Translation. *Mol. Cell* 68, 504-514.e7 (2017).

13. Trainor, B. M. & Shcherbik, N. Short and Sweet: Viral 5`-UTR as a Canonical and Non-Canonical Translation Initiation Switch. *J. Cell. Immunol.* 3, 296–304 (2021).

14. Tirosh, O. *et al.* The Transcription and Translation Landscapes during Human Cytomegalovirus Infection Reveal Novel Host-Pathogen Interactions. *PLoS Pathog.* 11, e1005288 (2015).

15. Finkel, Y. *et al.* SARS-CoV-2 uses a multipronged strategy to impede host protein synthesis. *Nature* 594, 240–245 (2021).

16. Hoang, H.-D. *et al.* Induction of an Alternative mRNA 5′ Leader Enhances Translation of the Ciliopathy Gene Inpp5e and Resistance to Oncolytic Virus Infection. *Cell Rep.* 29, 4010-4023.e5 (2019).

17. Dai, A. *et al.* Ribosome Profiling Reveals Translational Upregulation of Cellular Oxidative Phosphorylation mRNAs during Vaccinia Virus-Induced Host Shutoff. *J. Virol.* 91, e01858-16 (2017).

18. Decoding viral infection by ribosome profiling - PubMed. https://pubmed.ncbi.nlm.nih.gov/25810547/.

19. Meyuhas, O. & Kahan, T. The race to decipher the top secrets of TOP mRNAs. *Biochim. Biophys. Acta* 1849, 801–811 (2015).

20. Masvidal, L., Hulea, L., Furic, L., Topisirovic, I. & Larsson, O. mTOR-sensitive translation: Cleared fog reveals more trees. *RNA Biol.* 14, 1299–1305 (2017).

21. Piccirillo, C. A., Bjur, E., Topisirovic, I., Sonenberg, N. & Larsson, O. Translational control of immune responses: from transcripts to translatomes. *Nat. Immunol.* 15, 503–511 (2014).

22. Xu, T. *et al.* Metabolic control of TH17 and induced Treg cell balance by an epigenetic mechanism. *Nature* 548, 228–233 (2017).

23. Wang, J., Zhang, X., Greene, G. H., Xu, G. & Dong, X. PABP/purine-rich motif as an initiation module for cap-independent translation in pattern-triggered immunity. *Cell* 185, 3186-3200.e17 (2022).

24. Xu, G. *et al.* Global translational reprogramming is a fundamental layer of immune regulation in plants. *Nature* 545, 487–490 (2017).

25. Beisang, D. & Bohjanen, P. R. Perspectives on the ARE as it turns 25 years old. *Wiley Interdiscip. Rev. RNA* 3, 719–731 (2012).

26. Arif, A. *et al.* The GAIT translational control system. *Wiley Interdiscip. Rev. RNA* 9, e1441 (2018).

27. Shalhout, S. Z., Miller, D. M., Emerick, K. S. & Kaufman, H. L. Therapy with oncolytic viruses: progress and challenges. *Nat. Rev. Clin. Oncol.* 20, 160–177 (2023).

28. Lin, D., Shen, Y. & Liang, T. Oncolytic virotherapy: basic principles, recent advances and future directions. *Signal Transduct. Target. Ther.* 8, 156 (2023).

29. Pol, J. G. *et al.* Maraba virus as a potent oncolytic vaccine vector. *Mol. Ther. J. Am. Soc. Gene Ther.* 22, 420–429 (2014).

30. Brun, J. *et al.* Identification of Genetically Modified Maraba Virus as an Oncolytic Rhabdovirus. *Mol. Ther.* 18, 1440–1449 (2010).

31. Jafarnejad, S. M. *et al.* Translational control of ERK signaling through miRNA/4EHP-directed silencing. *eLife* 7, e35034 (2018).

32. Rusinova, I. *et al.* Interferome v2.0: an updated database of annotated interferon-regulated genes. *Nucleic Acids Res.* 41, D1040-1046 (2013).

33. Bailey, T. L. *et al.* MEME SUITE: tools for motif discovery and searching. *Nucleic Acids Res.* 37, W202-208 (2009).

34. Vidigal, J. A. & Ventura, A. Rapid and efficient one-step generation of paired gRNA CRISPR-Cas9 libraries. *Nat. Commun.* 6, 8083 (2015).

35. Pol, J. G. *et al.* Maraba virus as a potent oncolytic vaccine vector. *Mol. Ther. J. Am. Soc. Gene Ther.* 22, 420–429 (2014).

36. Lauer, U. M. & Beil, J. Oncolytic viruses: challenges and considerations in an evolving clinical landscape. *Future Oncol.* 18, 2713–2732 (2022).

37. Pol, J. G. *et al.* Development and applications of oncolytic Maraba virus vaccines. *Oncolytic Virotherapy* 7, 117–128 (2018).

38. Hassanzadeh, G. *et al.* Characterizing Cellular Responses During Oncolytic Maraba Virus Infection. *Int. J. Mol. Sci.* 20, 580 (2019).

39. Schott, J. *et al.* Translational regulation of specific mRNAs controls feedback inhibition and survival during macrophage activation. *PLoS Genet.* 10, e1004368 (2014).

40. Beisang, D. & Bohjanen, P. R. Perspectives on the ARE as it turns 25 years old. *Wiley Interdiscip. Rev. RNA* 3, 719–731 (2012).

41. Shaw, G. & Kamen, R. A conserved AU sequence from the 3' untranslated region of GM-CSF mRNA mediates selective mRNA degradation. *Cell* 46, 659–667 (1986).

42. Leppek, K., Das, R. & Barna, M. Functional 5′ UTR mRNA structures in eukaryotic translation regulation and how to find them. *Nat. Rev. Mol. Cell Biol.* 19, 158–174 (2018).

43. Bal, N. V. *et al.* Upstream Open Reading Frames Located in the Leader of Protein Kinase Mζ mRNA Regulate Its Translation. *Front. Mol. Neurosci.* 9, (2016).

44. Young, S. K. & Wek, R. C. Upstream Open Reading Frames Differentially Regulate Gene-specific Translation in the Integrated Stress Response*. *J. Biol. Chem.* 291, 16927–16935 (2016).

45. Jürgens, L. *et al.* Somatic Functional Deletions of Upstream Open Reading Frame-Associated Initiation and Termination Codons in Human Cancer. *Biomedicines* 9, 618 (2021).

46. Morris, D. R. & Geballe, A. P. Upstream Open Reading Frames as Regulators of mRNA Translation. *Mol. Cell. Biol.* 20, 8635–8642 (2000).

47. Melo, E. O., Dhalia, R., de Sa, C. M., Standart, N. & de Melo Neto, O. P. Identification of a C-terminal Poly(A)-binding Protein (PABP)-PABP Interaction Domain: ROLE IN COOPERATIVE BINDING TO POLY(A) AND EFFICIENT CAP DISTAL TRANSLATIONAL REPRESSION*. *J. Biol. Chem.* 278, 46357–46368 (2003).

48. Cap-independent translation is required for starvation-induced differentiation in yeast - PubMed. https://pubmed.ncbi.nlm.nih.gov/17761883/.

49. Halbeisen, R. E. & Gerber, A. P. Stress-Dependent Coordination of Transcriptome and Translatome in Yeast. *PLOS Biol.* 7, e1000105 (2009).

50. Wang, C. *et al.* RNA-seq and Ribosome Profiling Reveal the Translational Landscape of Rice in Response to Rice Stripe Virus Infection. *Viruses* 16, 1866 (2024).

51. Hsieh, A. C. *et al.* The translational landscape of mTOR signalling steers cancer initiation and metastasis. *Nature* 485, 55–61 (2012).

52. Schmidt, T. *et al.* eIF4A1-dependent mRNAs employ purine-rich 5'UTR sequences to activate localised eIF4A1-unwinding through eIF4A1-multimerisation to facilitate translation. *Nucleic Acids Res.* 51, 1859–1879 (2023).

53. Wilczynska, A. *et al.* eIF4A2 drives repression of translation at initiation by Ccr4-Not through purine-rich motifs in the 5'UTR. *Genome Biol.* 20, 262 (2019).

54. Dhungel, P., Cao, S. & Yang, Z. The 5'-poly(A) leader of poxvirus mRNA confers a translational advantage that can be achieved in cells with impaired cap-dependent translation. *PLoS Pathog.* 13, e1006602 (2017).

55. Wilczynska, A. *et al.* eIF4A2 drives repression of translation at initiation by Ccr4-Not through purine-rich motifs in the 5'UTR. *Genome Biol.* 20, 262 (2019).

56. Wang, J., Zhang, X., Greene, G. H., Xu, G. & Dong, X. PABP/purine-rich motif as an initiation module for cap-independent translation in pattern-triggered immunity. *Cell* 185, 3186-3200.e17 (2022).

57. de Rozières, C. M. *et al.* PABP1 Drives the Selective Translation of Influenza A Virus mRNA. *J. Mol. Biol.* 434, 167460 (2022).

58. Liu, Z. *et al.* Akabane virus infection induces PABP1 nuclear retention and inhibits IFN-β production. *Virology* 619, 110878 (2026).

59. Tibbetts, A. S. & Appling, D. R. Compartmentalization of Mammalian folate-mediated one-carbon metabolism. *Annu. Rev. Nutr.* 30, 57–81 (2010).

60. Kikuchi, G., Motokawa, Y., Yoshida, T. & Hiraga, K. Glycine cleavage system: reaction mechanism, physiological significance, and hyperglycinemia. *Proc. Jpn. Acad. Ser. B Phys. Biol. Sci.* 84, 246–263 (2008).

61. Martínez-Reyes, I. & Chandel, N. S. Mitochondrial TCA cycle metabolites control physiology and disease. *Nat. Commun.* 11, 102 (2020).

62. West, A. P. *et al.* Mitochondrial DNA stress primes the antiviral innate immune response. *Nature* 520, 553–557 (2015).

63. Pakos-Zebrucka, K. *et al.* The integrated stress response. *EMBO Rep.* 17, 1374–1395 (2016).

64. Liu, R. & Li, S. Phosphorylation of FBXL3 mediates GLDC polyubiquitination to suppress MHC-I expression and promote cancer immune evasion. *Cell Insight* 5, 100308 (2026).

65. Fraser-Pitt, D. *et al.* Cysteamine-mediated blockade of the glycine cleavage system modulates epithelial cell inflammatory and innate immune responses to viral infection. *Biochem. Biophys. Res. Commun.* 677, 168–181 (2023).

66. Zhou, J. *et al.* Identification and characterization of GLDC as host susceptibility gene to severe influenza. *EMBO Mol. Med.* 11, e9528 (2019).

4. CHAPTER FIVE: GENERAL DISCUSSION

5.1 Physical and Delivery Barriers in Oncolytic Virotherapy

Physical and delivery barriers are the first limiting factors that restrict the therapeutic success of oncolytic virotherapy. One of the essential aspects to augment the therapeutic effect of OV lies in the capacity to penetrate various physical barriers to deliver and distribute viral particles evenly throughout the tumour bed. Therefore, optimizing virus delivery by experimenting with novel approaches is an important and complementary part of successful oncolytic virotherapy.

Previous observations demonstrated that oncolytic virotherapy, even in clinically advanced systems still faces serious bottlenecks in delivery, which remains one of the primary technical limitations for clinical applications. Intralesional injection remains the most applicable delivery method for OV in clinical setting, yet numerous barriers hinder the delivery of the virus solution to solid tumours. Structural characteristics of the tumour microenvironment, such as dense extracellular matrix, high interstitial fluid pressure, and distorted vascular architecture severely limit virus solution retention and spreading throughout the tumour[1,2]. These physical obstacles restrict the fraction of tumour cells that could be efficiently infected and decrease viral multiplication and therapeutic efficiency[1,3]. Besides these structural limitations, oncolytic viruses still cannot be efficiently delivered systemically due to other barriers including neutralization due to pre-existing immunity, sequestration in organs such as liver and spleen, and lack of extravasation to the tumour bed[4].

For those reasons, novel delivery strategies have been extensively explored. Nanoparticle encapsulation, PEGylation, biomimetic vesicles, and cell-based carriers are some of the strategies that have been designed in the context of solid tumours to protect viral particles against immune clearance and increase tumour targeting[5,6]. For example, polymer- and liposome-based vehicles have been shown to enhance stability and extend circulation, and mesenchymal stem cells have been investigated as tumour-homing vehicles that can also protect viruses against pre-existing immunity[6,7]. Nevertheless, these methods tend to be costly in terms of needing significant changes in viral particles or integration of complicated delivery systems and are constrained by their capacity to generate efficient and consistent infiltration of dense tumour tissues. Additionally,

capsid or viral engineering alone often is not enough to overcome the intrinsic physical barriers of solid tumours, which further supports the idea that a better viral design does not necessarily translate to a better intratumoural distribution. Our study shows that needle-free injection (NFI) is a simple, non-invasive physical method that does not need any modification of the viral genome or the addition of engineering to other delivery systems and can be effectively used to achieve the improvement of delivery. In contrast to the traditional needle-based delivery system where there is a tendency toward local deposition and restricted penetration, NFI employs a high-pressure jet system to distribute viral particles in tumour tissue, enhancing spatial distribution and maximizing the probability of productive infection in tumour regions. Significantly, needle-free injection systems have been widely tested clinically and have been shown to be similarly immunogenic in various vaccines such as influenza, poliovirus, and measles-mumps-rubella and have also been shown to drive better tissue distribution and in certain instances, dose-sparing[8]. These characteristics enable NFI as a clinically translatable delivery platform. We have shown that NFI can improve viral spread in tumours and maintain infectivity and therapeutic action, indicating that mechanisms of physical delivery alone can dramatically affect treatment outcomes. Our strategy, in contrast to current methods that use engineering the virus itself, involves engineering the physical delivery of the virus, an easier and more clinically translatable approach to augment intratumoural delivery in solid tumours. Hence, enhanced viral dissemination will increase tumour cell lysis, release of tumour-associated antigens and dendritic cell and tumour-specific T cell activation[8]. Therefore, the ability to optimize delivery can not only enhance direct oncolysis but also enhance antitumour immunity, which further helps boost the efficacy of therapy

5.2 Translation control in antiviral immune response

Viral infection induces an antiviral state in host cells that is characterized by activation of interferon signaling pathways and induction of a broad repertoire of interferon-stimulated genes. However, this state is not defined simply by transcriptional activation. A central feature of antiviral defence is that gene expression is also regulated at the level of mRNA translation. Viral infection activates mechanisms that globally constrain protein synthesis, including PKR-dependent phosphorylation of eIF2α and IFIT-mediated inhibition of vulnerable RNAs that lack specific structural features, such as 2′-O methylation on the ribose of the first transcribed nucleotide or the presence of an uncapped 5′ triphosphate group, yet this does not produce a total translational

shutdown[9–11]. Rather, it creates a reprogrammed translational environment in which some transcripts remain poorly engaged by ribosomes while others are selectively favored[12,13]. A well-established example to showcase the importance of translation control during the antiviral state is IRF7, a master transcription factor of interferon signaling whose mRNA is translationally repressed by 4E-BPs. Relief of this repression enhances type I interferon production and antiviral resistance[14,15]. Likewise, m6A-dependent regulation has been shown to enhance translation of selected interferon-stimulated genes such as IFITM1 and MX1, demonstrating that efficient antiviral protein production depends not only on mRNA induction but also on selective ribosome recruitment[16,17]. More recently, Viperin (RSAD2) is a well-characterized interferon-stimulated antiviral protein that not only inhibits viral replication through production of nucleotide analogs such as ddhCTP, but also modulates host translation by inducing ribosome collision-dependent translational inhibition, highlighting the direct link between innate immunity and control of protein synthesis[18]. Notably, emerging evidence identifies INPP5E as an antiviral effector selectively induced at the level of translation during viral infection, providing a clear example of how translational control can shape the antiviral proteome[19].

This framework is highly consistent with the MG1 translatome data. In the interferon-related mRNA-high / TE-low heatmaps, many transcripts display strong transcriptional induction but only modest ribosome-protected fragment signal and markedly reduced translational efficiency. This pattern indicates that transcriptional activation is not matched by efficient translation and supports the presence of a translational bottleneck within the antiviral response. In practical terms, MG1-infected cells appear capable of mounting a broad interferon- and cytokine-rich transcriptional program, but translation acts as a filtering step that restricts which of these transcripts are ultimately converted into protein. This interpretation is strongly supported by ribosome-profiling studies in other viral systems. During SARS-CoV-2 infection, transcripts encoding IFNB1, IFNL1–3, IL6, and CCL5 were shown to be strongly induced at the RNA level yet remain restricted at the post-transcriptional level, with limited ribosome occupancy relative to their transcriptional upregulation[20]. The mRNA-high/TE-low interferon-related genes in the MG1 dataset therefore resemble a cytokine-wave-like transcriptional response whose magnitude is subsequently restrained by translation. This is an important conceptual point, because the antiviral state is not simply “on” or “off” at the mRNA level; rather, it is quantitatively sculpted at the stage of ribosome recruitment.

A first major implication of these transcriptionally inflated but translationally restricted heatmaps is that they likely capture a regulated attempt to prevent excessive inflammatory output. Genes such as IFNB1, CCL5, CXCL10, CXCL9, IL8, CXCL2, CXCL3, TNFAIP3, HERC5, OASL, IFIT1, and RSAD2 are classical components of antiviral and inflammatory signaling[20], yet in the MG1 heatmaps many of them show a disproportion between mRNA abundance and translational efficiency. This suggests that transcriptional activation of inflammation does not automatically commit the cell to large-scale cytokine protein production. From a biological perspective, such a translational checkpoint is plausible and likely advantageous: unrestricted translation of inflammatory cytokines could amplify tissue-damaging responses or accelerate immune pathology, whereas a translation-level filter enables the infected cell to prime the antiviral program transcriptionally while controlling the magnitude and timing of protein output. In this sense, the MG1 dataset supports the view that the antiviral response includes a broad transcriptional reserve of inflammatory transcripts, only a fraction of which are ultimately allowed to proceed to efficient translation.

A second important point is that several genes within the mRNA-high/TE-low lists are not merely passive readouts of interferon signaling, but are themselves mechanistically connected to post-transcriptional control of innate immunity. A particularly strong example is OASL1-related biology. In mouse cells, Oasl1 binds the 5′UTR of Irf7 mRNA and inhibits its translation, thereby limiting type I interferon production; loss of Oasl1 enhances interferon induction and improves viral control[21]. This is highly relevant to our MG1 data because it demonstrates that interferon-stimulated genes can themselves impose translational brakes on the antiviral response. Similarly, murine Ifit1b has been shown to bind cap1-RNA, modulate host translation, and restrict coronavirus infection, placing IFIT-family biology directly at the interface between innate immunity and translational control[22]. Another strong example is HERC5, which is mechanistically linked to the translational machinery because it associates with polysomes and mediates co-translational ISGylation (mechanism in which the protein Interferon-Stimulated Gene 15 (ISG15) is conjugated covalently to the target proteins, a key component of the innate antiviral immune response of IFN type I) of newly synthesized proteins[23]. Together, these studies support the idea that the interferon system is not simply transcribed and then translated in a linear manner; rather, it contains built-in post-transcriptional regulators that shape how much of the induced program is

actually expressed as protein. Consistent with our data, where many interferon-related transcripts appear transcriptionally primed but translationally restrained.

A third point is that several inflammatory genes in the transcriptionally induced but translationally restricted group are well known to be controlled through AU-rich element (ARE)-dependent post-transcriptional mechanisms[24]. PTGS2/COX-2 is a classic example: its 3′UTR contains a conserved ARE that regulates both mRNA stability and translation, and dysregulation of this mechanism contributes to pathological overexpression[25]. More broadly, ARE-binding proteins such as ZFP36/TTP regulate the fate of inflammatory transcripts by promoting mRNA decay and/or translational repression[26]. This literature provides a strong mechanistic framework for understanding why inflammatory genes such as PTGS2, TNFAIP3, IL8, and related transcripts can be robustly induced at the mRNA level in the MG1 dataset while remaining translationally dampened. Importantly, this interpretation avoids the misleading conclusion that these genes are biologically unimportant simply because their translational efficiency is low. On the contrary, their low TE may reflect active post-transcriptional governance of inflammatory amplitude, duration, and timing. Notably, a transcript can be highly relevant to the antiviral state even when its protein output is deliberately restrained[27]. Given that many of these genes encode potent cytokines and immune mediators, such translational restraint likely serves to control the magnitude, timing, and duration of the inflammatory response

In contrast to this transcriptionally expansive but translationally constrained arm, the interferon-related mRNA-low-or-unchanged/TE-high heatmaps reveal a second arm of the antiviral response: a smaller subset of transcripts that are selectively prioritized for translation despite weak transcriptional support. This is an equally important finding. It shows that translation is not functioning only as a suppressive filter but also as an active selector of biological priorities. In our data, many genes display low or unchanged mRNA abundance together with strong RPF signal and high translational efficiency, indicating preferential ribosome recruitment under conditions in which global translation is constrained. This pattern is consistent with the broader literature showing that viral infection remodels translation rather than uniformly shutting it down, allowing only selected transcripts to retain ribosome access. In the MG1 setting, this translationally privileged group likely represents proteins that the infected cell “chooses” to produce under stress

because they support adaptation, defence, survival decisions, or clinically meaningful immune functions.

One of the strongest examples in this translationally prioritized group is IGF2BP1. IGF2BP1 is a well-established RNA-binding protein that regulates mRNA stability and translation and has been repeatedly implicated in tumour progression, metastasis, and therapeutic resistance[28–30]. Because IGF2BP1 itself can reshape post-transcriptional gene-expression programs, its selective translation during MG1 infection may have disproportionate biological consequences: producing more IGF2BP1 could amplify downstream translational remodeling and thereby reinforce the proteomic state of infected tumour cells. This makes IGF2BP1 particularly valuable because it connects the MG1 translation data not only to antiviral stress, but also to cancer-cell adaptation and therapeutic vulnerability. More broadly, it illustrates why low mRNA abundance should not be interpreted as lack of importance. A transcript with weak transcriptional induction but high translational efficiency may exert much greater biological influence than a highly abundant transcript that remains poorly translated.

A similarly important example is GLDC, which in the MG1 dataset is low at the mRNA level yet selectively translated. This pattern is mechanistically compelling because the literature already links GLDC to antiviral innate immunity through metabolism[31]. GLDC regulates glycine cleavage and pyrimidine biosynthesis, and experimental inhibition of GLDC amplifies type I interferon and ISG responses while suppressing influenza replication. These findings established a GLDC–pyrimidine biosynthesis–innate immunity axis, indicating that glycine metabolism is directly connected to antiviral signaling. In the context of the MG1 infection, selective translation of GLDC therefore suggests that MG1 infection recruits metabolic effectors into the antiviral program through translational prioritization. This is important finding because the genes privileged for translation are not limited to canonical cytokines or pattern-recognition molecules, but also include metabolic regulators that influence innate immunity. From a translation control perspective, this is the information that will be overlooked by transcriptomic analysis. A transcript with low mRNA abundance might be discarded as biologically irrelevant, yet our data show that such a gene can be translationally activated and potentially functionally important.

Other genes in the TE-high sets further support the idea of directed stress adaptation. BHLHE41 is a stress-responsive transcription factor associated with adaptive cellular programs. MAPK13, a

p38-family kinase, links stress and inflammatory signaling and has been implicated in post-viral epithelial remodeling. Even when the literature does not identify each of these genes as a canonical example of translation-level control, their selective enrichment in the TE-high panels strongly suggests that MG1 infection favors transcripts associated with cellular adaptation, injury responses, and reprogramming under translational stress. Likewise, several genes in these TE-high lists have clear immune or therapeutic relevance. IL3RA/CD123 is an established therapeutic target in hematologic malignancies[32]. CLEC7A has recognized immune and therapeutic relevance in gliomas[33]. HLA-DPA1 and PECAM1 point toward altered immune recognition and cell-interaction programs[34]. The key point is not that all of these genes are already known and well-established translation-controlled genes in the literature, but that our data identify them as preferentially translated interferon-related transcripts during MG1 infection. That observation alone is useful scientifically because it nominates a set of genes that may have been undervalued in transcript-centric analyses and that could be explored in future work as functional mediators, biomarkers, or therapeutic targets.

Taken together, the two classes of interferon-related gene sets support a unified model in which MG1 infection partitions the host response into two coupled but distinct layers. The first layer is a broad transcriptional interferon/cytokine arm, exemplified by genes such as IFNB1, CCL5, CXCL10, CXCL9, IL8, OASL, IFIT1B, HERC5, TNFAIP3, and PTGS2, many of which are transcriptionally robust but translationally restrained. The second layer is a smaller translationally prioritized arm, exemplified by IGF2BP1, GLDC, BHLHE41, MAPK13, IL3RA, HLA-DPA1, PECAM1, and CLEC7A, in which low or unchanged mRNA abundance is offset by enhanced ribosome recruitment and high TE. This dual architecture has important implications. First, it explains why mRNA abundance alone can be a poor predictor of protein output during OV infection. Second, it argues that translation is not merely a downstream readout of interferon signaling, but a major regulatory interface that determines which elements of the antiviral program are actually executed. Third, it highlights a practical opportunity for the field: genes overlooked because they are weakly transcribed may still be biologically and therapeutically important if they are translationally prioritized. In that sense, these data do more than document uncoupling between mRNA and translation, they provide a rationale for considering translation itself as a discovery layer for antiviral biology and as a potential therapeutic strategy.

5.3 Harnessing Translation Control Mechanisms for Therapy: Pharmacological approaches

Beyond the fundamental biological role of Translation control for protein synthesis, translation has increasingly been harnessed as an engineering tool across multiple therapeutic platforms. The development of novel drugs targeting these translation regulators have provided compelling evidence in neurodegenerative diseases. Several studies have demonstrated that modulation of the ISR, particularly through targeting the eIF2α–eIF2B axis, can restore proper protein synthesis and confer neuroprotection[35–38]

Additionally, cancer is among the diseases in which translation control mechanisms are increasingly being exploited as therapeutic strategies. In estrogen receptor (ER) driven tumours, such as wild-type ER tumours, estrogen receptor 1 (ESR1) mutation-driven tumours, estrogen receptor fusion-driven tumours, and endocrine therapy resistant tumours, pharmacological inhibition of eIF4A using rocaglates such as zotatifin suppresses the translation of estrogen receptor mRNA. As a result, this reduces tumour growth, and also overcomes resistance to endocrine therapy (therapies that inhibit estrogen signalling such as selective estrogen receptor degraders, fulvestrant)[39]. Critically, blocking eIF4A together with fulvestrant enhance the suppression of ER expression and growth, resulting in greater anti-tumour activity in vitro and in vivo, as well as responses in resistant patients[39,40]. In this regard, recent studies have shown that cancer cells, especially in aggressive cancers like triple-negative breast cancer, exhibit a broader dependency on eIF4A for translation that is distinct from normal cells, where second-generation inhibitors of eIF4A (e.g., MG-002) suppress translation of oncogenic mRNAs, limit tumour growth, and metastatic potential, while leaving normal cells intact[39,40]. Notably, these inhibitors preferentially target mRNAs containing polypurine-rich 5′UTR[39–42]. The 5′UTR of ESR1 has regulatory elements to enable eIF4E-independent translation; however, this translation is still dependent on the RNA helicase activity of eIF4A[39,40]. Interestingly, the translationally active R-motif–rich mRNAs observed upon viral infection may form structured RNA elements, suggesting that such motifs could confer selective translational regulation through increased dependency on RNA helicases such as eIF4A.

Rapamycin inhibitors have demonstrated antitumour activity across different malignancies clinically. Rapamycin (sirolimus) is an allosteric inhibitor of mTORC1 that suppresses translation

initiation via inhibiting activity of mTORC1 that prevent 4E-BP1 from competing for eIF4E and activation of ribosomal S6 kinases, ultimately reducing cap-dependent protein synthesis. Everolimus, a second-generation rapamycin derivative, has shown benefit in hormone receptor-positive advanced breast cancer, advanced renal cell carcinoma after prior targeted therapy, pancreatic neuroendocrine tumours, and neuroendocrine tumours of the gastrointestinal tract or lung[43–46]. Temsirolimus, another mTORC1 inhibitor, improved overall survival in poor-prognosis metastatic renal cell carcinoma[47]. Nab-sirolimus, an albumin-bound formulation of sirolimus, showed durable activity in malignant perivascular epithelioid cell tumours[48].

Even though eIF2α / ISR have important role in cancer progression and adaption to harsh conditions[49–51], their targets in cancer is clinically less established. At present, no eIF2α-directed therapy has achieved the same broad clinical validation in cancer as mTOR inhibitors, and many classic ISR modulators remain preclinical. However, the dopamine receptor D2 antagonist imipridone ONC201 (dordaviprone) provides a notable translational example because its antitumour activity has been linked to activation of the ISR, including ATF4 induction downstream of eIF2α kinases[52]. Clinical studies in H3 K27M-mutant diffuse midline glioma have reported that ONC201 was well tolerated and produced durable, clinically meaningful responses in subsets of patients, and a randomized phase III trial is ongoing[53–55]. ONC201 (dordaviprone) is a small-molecule anticancer agent that activates the integrated stress response, leading to phosphorylation of eIF2α, suppression of global protein synthesis, and selective translation of stress-responsive genes such as ATF4, ultimately promoting tumour cell death[56]. Thus, while the eIF2α pathway has not yet yielded a broadly adopted translation-targeted cancer therapy, it is emerging as a clinically relevant stress-associated translation pathway for therapeutic targeting.

Nevertheless, in these advances, the majority of pharmacological modalities that address translation are based on global or pathway-based regulation of the translational machinery, which is not transcript-specific in nature. Inhibitors of many major components of mTOR or eIF4A have a widespread effect on cap-dependent translation, and hence on disease-promoting and housekeeping mRNAs. Such non-selectivity may cause unintentional repression of vital cellular proteins, which will cause toxicity and narrow therapeutic indices[57–59]. In fact, mTOR inhibitors rapamycin and rapamycin analogs are linked with metabolic disturbances, immunosuppression, and feedback stimulation of compensatory signaling pathways, including PI3K/AKT, capable of

decreasing long-term therapy effect[60]. Similarly, targeting core translation initiation factors, such as eIF4A, may disproportionately affect transcripts with complex or structured 5′UTRs, yet still cause global perturbation of the cellular translatome, owing to the central role of these factors in protein synthesis. This extensive effect is especially applicable in dynamic biological conditions like viral infection or stress responses, in which global repression of translation already exists, and additional pharmacological repression can only worsen cellular dysfunction. Moreover, efforts to overcome resistance often arise, such as rewiring of translational regulatory pathways, activation of other initiation pathways, or targeting tumour cells with decreased reliance on specific translation factors.

Moreover, pharmacological modulation of stress-responsive pathways introduces significant complexity, as these pathways exert dual and opposing effects on translation. Therapeutic activation of the ISR can suppress protein synthesis but also enhance cellular adaptation and survival programs, whereas inhibition of the ISR may restore global translation yet inadvertently support viral replication or tumour progression. This context-dependent duality makes targeting the ISR particularly challenging in clinical settings.

Pharmacological approaches can relatively effectively address major nodes of the translational machinery, but are frequently not precise enough to allow specific transcripts to be regulated. This highlights the necessity of other methods that allow transcript-specific regulation of translation, including using endogenous cis-regulatory factors in untranslated regions of mRNA, which could offer a more targeted and context-specific means of regulating protein expression hence therapeutic benefits.

5.4 Harnessing Translation Control Mechanisms for Therapy: Non-Pharmacological Approaches

New non-pharmacological approaches are developed and gaining a huge interest to regulate protein synthesis using direct manipulation of RNA characteristics and regulatory factors. They involve antisense and steric-blocking oligonucleotides, which regulate ribosome access or translation factor binding, and splice-switching strategies that regulate mRNA isoform repertoire and downstream translational production. Simultaneously, UTR engineering has been applied to control protein expression more precisely, with translational efficiency improved by alterations in

the 5′UTR, and cell-type-specific regulation by cell-type-specific microRNA responsiveness mediated by incorporation into the 3′UTR[61–65].

Unlike the global pharmacological approaches, these RNA-based approaches provide a greater level of transcript specificity through direct encoding of regulatory elements in the mRNA. This is more applicable to my finding where I illustrate that intrinsic mRNA characteristics are correlated with increased translational efficiency in conditions of viral infection. Considering that the oncolytic viruses act within a highly restrictive and reprogrammed translational context, these results suggest a model whereby engineering or exploitation of cis-regulatory RNA elements can offer a more specific and context-adapted approach to maximize therapeutic transgene expression, to supplement current strategies of delivery, immune activation, and viral design.

OV have been extensively engineered to increase their safety, delivery, tumour selectivity and therapeutic efficacy, using approaches like virulence attenuation, tumour-specific targeting with promoters and regulation using microRNAs. Moreover, a lot of effort has been invested in maximizing the expression of therapeutic transgenes via transcription control using strong promoters[66–68]. Nonetheless, although protein synthesis is central to the process of determining viral replication and therapeutic output, translation-level control has yet to be a design principle in OV engineering, and the majority of strategies have been based on transcriptional or post-entry control. However, there are evidence suggesting the potential of translation engineering in designing enhanced OV. For example, the oncolytic poliovirus PVSRIPO, which is engineered by substituting the native poliovirus IRES with a heterologous type I IRES which is based on a human rhinovirus type 2 (HRV2)[69]. This modification alters the translational tropism of the virus, reducing the expression of viral proteins in normal neuronal cells and maintaining an active cap-independent translation in cancer cells where signaling pathways are often dysregulated and protein translation control is often altered. IRES elements in the endogenous transcripts such as VEGF-A and FGF2 facilitate continued protein synthesis under hypoxic or stress conditions, thereby supporting angiogenesis and stress adaptation. These properties have been directly exploited in therapeutic systems, where IRES elements are incorporated into multicistronic gene therapy vectors to enable coordinated expression of multiple genes from a single transcript while maintaining translation in restrictive environments[70]. For example, IRES-based constructs are widely used in viral and non-viral vectors, including engineered immune cell therapies and gene

delivery platforms, to ensure stable expression of therapeutic transgenes even when cap-dependent translation is suppressed[71]. Notably, the IRES-mediated activity can facilitate viral protein synthesis in the state of translational stress, such as that caused by host antiviral responses, such as type I interferon signaling, which underlines the ability of optimised RNA elements to partially circumvent host translational repression[69,72].

MicroRNAs (miRNAs) are small non-coding RNAs that control the expression of genes by inhibiting the translation of target transcripts. miRNA are associated with interacting with miRNA response elements (MREs) in the 3′UTR, also in the 5′UTR and coding regions, and induces translational repression of target mRNAs[73]. miRNAs translational control strategy has been used in the context of oncolytic virotherapy to increase tumour selectivity and therapeutic efficacy. In particular, viral miRNAs (MREs or miRTs) have been inserted into the viral genomes so that cell-type-specific repression of viral protein synthesis can be achieved and hence enhance its safety. In normal tissues, where the cognate miRNAs are strongly expressed, miRNAs binding to viral transcripts represses the expression of key viral genes, resulting in restricted viral replication and toxicity. This strategy has been implemented using neuronal miRNAs such as miR-124 and miR-128, muscle-enriched miRNAs such as miR-1 and miR-133, and tumour-suppressive miRNAs such as miR-143, across multiple oncolytic platforms including HSV-1, adenovirus, VSV, measles virus, and coxsackievirus B3 (CVB3)[74–76], where insertion of miRTs into 3′UTR or combined 5′/3′UTR regions of viral transcripts enhances translational restriction in normal tissues while preserving robust viral protein synthesis in tumours. Furthermore, positioning of miRTs within untranslated regions directly modulates translational efficiency. In addition to detargeting strategies, miRNAs can also enhance oncolytic virus activity by modulating host translational landscapes; for example, miR-99b, miR-485, and miR-26b have been shown to promote adenoviral replication in cancer cells[74,77,78], suggesting that specific miRNAs can facilitate viral protein synthesis or alleviate antiviral translational barriers. Aside from miRNA, incorporating other translation modifying cis-element to the UTRs also showed promising results. Designing of therapeutic constructs containing an eIF4E-responsive 5′UTR demonstrated preferential translation in cancer cells, while remaining poorly translated in normal cells, resulting in selective expression of reporter and therapeutic genes, including herpes simplex virus thymidine kinase (HSV-TK), and enabling targeted cell killing upon prodrug treatment with ganciclovir, generating sufficient enzyme to convert ganciclovir into its cytotoxic form, thereby conferring selective

cytotoxicity[79]. This construct depends on structurally complex 5′UTRs on elevated eIF4E/eIF4F activity for efficient ribosome recruitment, such that transcripts remain translationally repressed in normal cells despite comparable mRNA levels, but are efficiently translated in cancer cells with dysregulated cap-dependent translation. Furthermore, when combined with transcriptional targeting strategies such as prostate-specific promoters (e.g., ARR2PB), this approach enables multi-layered control of gene expression, ensuring both tissue-specific transcription and context-dependent translation[79].

Recent advances in gene therapy design indicate a shift from exclusively optimizing transcriptional elements, such as strong promoters (e.g., CMV), toward incorporating regulatory features that enhance protein output at the level of translation. The study of translational control as a therapeutic stratum has grown significantly in the last several years, and novel high-throughput experimental and theoretical approaches have been developed to systematically discover mRNA characteristics that regulate translational efficiency and protein production. For example, a generative adversarial network-based model (UTRGAN) was developed to generate synthetic 5′UTRs optimized for translation efficiency, ribosome load, and protein expression. These engineered UTRs achieved up to a 34-fold increase in predicted translation efficiency and significantly enhanced protein production in vitro when applied to therapeutic targets such as TNF-α[80]. Importantly, this framework is designed for applications across mRNA-based therapeutics, including protein replacement therapies, gene editing, vaccination, and cancer immunotherapy[80]. Another study where they used high-throughput screening of approximately 12,000 natural and synthetic 5′UTRs, generated through integration of RNA-seq and ribosome profiling datasets with computational modeling, which identified synthetic UTRs capable of significantly increasing protein production independent of promoter strength[81]. Although initially validated in reporter systems, this strategy has clear therapeutic implications. Optimization of translation via 5'UTR optimization leads to an increase in protein expression at lower doses of vectors, increasing therapeutic efficacy with a decrease in toxicity, manufacturing load and immune adverse responses related to high dosage delivery[81]. Recent studies using RNA-seq, ribosome profiling, and CLIP-seq datasets further expand on this concept by demonstrating that endogenous 5′UTRs derived from ribosomal protein mRNAs, including RPS9, RPL18, and RPL35, can markedly enhance translation efficiency across multiple cell types and in vivo systems. These studies identified UTR features that promote efficient ribosome recruitment and interaction with translation-regulatory

RNA-binding proteins such as LARP1 and LARP4[82]. Importantly, incorporation of these optimized 5′UTRs into synthetic mRNAs significantly improved protein output in preclinical models of aging and metabolic dysfunction, conditions characterized by impaired translational capacity[82]. This is especially applicable in the gene therapy platform like AAV where dose restriction is a significant issue.

Although many studies have extensively explored translation-enhancing UTRs in the context of normal cells and tissues, less is known about elements that can sustain or enhance translation in restrictive environments, such as those imposed by viral infection. Although these methods have mainly been applied to non-viral based gene delivery and cancer therapeutic delivery systems, our results studying oncolytic virotherapy show that viral and host-derived RNA elements can be used to overcome the highly restrictive translational environment induced by infection and increase the expression of therapeutic transgenes. For example, incorporation of the HSV1 US11 5′UTR upstream of the GM-CSF transgene resulted in enhanced protein expression, demonstrating that viral-derived UTR elements can be leveraged to overcome translational limitations in infected cells. The poly-R motif, being able to enhacing translation specifically during the antiviral state, can also be another potent cis-element to improve transgene expression from OV genome to ensure high protein output during OV-induced antiviral state.

Moreover, improving protein production and mRNA stability has also been exploited to enhance overall protein output. Across the vaccine and mRNA-therapy literature, the central strategy is to redesign the RNA itself so that it is translated more efficiently, remains stable longer, avoids excessive innate sensing, and produces more protein at a lower dose. The main parts that are engineered are the 5′ cap, 5′UTR, coding sequence, 3′UTR, and poly(A) tail, and these elements work together rather than independently. The strongest clinical proof comes from mRNA vaccines, especially the COVID-19 vaccines, which validated the idea that rationally optimized mRNA structure can support potent and safe protein expression in humans[83–85]. Machine learning–based and high-throughput methods have been developed to systematically design and optimize 3′UTRs[86]. Through a massively parallel reporter assay (MPRA), a large dataset of approximately 180,000 natural and synthetic 3′UTRs have been generated and quantified for their effects on mRNA half-life[86]. This dataset was then used to train predictive models linking sequence features to mRNA stability, enabling iterative design of synthetic 3′UTRs with enhanced performance[86].

These optimized 3′UTRs significantly improved mRNA stability and led to markedly increased protein production, reaching up to 30–100-fold in vivo compared to standard UTR benchmarks[86]. Altogether, this study indicates that 3′UTRs represent programmable regulatory elements that can be engineered to increase the effectiveness of mRNA-based therapeutics.

The clearest clinical proof that translation control can be engineered to improve therapy comes from the approved nucleoside-modified mRNA COVID-19 vaccines, particularly BNT162b2 and mRNA-1273. These vaccines were not simply antigen-encoding RNAs; they were structurally optimized transcripts designed to maximize protein output while limiting innate immune sensing. The core strategy included a 5′ cap, optimized 5′ and 3′ untranslated regions (UTRs), a poly(A) tail, and modified uridines to prevent activation of innate RNA sensors that otherwise induce type I interferons and suppress translation. In this framework, the UTRs regulate transcript stability and ribosome recruitment, the cap and poly(A) tail cooperate to promote mRNA circularization and translation initiation, and nucleoside modification increases translational capacity by reducing recognition by TLRs and RIG-I-like pathways. These principles were clinically validated by the success of Pfizer–BioNTech's BNT162b2 and Moderna's mRNA-1273, both of which achieved >94% efficacy in phase III trials and became approved vaccines[83,84]. An example of sequence-level translational optimization within an approved product is BNT162b2, which uses a nucleoside-modified mRNA in which uridines are replaced by N1-methylpseudouridine to enhance translation and reduce innate immune activation. In addition, its poly(A) tail incorporates a 10-base UGC linker, yielding an A30-linker-A70 configuration, which helps stabilize long poly(A) tracts during plasmid production while preserving the tail length needed for efficient translation initiation. In the same clinical lineage, mRNA-1273 also belongs to the nucleoside-modified mRNA class and was developed using the same general design logic of cap optimization, modified nucleosides, and carefully selected non-coding elements to support high antigen output in vivo[83,84]. These vaccines, therefore, represent robust examples to show that intrinsic mRNA structure can be deliberately engineered to enhance translation in a clinically approved setting.

A second clinically relevant strategy is illustrated by CureVac's CVnCoV, which took a somewhat different approach. Rather than relying on nucleoside modification, the platform used sequence engineering and codon optimization to deplete uridines and increase GC content, thereby

reducing innate sensing while improving translation. CVnCoV have entered phase III clinical trials, making it an important example of translation-oriented RNA design in the clinic even though it did not become an approved vaccine[83,84]. Its development highlights that translation can be enhanced not only by modifying the non-coding regions, but also by redesigning the coding region itself to favor translational efficiency and reduce inhibitory immune signaling. The same translational design principle became even more explicit in CV2CoV, CureVac's second-generation SARS-CoV-2 candidate. Unlike CVnCoV, CV2CoV was specifically reported to be optimized to improve translation and immunogenicity, the exact non-coding elements used: a 5′UTR from the human hydroxysteroid 17-β-dehydrogenase 4 gene and a 3′UTR from the human proteasome 20S subunit β3 gene, whereas the earlier CVnCoV construct used a 3′UTR from the human α-haemoglobin gene. In preclinical studies, this redesign increased protein expression by about 1.8-fold relative to CVnCoV and improved induction of cross-neutralizing antibodies[84]. This is one of the clearest examples in the vaccine literature showing that changing the UTRs alone can measurably improve the translational and immunological performance of an mRNA therapeutic. CV2CoV is therefore an important clinical-trial-era example of direct UTR engineering, even if the specific construct itself remained at the candidate stage rather than achieving approval.

Other examples of translation engineering in vaccine design include the Respiratory Syncytial Virus (RSV) mRNA vaccines mRNA-1777 and its improved version mRNA-1345. these RSV candidates were in clinical trials, both targeting the prefusion F protein. Importantly, mRNA-1345 was reported to be further engineered and codon-optimized to enhance translation and immunogenicity relative to mRNA-1777, and interim phase I data suggested markedly higher neutralizing antibody titres with the redesigned candidate[84]. Similarly, a tuberculosis mRNA vaccine study compared multiple 5′UTRs and found that the 5′UTRs from HBB, HSPA1A, Rabb, H4C2, and especially the adenoviral tripartite leader (TPL) sequence produced higher luciferase expression in DC2.4 dendritic cells than the 5′UTRs used in BNT162b2 and mRNA-1273. More importantly, when TPL was inserted into an mRNA vaccine encoding a multiepitope tuberculosis antigen, it improved the T-cell response in mice compared with the Moderna-derived 5′UTR backbone. This is a direct demonstration that replacing the 5′UTR can enhance translational performance and immunological output[87]. However, this work is preclinical, not clinical, and the same study also emphasizes that the effect was cell-type specific, since the same UTR advantages were not reproduced in THP1 cells. Some 3′UTR combinations such as AES-HBB and mtRNR-

HBB yielded lower luciferase output than the mRNA-1273-derived 3′UTR or combinations such as AES-AES and mtRNR-mtRNR, implying that 3′UTR choice can influence translation indirectly through effects on RNA stability and degradation[87]. These context-dependent effects are thought to be through interactions with RNA-binding proteins and microRNAs, further supporting the idea that UTRs do not act in isolation but are read differently by distinct cellular translational environments.

A minimalistic synthetic mRNAs with extremely short UTRs can remain highly functional *in vitro* and *in vivo*, with performance comparable to common augmented mRNAs containing globin UTRs or UTRs found in licensed vaccines. This suggests that translational enhancement can be achieved either by introducing favorable regulatory elements or by removing inhibitory sequence complexity. In other words, the field is not converging on one universal UTR design, but on the broader principle that non-coding elements in mRNA architecture is programmable and therapeutically tunable. mRNA vaccines use optimized RNA, but that translation control itself has become a therapeutic design principle. The clinical field has already shown that modifying the RNA molecule at the level of the 5′ cap, 5′UTR, coding sequence, 3′UTR, poly(A) tail, and nucleoside chemistry can increase protein output, improve stability, and reduce innate translational repression. Our work extends that principle into a different and far more restrictive biological setting, namely oncolytic virus-infected cells, where translation is already heavily reprogrammed by infection. In that context, viral or host-derived UTR elements are not simply optimization tools but a strategy to preserve transgene expression under conditions in which standard translation is suppressed.

5.5 Dysregulation of Translation in Diseases and Potential Application

Emerging evidence highlights translational dysregulation as a fundamental mechanism underlying multiple disease states[88]. Cancer represents one of the most extensively studied contexts in which translational control is dysregulated. Although there is substantial evidence supporting the role of translational dysregulation in cancer, it remains less well characterized than transcriptional regulation. Cancer cells rely heavily on protein output for proliferation, survival, metastasis, and resistance to therapy. Notably, translational dysregulation in cancer occurs at multiple levels, including tRNA abundance and modification, ribosome composition and biogenesis, translation initiation and elongation factors, and mRNA modifications that influence

translational efficiency. The table below summarizes selected examples of translation-associated defects across various cancer types and their functional consequences.

Cancer type	Category	Representative translation-control defect	Reported consequence	Functional role in cancer
Breast cancer	tRNA charging	Reduced leucyl-tRNA synthetase (LARS) activity and altered selective charging of tRNA-Leu(CAG)	LARS downregulation reduces tRNA-Leu(CAG) availability, leading to codon-dependent translational repression of leucine-rich tumour suppressor mRNAs[89,90].	Driver
Breast cancer	Ribosomes	Ribosomal Protein L15 (RPL15) overexpression in circulating tumour cells and metastatic cells	Selectively enhances translation of ribosomal proteins and cell-cycle regulators, increasing metastatic outgrowth[91].	Driver
Breast cancer	Translation initiation	High eIF4A dependence in advanced disease	Supports translation of ERα, cyclin D1, and CDK4; eIF4A inhibition suppresses tumour growth and can enhance endocrine therapy response[39,40].	Driver / therapeutic target
Breast cancer	mTOR-translational axis	Dysregulated 4E-BP1/S6K signaling	Associated with enhanced proliferation, invasion, and endocrine-therapy behavior, consistent with elevated cap-dependent translation[92,93].	Mixed: association + functional support
Colorectal cancer	Translation initiation	eIF3a overexpression	Drives translational upregulation of Cdc42 and ras homologue family member A (RhoA), promoting proliferation, motility, and metastasis[94,95].	Driver
Colorectal cancer	tRNA modification	Epigenetic loss of TYW2 causing wybutosine/guanosine hypomodification of tRNA	Increases ribosomal frameshifting and is linked to EMT-like features, migration, and poor outcome[96].	Driver
Colorectal cancer	mRNA modification affecting translation	Elevated m6A/YTHDF3-dependent translational control in oxaliplatin-resistant CRC	Facilitates recruitment of translational machinery to resistance-associated transcripts and promotes chemotherapy resistance[97].	Driver
Non-small cell lung cancer	Translation initiation	Overexpression/phosphorylation of eIF4E	Correlates with advanced stage and poor prognosis, supporting aberrant cap-dependent translation in NSCLC progression[98,99].	Mainly associative, with mechanistic support

Prostate cancer	Translation initiation	Dysregulated eIF4E phosphorylation and cap-dependent translation	Supports disease progression and has been implicated in resistance to hormonal therapy and chemotherapy[100,101].	Mixed: association + mechanistic support
Prostate cancer	Ribosome / ribosomal stress	Proviral Integration Site for Moloney murine leukemia virus 1 (PIM1) – MYC proto-oncogene – Ribosomal Protein S7 axis ribosomal stress axis	Promotes cell growth and tumour progression through abnormal ribosomal biogenesis/stress signaling[102,103].	Driver
Pancreatic ductal adenocarcinoma	Translation elongation	Upregulated and hypusinated eIF5A	Promotes PDAC growth, migration, invasion, and metastasis; genetic or pharmacologic inhibition suppresses these phenotypes[104,105].	Driver
Pancreatic ductal adenocarcinoma	Translation initiation downstream of KRAS	eIF4A/eIF4E-dependent translation of ADP-ribosylation factor 6 and its effector AMAP1	Enhances invasion and metastasis in KRAS-driven pancreatic cancer[106].	Driver
Pancreatic ductal adenocarcinoma	Ribosome biogenesis	High dependency on nucleolar/ribosome-biogenesis programs	Creates a therapeutic vulnerability; ribosome-biogenesis inhibition can reinforce senescence or cell death in pancreatic cancer models[107,108].	Therapeutic vulnerability; causal role still being refined
Gastric cancer	Translation initiation	EIF3B overexpression	Associated with poor prognosis and functionally promotes gastric cancer progression, including through PI3K/AKT/mTOR-linked programs[109].	Driver / prognostic marker
Gastric cancer	tRNA-derived small RNAs	Deregulated tRFs/tsRNAs	Linked to altered translational regulation and show promise as diagnostic/prognostic biomarkers; functional evidence exists but is less mature than for initiation factors[110,111].	Mostly associative, emerging functional role
Hepatocellular carcinoma	mRNA modification affecting translation	m6A-dependent translational regulation including the PDK4 axis	Promotes tumour growth by enhancing translation of metabolic and growth-related transcripts[112,113].	Driver / mechanistic support
Hepatocellular carcinoma	Ribosome / translational apparatus	Elevated translational machinery markers, including phospho-RPS6,	Associated with HCC progression and supports the concept that the translational	Mainly associative, therapeutically relevant

		and increased ribosome-biogenesis programs	apparatus itself is a biomarker and therapeutic node[114].	
Esophageal squamous cell carcinoma	tRNA modification	Upregulated METTL1/WDR4 causing increased tRNA m7G methylation	Selectively enhances translation of oncogenic programs and promotes ESCC progression; associated with poor prognosis[115].	Driver
Esophageal squamous cell carcinoma	Translation initiation	EIF3H overexpression	Promotes aggressive behavior and tumour progression, including enhanced proliferative and invasive phenotypes[116].	Driver
Esophageal squamous cell carcinoma	Translation elongation control	Elevated eEF2K/eEF2 signaling	Promotes progression and radioresistance; elongation control is a therapeutic target[117,118].	Driver / therapeutic target

Table 5. 1. Translation-associated defects across various cancer types and their functional consequences

Neurodegenerative disorders are increasingly being defined as diseases of translational control, where impaired protein synthesis leads to protein misfolding, aggregation, and eventually neuronal death. For instance, amyotrophic lateral sclerosis (ALS) is caused by mutations in RNA-binding proteins, such as TDP-43 and FUS, which accumulate in the cytoplasm, aggregate, and interfere with critical RNA processing. This leads to defects in mRNA splicing, transport and translation, resulting in proteotoxicity and motor neuron death[119,120]. Furthermore, a hexanucleotide repeat expansion in the non-coding region of the C9ORF72 (Chromosome 9 Open Reading Frame 72) gene is the most frequent genetic cause of ALS and frontotemporal dementia (FTD), with similar repeat expansions and repeat-associated non-AUG (RAN) translation observed in Huntington's disease, spinocerebellar ataxias, fragile X-associated tremor/ataxia syndrome, and myotonic dystrophy. RAN translation in C9ORF72 gives rise to dipeptide repeat (DPR) proteins[119,120]. Arginine-rich DPRs, such as poly-GR and poly-PR, disrupt protein translation by binding to translation initiation factors and ribosomes, thereby preventing proper ribosome assembly on mRNA and inhibiting translation initiation[119,120]. They also inhibit translation elongation by obstructing the ribosomal exit tunnel, resulting in ribosome stalling and global repression of protein synthesis. Additionally, mutations in ribosome quality control proteins such as NEMF and LTN1 disrupt stalled ribosome clearance and amplify the translational

dysfunction that is both a cause and a main feature in neurodegenerative diseases like ALS[121]. Disruption of the integrated stress response (ISR), with phosphorylation of eIF2α, also impairs global translation in neurodegenerative diseases such as ALS, Alzheimer's disease and Parkinson's disease[119,122]. Likewise, in leukoencephalopathy with vanishing white matter, mutations affecting eIF2B affect translation initiation by interfering with eIF2 recycling, leading to impaired protein synthesis in response to stress[119,120,123]. tRNA biology is also affected in certain neurodegenerative diseases; for instance, in Charcot–Marie–Tooth disease, mutations in aminoacyl-tRNA synthetases (e.g. GARS, glycyl-tRNA synthetase) cause defects in translation elongation through the depletion of charged tRNAs, resulting in ribosome stalling and the induction of stress pathways[124]. Add potential

Altered protein translation has also been implicated in the development of cardiovascular disease (CVD). Cardiac gene expression is highly regulated at the level of translation, affecting contractility, angiogenesis and stress responses, in addition to the more well-known regulation by transcription. Dysregulated translation can result in protein misfolding, proteostasis imbalance, and endoplasmic reticulum stress, all features of cardiac disease. Furthermore, altered activity of major signaling pathways, including PI3K/Akt/mTOR, drives changes in translational output that contribute to pathological cardiac hypertrophy. Regulation of elongation and translation factors has also been found to impact disease progression, showcasing the many levels at which translation has been implicated in CVD. These studies highlight the role of translation control in regulating cardiac function and suggest that modulating translational pathways may be a promising therapeutic approach .

5.6 Conclusion

Taken together, these studies reveal that translation is not simply a passive or secondary outcome of gene expression, but instead represents an independent and critical layer of regulation that controls protein production, cellular states and behaviors and ultimately cell fate. This is especially apparent in dynamic biological processes, such as viral infection, where transcription profiles are rapidly redefined and mRNA levels cannot be relied upon as a predictor of protein output. Rather, a targeted engagement of specific mRNAs by the translational machinery allows a nuanced response, even in the context of a global shutdown of translation.

In line with this notion, our studies of MG1-infected glioblastoma cells have shown a highly uncoupled transcriptional/translational response, with host transcripts displaying increased or sustained ribosome occupancy despite reduced transcript abundance. Likewise, our work based on HSV1 infection shows that successful protein synthesis during the infection process is not exclusively determined by the strength of transcription, but also relies on specific mRNA features that support translation in the hostile antiviral environment. These findings demonstrate that translation is a critical control point in both host antiviral responses and the functional outcome of oncolytic viruses.

Critically, my studies go beyond providing mechanistic understanding by showing that both distribution and translation are key factors in oncolytic virotherapy. As demonstrated in this thesis, enhancing viral spread through methods such as needle-free injection improves targeting of tumours, and engineering transgene expression at the level of translation allows for continued protein expression under the influence of antiviral immune responses. In addition, the discovery of a purine-rich cis-regulatory element that drives selective translation suggests that harnessing intrinsic mechanisms of translational control can be used to improve therapeutic design

Overall, this thesis offers a strategy for rationally enhancing the therapeutic potential of oncolytic virus platforms through physical delivery and molecular control of gene expression. This work provides evidence that modulating translational efficiency, rather than focusing exclusively on transcription-based approaches, is a promising and underused strategy to improve therapeutic effectiveness. More generally, this study highlights the role of translation as a dynamic and programmable component of gene regulation, with implications beyond virotherapy for other types of gene-based therapies.

Table 4. 2: List of transcriptionally upregulated genes

Tracking_ID	Gene_Short_Name	MG1/MOCK mRNA	MG1/MOCK RPF	MG1/MOCK TE
ENSG00000182393.3	IFNL1	380.2794002	N/A	N/A
ENSG00000171855.7	IFNB1	262.2825124	60.28989307	0.229866233
ENSG00000183709.8	IFNL2	94.74728647	11.30716028	0.119340202
ENSG00000138755.6	CXCL9	89.13071598	N/A	N/A
ENSG00000154646.9	TMPRSS15	68.66310653	N/A	N/A
ENSG00000135114.14	OASL	68.38435827	15.33223949	0.22420682
ENSG00000169245.6	CXCL10	60.42499505	9.704198402	0.160599076
ENSG00000242412.1	DBIL5P2	59.70180931	N/A	N/A
ENSG00000277632.2	CCL3	49.67104689	N/A	N/A
ENSG00000104689.10	TNFRSF10A	42.52520636	1.422080534	0.033440885
ENSG00000141682.12	PMAIP1	41.32015169	N/A	N/A
ENSG00000105642.16	KCNN1	36.56240102	N/A	N/A
ENSG00000248802.1	ENSG00000248802	35.9837309	N/A	N/A
ENSG00000134588.13	USP26	33.68368655	N/A	N/A
ENSG00000073756.13	PTGS2	33.52401677	5.371166752	0.160218472
ENSG00000257067.6	LINC02703	33.02480728	N/A	N/A
ENSG00000124256.15	ZBP1	32.74271927	2.773091055	0.084693364
ENSG00000115616.3	SLC9A2	31.99405458	N/A	N/A
ENSG00000226308.2	ENSG00000226308	31.90792573	N/A	N/A
ENSG00000163121.10	NEURL3	30.34030895	11.23959169	0.370450799
ENSG00000134321.13	RSAD2	30.30221953	9.958379301	0.32863531
ENSG00000169429.12	CXCL8	29.09486248	4.321048845	0.148515871
ENSG00000176058.13	TPRN	24.45864973	0.47177276	0.019288586
ENSG00000013725.14	CD6	23.84328074	0.134699308	0.005649361
ENSG00000271503.6	CCL5	23.44639549	3.352019849	0.142965252
ENSG00000113924.12	HGD	22.55170067	N/A	N/A
ENSG00000196277.17	GRM7	22.15315708	0.461024175	0.020810766
ENSG00000136826.15	KLF4	21.38236164	14.18536135	0.663414154
ENSG00000204010.3	IFIT1B	20.71403143	1.912311935	0.09231964
ENSG00000163734.4	CXCL3	20.12880242	7.854111648	0.390192694
ENSG00000137441.8	FGFBP2	20.04014742	N/A	N/A
ENSG00000133246.12	PRAM1	17.79230503	1.528308179	0.085897143
ENSG00000233930.4	KRTAP5-AS1	17.704242	N/A	N/A
ENSG00000199568.1	RNU5A-1	17.52776535	0.886600095	0.050582609
ENSG00000184254.17	ALDH1A3	17.51352582	N/A	N/A
ENSG00000200708.1	RN7SKP93	17.17715058	1.84045956	0.107145801
ENSG00000248124.11	RRN3P1	16.97299567	0.116838238	0.006883772
ENSG00000186265.10	BTLA	16.71512317	N/A	N/A
ENSG00000206863.1	RNU5A-6P	16.62448238	0.838685548	0.050448822
ENSG00000157551.19	KCNJ15	16.06462617	0.022036314	0.001371729

ENSG00000202444.1	RNU5E-6P	15.95530174	1.51414982	0.094899479
ENSG00000205445.3	KRTAP10-2	15.65725627	N/A	N/A
ENSG00000185745.10	IFIT1	15.33366318	2.880868114	0.187878661
ENSG00000162772.17	ATF3	15.28624206	1.513454057	0.099007595
ENSG00000278338.4	VWA8-AS1	15.08082123	N/A	N/A
ENSG00000149090.13	PAMR1	15.07275529	N/A	N/A
ENSG00000258602.2	LINC01629	14.99721744	N/A	N/A
ENSG00000081041.9	CXCL2	14.86523924	0.926874132	0.06235178
ENSG00000289322.2	ENSG00000289322	14.70322433	3.038715048	0.206669978
ENSG00000147432.7	CHRNB3	14.61221084	0	0
ENSG00000156966.7	B3GNT7	14.53693558	3.160065232	0.217381801
ENSG00000199677.1	Y_RNA	14.53189686	1.095511194	0.075386662
ENSG00000205702.12	CYP2D7	13.73449433	N/A	N/A
ENSG00000197816.16	CCDC180	13.45911416	0.152431347	0.011325511
ENSG00000164690.8	SHH	13.10454632	N/A	N/A
ENSG00000201643.1	SNORA14A	13.02271062	1.207610419	0.092731111
ENSG00000279220.4	CMKLR2-AS	13.01436822	N/A	N/A
ENSG00000231345.3	BEND3P1	12.7098191	0.975692986	0.076766866
ENSG00000178175.12	ZNF366	12.70768714	0.358141259	0.02818304
ENSG00000201516.1	ENSG00000201516	12.5948309	N/A	N/A
ENSG00000222644.1	RNU2-16P	12.56866775	N/A	N/A
ENSG00000239127.1	SNORD125	12.50579889	0	0
ENSG00000266014.2	ENSG00000266014	12.28211156	N/A	N/A
ENSG00000154654.15	NCAM2	11.90934153	0	0
ENSG00000290729.1	ENSG00000290729	11.78828646	1.296667549	0.109996271
ENSG00000286451.1	ENSG00000286451	11.78789781	N/A	N/A
ENSG00000175003.15	SLC22A1	11.7316249	N/A	N/A
ENSG00000252802.1	Y_RNA	11.66732214	4.364767116	0.374101877
ENSG00000174473.16	GALNTL6	11.25244663	0	0
ENSG00000254242.2	ENSG00000254242	11.24363986	N/A	N/A
ENSG00000166341.9	DCHS1	11.21420958	7.033513476	0.627196542
ENSG00000291065.1	ENSG00000291065	11.173901	N/A	N/A
ENSG00000146054.18	TRIM7	11.11902152	5.650214655	0.508157543
ENSG00000237927.1	ENSG00000237927	11.02733499	N/A	N/A
ENSG00000162738.7	VANGL2	10.84092469	1.030523089	0.095058597
ENSG00000201782.1	RN7SKP226	10.83877282	0.980783976	0.090488471
ENSG00000278239.1	ENSG00000278239	10.83632633	N/A	N/A
ENSG00000133328.4	PLAAT2	10.83371039	1.082460237	0.099915929
ENSG00000236956.2	NF1P8	10.83234696	1.091129632	0.10072883
ENSG00000197140.15	ADAM32	10.82684799	5.343789443	0.493568345
ENSG00000115850.10	LCT	10.8258934	0.530376417	0.048991469
ENSG00000164270.19	HTR4	10.78974232	N/A	N/A
ENSG00000228412.9	LNC-LBCS	10.64272451	N/A	N/A

ENSG00000201801.1	RNU5E-4P	10.60420988	1.272476155	0.119997262
ENSG00000167772.12	ANGPTL4	10.51831026	N/A	N/A
ENSG00000182782.8	HCAR2	10.45842371	3.047358565	0.291378381
ENSG00000117090.16	SLAMF1	10.37422229	N/A	N/A
ENSG00000167874.7	TMEM88	10.05954113	0	0
ENSG00000178199.14	ZC3H12D	9.87437058	N/A	N/A
ENSG00000115267.10	IFIH1	9.664460545	1.301220845	0.13463978
ENSG00000115009.13	CCL20	9.636421692	N/A	N/A
ENSG00000246223.10	LINC01550	9.632659211	N/A	N/A
ENSG00000173662.21	TAS1R1	9.623512636	N/A	N/A
ENSG00000272181.1	ENSG00000272181	9.592341258	0	0
ENSG00000271428.1	MPHOSPH6P1	9.58789459	0.156138716	0.016284985
ENSG00000200816.1	SNORA38	9.563263544	2.07717002	0.217203051
ENSG00000120738.8	EGR1	9.517738973	2.825584823	0.296875637
ENSG00000163915.7	IGF2BP2-AS1	9.343422696	N/A	N/A
ENSG00000207281.1	Y_RNA	9.224475385	3.449431246	0.373943352
ENSG00000070190.13	DAPP1	9.146736633	N/A	N/A
ENSG00000283632.4	EXOC3L2	9.10155815	N/A	N/A
ENSG00000259062.2	ACTN1-DT	9.095586563	0	0
ENSG00000240964.3	RN7SL751P	9.081513009	N/A	N/A
ENSG00000255398.3	HCAR3	9.055060954	N/A	N/A
ENSG00000252231.1	RNA5SP67	9.027842126	1.965458655	0.217710791
ENSG00000186038.9	HTR3E	8.980143095	N/A	N/A
ENSG00000200041.1	Y_RNA	8.970279776	1.198390054	0.133595616
ENSG00000201228.1	Y_RNA	8.854788093	0.784069406	0.088547506
ENSG00000104826.15	LHB	8.816917783	0	0
ENSG00000230373.9	GOLGA6L5P	8.615813015	0.88133731	0.102292994
ENSG00000163508.13	EOMES	8.600869721	1.284547983	0.149350941
ENSG00000267334.1	KIF18B-DT	8.5996073	N/A	N/A
ENSG00000230585.2	PHB1P12	8.598989481	N/A	N/A
ENSG00000200475.1	RN7SKP162	8.591459831	1.150844591	0.133952159
ENSG00000229292.2	RFPL4AL1	8.590944266	N/A	N/A
ENSG00000231449.1	ENSG00000231449	8.589897132	N/A	N/A
ENSG00000256325.1	ENSG00000256325	8.589125827	N/A	N/A
ENSG00000199787.1	SNORA80C	8.561602343	1.094290067	0.127813699
ENSG00000200336.1	RNA5SP333	8.522188693	N/A	N/A
ENSG00000171533.12	MAP6	8.510233578	N/A	N/A
ENSG00000138315.13	OIT3	8.456208562	N/A	N/A
ENSG00000140807.7	NKD1	8.431629033	N/A	N/A
ENSG00000276085.1	CCL3L1	8.38914318	N/A	N/A
ENSG00000169435.14	RASSF6	8.382162047	0	0
ENSG00000255974.8	CYP2A6	8.28256212	N/A	N/A
ENSG00000224289.1	IFIT6P	8.252163017	1.573623524	0.190692249

ENSG00000239043.1	SNORD127	8.247752705	0.747967637	0.090687447
ENSG00000105967.16	TFEC	8.238969514	N/A	N/A
ENSG00000251766.1	RNA5SP518	8.17177903	N/A	N/A
ENSG00000287750.3	LINC03026	8.167823725	N/A	N/A
ENSG00000282024.1	ENSG00000282024	8.131789545	N/A	N/A
ENSG00000279537.1	ENSG00000279537	8.10005347	N/A	N/A
ENSG00000240309.1	MTCO1P6	8.099676575	N/A	N/A
ENSG00000265145.1	SNORD53	8.091072585	1.580800838	0.195375931
ENSG00000231119.2	ENSG00000231119	8.089536473	1.030564275	0.127394725
ENSG00000200849.1	Y_RNA	8.076214723	2.992518575	0.370534796
ENSG00000154451.15	GBP5	8.037036854	0.580476692	0.072225212
ENSG00000123407.4	HOXC12	8.028621647	0.466754976	0.058136377
ENSG00000234813.1	ENSG00000234813	7.994784785	0.081964762	0.010252279
ENSG00000252207.1	RNA5SP365	7.960639583	N/A	N/A
ENSG00000218416.4	GPC1-AS1	7.943922657	0.274830531	0.034596325
ENSG00000239180.1	Y_RNA	7.910518344	0.374394387	0.047328679
ENSG00000171747.9	LGALS4	7.769543245	N/A	N/A
ENSG00000228198.3	OR2M3	7.760502504	1.082460548	0.139483306
ENSG00000265168.1	ENSG00000265168	7.716887101	N/A	N/A
ENSG00000128268.12	MGAT3	7.641929493	N/A	N/A
ENSG00000200889.1	RNU4-13P	7.570496975	0.700722675	0.092559666
ENSG00000258910.3	LINC01956	7.564770165	0.833559078	0.110189611
ENSG00000128016.7	ZFP36	7.557734593	2.777101598	0.367451591
ENSG00000228221.6	LINC00578	7.538366536	N/A	N/A
ENSG00000231057.5	NEK2-DT	7.502696955	N/A	N/A
ENSG00000229484.3	LINC02766	7.479730616	0	0
ENSG00000200534.1	SNORA33	7.476432945	1.120297675	0.149843874
ENSG00000249145.5	LINC02517	7.444214972	N/A	N/A
ENSG00000259675.4	ENSG00000259675	7.431952786	N/A	N/A
ENSG00000289725.1	ENSG00000289725	7.42083467	N/A	N/A
ENSG00000290376.1	HERC2P3	7.395987992	4.884943987	0.660485657
ENSG00000008118.10	CAMK1G	7.337709292	5.961426471	0.812436993
ENSG00000163618.18	CADPS	7.303506609	0	0
ENSG00000230006.10	ANKRD36BP2	7.250196788	0.243371145	0.033567523
ENSG00000065357.20	DGKA	7.198554757	0.748990489	0.104047342
ENSG00000204428.12	LY6G5C	7.189279967	N/A	N/A
ENSG00000234570.1	ZFRP1	7.175360627	0.337177791	0.046991058
ENSG00000276956.1	RN7SL769P	7.172429564	1.53635986	0.214203548
ENSG00000260325.2	HSPB9	7.171058533	N/A	N/A
ENSG00000291218.1	ENSG00000291218	7.165865184	0	0
ENSG00000252906.1	SCARNA3	7.044264466	0.691725765	0.098197018
ENSG00000130561.17	SAG	6.915605533	N/A	N/A
ENSG00000228697.6	ENSG00000228697	6.840815651	N/A	N/A

ENSG00000252612.1	Y_RNA	6.823684558	0.885848175	0.129819626
ENSG00000181847.12	TIGIT	6.801216352	N/A	N/A
ENSG00000250166.4	C2CD5-AS1	6.794796255	0	0
ENSG00000145087.14	STXBP5L	6.750325189	N/A	N/A
ENSG00000207154.1	RNU1-46P	6.736006829	0.709309233	0.105301145
ENSG00000281156.1	MIR3651	6.723483403	1.186290748	0.176439901
ENSG00000223573.7	TINCR	6.705229702	N/A	N/A
ENSG00000187513.9	GJA4	6.685464116	0.916420339	0.137076547
ENSG00000200738.1	RNA5SP472	6.651683533	0	0
ENSG00000068976.14	PYGM	6.619869971	4.032797392	0.609195862
ENSG00000289431.2	ENSG00000289431	6.589131049	N/A	N/A
ENSG00000201377.1	RNY4P23	6.549725194	1.475907685	0.225338872
ENSG00000196844.9	PATE2	6.541916345	N/A	N/A
ENSG00000289697.1	ENSG00000289697	6.464557926	0.213977811	0.033100146
ENSG00000130775.16	THEMIS2	6.431055315	N/A	N/A
ENSG00000287620.1	ENSG00000287620	6.426468963	1.836133013	0.285714134
ENSG00000227613.1	QRSL1P2	6.426084184	0	0
ENSG00000234143.1	UGT1A13P	6.425143071	0.959763227	0.149376164
ENSG00000261334.1	ENSG00000261334	6.424567362	1.951850457	0.303810412
ENSG00000234695.1	TFPI2-DT	6.424225456	N/A	N/A
ENSG00000115263.15	GCG	6.422971213	0	0
ENSG00000165841.11	CYP2C19	6.40151919	N/A	N/A
ENSG00000105697.9	HAMP	6.401373595	N/A	N/A
ENSG00000254376.2	SOX5P1	6.400358298	0.357656928	0.055880767
ENSG00000232926.1	ENSG00000232926	6.398811276	N/A	N/A
ENSG00000248729.1	MTCO1P30	6.397965802	N/A	N/A
ENSG00000279687.1	ENSG00000279687	6.396462154	N/A	N/A
ENSG00000213060.4	ENSG00000213060	6.395058197	N/A	N/A
ENSG00000280916.4	FOXCUT	6.394898077	N/A	N/A
ENSG00000214211.2	CTAGE14P	6.39422083	0.509237324	0.079640247
ENSG00000245928.2	SDAD1-AS1	6.394063394	N/A	N/A
ENSG00000145945.7	FAM50B	6.394040166	N/A	N/A
ENSG00000290609.1	ENSG00000290609	6.39402216	0	0
ENSG00000262503.1	ENSG00000262503	6.393110738	N/A	N/A
ENSG00000244125.1	ENSG00000244125	6.391017904	N/A	N/A
ENSG00000171772.17	SYCE1	6.380796173	1.038536146	0.162759649
ENSG00000232884.11	ENSG00000232884	6.327658234	N/A	N/A
ENSG00000118503.17	TNFAIP3	6.252948449	3.166742659	0.506439912
ENSG00000146005.4	PSD2	6.233118954	2.269599562	0.364119405
ENSG00000201253.1	RNU4-10P	6.204450092	0.297365123	0.047927716
ENSG00000265222.1	ENSG00000265222	6.200894782	N/A	N/A
ENSG00000291108.1	SEPTIN7P11	6.197508844	N/A	N/A
ENSG00000159625.15	DRC7	6.18597835	N/A	N/A

ENSG00000265706.1	SNORD53B	6.149485649	0.663217575	0.107849276
ENSG00000138646.9	HERC5	6.146773294	1.004222345	0.163373903
ENSG00000261043.5	ENSG00000261043	6.142192283	N/A	N/A
ENSG00000170345.10	FOS	6.081836119	5.472000189	0.899728319
ENSG00000202430.1	RNA5SP88	6.057092988	N/A	N/A
ENSG00000273972.1	ENSG00000273972	6.051092672	N/A	N/A
ENSG00000150656.15	CNDP1	6.028913218	N/A	N/A
ENSG00000236384.7	LINC00479	6.016243322	N/A	N/A

Table 4. 3: List of translationally upregulated genes

Tracking_ID	Gene_Short_Name	MG1/MOCK mRNA	MG1/MOCK RPF	MG1/MOCK TE
ENSG00000185974.7	GRK1	0.063339372	8.135588229	128.4444093
ENSG00000007350.17	TKTL1	0.056707626	6.651108453	117.287726
ENSG00000249550.8	LINC01234	0.106048934	12.08560324	113.9625152
ENSG00000269696.3	ZNF470-DT	0.040283919	4.435762351	110.1124821
ENSG00000170074.20	FAM153A	0.037975297	3.026405138	79.69404811
ENSG00000081189.17	MEF2C	0.568402769	42.3387877	74.48730026
ENSG00000156711.17	MAPK13	0.148649255	10.83664509	72.90076946
ENSG00000205592.16	MUC19	0.040688093	2.05298817	50.4567308
ENSG00000196668.4	LINC00173	0.02595739	1.297468268	49.98454174
ENSG00000240790.3	SND1-DT	0.194703042	9.250490607	47.51076565
ENSG00000198838.14	RYR3	0.678197273	31.9087859	47.04941644
ENSG00000278932.6	ENSG00000278932	0.027562156	1.19202257	43.24852362
ENSG00000136378.15	ADAMTS7	0.290155581	12.53942756	43.2162205
ENSG00000282458.1	WASH5P	0.050763538	2.152989413	42.41212269
ENSG00000261371.6	PECAM1	1.146316899	47.57300544	41.50074511
ENSG00000120049.20	KCNIP2	0.093286241	3.684961706	39.50166352
ENSG00000123095.6	BHLHE41	0.176209551	6.476263816	36.75319404
ENSG00000147437.10	GNRH1	0.443641335	16.1619089	36.43012416
ENSG00000137726.17	FXYD6	0.166178801	5.78539823	34.81429759
ENSG00000106341.11	PPP1R17	0.281961351	9.41836847	33.4030477
ENSG00000213463.5	SYNJ2BP	0.468039716	14.84276874	31.71262656
ENSG00000225898.1	ENSG00000225898	0.168090428	5.217592727	31.04039164
ENSG00000235263.1	ENSG00000235263	0.13910426	4.217613216	30.31979911
ENSG00000145794.17	MEGF10	0.734211565	21.29312986	29.0013545
ENSG00000279520.1	ENSG00000279520	0.134661926	3.891374256	28.89736074
ENSG00000000971.17	CFH	0.046907761	1.353988268	28.86490945
ENSG00000269235.4	ZNF350-AS1	0.166645725	4.442733101	26.65974842
ENSG00000102452.18	NALCN	0.293076624	7.735664906	26.3946841
ENSG00000159217.10	IGF2BP1	0.138896753	3.601631293	25.93027711
ENSG00000100385.15	IL2RB	0.681369277	17.51664551	25.70800606

ENSG00000277511.2	ENSG00000277511	0.077252362	1.957261565	25.33594454
ENSG00000071073.13	MGAT4A	0.276294382	6.808976977	24.64392117
ENSG00000174951.12	FUT1	0.364043221	8.949169594	24.58271184
ENSG00000228484.3	ENSG00000228484	0.085043864	2.06077972	24.23196247
ENSG00000106809.11	OGN	0.452856089	10.80700467	23.86410369
ENSG00000254413.8	CHKB-CPT1B	0.670154117	15.40241144	22.98338703
ENSG00000237877.8	LINC01473	0.485362542	10.96742441	22.59635521
ENSG00000239945.1	ENSG00000239945	0.046219396	1.038584286	22.47074559
ENSG00000178445.10	GLDC	0.155018572	3.41578741	22.03469797
ENSG00000287262.1	ENSG00000287262	0.0950888	2.061038202	21.67487878
ENSG00000265702.2	ENSG00000265702	0.705383103	14.93631094	21.17475012
ENSG00000188611.17	ASAH2	0.739109807	15.51955863	20.99763591
ENSG00000085563.15	ABCB1	0.701341377	14.15264299	20.17939259
ENSG00000149243.17	KLHL35	0.547103044	10.98128665	20.07169725
ENSG00000005844.19	ITGAL	1.14339078	22.63718612	19.79829338
ENSG00000163072.16	NOSTRIN	0.140671395	2.768651911	19.68169805
ENSG00000259349.4	APPBP2-DT	0.106274132	2.073409287	19.51000908
ENSG00000028137.19	TNFRSF1B	0.477495212	9.28978273	19.45523744
ENSG00000225706.3	PTPRD-AS1	0.111109775	2.10031566	18.9030683
ENSG00000008710.20	PKD1	0.088832764	1.678488925	18.89493081
ENSG00000278879.1	ENSG00000278879	0.493354291	9.233999219	18.71677086
ENSG00000261613.2	ENSG00000261613	0.442111347	8.03792215	18.18076419
ENSG00000059145.19	UNKL	0.311993314	5.648779677	18.10545107
ENSG00000162572.21	SCNN1D	0.48331456	8.7434888	18.09067948
ENSG00000271851.1	ENSG00000271851	0.277890725	4.966194898	17.87103508
ENSG00000275437.1	ENSG00000275437	0.328483905	5.721981325	17.41936589
ENSG00000077616.11	NAALAD2	0.419752355	7.296407662	17.38264854
ENSG00000231389.8	HLA-DPA1	0.12665542	2.182138408	17.22893819
ENSG00000170190.16	SLC16A5	0.177685989	2.936249767	16.52493695
ENSG00000182511.12	FES	0.167776257	2.666818442	15.8950884
ENSG00000203926.5	SPANXA2	0.207332292	3.277891167	15.80984387
ENSG00000263786.1	ENSG00000263786	0.126016161	1.953942819	15.50549395
ENSG00000127241.18	MASP1	0.568368525	8.74393766	15.38427496
ENSG00000267106.9	ZNF561-AS1	0.601676777	9.170151959	15.24099368
ENSG00000246922.10	UBAP1L	0.549012588	8.309920197	15.1361196
ENSG00000287574.1	ENSG00000287574	0.097775207	1.478832613	15.12482209
ENSG00000227373.6	RABGAP1L-DT	0.1133091	1.694296207	14.95286975
ENSG00000147408.16	CSGALNACT1	0.32793097	4.89697713	14.93295109
ENSG00000198885.10	ITPRIPL1	0.616420726	8.907967723	14.45111649
ENSG00000250575.1	ENSG00000250575	0.43073767	6.182260457	14.35272763
ENSG00000167100.15	SAMD14	0.453909041	6.447242468	14.20382034
ENSG00000153253.20	SCN3A	1.148324323	16.27998202	14.1771638
ENSG00000184163.3	C1QTNF12	0.228335555	3.230881731	14.1497093

ENSG00000283674.3	ENSG00000283674	0.082682659	1.121205319	13.56034419
ENSG00000283674.3	ENSG00000283674	0.082682659	1.121205319	13.56034419
ENSG00000271427.1	ENSG00000271427	0.229390601	3.107563904	13.54704113
ENSG00000261526.3	ENSG00000261526	0.080912288	1.084577209	13.40435713
ENSG00000118420.17	UBE3D	0.720252826	9.644536398	13.39048741
ENSG00000280254.1	ENSG00000280254	0.272424347	3.64713846	13.38771111
ENSG00000108830.10	RND2	0.096358411	1.2875841	13.36244644
ENSG00000240137.8	ERICH6-AS1	0.194321404	2.584338369	13.29929858
ENSG00000265916.1	ENSG00000265916	0.248496166	3.269245219	13.15611934
ENSG00000182621.18	PLCB1	0.828330735	10.88440173	13.14016402
ENSG00000279413.1	ENSG00000279413	0.114541304	1.491078826	13.01782648
ENSG00000235742.1	ENSG00000235742	0.242655076	3.107556857	12.80647784
ENSG00000276791.1	ENSG00000276791	0.319952795	4.09678024	12.80432709
ENSG00000008323.16	PLEKHG6	1.57104485	20.09541795	12.79111666
ENSG00000177234.7	LINC01561	0.145698336	1.86275561	12.78501632
ENSG00000257027.1	ENSG00000257027	0.222332332	2.755840538	12.39514068
ENSG00000197978.10	GOLGA6L9	1.426317638	17.48493601	12.25879534
ENSG00000253394.7	LINC00534	0.173406881	2.097983098	12.09861506
ENSG00000131969.15	ABHD12B	1.079438553	13.03337175	12.07421369
ENSG00000149256.16	TENM4	0.681008756	8.171044659	11.99844288
ENSG00000149256.16	TENM4	0.681008756	8.171044659	11.99844288
ENSG00000285367.3	ENSG00000285367	0.156400932	1.852762501	11.846237
ENSG00000085831.16	TTC39A	0.065639171	0.773043112	11.77716143
ENSG00000198691.14	ABCA4	0.083034198	0.975623068	11.7496537
ENSG00000266921.2	ZNF230-DT	0.266034116	3.11137774	11.69540878
ENSG00000113520.11	IL4	0.346825879	4.016187834	11.57983897
ENSG00000268087.1	ENSG00000268087	0.175659888	2.03296533	11.57330424
ENSG00000269929.5	MIRLET7A1HG	0.076175316	0.879318186	11.54334803
ENSG00000288823.1	ENSG00000288823	0.094925347	1.095513998	11.54079527
ENSG00000200693.2	U3	0.244752513	2.810527799	11.48314175
ENSG00000090006.18	LTBP4	0.265051392	3.038017808	11.4619953
ENSG00000178662.16	CSRNP3	0.239290614	2.70511948	11.30474546
ENSG00000226471.7	ENSG00000226471	0.04610704	0.516784636	11.20836723
ENSG00000289004.2	ENSG00000289004	0.174894146	1.952107923	11.16165385
ENSG00000233818.1	CLDN14-AS1	0.200099965	2.213468462	11.06181336
ENSG00000188152.13	NUTM2G	0.233275856	2.566500821	11.00199938
ENSG00000172382.10	PRSS27	1.172553903	12.80124207	10.91740178
ENSG00000233626.2	ENSG00000233626	0.195336736	2.123459468	10.87076352
ENSG00000229267.3	SNHG31	0.964014553	10.47352268	10.86448608
ENSG00000221923.9	ZNF880	0.484789329	5.249537688	10.82849265
ENSG00000188981.11	MSANTD1	0.383619711	4.150206728	10.81854401
ENSG00000162552.15	WNT4	0.1733685	1.831172246	10.56231232
ENSG00000260540.2	ABHD17AP8	0.092988446	0.977680222	10.51399678

ENSG00000259345.7	ENSG00000259345	0.112942713	1.186685	10.50696381
ENSG00000205853.12	RFPL3S	0.226539114	2.372689548	10.47364188
ENSG00000261098.1	ENSG00000261098	0.60859855	6.291013336	10.33688519
ENSG00000182749.6	PAQR7	0.216004943	2.18214715	10.10230191
ENSG00000066405.13	CLDN18	0.097050299	0.978917828	10.08670598
ENSG00000289480.1	ENSG00000289480	1.060694698	10.55137072	9.947603902
ENSG00000273311.1	DGCR11	0.325089207	3.232152604	9.942355937
ENSG00000177301.16	KCNA2	0.345160755	3.412936681	9.887962727
ENSG00000177301.16	KCNA2	0.345160755	3.412936681	9.887962727
ENSG00000196358.12	NTNG2	0.18520012	1.831013336	9.886674674
ENSG00000111252.11	SH2B3	0.451160862	4.435557837	9.831433122
ENSG00000254718.6	ENSG00000254718	0.73727019	7.214376625	9.785254745
ENSG00000128594.8	LRRC4	0.565519649	5.514987881	9.752071193
ENSG00000279631.1	ENSG00000279631	0.310781879	3.022917699	9.726814533
ENSG00000063015.21	SEZ6	0.07404996	0.720139884	9.725054332
ENSG00000105717.14	PBX4	0.276266594	2.684913845	9.718561357
ENSG00000260196.1	ENSG00000260196	0.513292109	4.978966999	9.700065354
ENSG00000251615.3	ENSG00000251615	0.613957749	5.839415363	9.511102963
ENSG00000204929.13	LINC02934	0.592732216	5.621099026	9.483370189
ENSG00000276592.1	PHB1P6	0.503627063	4.73612336	9.404028705
ENSG00000279799.1	ENSG00000279799	0.10759597	0.988800602	9.189940849
ENSG00000269729.1	ENSG00000269729	0.07725705	0.70674928	9.148023148
ENSG00000274677.1	ENSG00000274677	0.230846669	2.064548605	8.943376182
ENSG00000259959.1	ENSG00000259959	0.554286808	4.946456233	8.924001365
ENSG00000287089.1	ENSG00000287089	0.905047384	8.073736697	8.920788943
ENSG00000250742.6	LINC02381	0.464740817	4.138056717	8.904009655
ENSG00000235244.6	DANT2	0.277288656	2.461303853	8.87632363
ENSG00000196756.15	SNHG17	0.198459524	1.751525638	8.82560636
ENSG00000273796.2	ENSG00000273796	0.289955313	2.539548187	8.758412326
ENSG00000258599.2	ENSG00000258599	0.081153821	0.710628392	8.756561106
ENSG00000042317.17	SPATA7	0.27085464	2.365622436	8.73391881
ENSG00000215417.13	MIR17HG	0.055438689	0.484186864	8.733735876
ENSG00000182575.8	NXPH3	0.467097466	4.072622713	8.718999801
ENSG00000251661.3	ENSG00000251661	0.603382445	5.214605663	8.642289322
ENSG00000286416.1	ENSG00000286416	0.331792722	2.861849605	8.625414045
ENSG00000169327.5	OR5AU1	0.958208738	8.253675227	8.613650555
ENSG00000189367.15	KIAA0408	0.764325236	6.57908408	8.607702289
ENSG00000198835.4	GJC2	0.284630081	2.442756263	8.582214003
ENSG00000232735.2	ATG4AP1	0.239278899	2.044869266	8.545965694
ENSG00000272468.1	ENSG00000272468	0.348836497	2.972690721	8.521730804
ENSG00000140986.8	RPL3L	0.597925694	5.092312356	8.516630756
ENSG00000290888.1	ENSG00000290888	0.128695139	1.068706754	8.304173446
ENSG00000260675.1	TCERG1P2	0.111356402	0.92355672	8.293701183

ENSG00000272219.1	ENSG00000272219	0.367405291	3.035222571	8.261238049
ENSG00000228857.3	ACTR3-AS1	0.504622322	4.148742068	8.221479491
ENSG00000248323.8	LUCAT1	0.324157249	2.645051219	8.15977809
ENSG00000229152.2	ANKRD10-IT1	0.591976474	4.812131439	8.128923441
ENSG00000218187.2	ENSG00000218187	0.375022122	3.043871452	8.116511725
ENSG00000197213.11	ZSCAN5B	0.398451836	3.219674471	8.080460866
ENSG00000197191.7	CYSRT1	0.620183258	4.999232401	8.06089545
ENSG00000128346.11	C22orf23	0.301680243	2.426953425	8.04478743
ENSG00000262228.3	ENSG00000262228	0.26955948	2.16492305	8.031337101
ENSG00000279443.1	ENSG00000279443	0.61279714	4.921337458	8.030940648
ENSG00000289268.1	ENSG00000289268	0.479332062	3.83232389	7.995133623
ENSG00000172243.18	CLEC7A	0.476534856	3.804624676	7.983937861
ENSG00000289827.1	ENSG00000289827	0.128245136	1.022428897	7.972457501
ENSG00000226220.1	CICP22	0.477501164	3.804370011	7.967247617
ENSG00000028277.22	POU2F2	0.230717307	1.830748883	7.935030573
ENSG00000279103.1	ENSG00000279103	0.138834474	1.091073541	7.858808451
ENSG00000226554.1	MTCL1P1	0.218696182	1.716659206	7.84951613
ENSG00000261799.1	ENSG00000261799	0.625885501	4.905558339	7.837788747
ENSG00000132874.15	SLC14A2	0.236519447	1.850431828	7.823592735
ENSG00000254187.1	ENSG00000254187	0.080767881	0.631646803	7.820519704
ENSG00000275329.1	ENSG00000275329	0.139330767	1.086866203	7.800618832
ENSG00000215168.2	ATXN7L3P1	0.276372085	2.143091978	7.754372086
ENSG00000249908.2	BRD9P2	0.148013151	1.146903378	7.748658611
ENSG00000227573.2	ENSG00000227573	0.069072161	0.533564082	7.724734198
ENSG00000254847.1	ENSG00000254847	0.424915047	3.26922549	7.693833193
ENSG00000229808.1	ENSG00000229808	0.255882624	1.96274497	7.670489462
ENSG00000226338.1	ENSG00000226338	0.478467801	3.668981165	7.668188241
ENSG00000071655.18	MBD3	0.400484974	3.057697978	7.634988016
ENSG00000289911.1	ENSG00000289911	0.309615361	2.360964372	7.625475567
ENSG00000074181.9	NOTCH3	0.329292426	2.506034816	7.610362749
ENSG00000169282.18	KCNAB1	0.383344953	2.907692918	7.585055959
ENSG00000272572.1	ENSG00000272572	0.258791645	1.962142005	7.581937206
ENSG00000073803.14	MAP3K13	0.406937785	3.071322646	7.547400997
ENSG00000240487.1	ATOSBP1	0.288628042	2.173630325	7.530904854
ENSG00000163141.20	BNIPL	1.046155173	7.863645176	7.516710119
ENSG00000149488.14	TMC2	0.434968465	3.269245028	7.516050682
ENSG00000215481.9	BCRP3	0.821724172	6.151933417	7.486616104
ENSG00000103154.10	NECAB2	0.140281771	1.049815783	7.483622263
ENSG00000236536.2	ENSG00000236536	0.225827413	1.688145528	7.475379108
ENSG00000289519.1	ENSG00000289519	0.438782639	3.264608215	7.440149007
ENSG00000104894.12	CD37	0.36908723	2.735387698	7.411222803
ENSG00000265018.7	AGAP12P	0.800729384	5.928803143	7.404253254
ENSG00000272501.1	ENSG00000272501	0.279427727	2.064544192	7.388472917

ENSG00000267649.1	ENSG00000267649	0.238840149	1.763584321	7.383952512
ENSG00000244264.3	RN7SL597P	0.681142952	4.994080864	7.331913001
ENSG00000280294.1	ENSG00000280294	0.409499737	2.987660264	7.295878345
ENSG00000280106.1	ENSG00000280106	0.410820363	2.995842927	7.292342833
ENSG00000189145.7	RPL32P36	0.126150766	0.918302002	7.279400899
ENSG00000279821.1	ENSG00000279821	0.292971659	2.119150194	7.233294173
ENSG00000261485.1	PAN3-AS1	0.269520767	1.947429852	7.225528003
ENSG00000289523.1	ENSG00000289523	0.258329898	1.850435961	7.163073183
ENSG00000260942.1	CAPN10-DT	0.293383581	2.091712667	7.129617345
ENSG00000168792.5	ABHD15	0.356698455	2.539778997	7.120241087
ENSG00000169598.17	DFFB	0.556273775	3.955425372	7.11057315
ENSG00000129295.10	DNAAF11	0.302191733	2.141766263	7.087441615
ENSG00000280128.1	ENSG00000280128	0.4448737	3.152379677	7.086010426
ENSG00000271780.2	ENSG00000271780	0.843232605	5.964750264	7.073671282
ENSG00000066056.14	TIE1	0.066068234	0.467235512	7.072014496
ENSG00000261512.2	ENSG00000261512	0.331823668	2.341949504	7.057813322
ENSG00000289207.1	ENSG00000289207	0.149645294	1.05577271	7.055168119
ENSG00000107611.16	CUBN	0.311657262	2.196121202	7.046590825
ENSG00000205085.13	GARIN1A	1.889328067	13.29839177	7.038688516
ENSG00000185864.18	NPIPB4	0.659356658	4.628324022	7.019454447
ENSG00000234807.8	LINC01135	0.266323717	1.858168647	6.977105421
ENSG00000271408.1	NAPGP1	0.608591092	4.234832518	6.958420149
ENSG00000287562.1	ENSG00000287562	0.455103013	3.160054348	6.943602343
ENSG00000226180.3	ENSG00000226180	0.571432397	3.96489839	6.938525728
ENSG00000159958.7	TNFRSF13C	0.623848804	4.295978002	6.886248681
ENSG00000288610.1	ENSG00000288610	0.215524156	1.477137178	6.853696622
ENSG00000247556.7	OIP5-AS1	0.363431144	2.48594624	6.840212452
ENSG00000108813.12	DLX4	0.321193844	2.179383441	6.785259059
ENSG00000259291.2	ZNF710-AS1	0.421411682	2.850880381	6.765072027
ENSG00000148655.15	LRMDA	0.608363894	4.105271369	6.748052295
ENSG00000120215.10	MLANA	0.152864019	1.030385046	6.740533521
ENSG00000033050.9	ABCF2	0.534114936	3.599737109	6.739630122
ENSG00000130283.9	GDF1	0.348876266	2.345302792	6.722448677
ENSG00000226209.1	RBISP1	0.08083944	0.543433471	6.72238046
ENSG00000177238.14	TRIM72	0.444711587	2.977542841	6.695446954
ENSG00000289600.1	ENSG00000289600	0.162428289	1.086765193	6.690738407
ENSG00000279773.1	ENSG00000279773	0.249983823	1.661898738	6.648025137
ENSG00000196924.19	FLNA	0.153604904	1.021069493	6.647375626
ENSG00000227775.3	ENSG00000227775	0.445035631	2.948943234	6.626308169
ENSG00000139714.12	MORN3	0.211719711	1.401953156	6.621741297
ENSG00000291299.2	ENSG00000291299	0.104931636	0.694690841	6.62041372
ENSG00000162006.9	MSLNL	0.446471457	2.955673633	6.620072996
ENSG00000213940.4	ENSG00000213940	0.399124795	2.63834569	6.610327712

ENSG00000231010.1	ENSG00000231010	0.598649233	3.953317454	6.603729254
ENSG00000123977.10	DAW1	0.408356276	2.695605218	6.601111276
ENSG00000141854.10	MISP3	0.040525748	0.267093067	6.59070053
ENSG00000161328.11	LRRC56	0.11551969	0.760673943	6.584799029
ENSG00000289412.2	ENSG00000289412	0.144286786	0.949894424	6.5833778
ENSG00000263412.3	NFE2L1-DT	0.199599566	1.311654977	6.571432012
ENSG00000248367.2	ENSG00000248367	0.082119452	0.537116044	6.540667691
ENSG00000289754.1	ENSG00000289754	0.347021568	2.263056792	6.521372165
ENSG00000164398.15	ACSL6	0.277390398	1.808601292	6.520057318
ENSG00000277144.1	ENSG00000277144	0.804883183	5.212048318	6.475533872
ENSG00000188013.6	MEIS3P2	0.229702187	1.480641107	6.445916464
ENSG00000272690.6	LINC02018	0.114919315	0.738061429	6.422431501
ENSG00000290048.1	ENSG00000290048	0.490378648	3.138644088	6.400450139
ENSG00000284419.1	MIR663A	0.208097957	1.329297006	6.387842668
ENSG00000233429.9	HOTAIRM1	0.395571064	2.525817707	6.385243858
ENSG00000119681.12	LTBP2	0.362927326	2.309198487	6.362702176
ENSG00000271387.1	C1orf21-DT	0.306908191	1.949633727	6.352498196
ENSG00000225950.9	NTF4	0.315384122	1.994606818	6.324372973
ENSG00000267731.1	ENSG00000267731	0.634504427	4.00174456	6.30688202
ENSG00000287091.1	ENSG00000287091	0.133938348	0.84120556	6.280543053
ENSG00000266371.1	ENSG00000266371	0.326932327	2.052990117	6.279556803
ENSG00000287021.1	ENSG00000287021	0.155654338	0.973717641	6.255640902
ENSG00000086730.17	LAT2	0.725059639	4.521192508	6.235614653
ENSG00000142623.11	PADI1	0.299581582	1.867978012	6.235289892
ENSG00000288557.1	ENSG00000288557	0.531501901	3.291456567	6.192746551
ENSG00000269911.1	FAM226B	0.076728065	0.474095062	6.178900292
ENSG00000197779.15	ZNF81	0.295405801	1.814170855	6.141283784
ENSG00000162599.18	NFIA	0.375882743	2.303243853	6.127559443
ENSG00000233297.4	RASA4DP	0.396084835	2.424792795	6.121902641
ENSG00000218226.1	TATDN2P2	0.749085554	4.579730842	6.113762065
ENSG00000184368.16	MAP7D2	0.194759066	1.190581622	6.113099883
ENSG00000156381.9	ANKRD9	0.346868372	2.117556671	6.104784521
ENSG00000288075.1	ENSG00000288075	0.397735519	2.424833756	6.096598465
ENSG00000197852.12	INKA2	0.251905422	1.535550305	6.095741391
ENSG00000277715.1	ENSG00000277715	0.330125774	2.003966125	6.07031102
ENSG00000240859.3	LINC03014	0.053228451	0.320770416	6.026296283
ENSG00000252690.3	ENSG00000252690	0.262892465	1.583663876	6.023998744
ENSG00000183570.17	PCBP3	0.090043801	0.541228993	6.010730177
ENSG00000229291.1	LINC02768	0.953098629	5.728556283	6.010454858
ENSG00000204172.12	AGAP9	0.847764902	5.094938469	6.009848319
ENSG00000168878.19	SFTPB	0.199394912	1.198199436	6.009177579

5.7 References

1. Jin, K.-T. *et al.* Oncolytic Virotherapy in Solid Tumors: The Challenges and Achievements. *Cancers* **13**, 588 (2021).
2. Vähä-Koskela, M. & Hinkkanen, A. Tumor Restrictions to Oncolytic Virus. *Biomedicines* **2**, 163–194 (2014).
3. Zheng, M., Huang, J., Tong, A. & Yang, H. Oncolytic Viruses for Cancer Therapy: Barriers and Recent Advances. *Mol. Ther. Oncolytics* **15**, 234–247 (2019).
4. Russell, S. J., Peng, K.-W. & Bell, J. C. Oncolytic virotherapy. *Nat. Biotechnol.* **30**, 658–670 (2012).
5. Li, L., Liu, S., Han, D., Tang, B. & Ma, J. Delivery and Biosafety of Oncolytic Virotherapy. *Front. Oncol.* **10**, 475 (2020).
6. Zhu, J., Ma, J., Huang, M., Deng, H. & Shi, G. Emerging delivery strategy for oncolytic virotherapy. *Mol. Ther. Oncol.* **32**, 200809 (2024).
7. Cao, Y., Dong, X. & Chen, X. Polymer-Modified Liposomes for Drug Delivery: From Fundamentals to Applications. *Pharmaceutics* **14**, 778 (2022).
8. Yu, C. & Walter, M. *Needleless Injectors for the Administration of Vaccines: A Review of Clinical Effectiveness*. (Canadian Agency for Drugs and Technologies in Health, Ottawa (ON), 2020).
9. Diamond, M. S. & Farzan, M. The broad-spectrum antiviral functions of IFIT and IFITM proteins. *Nat. Rev. Immunol.* **13**, 46–57 (2013).
10. Stern-Ginossar, N., Thompson, S. R., Mathews, M. B. & Mohr, I. Translational Control in Virus-Infected Cells. *Cold Spring Harb. Perspect. Biol.* **11**, a033001 (2019).

11. Walsh, D., Mathews, M. B. & Mohr, I. Tinkering with Translation: Protein Synthesis in Virus-Infected Cells. *Cold Spring Harb. Perspect. Biol.* **5**, a012351 (2013).

12. Kumar, P. *et al.* Inhibition of translation by IFIT family members is determined by their ability to interact selectively with the 5′-terminal regions of cap0-, cap1- and 5′ppp-mRNAs. *Nucleic Acids Res.* **42**, 3228–3245 (2014).

13. Liu, Y. *et al.* The role of host eIF2α in viral infection. *Virol. J.* **17**, 112 (2020).

14. Erickson, A. K. & Gale, M. Regulation of interferon production and innate antiviral immunity through translational control of IRF-7. *Cell Res.* **18**, 433–435 (2008).

15. Colina, R. *et al.* Translational control of the innate immune response through IRF-7. *Nature* **452**, 323–328 (2008).

16. Kroczynska, B., Mehrotra, S., Arslan, A. D., Kaur, S. & Platanias, L. C. Regulation of Interferon-Dependent mRNA Translation of Target Genes. *J. Interferon Cytokine Res.* **34**, 289–296 (2014).

17. McFadden, M. J. *et al.* Post-transcriptional regulation of antiviral gene expression by N6-methyladenosine. *Cell Rep.* **34**, 108798 (2021).

18. Hsu, J. C.-C. *et al.* Viperin triggers ribosome collision-dependent translation inhibition to restrict viral replication. *Mol. Cell* **82**, 1631-1642.e6 (2022).

19. Hoang, H.-D. *et al.* Induction of an Alternative mRNA 5' Leader Enhances Translation of the Ciliopathy Gene Inpp5e and Resistance to Oncolytic Virus Infection. *Cell Rep.* **29**, 4010-4023.e5 (2019).

20. Alexander, M. R. *et al.* Ribosome-Profiling Reveals Restricted Post Transcriptional Expression of Antiviral Cytokines and Transcription Factors during SARS-CoV-2 Infection. *Int. J. Mol. Sci.* **22**, 3392 (2021).

21. Lee, M. S., Kim, B., Oh, G. T. & Kim, Y.-J. OASL1 inhibits translation of the type I interferon-regulating transcription factor IRF7. *Nat. Immunol.* **14**, 346–355 (2013).

22. Mears, H. V. & Sweeney, T. R. Mouse Ifit1b is a cap1-RNA–binding protein that inhibits mouse coronavirus translation and is regulated by complexing with Ifit1c. *J. Biol. Chem.* **295**, 17781–17801 (2020).

23. Durfee, L. A., Lyon, N., Seo, K. & Huibregtse, J. M. The ISG15 Conjugation System Broadly Targets Newly Synthesized Proteins: Implications for the Antiviral Function of ISG15. *Mol. Cell* **38**, 722–732 (2010).

24. Dolicka, D., Sobolewski, C., Correia de Sousa, M., Gjorgjieva, M. & Foti, M. mRNA Post-Transcriptional Regulation by AU-Rich Element-Binding Proteins in Liver Inflammation and Cancer. *Int. J. Mol. Sci.* **21**, 6648 (2020).

25. Dixon, D. A. Dysregulated post-transcriptional control of COX-2 gene expression in cancer. *Curr. Pharm. Des.* **10**, 635–646 (2004).

26. Brooks, S. A. & Blackshear, P. J. Tristetraprolin (TTP): Interactions with mRNA and proteins, and current thoughts on mechanisms of action. *Biochim. Biophys. Acta* **1829**, 666–679 (2013).

27. Mazumder, B., Li, X. & Barik, S. Translation Control: A Multifaceted Regulator of Inflammatory Response. *J. Immunol. Baltim. Md 1950* **184**, 3311–3319 (2010).

28. Ma, S., Qin, Y. & Ren, W. Insulin-like growth factor 2 mRNA-binding protein 1 (IGF2BP1) in hematological diseases. *Mol. Med.* **30**, 165 (2024).

29. Leclair, N. K. *et al.* The RNA-binding protein IGF2BP1 regulates stability of mRNA transcribed from FOXM1 target genes in hypermitotic meningiomas. *Acta Neuropathol. (Berl.)* **148**, 28 (2024).

30. Xi, Y. & Wang, Y. IGF2BP1, a New Target to Overcome Drug Resistance in Melanoma? *Front. Pharmacol.* **13**, 947363 (2022).

31. Zhou, J. *et al.* Identification and characterization of GLDC as host susceptibility gene to severe influenza. *EMBO Mol. Med.* **11**, e9528 (2019).

32. Pelosi, E., Castelli, G. & Testa, U. CD123 a Therapeutic Target for Acute Myeloid Leukemia and Blastic Plasmocytoid Dendritic Neoplasm. *Int. J. Mol. Sci.* **24**, 2718 (2023).

33. Wang, J. *et al.* CLEC7A regulates M2 macrophages to suppress the immune microenvironment and implies poorer prognosis of glioma. *Front. Immunol.* **15**, 1361351 (2024).

34. Cruz-Tapias, P., Castiblanco, J. & Anaya, J.-M. Major histocompatibility complex: Antigen processing and presentation. in *Autoimmunity: From Bench to Bedside [Internet]* (El Rosario University Press, 2013).

35. Halliday, M. *et al.* Partial restoration of protein synthesis rates by the small molecule ISRIB prevents neurodegeneration without pancreatic toxicity. *Cell Death Dis.* **6**, e1672 (2015).

36. Halliday, M. *et al.* Repurposed drugs targeting eIF2α-P-mediated translational repression prevent neurodegeneration in mice. *Brain J. Neurol.* **140**, 1768–1783 (2017).

37. Sidrauski, C., McGeachy, A. M., Ingolia, N. T. & Walter, P. The small molecule ISRIB reverses the effects of eIF2α phosphorylation on translation and stress granule assembly. *eLife* **4**, e05033 (2015).

38. Wong, Y. L. *et al.* eIF2B activator prevents neurological defects caused by a chronic integrated stress response. *eLife* **8**, e42940 (2019).

39. Boyer, J. A. *et al.* eIF4A controls translation of estrogen receptor alpha and is a therapeutic target in advanced breast cancer. *Proc. Natl. Acad. Sci. U. S. A.* **122**, e2424286122.

40. Cencic, R. *et al.* A second-generation eIF4A RNA helicase inhibitor exploits translational reprogramming as a vulnerability in triple-negative breast cancer. *Proc. Natl. Acad. Sci. U. S. A.* **121**, e2318093121 (2024).

41. Chu, J. *et al.* Rocaglates Induce Gain-of-Function Alterations to eIF4A and eIF4F. *Cell Rep.* **30**, 2481-2488.e5 (2020).

42. Iwasaki, S. *et al.* The Translation Inhibitor Rocaglamide Targets a Bimolecular Cavity between eIF4A and Polypurine RNA. *Mol. Cell* **73**, 738-748.e9 (2019).

43. Baselga, J. *et al.* Everolimus in postmenopausal hormone-receptor-positive advanced breast cancer. *N. Engl. J. Med.* **366**, 520–529 (2012).

44. Motzer, R. J. *et al.* Efficacy of everolimus in advanced renal cell carcinoma: a double-blind, randomised, placebo-controlled phase III trial. *Lancet* **372**, 449–456 (2008).

45. Yao, J. C. *et al.* Everolimus for advanced pancreatic neuroendocrine tumors. *N. Engl. J. Med.* **364**, 514–523 (2011).

46. Yao, J. C. *et al.* Everolimus for the treatment of advanced, non-functional neuroendocrine tumours of the lung or gastrointestinal tract (RADIANT-4): a randomised, placebo-controlled, phase 3 study. *Lancet* **387**, 968–977 (2016).

47. Hudes, G. *et al.* Temsirolimus, interferon alfa, or both for advanced renal-cell carcinoma. *N. Engl. J. Med.* **356**, 2271–2281 (2007).

48. Wagner, A. J. *et al.* nab-Sirolimus for Patients With Malignant Perivascular Epithelioid Cell Tumors. *J. Clin. Oncol. Off. J. Am. Soc. Clin. Oncol.* **39**, 3660–3670 (2021).

49. McConkey, D. J. The integrated stress response and proteotoxicity in cancer therapy. *Biochem. Biophys. Res. Commun.* **482**, 450–453 (2017).

50. Tian, X. *et al.* Targeting the Integrated Stress Response in Cancer Therapy. *Front. Pharmacol.* **12**, (2021).

51. Lines, C. L., McGrath, M. J., Dorwart, T. & Conn, C. S. The integrated stress response in cancer progression: a force for plasticity and resistance. *Front. Oncol.* **13**, 1206561 (2023).

52. Kline, C. L. B. *et al.* ONC201 kills solid tumor cells by triggering an integrated stress response dependent on ATF4 activation by specific eIF2α kinases. *Sci. Signal.* **9**, ra18 (2016).

53. Chi, A. S. *et al.* Pediatric and adult H3 K27M-mutant diffuse midline glioma treated with the selective DRD2 antagonist ONC201. *J. Neurooncol.* **145**, 97–105 (2019).

54. Gardner, S. L. *et al.* Phase I dose escalation and expansion trial of single agent ONC201 in pediatric diffuse midline gliomas following radiotherapy. *Neuro-Oncol. Adv.* **4**, vdac143 (2022).

55. Arrillaga-Romany, I. *et al.* ACTION: a randomized phase 3 study of ONC201 (dordaviprone) in patients with newly diagnosed H3 K27M-mutant diffuse glioma. *Neuro-Oncol.* **26**, S173–S181 (2024).

56. Prabhu, V. V. *et al.* ONC201 and imipridones: Anti-cancer compounds with clinical efficacy. *Neoplasia N. Y. N* **22**, 725–744 (2020).

57. Zafar, A., Khatoon, S., Khan, M. J., Abu, J. & Naeem, A. Advancements and limitations in traditional anti-cancer therapies: a comprehensive review of surgery, chemotherapy, radiation therapy, and hormonal therapy. *Discov. Oncol.* **16**, 607 (2025).

58. Kezic, A., Popovic, L. & Lalic, K. mTOR Inhibitor Therapy and Metabolic Consequences: Where Do We Stand? *Oxid. Med. Cell. Longev.* **2018**, 2640342 (2018).

59. Cunningham, T. A., Chapman, E. & Schatz, J. H. eIF4A inhibition: ready for primetime? *Oncotarget* **9**, 35515–35516 (2018).

60. Panwar, V. *et al.* Multifaceted role of mTOR (mammalian target of rapamycin) signaling pathway in human health and disease. *Signal Transduct. Target. Ther.* **8**, 375 (2023).

61. Ma, S., Howden, S. A. & Keane, S. C. Use of steric blocking antisense oligonucleotides for the targeted inhibition of junction containing precursor microRNAs. *bioRxiv* 2024.04.08.588531 (2024) doi:10.1101/2024.04.08.588531.

62. Ma, X. *et al.* Enhancing mRNA translation efficiency by introducing sequence optimized AU-rich elements in 3′ UTR via HuR anchorage. *Mol. Ther. Nucleic Acids* **36**, 102485 (2025).

63. Szukowska, A., Żuk, M., Sztompke, J., Bednarz, B. & Kaźmierczak, U. Application of Antisense Oligonucleotides as an Alternative Approach for Gene Expression Control and Functional Studies. *Int. J. Mol. Sci.* **26**, 10524 (2025).

64. Ling, H., Fabbri, M., Calin, G. A. & Calin, G. A. MicroRNAs and other non-coding RNAs as targets for anticancer drug development. *Nat. Rev. Drug Discov.* **12**, 847–865 (2013).

65. Boti, M. A., Diamantopoulos, M. A. & Scorilas, A. RNA-Targeting Techniques: A Comparative Analysis of Modern Approaches for RNA Manipulation in Cancer Research and Therapeutics. *Genes* **16**, 1168 (2025).

66. Naldini, L. Gene therapy returns to centre stage. *Nature* **526**, 351–360 (2015).

67. Qin, J. Y. *et al.* Systematic comparison of constitutive promoters and the doxycycline-inducible promoter. *PloS One* **5**, e10611 (2010).

68. Zeng, J. *et al.* Exploring the Potential of Cytomegalovirus-Based Vectors: A Review. *Viruses* **15**, 2043 (2023).

69. Dighe, O. R. *et al.* Emerging Recombinant Oncolytic Poliovirus Therapies Against Malignant Glioma: A Review. *Cureus* **15**, e34028.

70. Huez, I. *et al.* Two Independent Internal Ribosome Entry Sites Are Involved in Translation Initiation of Vascular Endothelial Growth Factor mRNA. *Mol. Cell. Biol.* **18**, 6178–6190 (1998).

71. Marques, R., Lacerda, R. & Romão, L. Internal Ribosome Entry Site (IRES)-Mediated Translation and Its Potential for Novel mRNA-Based Therapy Development. *Biomedicines* **10**, 1865 (2022).

72. Walton, R. W., Brown, M. C., Sacco, M. T. & Gromeier, M. Engineered Oncolytic Poliovirus PVSRIPO Subverts MDA5-Dependent Innate Immune Responses in Cancer Cells. *J. Virol.* **92**, e00879-18 (2018).

73. O'Brien, J., Hayder, H., Zayed, Y. & Peng, C. Overview of MicroRNA Biogenesis, Mechanisms of Actions, and Circulation. *Front. Endocrinol.* **9**, 402 (2018).

74. Toropko, M., Chuvpilo, S. & Karabelsky, A. miRNA-Mediated Mechanisms in the Generation of Effective and Safe Oncolytic Viruses. *Pharmaceutics* **16**, (2024).

75. Mazzacurati, L. *et al.* Use of miRNA response sequences to block off-target replication and increase the safety of an unattenuated, glioblastoma-targeted oncolytic HSV. *Mol. Ther. J. Am. Soc. Gene Ther.* **23**, 99–107 (2015).

76. Kelly, E. J. & Russell, S. J. MicroRNAs and the regulation of vector tropism. *Mol. Ther. J. Am. Soc. Gene Ther.* **17**, 409–416 (2009).

77. Rovira-Rigau, M. *et al.* Bioselection Reveals miR-99b and miR-485 as Enhancers of Adenoviral Oncolysis in Pancreatic Cancer. *Mol. Ther.* **27**, 230–243 (2019).

78. St-Cyr, G. *et al.* Remodeling the tumor immune microenvironment with oncolytic viruses expressing miRNAs. *Front. Immunol.* **13**, (2023).

79. Yu, D. *et al.* Targeting and killing of prostate cancer cells using lentiviral constructs containing a sequence recognized by translation factor eIF4E and a prostate-specific promoter. *Cancer Gene Ther.* **13**, 32–43 (2006).

80. UTRGAN: learning to generate 5′ UTR sequences for optimized translation efficiency and gene expression | Bioinformatics Advances | Oxford Academic. https://academic.oup.com/bioinformaticsadvances/article/5/1/vbaf134/8160017.

81. Cao, J. *et al.* High-throughput 5′ UTR engineering for enhanced protein production in non-viral gene therapies. *Nat. Commun.* **12**, 4138 (2021).

82. Yoon, S. *et al.* Designing 5′ UTR sequences improves the capacity of mRNA therapeutics in preclinical models of aging and obesity. *Mol. Ther.* **34**, 2098–2118 (2026).

83. Szabó, G. T., Mahiny, A. J. & Vlatkovic, I. COVID-19 mRNA vaccines: Platforms and current developments. *Mol. Ther.* **30**, 1850–1868 (2022).

84. Chaudhary, N., Weissman, D. & Whitehead, K. A. mRNA vaccines for infectious diseases: principles, delivery and clinical translation. *Nat. Rev. Drug Discov.* **20**, 817–838 (2021).

85. Kim, S. C. *et al.* Modifications of mRNA vaccine structural elements for improving mRNA stability and translation efficiency. *Mol. Cell. Toxicol.* **18**, 1–8 (2022).

86. Morrow, A. K. *et al.* ML-driven design of 3’ UTRs for mRNA stability. 2024.10.07.616676 Preprint at https://doi.org/10.1101/2024.10.07.616676 (2025).

87. Reshetnikov, V. *et al.* Untranslated Region Sequences and the Efficacy of mRNA Vaccines against Tuberculosis. *Int. J. Mol. Sci.* **25**, 888 (2024).

88. Jia, X. *et al.* Protein translation: biological processes and therapeutic strategies for human diseases. *Signal Transduct. Target. Ther.* **9**, 44 (2024).

89. Passarelli, M. C. *et al.* Leucyl-tRNA synthetase is a tumour suppressor in breast cancer and regulates codon-dependent translation dynamics. *Nat. Cell Biol.* **24**, 307–315 (2022).

90. Vincent, C. T. & Schneider, R. J. Selective tRNA charging in breast cancer. *Nat. Cell Biol.* **24**, 287–289 (2022).

91. Ebright, R. Y. *et al.* Deregulation of ribosomal protein expression and translation promotes breast cancer metastasis. *Science* **367**, 1468–1473 (2020).

92. Karlsson, E. *et al.* The mTOR effectors 4EBP1 and S6K2 are frequently coexpressed, and associated with a poor prognosis and endocrine resistance in breast cancer: a retrospective study including patients from the randomised Stockholm tamoxifen trials. *Breast Cancer Res. BCR* **15**, R96 (2013).

93. Sridharan, S. & Basu, A. Distinct Roles of mTOR Targets S6K1 and S6K2 in Breast Cancer. *Int. J. Mol. Sci.* **21**, 1199 (2020).

94. Mei, C. *et al.* eIF3a Regulates Colorectal Cancer Metastasis via Translational Activation of RhoA and Cdc42. *Front. Cell Dev. Biol.* **10**, 794329 (2022).

95. Huo, C. *et al.* eIf3a mediates malignant biological behaviors in colorectal cancer through the PI3K/AKT signaling pathway. *Cancer Biol. Ther.* **25**, 2355703 (2024).

96. Rosselló-Tortella, M. *et al.* Epigenetic loss of the transfer RNA-modifying enzyme TYW2 induces ribosome frameshifts in colon cancer. *Proc. Natl. Acad. Sci. U. S. A.* **117**, 20785–20793 (2020).

97. Zhao, Y. *et al.* YTHDF3 Facilitates eIF2AK2 and eIF3A Recruitment on mRNAs to Regulate Translational Processes in Oxaliplatin-Resistant Colorectal Cancer. *ACS Chem. Biol.* **17**, 1778–1788 (2022).

98. Yoshizawa, A. *et al.* Overexpression of Phospho-eIF4E Is Associated with Survival through AKT Pathway in Non–Small Cell Lung Cancer. *Clin. Cancer Res. Off. J. Am. Assoc. Cancer Res.* **16**, 240–248 (2010).

99. Dai, L. *et al.* Targeting EIF4F complex in non-small cell lung cancer cells. *Oncotarget* **8**, 55731–55735 (2017).

100. Ramamurthy, V. P., Ramalingam, S., Kwegyir-Afful, A. K., Hussain, A. & Njar, V. C. O. Targeting of protein translation as a new treatment paradigm for prostate cancer. *Curr. Opin. Oncol.* **29**, 210–220 (2017).

101. D'Abronzo, L. S. & Ghosh, P. M. eIF4E Phosphorylation in Prostate Cancer. *Neoplasia N. Y. N* **20**, 563–573 (2018).

102. Iadevaia, V. *et al.* PIM1 kinase is destabilized by ribosomal stress causing inhibition of cell cycle progression. *Oncogene* **29**, 5490–5499 (2010).

103. Zhang, C. *et al.* Kinase PIM1 promotes prostate cancer cell growth via c-Myc-RPS7-driven ribosomal stress. *Carcinogenesis* **40**, 52–60 (2019).

104. Fujimura, K. *et al.* A hypusine-eIF5A-PEAK1 switch regulates the pathogenesis of pancreatic cancer. *Cancer Res.* **74**, 6671–6681 (2014).

105. Fujimura, K. *et al.* Eukaryotic Translation Initiation Factor 5A (EIF5A) Regulates Pancreatic Cancer Metastasis by Modulating RhoA and Rho-associated Kinase (ROCK) Protein Expression Levels. *J. Biol. Chem.* **290**, 29907–29919 (2015).

106. Shin, S. *et al.* Translational alterations in pancreatic cancer: a central role for the integrated stress response. *NAR Cancer* **4**, zcac031 (2022).

107. Chaudhary, S., Siddiqui, J. A., Pothuraju, R. & Bhatia, R. Ribosome biogenesis, altered metabolism and ribotoxic stress response in pancreatic ductal adenocarcinoma tumor microenvironment. *Cancer Lett.* **612**, 217484 (2025).

108. Rowell, MC. *et al.* Targeting ribosome biogenesis reinforces ERK-dependent senescence in pancreatic cancer. *Cell Cycle* **22**, 2172–2193.

109. Wang, L. *et al.* EIF3B is associated with poor outcomes in gastric cancer patients and promotes cancer progression via the PI3K/AKT/mTOR signaling pathway. *Cancer Manag. Res.* **11**, 7877–7891 (2019).

110. Kohansal, M. *et al.* tRNA-derived fragments in gastric cancer: Biomarkers and functions. *J. Cell. Mol. Med.* **26**, 4768–4780 (2022).

111. Xie, Y., Zhang, S., Yu, X., Ye, G. & Guo, J. Transfer RNA-derived fragments as novel biomarkers of the onset and progression of gastric cancer. *Exp. Biol. Med.* **248**, 1095–1102 (2023).

112. Li, Z. *et al.* N6-methyladenosine regulates glycolysis of cancer cells through PDK4. *Nat. Commun.* **11**, 2578 (2020).

113. Jia, X. *et al.* Protein translation: biological processes and therapeutic strategies for human diseases. *Signal Transduct. Target. Ther.* **9**, 44 (2024).

114. Scagliola, A., Miluzio, A. & Biffo, S. Translational Control of Metabolism and Cell Cycle Progression in Hepatocellular Carcinoma. *Int. J. Mol. Sci.* **24**, 4885 (2023).

115. Han, H. *et al.* N7-methylguanosine tRNA modification promotes esophageal squamous cell carcinoma tumorigenesis via the RPTOR/ULK1/autophagy axis. *Nat. Commun.* **13**, 1478 (2022).

116. Guo, X. *et al.* EIF3H promotes aggressiveness of esophageal squamous cell carcinoma by modulating Snail stability. *J. Exp. Clin. Cancer Res. CR* **39**, 175 (2020).

117. Zhu, H. *et al.* eEF2K promotes progression and radioresistance of esophageal squamous cell carcinoma. *Radiother. Oncol. J. Eur. Soc. Ther. Radiol. Oncol.* **124**, 439–447 (2017).

118. Jia, X. *et al.* Toosendanin targeting eEF2 impedes Topoisomerase I & II protein translation to suppress esophageal squamous cell carcinoma growth. *J. Exp. Clin. Cancer Res. CR* **42**, 97 (2023).

119. Wang, S. & Sun, S. Translation dysregulation in neurodegenerative diseases: a focus on ALS. *Mol. Neurodegener.* **18**, 58 (2023).

120. Bosco, D. A. Translation dysregulation in neurodegenerative disorders. *Proc. Natl. Acad. Sci.* **115**, 12842–12844 (2018).

121. Martin, P. B. *et al.* NEMF mutations that impair ribosome-associated quality control are associated with neuromuscular disease. *Nat. Commun.* **11**, 4625 (2020).

122. Bond, S., Lopez-Lloreda, C., Gannon, P. J., Akay-Espinoza, C. & Jordan-Sciutto, K. L. The Integrated Stress Response and Phosphorylated Eukaryotic Initiation Factor 2α in Neurodegeneration. *J. Neuropathol. Exp. Neurol.* **79**, 123–143 (2020).

123. Li, W., Wang, X., van der Knaap, M. S. & Proud, C. G. Mutations Linked to Leukoencephalopathy with Vanishing White Matter Impair the Function of the Eukaryotic Initiation Factor 2B Complex in Diverse Ways. *Mol. Cell. Biol.* **24**, 3295–3306 (2004).

124. Mendonsa, S., von Kuegelgen, N., Bujanic, L. & Chekulaeva, M. Charcot–Marie–Tooth mutation in glycyl-tRNA synthetase stalls ribosomes in a pre-accommodation state and activates integrated stress response. *Nucleic Acids Res.* **49**, 10007–10017 (2021).

125. Baliga, U. K. *et al.* Translational Control in Cardiac Pathophysiology and Therapeutic Development: When mRNA Meets the Heart. *Int. J. Mol. Sci.* **26**, (2025).